ABSTRACT

Title of Document:	BEHAVIOR OF FIBER REINFORCED POLYMER COMPOSITE PILES WITH ELLIPTICAL CROSS SECTIONS IN INTEGRAL ABUTMENT BRIDGE FOUNDATIONS
	Yahya Aliabadizadeh PE, 2016
Directed By:	Professor Amde M. Amde , Department of Civil and Environmental Engineering

Every year in the US and other cold-climate countries considerable amount of money is spent to restore structural damages in conventional bridges resulting from (or "caused by") salt corrosion in bridge expansion joints. Frequent usage of deicing salt in conventional bridges with expansion joints results in corrosion and other damages to the expansion joints, steel girders, stiffeners, concrete rebar, and any structural steel members in the abutments.

The best way to prevent these damages is to eliminate the expansion joints at the abutment and elsewhere and make the entire bridge abutment and deck a continuous monolithic structural system. This type of bridge is called Integral Abutment Bridge which is now widely used in the US and other cold-climate countries. In order to

provide lateral flexibility, the entire abutment is constructed on piles. Piles used in integral abutments should have enough capacity in the perpendicular direction to support the vertical forces. In addition, piles should be able to withstand corrosive environments near the surface of the ground and maintain their performance during the lifespan of the bridge.

Fiber Reinforced Polymer (FRP) piles are a new type of pile that can not only accommodate large displacements, but can also resist corrosion significantly better than traditional steel or concrete piles. The use of FRP piles extends the life of the pile which in turn extends the life of the bridge.

This dissertation studies FRP piles with elliptical shapes. The elliptical shapes can simultaneously provide flexibility and stiffness in two perpendicular axes. The elliptical shapes can be made using the filament winding method which is a less expensive method of manufacturing compared to the pultrusion or other manufacturing methods. In this dissertation a new way is introduced to construct the desired elliptical shapes with the filament winding method.

Pile specifications such as dimensions, number of layers, fiber orientation angles, material, and soil stiffness are defined as parameters and the effects of each parameter on the pile stresses and pile failure have been studied. The ANSYS software has been used to model the composite materials. More than 14,000 nonlinear finite element pile models have been created, each slightly different from the others. The outputs of analyses have been used to draw curves. Optimum values of the parameters have been defined using generated curves. The best approaches to find optimum shape, angle of fibers and types of composite material have been discussed.

BEHAVIOR OF FIBER-REINFORCED POLYMER COMPOSITE PILES WITH ELLIPTICAL CROSS SECTIONS IN INTEGRAL ABUTMENT BRIDGE FOUNDATIONS

By

Yahya Aliabadizadeh PE

Dissertation submitted to the Faculty of the Graduate School of the
University of Maryland, College Park, in partial fulfillment
of the requirements for the degree of
Doctor of Philosophy
2016

Advisory Committee:
Professor Amde M. Amde, Advisor/Chairman
Professor Sherif M. Aggour
Professor Bilal M. Ayyub
Professor Chung C. Fu
Professor Sung Lee

A. Dedication

With great respect to my Mother and Father, who always encouraged and supported

me to continue my education and made me who I am.

With all my love to my dear wife Laleh.

To my dear daughter Ava and my dear son Aiden, whose own dissertation defenses I

hope to attend one day.

B. Acknowledgements

C. Table of Contents

D. List of Tables

E. List of Figures

F. List of Abbreviations and Variables

- **Abbreviations**

ACP: ANSYS Composite PrepPost

AGS: Advanced Grid Stiffened

APDL: ANSYS Parametric Design Language

CCA: Composite Cylinder Assemblage

CFFT: Concrete-Filled Fiber reinforced polymer Tubes

CFRP: Carbon Fiber Reinforced Plastic

CFST: Concrete-Filled Steel Tubes

CNC: Computer Numerical Control

DOD: Department of Defense

FE: Finite Element

FHWA: Federal Highway Administration

FRC: Fiber reinforced composites

FRP: Fiber Reinforced Polymer

GFRP: Glass FRP

GSCS: Generalized Self Consistent Scheme

HDPE: High Density Polyethylene

IAB: Integral Abutment bridges

PS: Parameter Set

RC: Reinforced Concrete

RF: Radio Frequency

RPP: Reinforced Polymeric Piling

SCC: Self Consolidating Concrete

SRP: Structurally reinforced plastic

UDC: Unidirectional Fiber Composite

- **FRP material variables**

ε Strain

σ Stress

1 material 1 direction

2 material 2 direction

3 out-of-plane normal direction

12 in plane shear

13 and 23 out of plane shear terms

I principal I direction

II principal II direction

III principal III direction

"t" tension

"c" compression

"tw" Tsai-Wu 2D and 3D

"th" Tsai-Hill 2D and 3D

k_f Plane strain bulk moduli for isotropic fibers

E_f Plane modulus of elasticity for isotropic fibers

ν_f Plane poison ratio for isotropic fibers

k_m Plane strain bulk moduli for matrix

E_m Plane modulus of elasticity for isotropic matrix

v_m Plane poison ratio for isotropic matrix

$\bar{\sigma}_{11}$ Average stress in principal direction

$\bar{\sigma}_{22}$ Average stress in direction 2

$\bar{\sigma}_{33}$ Average stress in direction 3

$\bar{\varepsilon}_{11}$ Average strain in principal direction

$\bar{\varepsilon}_{22}$ Average strain in direction 2

$\bar{\varepsilon}_{33}$ Average strain in direction 3

G_1^* Effective in plane Shear Modulus

G_2^* Effective out of plane shear modulus

G_3^* Effective out of plane shear modulus

v_{12}^* Major Poisson's ratio

v_{23}^* Minor Poisson's ratio

v_{13}^* Minor Poisson's ratio

E_1 Modulus in 1 direction

E_2 Modulus in 2 direction

E_3 Modulus in 3 direction

k^* Plane strain bulk modulus

k_f Fiber transverse bulk modulus

σ_{1t} In plane failure strength in uniaxial tension

σ_{1c} In plane failure strength in uniaxial compression

σ_{2t} In plane failure strength in uniaxial tension

σ_{2c} In plane failure strength in uniaxial compression

σ_{3t} Out of plane failure strength in uniaxial tension

σ_{3c} Out of plane failure strength in uniaxial compression

ε_{1t} In plane failure strain in uniaxial tension

ε_{1c} In plane failure strain in uniaxial compression

ε_{2t} In plane failure strain in uniaxial tension

ε_{2c} In plane failure strain in uniaxial compression

ε_{3t} Out of plane failure strain in uniaxial tension

ε_{3c} Out of plane failure strain in uniaxial compression

- **Soil variables**

n Shape Parameter

n_h Constant of subgrade reaction

k_h Initial Lateral Stiffness

p Generalized Soil lateral resistance

p_u Ultimate lateral soil resistance

y Generalized lateral displacement

α the soil cohesion factor

k_v Initial Slip resistance

q Generalized Soil slip resistance

f_{max} Ultimate soil Slip resistance

z Generalized slip displacement

$k_q =$ Initial Point Stiffness,

q Generalized Soil bearing resistance

q_{max} Ultimate soil Bearing resistance

z Generalized bearing displacement

ε_{50} Axial strain at 0.5 times peak stress difference

c_u Undrained cohesion

B Pile width

γ Effective unit weight of soil

x Depth from soil surface

φ Angle of internal Friction

k_p Passive pressure coefficient

k_a Active pressure coefficient

k_0 At rest pressure coefficient

y_{50} Displacement at one half ultimate soil reaction

α Shear strength reduction factor

c_a Adhesion between soil and pile

N Average standard penetration blow count

N_{corr} Corrected standard penetration test

z_c Relative displacement required to develop f_{max}

l_g Gross perimeter of the pile

1. Introduction

This dissertation focuses on Fiber Reinforced Polymer (FRP) piles with elliptical cross section used in Integral Abutment Bridge (IAB) structures.

Integral Abutment Bridges are structures where the superstructure and substructure move together to accommodate the required translation and rotation. There are no bridge expansion joints and in the case of Fully Integral Abutment Bridges, no bearings. In the United States of America (USA), there are more than 9,000 Fully Integral Abutment Bridges and 4,000 Semi-Integral Abutment Bridges. Integral Abutment Bridges have proven themselves to be less expensive to construct, easier to maintain, and more economical to own over their life span. European experience with Integral Abutments is significantly less, but what experience has been gained has been positive. As a result, the trend across Europe is towards increasing the percentage of Integral Abutment Bridges in newly constructed bridges.

Bridges are subjected to severe changes in temperature. This will cause bridges to expand and contract. The thermal displacement is a factor of bridge length, temperature variation and bridge material. The bridge material is almost constant for most of today's bridges. The temperature variation depends on the geographic location of the bridge and the climate. The bridge length is the other effecting factor. Currently, the longest jointless IAB ever built in the US is 1175 ft long (Houston Walker 2016). With a practical solution to accommodate larger thermal displacement the IAB length can be extended further.

Piles made of steel or timbers deteriorate over the years. Concrete piles may be more durable but when it comes to bridge piles, they do not present required flexibility. The

composite piles are a relatively newer generation of piles. They present a much longer life span. Besides, there are increasing types of composite to be used in piles. Composite piles also can accommodate much larger flexibility without affecting the vertical load carrying capacity.

Composite piles have been available in the North American market since the late 1980s, but to date their use has been limited mainly to marine fender piles, load-bearing piles for light structures, and experimental test piles (Iskander, et al., 2001). Composite piles have not yet gained wide acceptance in the civil engineering industry, primarily due to the lack of a long track record of performance, and the scarcity of well-documented field load tests. However, FRP composite piles may exhibit longer life cycle and improved durability in harsh marine environments, thereby presenting the potential for substantially reduced costs. Potential disadvantages of using composite piles are related to cost and performance. At present, composite piles are generally more expensive than traditional piles (Hoy 1995, Iskander and Hassan 1998). Drivability may be less efficient with these piles. Structural properties, including low bending stiffness and high axial capacity, could result in large lateral deformations. In IAB structures this can be an advantage. Currently, engineers and designers use H piles made of composite materials. There are a fewer number of sizes available to choose from. Compared to variations of the steel piles and concrete pile the number of choices is very limiting for the designers. The flexibility of the pile is the main reason for use as a replacement for the expansion joints. The pile requires enough rigidity in the lateral and vertical directions as well. The elliptical shape is proposed in this dissertation for its ability to

maintain the desired flexibly and stiffness in two independent perpendicular directions. The proposed method of production eases the production and reduces the cost. The pultrusion method, which is the dominant method of mass production, requires considerable budget in the beginning. This method will only be economical if it is used in mass production. Since the FRP piles are not popular, the low demand for this type of pile will keep the production low and expensive.

On the contrary the filament winding method is a relatively less expensive method used for production of round sections. With the solution proposed in this dissertation, FRP piles with elliptical cross section can be made with this method which will be more economical. More economical production will lead to more usage. More usage of FRPs will lead to more study. More study and research will bring better solutions. Currently FRP piles are not as popular as the steel and concrete piles.

In this dissertation numerous finite element models are created to show the stresses and failures resulting from applied forces and displacements. The conclusion at the end of the report summarizes the findings.

2. Integral Abutment Bridges

Integral Abutment Bridges are structures where the superstructure and substructure move together to accommodate the required translation and rotation resulting from temperature changes. There are no bridge expansion joints in integral abutment bridges, therefore no bearings and no damage due to salt penetration to the supports.
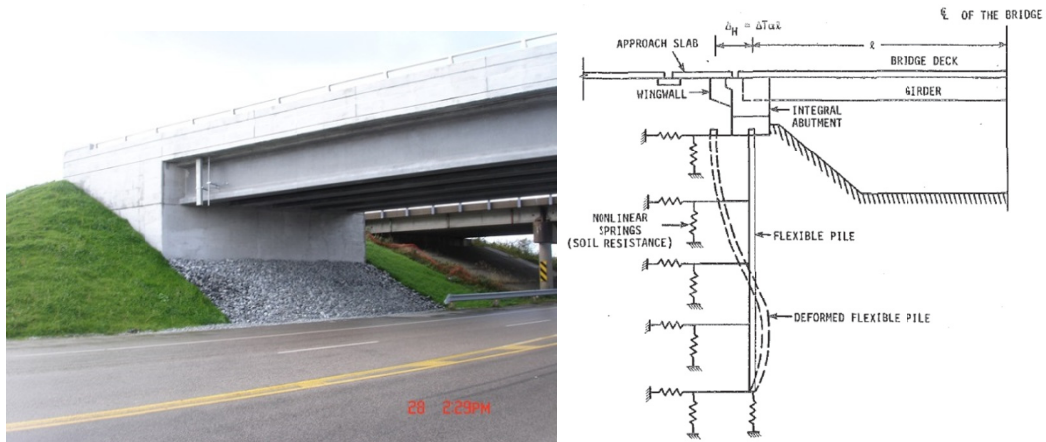
Figure 1 - (Left) example of Integral Abutment Bridge, (Right) Cross section of Integral Abutment Bridge with soil-Pile Interaction model (NS Department of Transportation and Infrastructure Renewal 2010-2013)

The entire abutments are supported on piles. The piles' lateral movement allows small movement to the abutment. Therefore, the need for an expansion joint is eliminated. The piles' lateral movement can absorb thermal expansion or contraction, vehicle braking force and similar axial forces in the bridge axial direction. Experience indicates that the expansion joint/bearing detail can be a significant post-construction maintenance item and thus an expense during the in-service life of a bridge. Therefore, the concept was developed to physically and structurally connect the superstructure and abutments as shown in Figure 1 to create what is referred to as an Integral Abutment Bridge (IAB). In doing so, the troublesome and costly

expansion joint/bearing detail is eliminated. IABs have been used for roads since at least the early 1930s in the U.S.A. However, they have seen more extensive use worldwide in recent years because of their economy of construction in a wide range of conditions. Over the years and in different countries IABs have also been called integral bridges, integral bridge abutments, jointless bridges, rigid-frame bridges and U-frame bridges. There is also a design variant called the semi-integral-abutment bridge which is not the subject of this dissertation.
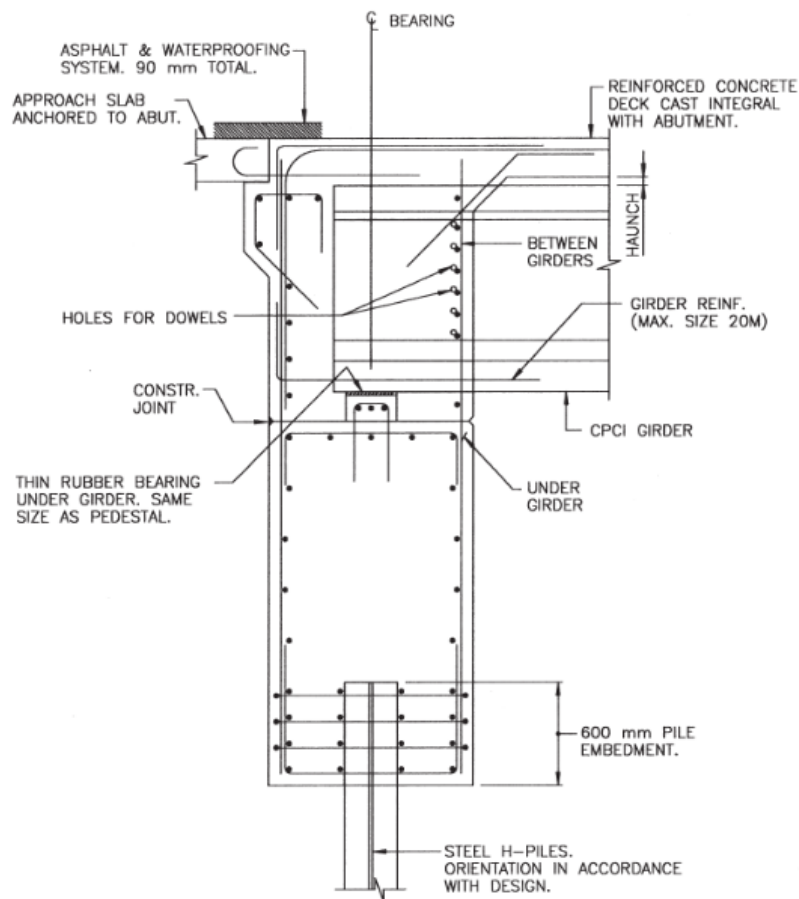
Figure 2 - Typical Detail for Integral Abutments with Steel Girders (Dicleli, Rational design approach for prestressed-concrete-girder integral bridges 2000)

Figure 2 is an example of the approach slab, abutment and bridge deck connection. This dissertation will clarify the ways to replace the costly expansion joints with less expensive elliptical FRP piles. The result will be a type of bridge which is not only cost effective but also long-lasting, maintenance free and Earth friendly.

One of the most important aspects of design, which can effect structure life and maintenance costs, is the reduction or elimination of roadway expansion joints and associated expansion bearings. Unfortunately, this is too often overlooked or avoided. Joints and bearings are expensive to buy, install, maintain and repair and more costly to replace. The most frequently encountered corrosion problem involves damaged expansion joints and broken seals that permit salt-laden runoff water from the roadway surface to attack the girder ends, bearings and supporting reinforced concrete substructures. Elastomeric glands get filled with dirt, rocks and trash, and ultimately fail to function. Many of our most costly maintenance problems originated with damaged joints. Bridge deck joints are subject to continual wear and heavy impact from repeated live loads as well as continual stages of movement from expansion and contraction caused by temperature changes, as well as creep and shrinkage or long term movement effects such as settlement and soil pressure. Joints are sometimes subject to impact loadings which can exceed their design capacity. Retaining hardware for joints are damaged and loosened by snowplows and the relentless pounding of heavy traffic. Broken hardware can become a hazard to motorists, and liability to owners.

Deck joints are routinely one of the last items installed on a bridge and are sometimes not given the necessary attention they deserve to ensure the desired performance.

While usually not a significant item based on cost, bridge deck joints can have a significant impact on a bridge performance. A wide variety of joints have been developed over the years to accommodate a wide range of movements, and promises of long lasting, durable, effective joints have led States to try many of them. Some joint types perform better than others, but all joints can cause maintenance problems. Bearings also are expensive to buy and install and more costly to replace. Over time, steel bearings tip over and seize up due to loss of lubrication or build-up of corrosion. Elastomeric bearings can split and rupture due to unanticipated movements or may ratchet out of position. Because of the underlying problems of installing, maintaining and repairing deck joints and bearings, many States have been eliminating joints and associated bearings where possible and are finding that jointless bridges can perform well without the continual maintenance issues inherent in joints. When deck joints are not provided, the thermal movements induced in bridge superstructures by temperature changes, creep and shrinkage must be accommodated by other means. Typically, provisions are made for movement at the ends of the bridge by one of two methods: integral or semi-integral abutments, along with a joint in the pavement or at the end of a reinforced concrete approach slab. Specific guidelines for designing and detailing jointless bridges have not yet been developed by AASHTO so the States have been relying on established experience.

A 1985 FHWA report on tolerable movement of highway bridges examined 580 abutments in 314 bridges in the United States and Canada. Over 75 percent of these abutments experienced movement, contrary to their designer's intent, typically much

greater movement vertically than horizontally. The following paragraph is from that report:

"The magnitude of the vertical movements tended to be substantially greater than the horizontal movements. This can be explained, in part, by the fact that in many instances the abutments moved inward until they became jammed against the beams or girders which acted as struts, thus preventing further horizontal movements. For those sill type abutments that had no backwalls, the horizontal movements were often substantially larger, with abutments moving inward until the beams were, in effect, extruded out behind the abutments."

The use of expansion joints and bearings to accommodate thermal movements does not avoid maintenance problems; rather, the provision to these items can often increase the maintenance problems. In this 40-year national experience, many savings have been realized in initial construction costs by eliminating joints and bearings and in long-term maintenance expenses from the elimination of joint replacement and the repair of both super- and substructures.

Designers should always consider the possibilities of minimum or no joint construction to provide the most durable and cost-effective structure. Steel superstructure bridges up to 400 feet long and concrete superstructure bridges up to 800 feet long have been built with no joints, even at the abutments.

The decisions made at the design stage account for over 80 percent of the influence on both cost (first and life-cycle) and quality (service life performance) of the structure. Decisions made in the initial stages of design establish a program that is difficult and costly to change once detailed design or construction begins. The

following quotation is very appropriate for bridge engineering: "Quality is never an accident. It is always the result of high intention, sincere effort, intelligent direction, and skillful execution. It represents the wise choice of many alternatives."

This is especially true when the Engineer begins the task of planning, designing and detailing a bridge structure. The variables are many, each of which has a different first and life-cycle cost factor. The question to be asked continuously throughout the entire process is, what value is added if minimum cost is not selected? Another question to be asked is, what features should be incorporated in the structure to reduce the first and life-cycle cost and enhance the quality? Most of the variables are controlled by the designer. These decisions influence the cost and quality of the project; for better or for worse. (Mistry 2000)

There are many advantages to the use of FRP piles in jointless bridges as many are performing well in service. There are long-term benefits to adopting FRP pile concepts and therefore there should be greater use of FRP piles in integral bridge construction. FRP piles require much less maintenance compared to equivalent bridges with expansion joints. In other words, jointless bridges last longer without the need for maintenance. Using FRP piles increases the life of the bridge to even greater extent.

This dissertation explains why we should use Integral Abutment and Jointless Bridges, and discusses some facts about FRP piles with elliptical cross section which is believed to be the best cross section for this type of bridge.

Until today, relatively little study has been performed on Integral Abutment Bridges. Within this study, even less is focused on FRP piles. And among the studies on FRP

piles almost no study has been done on FRP piles with elliptical cross section. As will be described in future chapters, the use of some types of FRP material is also environmentally friendly and can help the environment while providing the required stabilities at the same time.

3. Research Objectives and Approach Methodology

The piles used under integral abutment bridges should have a required stiffness in one direction and a different stiffness in the perpendicular direction. The pile should be flexible to allow the lateral displacement of the abutment along the bridge axis, and at the same time stiff enough to resist the moments, shears and axial load applied in the other directions.

Fiber composites have been a viable option in replacing traditional pile materials such as concrete and steel in harsh environmental conditions. However, driving composite piles requires careful consideration due to their relatively low stiffness. Currently, there are no specific guidelines on the installation of composite piles which limits their acceptance in load-bearing applications. There is a need therefore to understand their behavior in order for composite piles to be safely and economically used under the bridges.

The elliptical cross section is suggested as the best possible section that can be produced without the expensive cost of the pultrusion mold simply by using the filament winding method. The elliptical FRP piles have several variables. Thickness, orientation of the fibers, number of layers of fibers, eccentricity of the ellipse cross section, and size of the pile are some of the variables.

The main objective of this dissertation is to evaluate these variables and provide charts to show the best economic solution for the desired pile section properties. This can be achieved by modeling different piles and obtaining a point for each. Then the curve will be generated by connecting these dots. The optimum value of each variable will be the maximum or minimum point of each chart.

4. Fiber Reinforced Polymer (FRP) Piles

Every year in the US and other countries, considerable money is spent on piles damaged or deteriorated due to corrosion. Using FRP (Fiber Reinforced Polymer) piles appears to be the most feasible solution that eliminates the corrosion and deterioration problem.

Figure 3 shows the corrosion resistance of the FRP piles compared to other materials used for pile construction.

Wood Rots   **Steel Rusts**   **Concrete Crumbles**   **Fiberglass Lasts**

Figure 3 – Corrosion resistance of the FRP piles compared to other materials (Pearson Pilings 2016)

This becomes more important in structures in which the lifespan of the structure is directly effected by the resistance of the foundation against corrosion. Use of FRP material in IAB (Integral Abutment Bridges) structures becomes more important than usual when both the performance and lifespan of the bridge can be significantly increased with the help of this new technology.

Piles under the IAB structures should have a cross section which maintains enough flexibility in one direction and considerable rigidity in the perpendicular direction. An elliptical section can accommodate both requirements. In addition, pile flexibility can be achieved with optimum cross section without sacrificing the overall pile capacity. Piles with elliptical cross sections can be made using both filament winding and pultrusion methods. Square or rectangular shapes can only be made with pultrusion method. Pultrusion method usually has considerable cost of forming die manufacturing which significantly affects the feasibility of the product.

In contrast, the filament winding method has a relatively much lower cost of manufacturing. The filament winding mandrel can also be built much faster than the pultrusion forming die. Therefore, the elliptical cross sections will be the more feasible option for designers and engineers.

The circular or elliptical mandrel can be easily built with several methods. Using a steel pipe with a matching desired diameter for circular sections is very popular. Pressing a steel pipe sideways to achieve an elliptical shape is also recommended for elliptical cross sections. Manufacturers can make the desired shape by welding strips of steel plates. As an alternative solution, stiffener plates can be temporarily (or permanently) welded to an inner circular core. Then a covering thin plate (to be bent easily) can be welded or screwed to the inner circular core. By using this method any desired elliptical shape can be built without bearing the cost of rotating inner parts. This method also reduces the time to build a new rotating mandrel with the desired cross section. Figure 4 and Figure 5 show different elliptical cross sections built on the same inner core.

As shown, the covering thin plate can be mounted on elliptical stiffeners to achieve an elliptical surface.
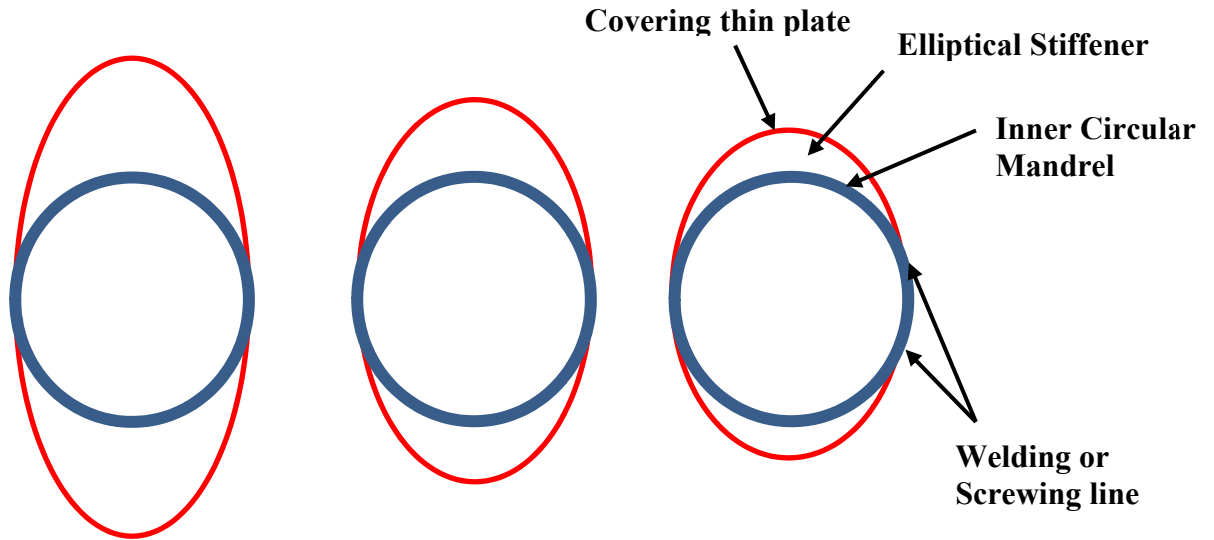
Figure 4 - Possibility of building different elliptical shapes on inner circular rotating mandrel by welding or bolting stiffener plates
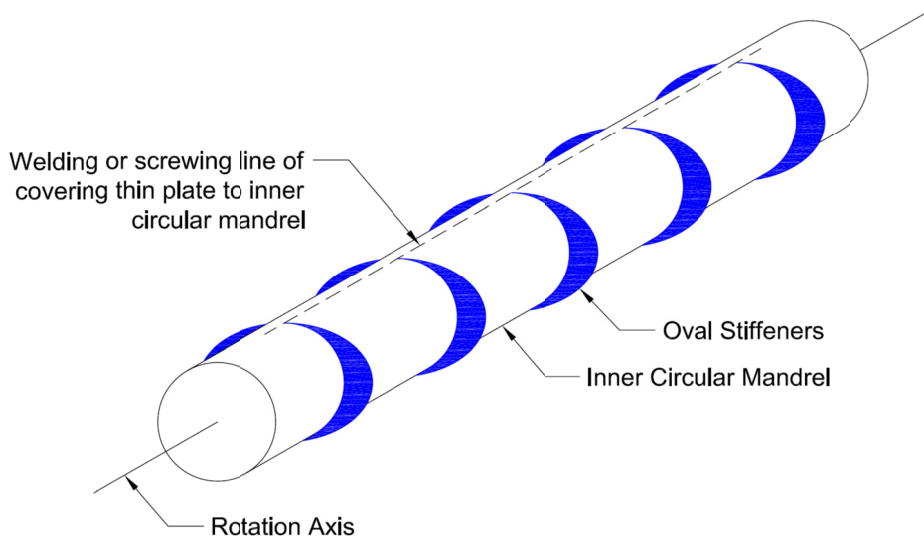
Figure 5 - Stiffener plates along the inner circular mandrel

Production of a custom made forming die requires weeks of precision manufacturing which only a handful of manufacturers can provide. In contrast, the rotating mandrel

or the elliptical stiffeners can be built in most steel shops. Using Computer Numerical

Control (CNC) technology to cut the crescents between the desired ellipse and inner

circular mandrel will reduce the time of production to a day. Even with hand cutting

the plates, minor errors in the production such as eccentricity of the mandrel do not

affect the quality of the final product. Therefore, the filament winding low cost

elliptical mandrel can also be produced in a much shorter time.

The filament winding method has several superior advantages over the pultrusion

method which directly relates to the subject of this study. The most important factors

are described as follows:

4.1. *Parameters affecting the pile capacity*

4.1.1.   Layer orientation

One of the parameters that can be easily adjusted in the production method is the orientation of the fibers. The piles with elliptical cross section can be built with a wide range of fiber orientation angle. The desired orientation angle can be easily achieved by fine tuning the filament guide movement with respect to mandrel rotation speed. The box cross sections inherently limit the fiber orientation from pultrusion manufacturing method while the elliptical and circular shapes produced with the filament winding method can have any fiber orientation angle.

4.2. *Number of layers*

The number of layers also can easily be reduced or increased in filament winding method by simply applying less or more passes of fibers over the lower layers. This is another important factor when a certain number of layers is desired. In the pultrusion method the forming die is made for a fixed number of fibers. Since it is impossible to add the number of layers in a pultrusion method, piles with more or less layers require a different forming die for each production which would not be feasible.

4.2.1.   Ellipse Eccentricity

Regarding the aforementioned manufacturing techniques, the desired elliptical shape can be easily and quickly built in the shop with considerably less cost. Since the forming die is not flexible, this would not be feasible while using the pultrusion forming die.

4.2.2.   Solution

This concludes that using the filament winding method is less expensive, faster and easier compared to the pultrusion method. The elliptical and circular shapes are the best cross sections that can be manufactured with the filament winding method. Therefore, the elliptical and circular cross sections are the most feasible cross sections to be used for FRP piles.

The current studies performed on FRP piles show that the pile capacity is affected by many factors such as layer orientation, cross section of the pile and also pile dimensions and thickness. Currently there is lack of information on how each of the mentioned factors could affect the piles with elliptical cross section. Almost no study is found on the optimization of piles with elliptical or oval cross section. This dissertation is conducted to define the behavior of the pile with regard to each factor. Then the best and optimum case is presented as the most economical section. This method can obviously be a great aid for the designers and engineers in order to design the IAB structures. Functionality of IAB structures highly depends on to the durability of the piling system. If a reliable system is known to withstand deterioration, fatigue and extreme loading while being feasible and easy to produce, it would be a great tool to overcome the bridge design and construction problems.

5. *Manufacturing Methods and Physical Properties*

A composite material (also called a composition material or shortened to composite) is a material made from two or more constituent materials with significantly different physical or chemical properties that, when combined, produce a material with characteristics different from the individual components. The individual components remain separate and distinct within the finished structure. The new material may be preferred for many reasons: common examples include materials which are stronger, lighter, or less expensive when compared to traditional materials.

The earliest man-made composite materials were straw and mud combined to form bricks for building construction. Ancient brick-making was documented by Egyptian tomb paintings. Wattle and daub is one of the oldest man-made composite materials, at over 6,000 years old. Concrete is also a composite material, and is used more than any other man-made material in the world. As of 2006, about 7.5 billion cubic meters of concrete are made each year which is more than one cubic meter for every person on Earth.

5.1. *Positive and Negative Features of Composite Designs*

The following characteristics are positive features of composite materials:

- Oriented stiffness and strength properties.

- Material properties adjustable by engineers (material design)

- Parameters to modify e.g. type of fibers and matrix, fiber volume fraction, fiber orientation, stacking sequence, layer thickness, fabrication method

- Significant reduced weight compared to metals

- High stiffness and strength properties with respect to weight

- High fatigue resistance

- Specific material characteristics possible (e.g. thermal stability due to negative coefficient of thermal expansion of carbon fibers)

- Reduced corrosion tendency

- Low moisture absorption

- Damping of vibrations

- Less sensitive to imperfections (geometrical and physical)

- Electrical conductivity or non-conductivity (depending on the materials used)

While having considerable advantages over the homogenous material, there are some disadvantages using composites. Of course not all of them apply to the usage of composite piles under bridges.

- Low stiffness and strength perpendicular to fiber direction

- Large thermal strains perpendicular to fiber direction

- Low inter-laminar shear stiffness and strength

- Long time durability (especially concerning environmental influence, e.g. heat, moisture, chemical, UV, aging …)

- Low heat resistance (e.g. low fire resistance of matrix material)

- Undesirable brittle failure behavior (safety concepts)

- Open questions concerning recycling

- Difficulties in damage detection (x-rays, ultrasonic, thermographic, nondestructive methods)

- Open questions concerning reparability

- Relatively high material costs

- Problems with conventional joints (bolts, rivet, adhesive)

- Sensitive with respect to the fabrication process (flaws, bubbles, dust)

5.2. *Previous Studies on Fiber Reinforced Plastic FRPs*

In April 1987 the first prototype recycled plastic pile was driven at the Port of Los Angeles (Horeczko 1995). The pile consisted of a segmented, 18 m (60 ft) long, 33 cm (13 in.) diameter recycled plastic, with a 12.5 cm (5 in.) diameter steel pipe core. Each 6 m (20 ft) segment was connected by a threaded coupling. Experience, however, has shown that steel core composite piling suffers from core delamination due to thermal stresses. Over the next few years, several vendors produced a variety of piling products made of virgin, recycled and hybrid composites. (Iskander 1998)

In 1995 Mirmiran and Shahawy conducted a study on fiber jacketing technique which was considered an effective retrofitting tool for existing columns and piles.

In 1996 Seible studied the development of advanced composite carbon shell systems for concrete columns in seismic zones. Ireman conducted an experimental study on damage propagation in composite structural elements in the same year.

Also in 1996 Mirmiran and Shahawy studied the behavior of the proposed column by developing two analytical tools; (1) a new passive confinement model for externally reinforced concrete columns, (2) a composite action model that evaluates the lateral stiffening effect of the jacket.

In 1998 Iskander conducted a paper considering the advantages and disadvantages of the FRP piles. Iskander counted good durability and environmental dividends as the most important advantages and high cost, less efficient drivability, high compressibility, and lack of a long-term track record as disadvantages of the FRP piles.

In 2000 Pando studied the behavior of FRP piles under different loadings. Short term versus long term axial and flexural strength as well as durability of the pile was studied. Pando concluded that the degradation of the FRP properties has a greater impact on the long-term flexural capacity of the pile. For the example presented, the long-term axial and flexural capacities were estimated to be 5 and 24 percent lower than the short-term capacities respectively.

In 2001 Davol et al. characterized the response of a circular external FRP jacket with inner concrete core under flexural loading. Compression behavior was discussed with emphasis on understanding the dilation behavior of the concrete core. A finite element model was proposed that predicted the longitudinal, hoop, and shear strains in the FRP shell. Large-scale experimental validation of the models was presented.

In the same year Pando described a simplified model for predicting the residual axial capacity of a concrete FRP pile subjected to tidal region moisture. The model showed that based on available data, the strength would reach a maximum reduction in capacity in about 150 days.

In the same year Iskander conducted a drivability study of FRP composite piles. Iskander concluded that several obstacles must be addressed before composite piling can be widely used. First, several FRP composite piles must be instrumented, installed, and load tested to support the analysis results and to answer many open questions. Second, allowable driving stresses of composite materials must be quantified. Third, prestressing of concrete-filled fiberglass piles must be verified. Fourth, long-term bond between composites and reinforcing elements must be

confirmed. Fifth, the durability of FRP piling, especially recycled composites, under actual field conditions must be validated.

In the same year Ashford compared the drivability of four composite piles to conventional steel and concrete piles and showed that all of the FRP piles can be reasonably expected to attain design bearing capacities of 400 kN (90 kips), but the extremely low impedance of glass fiber-reinforced matrix composite piles limits the ultimate capacity that can be achieved through impact driving.

In 2002 Hesham conducted a study on tapered FRP piles. The paper focused on design of tapered piles, toe driving and statnamic pile load testing.

In the same year Pando conducted experiments on FRP piles driven in the sand with more focus on the skin friction characteristics of FRP composite piles against sand. Pando compared the results of sand-to-composite pile interface shear tests on two types of FRP composite piles. The test results were compared with those from sand-to-concrete interface tests.

In 2003 Fam et al. conducted a test on FRP piles used for the first time in the construction of the substructure of the Route 40 highway bridge over the Nottoway River in Virginia. The piles consisted of 24.6 in. (625 mm) diameter concrete-filled glass fiber reinforced polymer (GFRP) circular tubes, with a 0.21 in. (5.3 mm) wall thickness.

Fam et al. concluded that 1) The use of concrete-filled FRP tubes as piling for bridge piers is practical and feasible; 2) The flexural strength of the 24" circular FRP pile with .213" thick GFRP tube is equal to a 20" square pile made of concrete and pre-stressed with fourteen 0.5" strands; 3) The FRP pile failed by fracture of GFRP on the

tension side, whereas the pre-stressed concrete pile failed by yielding of strands in tension followed by crushing of the concrete in compression; 4) Both the FRP pile and the concrete pile performed similarly during pile driving, axial load test and flexural test and analysis; 5) The initial cost of FRP piles is 77% higher than pre-stressed type. However, as production volume increases and by considering life cycle costs of the low maintenance composite piles, the cost comparison may shift in favor of FRP piles in corrosive environments; 6) No indications of unsatisfactory performance of FRP pile were reported by 2003.

In the same year Mirmiran et al. studied the stay-in-place FRP form for concrete columns. Mirmiran reviewed various design issues including confinement modelling, axial-flexural behavior, time-dependent behavior, buckling and slenderness, pile driving, seismic behavior, connections and modular construction, shear behavior, fatigue performance, and nondestructive testing and inspection of stay-in-place FRP concrete columns. The study showed the feasibility and effectiveness of the system for civil engineering applications.

In 2004 Mohammed conducted a study on toe driving of the FRP piles. In the study first the FRP pile was driven with a steel toe. Then self-consolidating concrete (SCC), a material that flows under gravity and assures the integrity of piles, was cast into fiberglass-reinforced polymer (FRP) tubes that provided corrosion-resistant reinforcement. The toe driving technique was proved to be very suitable for installing FRP piles in dense soils. Results from the driving tests and static load test indicated that FRP–SCC hybrid piles are a very competitive and attractive option for the deep foundations industry.

In 2005 Shao and Mirmiran conducted an experiment on six concrete-filled fiber reinforced polymer (FRP) tubes (CFFT). The study showed that CFFT can be designed with ductility behavior comparable to reinforced concrete members. Significant ductility can stem from the fiber architecture and interlaminar shear in the FRP tube. Moderate amounts of internal steel reinforcement in the range of 1–2% may further improve the cyclic behavior of CFFT.

Shao and Mirmiran also conducted another parallel study on cyclic analysis of CFFT piles. The study was carried out to evaluate the effect of CFFT parameters on its hysteretic response, and to compare the response with reinforced concrete (RC) and concrete-filled steel tubes (CFSTs). The study shows the feasibility of designing CFFT columns with comparable hysteretic performance to RC columns.

In the same year in the University of Maryland Civil and Environmental Engineering department, Yaser Jaradat submitted his dissertation titled "Soil-Structure Interaction of FRP Piles in Integral Abutment Bridges". Jaradat studied the FRP piles with box and circular cross sections. Pile stress and deflection and optimization charts were created and the optimum variables of the FRPs were defined for the subjected study. A double-I section that could be converted to a box by assuming the flange length equal to zero was the subject of this study. Jaradat concluded that:

1) The axial dead load which is applied at the beginning is of a major importance in increasing the capacity of the laterally deformed pile;

2) Changing the section geometry of the pile to reduce its moment of inertia while maintaining constant area has a minor effect on the stresses if the pile is fully driven in stiff soils;

3) Piles with larger cross-sectional areas produce lower stresses compared to smaller piles with equivalent loading;

4) The soil-pile stiffness for a single large pile is lower than that of multiple piles with an equivalent capacity when driven without predrilled holes;

5) Predrilled holes have a dramatic effect on stress reduction in piles in stiff soils. The stress reduction depends on the depth of the predrilled hole. A stress reduction of 70% or more can be achieved by using predrilled holes filled with loose sands;

6) Rectangular piles were found to be better than circular piles for geometrical optimization purposes. The section dimensions can be proportioned for lowest stress and stiffness;

7) Rectangular hollow piles are better than circular when subjected to lateral displacements. A hollow pile with a circular section experienced local buckling at some locations along its depth. Rectangular sections performed better without local buckling because the two sides parallel to the displacement direction (the webs) provided lateral support to the pile against local buckling;

8) The fiber orientations in the layers have a strong effect on the pile behavior. It is strongly recommended to have multiple layers with different fiber orientations. Increasing the number of layers up to a certain limit will improve the pile properties. The fiber orientations should be selected for best performance;

9) Due to the nature of concrete and its cracking under tension stresses, the section properties will not be stable under continuous lateral displacements. The loss of section under cracking increases the stresses on the composite shell which requires a change of fiber orientation for best performance as cracks keep growing;

10) The directional material properties have a major effect on the optimization results of layer orientations. The optimum fiber directions in each layer in the stack for the desired objective function change with the mechanical properties and their ratios in the composite material;

11) Plain concrete improves the pile axial stiffness and increases its load capacity when used as filler with FRP shells;

12) FRP improves the strength and the stiffness of confined concrete. The FRP shell strength, stiffness, thickness, and fiber structure are major factors in the percentage of the increase.

Jaradat's study was conducted on a FE model created in ANSYS software.

In 2006 the Federal Highway Administration (FHWA) published a comprehensive report titled "Behavior of fiber-reinforced polymer composite piles under vertical load". The report focused on mechanical short term behavior of FRP piles, behavior of FRP piles under vertical load and capacity evaluation.

In that same year the FHWA published another report titled "A Laboratory and Field Study of Composite Piles for Bridge Substructures". The report showed the field tests and axial , lateral and long term analysis of bridges with FRP piles.

In 2007 Fu, Amde and Robert studied the field performance of FRP deck in Harford County, Maryland. The study was performed on a bridge deck replacement project with new FRP deck. The study showed that the FRP deck can be effectively used in lieu of concrete deck.

In the same year Sakr studied wave equation analyses of tapered FRP–concrete piles in dense sand. The study concluded that the taper shape has a favorable effect on the

drivability and static resistance of piles. It is also found that the drivability of FRP–

SCC composite piles is similar to that of conventional pre-stressed concrete and steel

piles. However, empty FRP tubes required a much higher driving energy. Their low

flexural resistance along with risk of buckling can hinder their drivability in different

soil conditions.

In 2009 Gefu Ji performed a study on debonding between concrete and FRP

shells.Ji's study was in fact a continuation on Advanced Grid Stiffened (AGS) FRP.

The AGS-FRP tube was made of a lattice of interlaced FRP ribs that was wrapped

with a thin layer of FRP skin. The AGS-FRP tube was then filled with concrete. Test

results show a considerably increased compressive strength, elastic range, and

positive composite action due to the enhanced interfacial bonding strength through

mechanical interlocking.

In 2010 Guades conducted a study on the application of FRP composite in piling

systems. The study compared the common FRP composite pile systems. Guades

emphasized the necessity for more field tests to carefully assess and verify the

geotechnical performance of the composite piles to be used in developing reliable

design procedures.

In the same year Sadeghian developed a model for a moment connection between

circular concrete-filled FRP tubular CFFT members and RC footings. The connection

was based on the simple approach of direct embedment of the CFFT member into the

footing for a certain depth, and hence do not require the use of dowel bars or any

mechanical devices. The CFFT member was subjected to lateral or lateral and axial

loads at its free end. The model was capable of predicting the critical embedment

length of the CFFT member, which is the minimum length required to achieve material failure of the CFFT outside the footing, and bond failure inside the footing, simultaneously. If the actual embedment length was less than predicted, bond failure occurred prematurely at a lower capacity and the model could also predict the reduced strength. If the embedment was larger than the predicted critical embedment length, bond failure was avoided.

In 2012 Guades studied the driving performance of the FRP piles. Relative low stiffness of the FRP piles was evaluated in the study. It was concluded that the type of driving hammers used, resistance offered by the soil, the pile impedance, and the impact strength of the pile materials are the main factors that effect the driving performance of composite FRP piles.

In the same year Bozorg-Haddad and Iskander compared compressive creep of Reinforced Polymeric Piling (RPP) made of High Density Polyethylene (HDPE) and RPP reinforced with steel or fiber reinforced polymer rods (FRP, E-glass, or Fiberglass). The study showed that FRP has 0.5% (approximately half of HDPE) 100-year creep while loaded at an ultimate stress of 88 MPa (approximately ten times higher than HDPE).

In the same year Inkander performed a state of the art review on sustainable piling made of recycled polymers. He summarized the current state of the art in polymeric piling practice, including (1) the mechanical properties of piling made of recycled polymers; (2) the durability of recycled polymers in aggressive soils; (3) the compressive creep of recycled HDPE and FRP; (4) drivability; (5) design

considerations such as skin friction, end bearing, and buckling; and (6) load testing of polymeric piles.

In the same year Mohamed et al. evaluated concrete columns reinforced longitudinally with FRP bars and confined with FRP hoops and spirals under axial load. Fourteen full-scale circular RC columns were tested under concentric axial load. The columns were reinforced with longitudinal FRP bars and confined with circular FRP spirals or hoops. The test parameters included configuration of the confinement reinforcement (spirals versus hoops), hoop lap length, volumetric ratio, and FRP reinforcement type (glass versus carbon). The test results indicated that the GFRP and CFRP RC columns behaved similarly to columns reinforced with steel.

In 2014 Chyuan-Hwan et al conducted a study on reinforced concrete (RC) piles covered with FRP jacket. In order to compare the results seven reduced scale RC pile specimen were build and tested and the results were compared to the finite element analysis outputs.

As mentioned, FRP piles are a relatively new area of study. Unlike other materials used in construction which have been known to mankind for centuries, the FRP technology is in its early ages. On the other hand, advanced methods of study such as computer modeling and laboratory tests facilitate the understanding of FRP technology in a much faster pace.

The studies mentioned above focused on several topics. Nearly all studies indicate that:

1-   The FRP piles are suitable material to eliminate the corrosion issue.

2-   Most studies indicate that there is not enough and sometimes no reliable data about FRP piles.

FRP composites were used in aerospace and defense application before being used in piles and bridges. The first studies in FRP piles were conducted to study the repair and rehabilitation of marine structure piles that were corroded.

5.3. *Classification of Composite Piles Based on Shape and Appearance*

The application of composite piles was first recorded in the United States (US) when they were used in April 1987 at Berth 120 in the port of Los Angeles (Iskander & Hassan, 1998). These piles were composed of steel pipe core encased by recycled plastic shell and used for fendering applications.
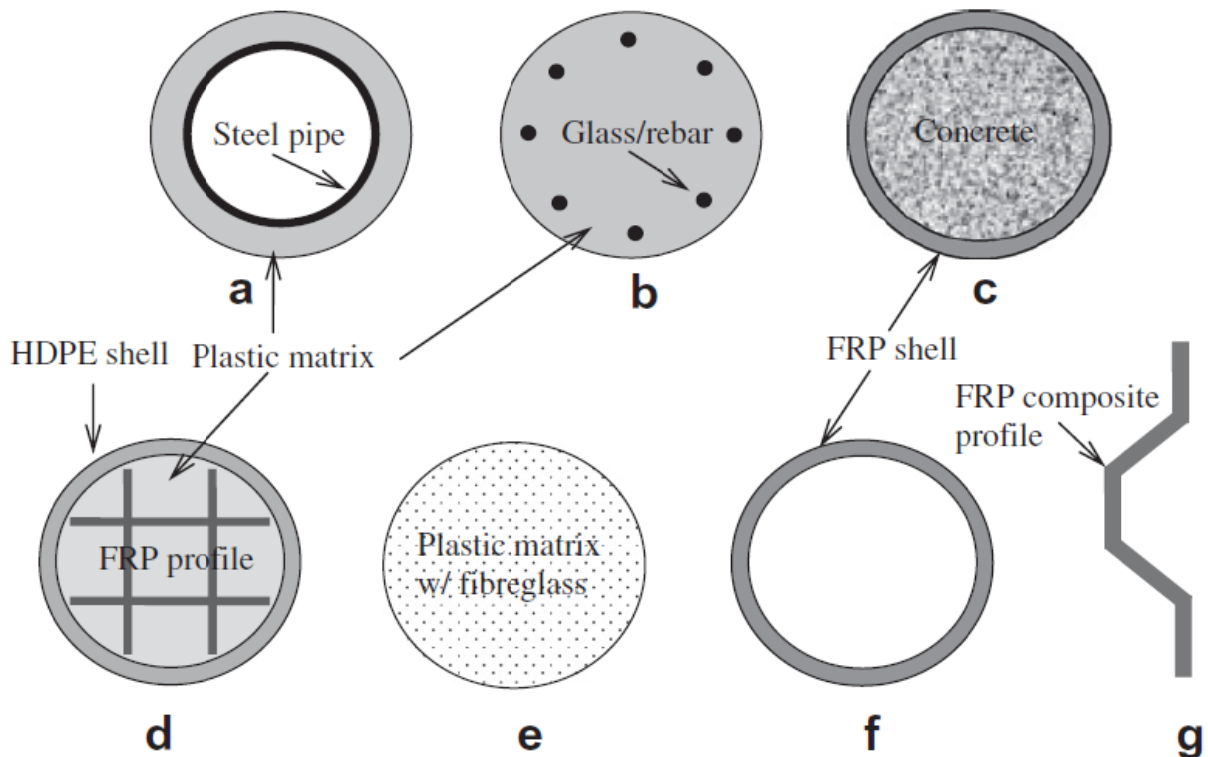
Figure 6 - Cross section view of the types of composite piles.

(a) Steel pipe core piles, (b) SRP piles, (c) Concrete-filled FRP piles, (d) Fiberglass pultruded piles, (e) Fiberglass reinforced plastic piles, (f) Hollow FRP piles and (g) FRP sheet piles. (Ernesto Guades, 2012)

To date, there are seven types of composite piles. These include: piles with steel pipe core, structurally reinforced plastic piles, concrete-filled FRP, fiberglass pultruded piles, fiberglass reinforced plastic piles, hollow FRP piles, and FRP sheet piles.

32

Figure 6 shows a schematic view of each type. The description and applications of each type of composite piles are presented in the following subsections.

5.3.1. Steel Pipe Core Piles

Steel pipe core piles consist of two layers: an inner steel layer and a thick outer plastic shell (Figure 6a). The inner layer provides the structural strength while the outer shell is used to protect the steel from corrosion. This type of pile is available in 8 to 24 in (200 to 600 mm) outer diameter and up to 75ft (23 m) long. The structural pipe cores range from 4 to 15 in (100 to 400 mm) outer diameter, with wall thicknesses between 0.25 and 1.5 in (6 and 40 mm). Early applications of this product suffered from delamination of the steel core from the plastic shell due to the difference in thermal stresses (Iskander & Hassan, State of Practice Review in FRP Composite Piling, 1998). These piles were observed to have cracks at the plastic shell surface a year after they were installed. The most common use of this type of pile is in fendering applications in regions with marine influence and change of the tide. However, steel pipe core piles are also considered potentially suitable for load-bearing applications. According to Pando et al., the design procedure of this type of composite pile would be essentially the same as for the traditional steel pipe pile if the plastic shell is used only in the upper portion of the pile that is exposed to corrosion.

5.3.2. Structurally Reinforced Plastic Piles

Structurally reinforced plastic (SRP) piles are composed of an extruded recycled plastic matrix reinforced with fiberglass rods or steel rebar (Figure 6b). The recycled materials are usually from waste plastic such as plastic milk jugs, soap bottles and

juice containers. SRP piles are produced using a continuous extrusion process which allows manufacturing of up to 32 m. The piles are available in diameters between 254 and 430 mm and are reinforced with 6 to 16 pieces of FRP or steel reinforcing rods of diameters ranging from 25 to 35 mm. SRP piles are mainly used in fendering applications and are regarded as potential load-bearing piles. Problems associated with these piles include the possibility of debonding of the reinforcing FRP rods and high creep rate related with the high polymeric content. This type of piles exhibits larger deflections under axial and lateral load (Miguel A. Pando, 2006) and causes problems during installation and handling due to their excessive deformation (Iskander & Hassan, State of Practice Review in FRP Composite Piling, 1998). One version of this pile is structurally reinforced by a steel cage with the bars welded to a continuous steel spiral.

5.3.3. Concrete-Filled FRP Piles

Concrete-filled FRP piles are comprised of an outer FRP shell with unreinforced concrete infill (Figure 6c). The FRP shell provides a stay-in-place structural formwork for the concrete infill, acts as non-corrosive reinforcement, gives confinement to concrete in compression, and protects the concrete from severe environmental effects (Mirmiran & Shahawy, A new concrete-filled hollow FRP composite column, 1996). On the other hand, the concrete infill offers the internal resistance in the compression zone and increases the stiffness of the member and prevents local buckling of the FRP tube.

This structural system is found to perform better than the equivalent prestressed and reinforced concrete structural members under combined axial and flexural loads.

Typically, concrete-filled FRP piles are available in diameters ranging from 203 to 610 mm, with wall thicknesses ranging between 4.6 and 9.1 mm. These piles are suitable for both fendering and load-bearing applications. An impending concern in using these piles is the interface bonding and delamination problem between FRP shell and concrete core. Recently, techniques and fabrication processes were developed to minimize the occurrence of delamination. These include the roughening of inside shell surface by applying a thin layer of epoxy sprayed with coarse silica and the application of bonding agents. Concrete-filled FRP piles were lately adopted in bridge rehabilitation projects in Virginia, USA (Ernesto Guades, 2012).

5.3.4. Fiberglass Pultruded Piles

Fiberglass pultruded piles are composed of an outer fiberglass sheet fitted with a fiberglass grid to provide structural strength (Figure 6d). The grid consists of two sets of orthogonal plates joined at four intersecting points and forming a tic-tac-toe pattern. The grid inserts are sometimes filled with high-density polyethylene (HDPE), plastic lumber, or polyethylene foam fills. The HDPE shell and fiberglass inserts are used to absorb the impact of horizontal load. These piles were used as fender piles in 1996 in a demonstration project at Berth 7 in Port Newark, New Jersey and in the Tiffany Pier Project. However, this type of composite pile was found to be unsuitable for load-bearing applications (Ernesto Guades, 2012).

5.3.5. Fiberglass Reinforced Plastic Piles

Fiberglass reinforced plastic piles consist of a recycled plastic matrix with randomly distributed fiberglass reinforcement (Figure 6e). The dense solid outer shell is bonded to the peripheral surface of the inner plastic core which is foam-filled to reduce weight. Trimax is the manufacturer of these composite piles and produces a variety of structural members that conform to lumber industry standards. These piles are available in 250 mm diameter with a standard length of 7.5 m. These composite piles were used in the construction of the Tiffany Street Pier in New York City as fender piles. The suitability of using these piles in load-bearing applications has not been studied since they did not undergo testing for bearing piles.

5.3.6. Hollow FRP Piles

Hollow FRP piles are an outer shell component of a concrete filled FRP composite system (Figure 6f). These piles typically consist of a thermosetting matrix reinforced with glass fibers forming a tubular section made either by filament winding, pultrusion, or resin transfer molding process. Some versions of these piles are coated with acrylic to protect against abrasion, UV and chemical attacks. The diameter and wall thickness of these piles can be varied up to 460 mm and 22 mm, respectively. Hollow FRP piles are considered potentially suitable in load-bearing applications.

5.3.7.   FRP Sheet Piles

FRP sheet piles are typically made of FRP pultruded sections with a corrugated-shape profile (Figure 6g). The single unit corrugated profile is composed of a symmetric double Z cross section. The available products on the market have section depths of 100–350 mm, widths from 400 to 460 mm, and wall thicknesses from 4 to 12 mm. FRP sheet piles are found to be increasingly used as waterfront retaining structures for both new installations and rehabilitations. The problem associated with using FRP sheet piles includes possible damage at their corners caused by ice impact and rubbing if installed in cold regions. Additionally, the asymmetrical shapes typically seen for FRP sheet piles make the testing of these materials more difficult than for many other commonly produced structural shapes. Earlier study on composite sheet piles includes recycled HDPE in tongue-and-groove profile reinforced with chopped glass fibers as potential material. As opposed to the other type of composite piles which carry vertical axial load, FRP sheet piles in general are used for a wall that resists horizontal loads. Similarly, the reported application of this type of pile is limited to seepage reduction, waterfront bulkhead or retaining walls, and protection from waves or storm water floods and not for load-bearing application.

5.4. *Classification of Composites Based on Reinforcement*

5.4.1. *Reinforcement Type*

Composite materials can be classified by the type of reinforcements used for the matrix material.

1. Particle Reinforced Composites

   Particle reinforced composites consist of particles of one material dispersed in a matrix of a second material. Particles may have any shape or size, but are generally spherical, ellipsoidal, polyhedral, or irregular in shape.
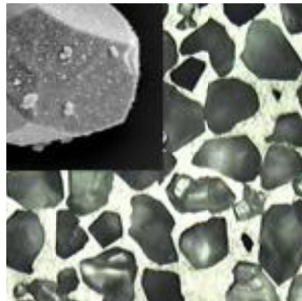
Figure 7 - Ceramic – Aluminum (Lissenden 2015)

2. Fiber Reinforced Composites

   Fiber reinforced composites (FRC) are composites where one material component (fiber) is used as a reinforcing material for the matrix.
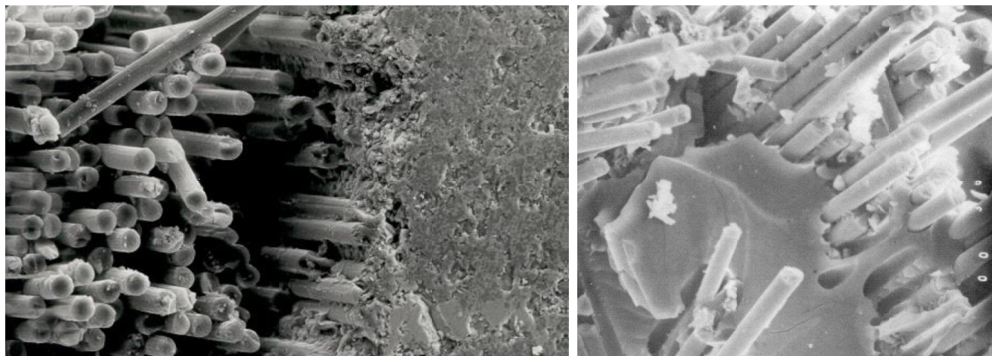
Figure 8 – Carbon Fiber Epoxy (left), Glass Fiber Epoxy (right) (Ultramet 2015)

The Fiber Reinforced Composites can also be divided to two groups:

2.1. Short Fiber Reinforced

2.2. Long Fiber Reinforced
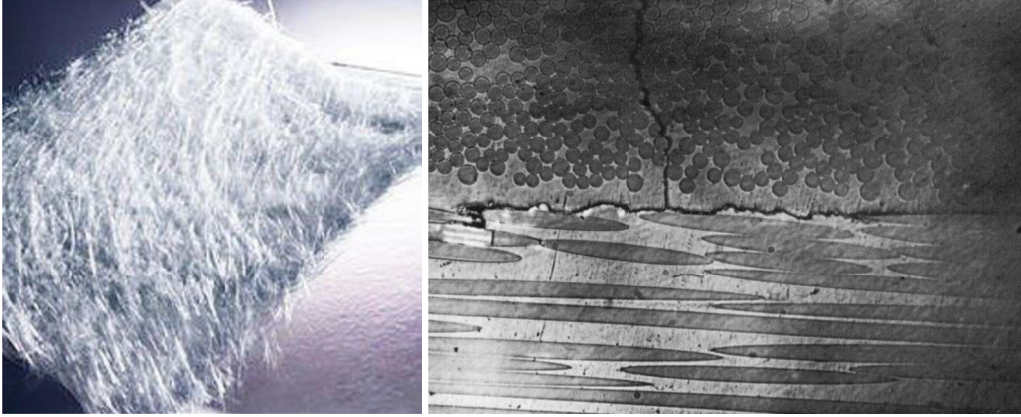
Figure 9 – Short Fiber Reinforced (left), Long Fiber Reinforced (right) (Ultramet 2015)

5.4.2.   *Direction of Reinforcement*

Depending on the direction the composite materials can be divided to random and

oriented reinforcement
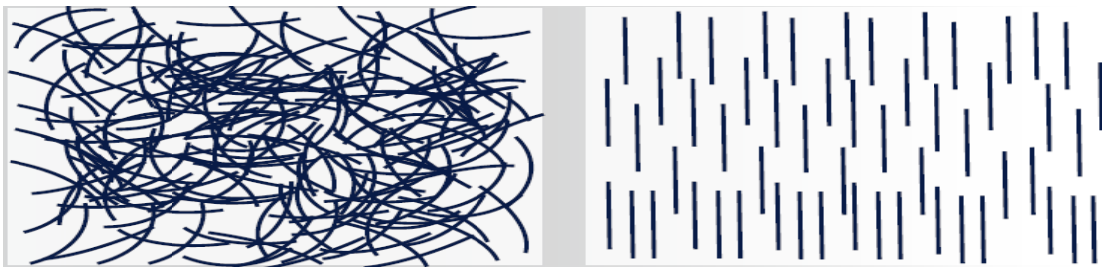
Figure 10 - Random and oriented short fiber reinforced composites (ANSYS Inc. 2016)

Figure 11 - Random and oriented long fiber reinforced composites (ANSYS Inc. 2016)

5.4.3. Reinforcement Forms

There are several reinforcement forms to make the composite materials. Figure 12 shows the most common types.

Unidirectional	Woven	Mat
Knits	Stitched	Braiding
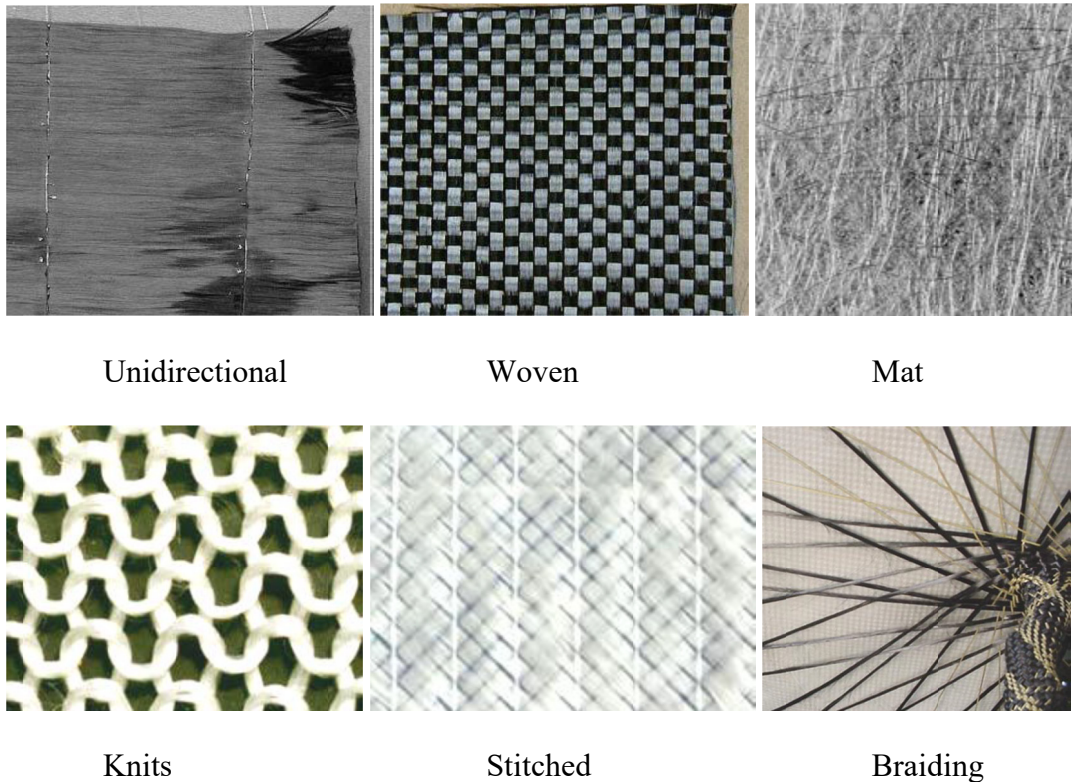
Figure 12 – Common types of reinforcements (ANSYS Inc. 2016)

5.5. Manufacturing Methods of FRP Piles

Fiberglass reinforced polymer (FRP) is most often referred to simply as "fiberglass" in practice (as in fiberglass tanks, fiberglass grating, fiberglass structural shapes, fiberglass boats, etc.). Used in this context, "fiberglass" is a composite consisting of a polymer resin matrix reinforced by embedded glass fibers. The strength of a fiberglass part is determined primarily by the type, orientation, quantity, and location of the glass fibers within the part. The resin binds the reinforcing glass together and

this resin/glass bond aids in developing stiffness in the part. The type of resin used determines corrosion resistance, flame resistance, and maximum operating temperature as well as contributing significantly to certain strength characteristics including resistance to impact and fatigue.

The following sections describe the development and manufacturing process of Fiber Reinforced Plastic Piles.

5.5.1. Pultrusion

Pultrusion is a manufacturing process for producing continuous lengths of FRP structural shapes. Raw materials include a liquid resin mixture (containing resin, fillers and specialized additives) and reinforcing fibers. The process involves pulling these raw materials (rather than pushing as is the case in extrusion) through a heated steel forming die using a continuous pulling device.

The reinforcement materials are in continuous forms such as rolls of fiberglass mat or doffs of fiberglass roving. As the reinforcements are saturated with the resin mixture ("wet-out") in the resin impregnator and pulled through the die, the gelation (or hardening) of the resin is initiated by the heat from the die and a rigid, cured profile is formed that corresponds to the shape of the die. While pultrusion machine design varies with part geometry, the basic pultrusion process concept is described in the following schematic.
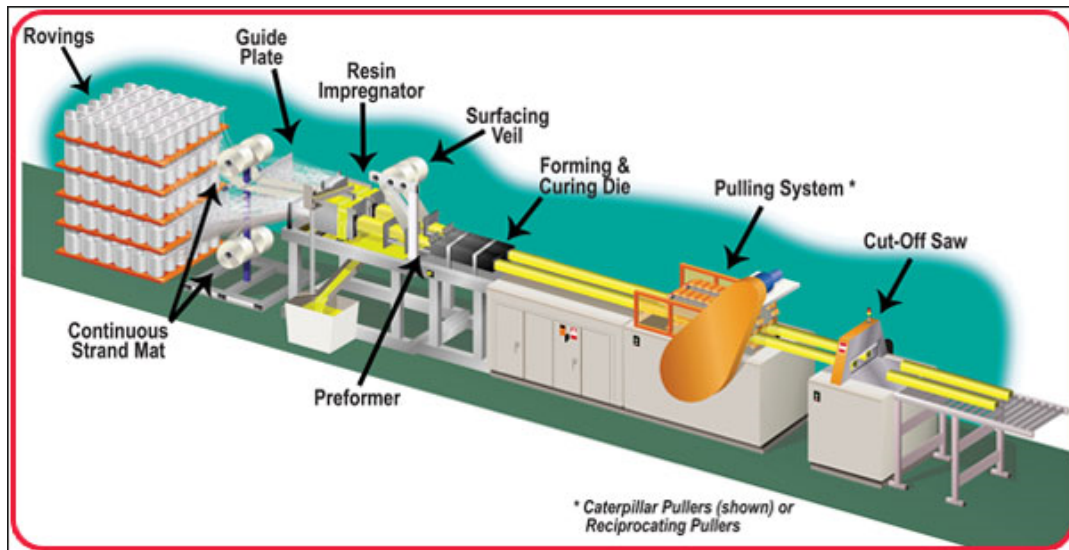
Figure 13 - Manufacturing FRP with Pultrusion method (Creative Pultrusion 2016)

The creels position the reinforcements for subsequent feeding into the guides. The reinforcement must be located properly within the composite and controlled by the reinforcement guides. The resin impregnator saturates (wets out) the reinforcement with a solution containing the resin, fillers, pigment, and catalyst plus any other

additives required. The interior of the resin impregnator is carefully designed to optimize the "wet-out" (complete saturation) of the reinforcements.

On exiting the resin impregnator, the reinforcements are organized and positioned for the eventual placement within the cross section form by the preformer. The preformer is an array of tooling which squeezes away excess resin as the product is moving forward and gently shapes the materials prior to entering the die. In the die the thermosetting reaction is heat activated (energy is primarily supplied electrically) and the composite is cured (hardened).

On exiting the die, the cured profile is pulled to saw for cutting to length. It is necessary to cool the hot part before it is gripped by pull block (made of durable urethane foam) to prevent cracking and /or deformation by the pull blocks. Two distinct pulling systems are used: a) Caterpillar counter-rotating type, b) hand-over-hand reciprocating type. In certain applications an RF (radio frequency wave generator) unit is used to preheat the composite before entering the die. When in use, the RF heater is positioned between the resin impregnator and the pre-former.

5.5.2. Hand Lay-up

This method involves building up layers of chopped glass or woven glass mat impregnated with catalyzed resin around a suitable mold. The reinforcement is then rolled for better wet-out and removing trapped air. This method does not appear to be practical for FRP piles.
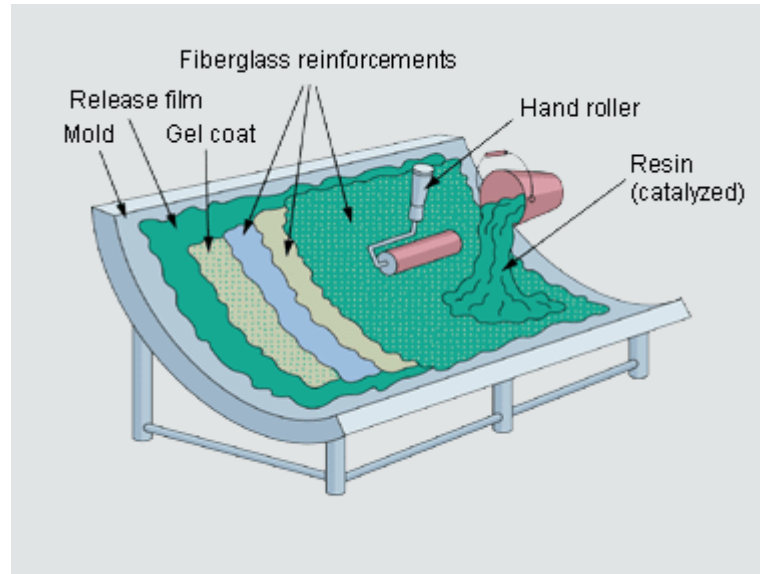
Figure 14 – Hand Lay-up method (Wacker 2015)

5.5.3. *Compression Molding*

This method is used for thermosets or thermoplastics. The process consists of placing a charge in the mold, which is subsequently closed and held at a high pressure, and then heating the mold to initiate cure reaction. Because of limitations in the size of the mold, this method of manufacturing does not appear to be practical for FRP piles which demand considerable length.

5.5.4.   *Resin Transfer Molding Process*

This method is similar to compression molding and appears not to be practical for FRP piles
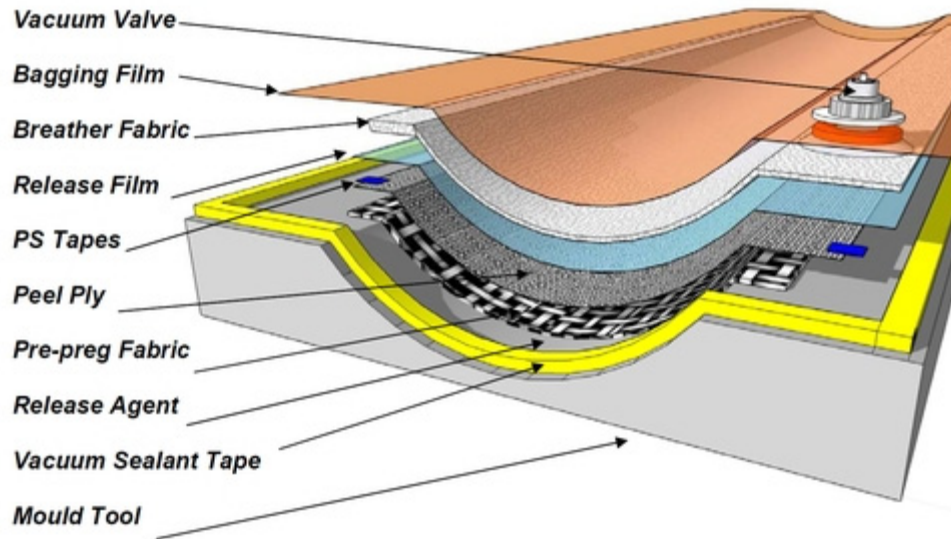
Figure 15 – Resin Transfer Molding Method (Aero Consultants AG 2015)

5.5.5.   *Injection Molding*

This method is for thermoplastic resins, commonly with short glass fibers as reinforcements. No chemical reaction occurs during the molding process.

5.5.6.   *Filament Winding*

Filament winding is a process where continuous fiber filaments called rovings, are saturated with catalyzed resin and helically wound around a mandrel. The fibers are fed through a device which moves up and down the length of rotating mandrel. The result is a high fiber-to-resin ratio (high strength-to-weight ratio) product. This method can produce circular or close to circular (e.g. octagonal) cross sections. In this

dissertation a new solution is proposed to make any elliptical shape using this method. As shown in Figure 5, the rotating mandrel can be modified for production of elliptical shapes.
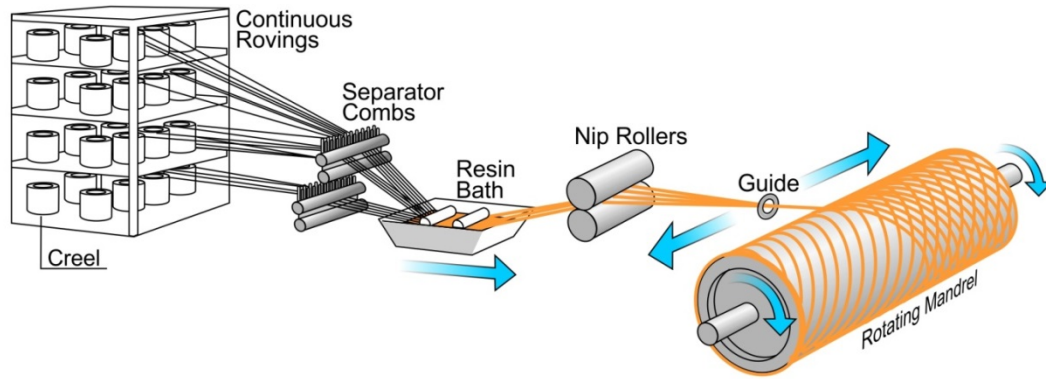
Figure 16 - Filament Winding (Nuplex 2015) (Direct Industry 2015)

5.6. *Types of Resins*

Three kinds of resin are used to make the FRP material: thermoplastic resins, thermoset resins and phenolic resins.

5.6.1. Thermoplastic Resins

Thermoplastic resins have a defined melting point after initial cooling, meaning they can be heated and reshaped and this shape is retained when re-cooled; however, thermoplastics can deform (creep) under loads, even at moderate temperature.

5.6.2. Thermoset Resins

Thermoset resins have no defined melting point, therefore cannot be heated and formed again. Once these resins have been processed with chemical cross-linking of the resin occurring, they take the shape of the die and harden upon cooling. When subjected to extreme heating, thermoset composites will degrade.

5.6.3. Phenolic Resins

Phenol formaldehyde resins are the oldest of all plastics, yet relatively new in composites / pultrusion. Phenolic composites are an option when superior fire resistance and minimum smoke emissions are required. Phenolic shapes can have "E-Glass" or carbon reinforcements; however, the higher reinforcement level makes carbon an expensive alternative. Transverse strength, pigmentation, and aesthetics are areas where phenolic profiles are not equal to standard shapes.

5.7. *Types of Fibers*

The fiber is an important constituent in composites. A great deal of research and development has been done with the fibers on the effects of the type, volume fraction, architecture, and orientation. The fiber generally occupies 30% - 70% of the matrix volume in the composites. The fibers can be chopped, woven, stitched, and/or braided. They are usually treated with sizings such as starch, gelatin, oil or wax to improve the bond as well as binders to improve the handling. The most common types of fibers used in advanced composites for structural applications are the glass fiber, aramid, carbon, boron, alumina, silicon carbide, quartz and ultrahigh molecular weight polyethylene. The fiberglass is the least expensive and carbon being the most expensive. The cost of aramid fibers is about the same as the lower grades of the carbon fiber. Other high-strength high-modulus fibers such as boron are at the present time considered to be economically prohibitive.

5.7.1.   *Glass Fibers*

Glass fiber is formed when thin strands of silica-based or other formulation glass are extruded into many fibers with small diameters suitable for textile processing. The technique of heating and drawing glass into fine fibers has been known for millennia; however, the use of these fibers for textile applications is more recent. Until this time, all glass fiber had been manufactured as staple (that is, clusters of short lengths of fiber). The first commercial production of glass fiber was in 1936. In 1938 Owens-Illinois Glass Company and Corning Glass Works joined to form the Owens-Corning

Fiberglas Corporation. When the two companies joined to produce and promote glass fiber, they introduced continuous filament glass fibers.

The glass fibers are divided into three classes -- E-glass, S-glass and C-glass. The E-glass is designated for electrical use and the S-glass for high strength. The C-glass is for high corrosion resistance, and it is uncommon for civil engineering application. Of the three fibers, the E-glass is the most common reinforcement material used in civil structures. It is produced from lime-alumina-borosilicate which can be easily obtained from an abundance of raw materials like sand. The fibers are drawn into very fine filaments with diameters ranging from 2 to 13 x10^{-6} m. The glass fiber strength and modulus can degrade with increasing temperature. Although the glass material creeps under a sustained load, it can be designed to perform satisfactorily. The fiber itself is regarded as an isotropic material and has a lower thermal expansion coefficient than that of steel. (Tang, 1997)

Table 1 - Typical cured epoxy/glass mechanical properties (Composite Material Handbook (DOD) 2013)

E Glass, Woven 7781 Style	Standard Structural	Dual Purpose Structural/Adhesive
Tensile Strength, ksi (MPa)	63 (430)	48 (330)
Tensile Modulus, Msi (GPa)	3.8 (36)	2.8 (19)
Compressive Strength, ksi (MPa)	60. (410)	50. (340)
Compressive Modulus, Msi (GPa)	3.6 (25)	3.2 (22)
Flexural Strength ksi, (MPa)	80. (550)	65 (450)
Flexural Modulus Msi, (GPa)	3.7 (26)	3.3 (23)
Interlaminar Shear ksi, (MPa)	2.6 (18)	3.8 (26)
Sandwich Peel, lb/in width (N/m width)	N.A.	30. (3.4)
Metal-to-Metal Peel, lb/lin. in. (N/lin. m)	N.A.	55 (6.3)
Specific Gravity gm/cm3 (lb/in3)	1.8 (0.065)	1.6 (0.058)
Cured Resin Content % Wt.	33	48

Table 2 - Typical properties of glass fibers (Composite Material Handbook (DOD) 2013)

		E	S-2	HR
Density	lb/in3	0.094	0.089	0.090
	gr/cm3	2.59	2.46	2.49
Tensile Strength	ksi	500	665	665
	MPa	34,450	45,818	45,818
Modulus of Elasticity	Msi	10.5	12.6	12.6
	GPa	72.35	86.81	86.81
% Ult. Elongation		4.8	5.4	5.4
Dielectric Constant at		6.3-6.7	4.9-5.3	NA

Table 3 - Chemical compositions of Glass Fibers

	%(wt)	E-Glass	S-2 Glass (Nominal)	HR Glass (B)
Silicon Dioxide (SiO2)		52-56 (A)	65	63.5 -65.0
Aluminum Oxide (Al2O3)		12-16 (A)	25	24.0 -25.5
Boron Oxide (B2O3)		5-10 (A)		
Calcium Oxide (CaO)		16-25 (A)		<0.5
Magnesium Oxide (MgO)		0-5 (A)	10	9.5 - 10.5
Lithium Oxide (Li2O)				
Potassium Oxide (K2O)	O.C.	0.0-0.2		
Sodium Oxide (Na2O)	O.C.	0-2		
Titanium Oxide (TiO2)	O.C.	0-1.5		
Cerium Oxide (CeO2)				
Zirconium Oxide (Zr2O2)				
Beryllium Oxide (BeO)				
Iron Oxide (Fe2O3)	O.C.	0.0-0.8		
Fluorine (F2)	O.C.	0.0-0.1		
Sulfate (SO2)				
Alkaline Oxides	PPG	0.5-1.5		
Calcium Fluoride (CAF)	PPG	0.0-0.8		
Finishes/Binders		0.5/3.0		

Table 4 - Typical corrosion resistance of glass fibers wt. loss % (Conditions: 200°F (96°C) - one week immersion) (Composite Material Handbook (DOD) 2013)

Fluid	E	S-2	SR
10% H2SO4	42	6.8	NA
10% HCL	43	4.4	NA
10% HNO3	43	3.8	NA
H2O (Distilled)	0.7	0.7	NA
10% Na OH	29	66	NA
10% KOH	23	66	NA

Table 5 - Basic strand fiber designations and strand counts (Composite Material Handbook (DOD) 2013)

Filament Diameter Designation		Strand Count (Number)		
SI	U.S. Customary	TEX	U.S. Customary	
(µm)	(Letter)	g/km	100 Yd. Cuts/Lb.	Yds./Lb.
5	D	11	450	45,000
7	E	22	225	22,500
9	G	733	150	15,000
10	H	45	110	11,000
13	K	66	75	7,500

Figure 17 - Glass fiber used in pultrusion and filament winding (Synthane Taylor 2015)

5.7.2. Advantages and Disadvantages

For many years glass composites have had a distinct strength-to-weight advantage. Although the rapid evolution of carbon and Aramid fibers have gained advantages, glass composite products have still prevailed in certain applications. Cost per weight or volume, certain armament applications, chemical or galvanic corrosion resistance, electrical properties, and availability of many product forms remain as examples of advantage. Coefficient of thermal expansion and modulus properties compared to

carbon composites may be considered as typical disadvantages. When compared to Aramid composites, glass has a disadvantage as to tensile properties but an advantage as to ultimate compression, shear properties, and moisture pick-up.

Commercial uses for glass products are many-fold. These include filtration devices, thermal and electrical insulation, pressure and fluid vessels, and structural products for automotive and recreation vehicles.

Because of the many product forms, structural applications are limitless to fabricate. If there are limitations, compared to other fibers, they may include low thermal and electrical conductivity or perhaps melting temperatures when compared to carbon fibers. (Composite Material Handbook (DOD) 2013)

5.7.3. Aramid Fibers

These are synthetic organic fibers consisting of aromatic polyamides. The Aramid fibers have excellent fatigue and creep resistance. Although there are several commercial grades of Aramid fibers available, the two most common ones used in structural applications are Kevlar® 29 and Kevlar® 49. The Young's Modulus curve for Kevlar® 29 is linear to a value of 83 GPa but then becomes slightly concave upward to a value of 100 GPa at rupture; whereas, for Kevlar® 49 the curve is linear to a value of 124 GPa at rupture (see **Error! Reference source not found.**). As an anisotropic material, its transverse and shear modulus are an order of magnitude less than those in the longitudinal direction. The fibers can have difficulty achieving a chemical or mechanical bond with the resin.

Table 6 – Typical properties of Aramid fibers (Tang 1997)

Typical Properties	Kevlar 29	Kevlar 49
Density (g/cm3)	1.44	1.44
Young's Modulus (GPa)	83/100	124
Tensile Strength (GPa)	2.27	2.27
Tensile Elongation (%)	2.8	1.8

Figure 18 – Aramid fibers used in FRP (Dupont 2015)

5.7.4.   Carbon Fibers (Graphite)

Carbon fibers are selected to achieve a high modulus (stiffer) composite. The carbon also makes the part electrically conductive. Carbon fiber reinforcements are 10 to 100 times as expensive as standard glass reinforcements depending on the grade used. The graphite or carbon fiber is made from three types of polymer precursors -- polyacrylonitrile (PAN) fiber, rayon fiber, and pitch. The tensile stress-strain curve is linear to the point of rupture. Although there are many carbon fibers available on the open market, they can be arbitrarily divided into three grades as shown.

They have lower thermal expansion coefficients than both the glass and Aramid fibers. The carbon fiber is an anisotropic material, and its transverse modulus is an order of magnitude less than its longitudinal modulus. The material has a very high fatigue and creep resistance. (Tang, 1997)

Table 7 – Typical properties of Carbon Fibers (Tang 1997)

Typical Properties	High Strength	High Modulus	Ultra-High Modulus
Density (g/cm³)	1.8	1.9	2.0 - 2.1
Young's Modulus (GPa)	230	370	520 - 620
Tensile Strength (GPa)	2.48	1.79	1.03 - 1.31
Tensile Elongation (%)	1.1	0.5	0.2

Since its tensile strength decreases with increasing modulus, its strain at rupture will also be much lower. Because of the material brittleness at higher modulus, it becomes critical in joint and connection details, which can have high stress concentrations. As a result of this phenomenon, carbon composite laminates are more effective with adhesive bonding that eliminates mechanical fasteners.
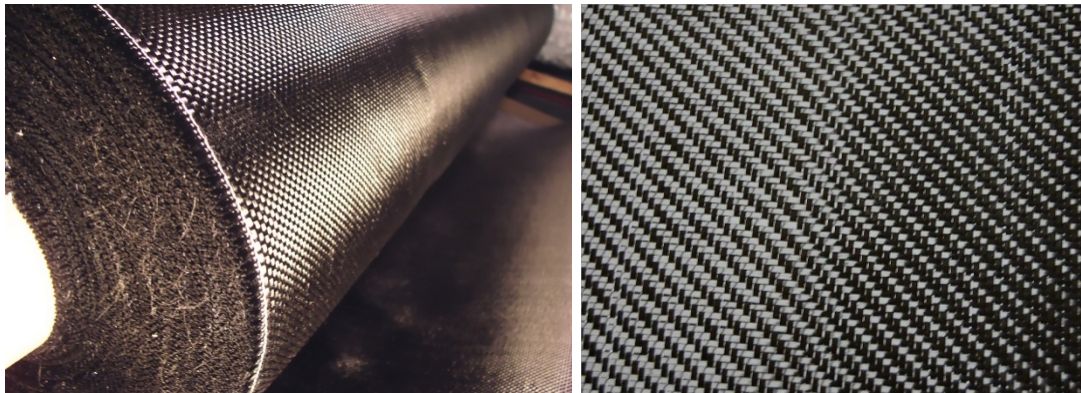
Figure 19 - Carbon fiber (Tap Plastics 2015)

6. *Structural Behavior*

Since the concrete filed FRP piles are the most common form of FRP piles, in this chapter the structural behavior of the FRP piles are studied.

6.1. *Short Term Behavior of FRP Piles*

The short-term axial and flexural structural behavior of concrete-filled FRP tubes has been studied by several researchers. A brief description is provided herein.

The FRP tube of a composite pile contributes structurally to the pile by primarily providing confinement to the concrete core. The beneficial effect of confinement on the total load carrying capacity of a short concrete-filled FRP tubular element (length-diameter ratio of 2) was studied by Fam and Rizkalla (Fam & Rizkalla, 2001), and is illustrated in Figure 20. The figure shows how the capacity of the composite stub significantly exceeds the load sharing capacity of the two individual materials. The load-strain curve starts to depart from the unconfined concrete curve in the vicinity of the unconfined concrete strength. As this stress level is approached the concrete core starts to experience significant micro-cracking as well as increased lateral expansion. In response to the lateral expansion of the concrete, the FRP shell applies a radial confining pressure, which continuously increases due to its linear elastic properties. The second slope of the load-strain curve is a function of the hoop tensile stiffness of the FRP shell, and the ultimate peak strength is governed by the hoop tensile strength of the FRP shell.
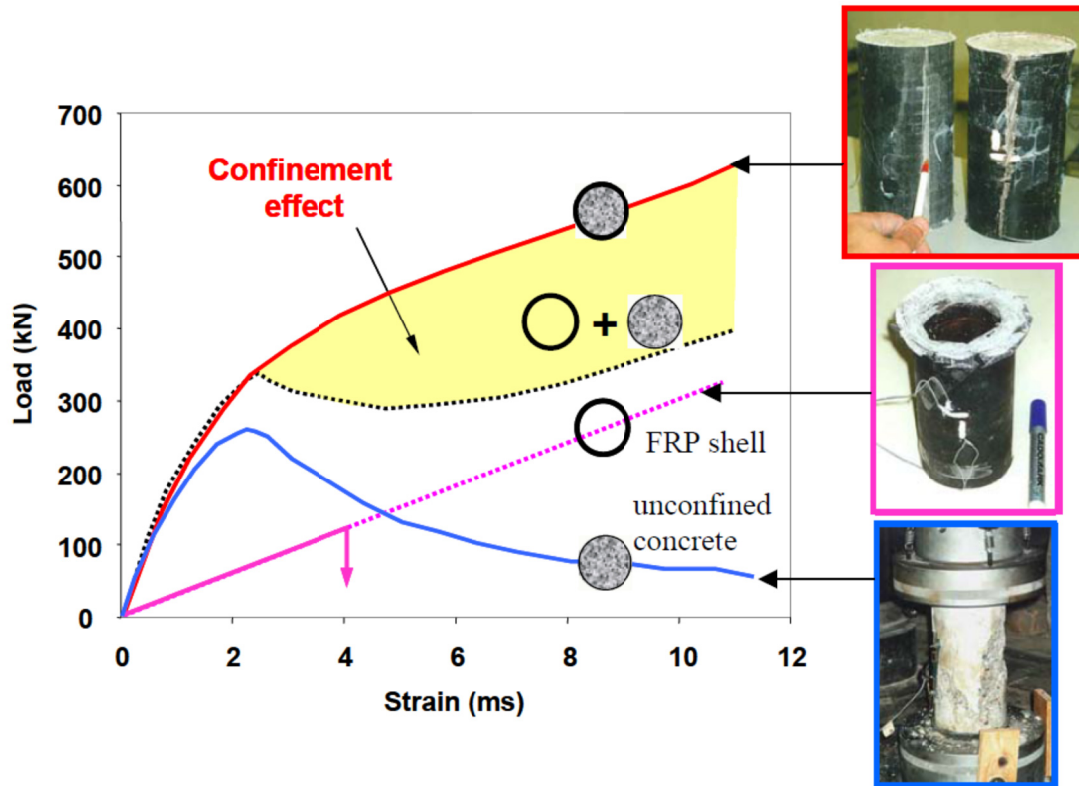
Figure 20 – Confinement effect in axially loaded FRP pile (Fam and Rizkalla 2001)

The short-term axial capacity of concrete-filled FRP tubes can be predicted using a confinement model such as the one proposed by Fam and Rizkalla (Fam & Rizkalla, 2001). This model is an incremental variable confinement model, which is based on equilibrium and radial displacement compatibility between the concrete core and the FRP tube and the constant confinement model.

The radial confinement pressure applied by the FRP shell can be obtained from equilibrium and by imposing radial displacement compatibility between the concrete core and the FRP shell. The load-strain response, predicted using the above model, and the experimental load-strain behavior for Test Stub No. 1 (from the Fam and

Rizkalla study) are shown. The figure shows good agreement between the model and the experimental results.
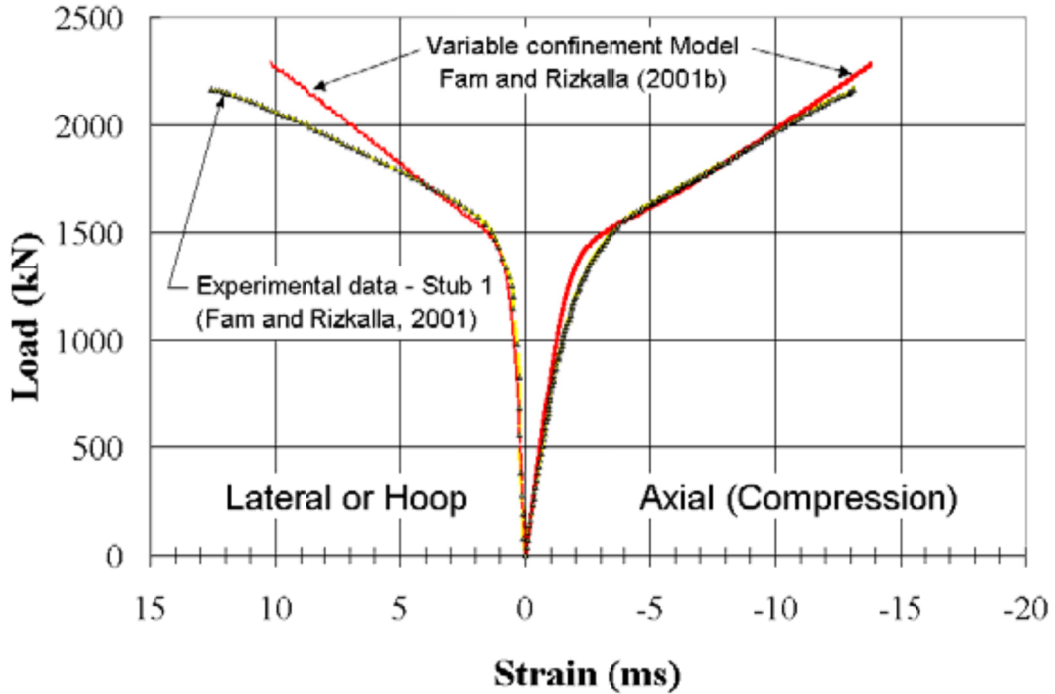
Figure 21 - Experimental versus predicted axial load-strain curves using the Fam and Rizkalla model (Fam and Rizkalla 2001)

6.2. *Damage Growth Under Cyclic Loading*

Just after compression strength reduction due to low velocity impact was recognized in the late 1970's, many composite research teams then took up investigating the fatigue behavior of impacted CFRP specimens. Among all available results, those shown in this section are drawn from a French-German collaborative program (Reference 7.7.1(a)) involving CEAT, Aerospatiale, DASA Munich and the WIM (in Erding).

In this program, specimens representative of real world stacking sequences were impacted with various energy levels but not higher than those corresponding to the creation of visible impact damages.

Usually impact damages that are to be assumed for fatigue (safe-life) investigations are those not sufficiently visible for being readily detectable. Those more severe, easily detectable, should not have to prove their capability to sustain a large number of fatigue cycles in service. These specimens were then tested in compression-compression fatigue (R = 10) in order to:

    i)   Plot Wöhler curves for several energy levels,

    ii) Monitor damage growth and residual static strength versus time.

Wöhler curves for the IM7/977-2 and the T800H/F-655-2 material references are reported in Figure 22 for various energy levels. The ratio between the endurance limit at 10^6 cycles and the initial static strength turned out to be between 0.50 and 0.75. This means that sizing a structure (with these materials) using ultimate loads should push fatigue loads down to a level likely to limit fatigue problems with low energy impact damages.

Figure 23 illustrates damage growth, measured by C-SCAN, versus fatigue cycles for the T800H/F655-2 material. Unrealistic fatigue stresses (above 75% of the static strength) were needed to allow such measurement. This illustration shows that, despite the log axis, damage growth starts very close to the end of the specimen lifetime (between 85% and 95% for all cases investigated in this program), with a very high slope.

From these results it is apparent that, as far as low velocity impact damages are concerned, assuming the possibility of a stable (or slow) growth approach for certification purposes may not be possible. This conclusion is also supported by other laboratory results such as, for example, those presented in "Damage Propagation in Composite Structural Element-Coupon Experiment and Analyses" (Ireman T. 1996) where very high slopes have also been shown for da/dN versus ΔG curves. These data were obtained on Double Cantilever Beam specimens made of two composite materials – the IM7/8552 and the HTA/6376 - and are representative of a mode I delamination growth phenomenon.
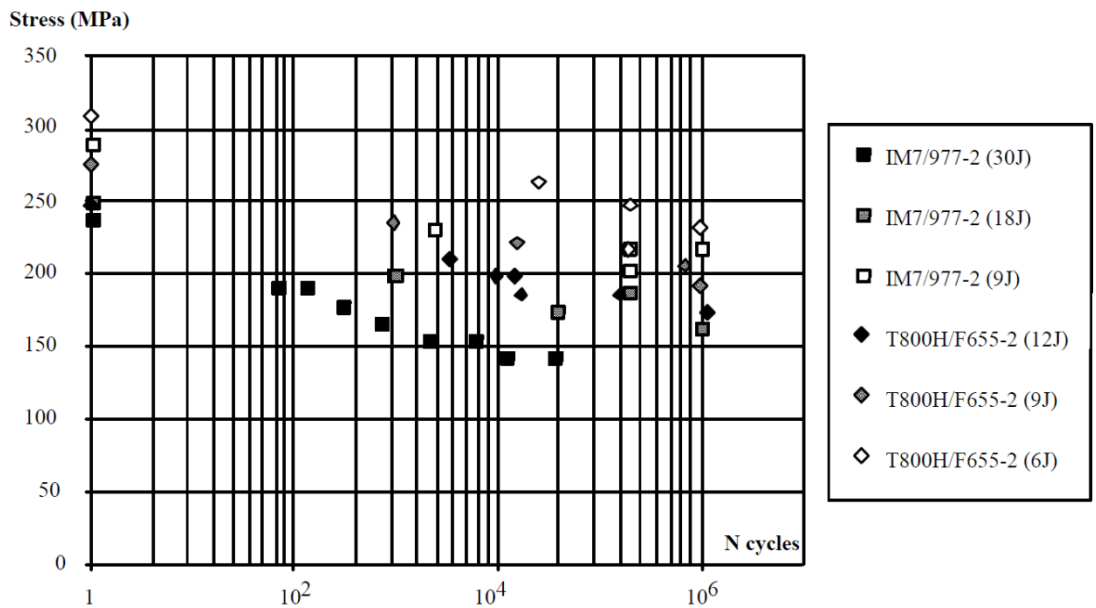
Figure 22 - Failure stress versus cycles for impact damaged laminates. (Composite Material Handbook (DOD) 2013)
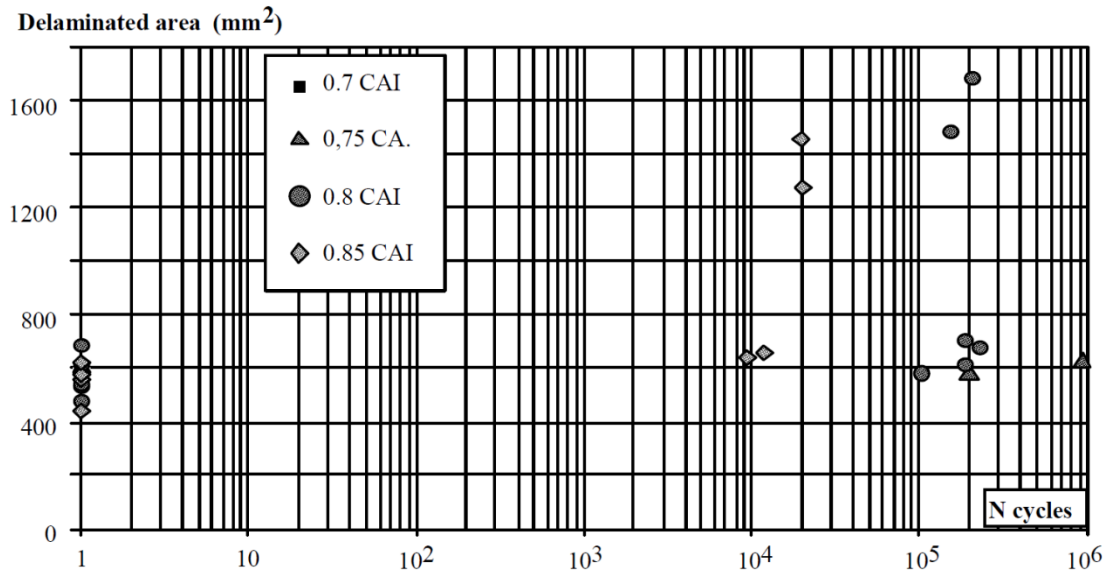
Figure 23 - Post-impact delamination size versus load cycles (Composite Material Handbook (DOD) 2013)

Since Integral Abutment Bridges are not subjected to high numbers of loading cycles and the maximum stresses are due to temperature changes, the FRP piles could be used under bridges.

7. Design Properties

7.1. Introduction

The purpose of this chapter is to provide an overview of techniques for analysis in the design of composite materials. Starting with the micromechanics of fiber and matrix in a lamina, analyses through simple geometric constructions in laminates are considered.

7.2. Basic Lamina Properties and Micromechanics

The strength of any given laminate under a prescribed set of loads is probably best determined by conducting a physical test. However, when many candidate laminates and different loading conditions are being considered, as in a preliminary design study, analysis methods for estimation of laminate strength become desirable. Because the stress distribution throughout the fiber and matrix regions of all the plies of a laminate is quite complex, precise analysis methods are not available. However, reasonable methods do exist which can be used to guide the preliminary design process.

Strength analysis methods may be grouped into different classes, depending upon the degree of detail of the stresses utilized. The following classes are of practical interest:

7.2.1. Laminate Level

Average values of the stress components in a laminate coordinate system are utilized. Laminate level stresses can be useful for translating measured strengths under single stress component tests into anticipated strength estimates for combined stress cases.

However this procedure does not help in the evaluation of alternate laminates for which test data do not exist.

7.2.2. Ply or Lamina Level

For this type of analysis, average values of the stress components within each ply are utilized. Ply level stresses are the commonly used approach to laminate strength. The average stresses in a given ply are used to calculate first ply failure and then subsequent ply failure leading to laminate failure.

7.2.3. Constituent Level

In this method, average values of the stress components within each phase (fiber or matrix) of each ply are utilized. Constituent level, or phase average stresses, eliminates some of the complexity of the micro-level stresses. They represent a useful approach to the strength of a unidirectional composite or ply. Micromechanics provides a method of analysis, presented in Section 8.4, for constituent level stresses. Micromechanics is the study of the relations between the properties of the constituents of a composite and the effective properties of the composite.

7.2.4. Micro Level

In micro-level analysis, local stresses of each point within each phase are utilized. Micro-level stresses could be used in appropriate failure criteria for each constituent to determine the external loads at which local failure would initiate. However, the uncertainties, due to departures from the assumed regular local geometry and the statistical variability of local strength make such a process impractical.

7.3. *Assumptions*

Several assumptions have been made for characterizing lamina properties:

7.3.1.   *Material Homogeneity*

Composites, by definition, are heterogeneous (Non-homogenous) materials. Mechanical analysis proceeds on the assumption that the material is homogeneous. This apparent conflict is resolved by considering homogeneity on microscopic and macroscopic scales. Microscopically, composite materials are certainly not homogeneous. However, on the macroscopic scale, they appear homogeneous and respond homogeneously when tested. The analysis of composite materials uses effective properties which are based on the average stress and average strain.

7.3.2.   *Material Orthotropy*

Orthotropy is the condition expressed by variation of mechanical properties as a function of orientation. Lamina exhibit orthotropy as the large difference in properties between the 0° and 90°directions. If a material is orthotropic, it contains planes of symmetry and can be characterized by four independent elastic constants.

7.3.3.   *Material Linearity*

Some composite material properties are nonlinear. The amount of nonlinearity depends on the property, type of specimen, and test environment. The stress-strain curves for composite materials are frequently assumed to be linear to simplify the analysis.

7.3.4. Residual Stresses

One consequence of the microscopic heterogeneity of a composite material is the thermal expansion mismatch between the fiber and the matrix. This mismatch causes residual strains in the lamina after curing. The corresponding residual stresses are often assumed not to affect the material's stiffness or its ability to strain uniformly.

7.4. Fiber Composites: Physical Properties

A unidirectional fiber composite (UDC) consists of aligned continuous fibers which are embedded in a matrix. The UDC physical properties are functions of fiber and matrix physical properties, of their volume fractions, and perhaps also of statistical parameters associated with fiber distribution. The fibers have, in general, circular cross-sections with little variability in diameter. A UDC is clearly anisotropic since properties in the fiber direction are very different from properties transverse to the fibers.

Properties of interest for evaluating stresses and strains are:

a) Elastic properties

b) Viscoelastic properties - static and dynamic

c) Thermal expansion coefficients

d) Moisture swelling coefficients

e) Thermal conductivity

f) Moisture diffusivity

A variety of analytical procedures may be used to determine the various properties of a UDC from volume fractions and fiber and matrix properties.

7.4.1. *Elastic Properties*

The elastic properties of a material are a measure of its stiffness. This information is necessary to determine the deformations which are produced by loads. In a UDC, the stiffness is provided by the fibers; the role of the matrix is to prevent lateral deflections of the fibers. For engineering purposes, it is necessary to determine such properties as Young's modulus in the fiber direction, Young's modulus transverse to the fibers, shear modulus along the fibers and shear modulus in the plane transverse to the fibers, as well as various Poisson's ratios. These properties can be determined in terms of simple analytical expressions. In the following equations, the subscript **f** refers to fiber and **m** refers to matrix. The subscript **1** refers to the fiber direction and **2** refers to the transverse to the fiber direction. **V** refers to volume fraction and ν refers to Poisson's ratio. Plane strain bulk moduli for isotropic fibers and matrix is defined in the following equations (Composite Material Handbook (DOD) 2013):

Plane strain bulk moduli for isotropic fibers

(Equation 7-1):

$$k_f = \frac{E_f}{2\left(1 - \nu_f - 2\nu_f^2\right)}$$

Plane strain bulk moduli for matrix

(Equation 7-2):

$$k_m = \frac{E_m}{2(1 - \nu_m - 2\nu_m^2)}$$

The effective elastic stress-strain relations of a typical transverse section of a UDC, based on average stress and average strain, have the form (Composite Material Handbook (DOD) 2013) :

(Equation 7-3):

$$\begin{cases} \bar{\sigma}_{11} = n^*\bar{\varepsilon}_{11} + l^*\bar{\varepsilon}_{22} + l^*\bar{\varepsilon}_{33} \\ \bar{\sigma}_{22} = l^*\bar{\varepsilon}_{11} + (k^* + G_2^*)\bar{\varepsilon}_{22} + (k^* - G_2^*)\bar{\varepsilon}_{33} \\ \bar{\sigma}_{33} = l^*\bar{\varepsilon}_{11} + (k^* - G_2^*)\bar{\varepsilon}_{22} + (k^* + G_2^*)\bar{\varepsilon}_{33} \end{cases}$$

(Equation 7-4):

$$\begin{cases} \bar{\sigma}_{12} = 2G_1^*\bar{\varepsilon}_{12} \\ \bar{\sigma}_{23} = 2G_2^*\bar{\varepsilon}_{23} \\ \bar{\sigma}_{13} = 2G_1^*\bar{\varepsilon}_{13} \end{cases}$$

with inverse:

(Equation 7-5):

$$\begin{cases} \bar{\varepsilon}_{11} = \dfrac{1}{E_1^*}\bar{\sigma}_{11} - \dfrac{v_{12}^*}{E_1^*}\bar{\sigma}_{22} - \dfrac{v_{12}^*}{E_1^*}\bar{\sigma}_{33} \\[2mm] \bar{\varepsilon}_{22} = -\dfrac{v_{12}^*}{E_1^*}\bar{\sigma}_{11} + \dfrac{1}{E_2^*}\bar{\sigma}_{22} - \dfrac{v_{23}^*}{E_2^*}\bar{\sigma}_{33} \\[2mm] \bar{\varepsilon}_{33} = -\dfrac{v_{12}^*}{E_1^*}\bar{\sigma}_{11} - \dfrac{v_{23}^*}{E_2^*}\bar{\sigma}_{22} + \dfrac{1}{E_2^*}\bar{\sigma}_{33} \end{cases}$$

Where an asterisk (*) denotes effective values. Figure 24 illustrates the loadings which are associated with these properties. The effective modulus k^* is obtained by subjecting a specimen to the average state of stress $\bar{\varepsilon}_{22} = \bar{\varepsilon}_{33}$ with all other strains vanishing, in which case it follows that:

(Equation 7-6):

$$(\bar{\sigma}_{22} + \bar{\sigma}_{33}) = 2k^*(\bar{\varepsilon}_{22} + \bar{\varepsilon}_{33})$$

Unlike the other properties listed above, k^* is of little engineering significance but is of considerable analytical importance.
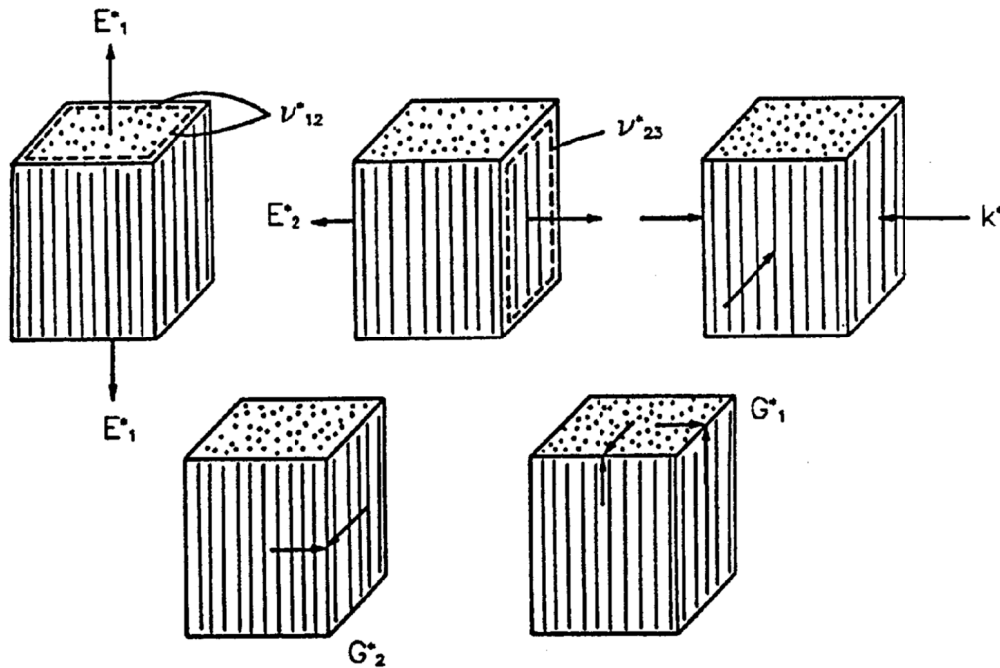
Figure 24 - Basic loading to define effective elastic properties (Composite Material Handbook (DOD) 2013)

Only five of the properties in **Error! Reference source not found.**equations are independent. The most important interrelations of properties are (Composite Material Handbook (DOD) 2013):

(Equation 7-7):

$$n^* = E_1^* + 4k^*v_{12}^{*2}$$

(Equation 7-8):

$$l^* = 2k^*v_{12}^*$$

(Equation 7-9):

$$\frac{4}{E_2^*} = \frac{1}{G_2^*} + \frac{4v_{12}^{*2}}{E_1^*}$$

(Equation 7-10):

$$\frac{2}{1-v_{23}^*} = 1 + \frac{k^*}{\left(1 + 4k^* \frac{v_{23}^{*2}}{E_1^*}\right) G_2^*}$$

Effective Transverse Shear Modulus,

(Equation 7-11):

$$G_2^* = \frac{E_2^*}{2(1 + v_{23}^*)}$$

Computation of effective elastic moduli is a very difficult problem in elasticity theory and only a few simple models permit exact analysis. One type of model consists of periodic arrays of identical circular fibers, e.g., square periodic arrays or hexagonal periodic arrays (Sendeckyj 1974). These models are analyzed by numerical finite difference or finite element procedures. Note that the square array is not a suitable model for the majority of UDCs since it is not transversely isotropic.

The composite cylinder assemblage (CCA) permits exact analytical determination of effective elastic moduli (Z. a. Hashin 1964). Consider a collection of composite cylinders, each with a circular fiber core and a concentric matrix shell. The size of the cylinders may vary but the ratio of core radius to shell radius is held constant. Therefore, the matrix and fiber volume fractions are the same in each composite cylinder. One strength of this model is the randomness of the fiber placement, while an undesirable feature is the large variation of fiber sizes. It can be shown that the latter is not a serious concern.

The analysis of the CCA gives closed form results for the effective properties, k^*, E_1^*, v_{12}^*, n^*, l^* and G_1^* and closed bounds for the properties G_2^*, E_2^* and v_{23}^*. Such results

will now be listed for isotropic fibers with the necessary modifications for transversely isotropic fibers (Z. Hashin 1979).

Plane strain bulk modulus,

(Equation 7-12):

$$k^* = \frac{k_m(k_f + G_m)V_m + k_f(k_m + G_m)V_f}{(k_f + G_m)V_m + (k_m + G_m)V_f} = k_m + \frac{V_f}{\frac{1}{k_f - k_m} + \frac{V_m}{k_m + G_m}}$$

Modulus in the fiber direction E_1 ,

(Equation 7-13):

$$E_1^* = E_m V_m + E_f V_f + \frac{4(\nu_f - \nu_m)^2 V_m V_f}{\frac{V_m}{k_f} + \frac{V_f}{k_m} + \frac{1}{G}} \approx E_m V_m + E_f V_f$$

The last is an excellent approximation for all UDC.

Major Poisson's ratio,

(Equation 7-14):

$$\nu_{12}^* = \nu_m V_m + \nu_f V_f + \frac{(\nu_f - \nu_m)\left(\frac{1}{k_m} - \frac{1}{k_f}\right) V_m V_f}{\frac{V_m}{k_f} + \frac{V_f}{k_m} + \frac{1}{G_m}}$$

Effective In Plane Shear Modulus,

(Equation 7-15):

$$G_1^* = G_m \frac{G_m V_m + G_f(1 + V_f)}{G_m(1 + V_f) + G_f V_m} = G_m + \frac{V_f}{\frac{1}{(G_f - G_m)} + \frac{V_m}{2G_m}}$$

As indicated earlier, the CCA analysis for G_2^* does not yield a result but only a pair of bounds which are in general quite close. (Z. Hashin 1974), (Z. a. Hashin 1964) and (Z. Hashin 1979). A preferred alternative is to use a method of approximation which

70

has been called the Generalized Self Consistent Scheme (GSCS). According to this method, the stress and strain in any fiber is approximated by embedding a composite cylinder in the effective fiber composite material. The volume fractions of fiber and matrix in the composite cylinder are those of the entire composite. Such an analysis results in a quadratic equation for G_2^* (Christensen 1984). Thus,

(Equation 7-16):

$$A \left(\frac{G_2^*}{G_m}\right)^2 + 2B \left(\frac{G_2^*}{G_m}\right) + C = 0$$

where:

(Equation 7-17):

$$A = 3v_f v_m^2 (\gamma - 1)(\gamma + \eta_f) \\ + \left[\gamma \eta_m + \eta_f \eta_m - (\gamma \eta_m - \eta_f)v_f^3\right]\left[v_f \eta_m (\gamma - 1) - (\gamma \eta_m + 1)\right]$$

(Equation 7-18):

$$B = -3v_f v_m^2 (\gamma - 1)(\gamma + \eta_f) \\ + \frac{1}{2}\left[\gamma \eta_m + (\gamma - 1)v_f + 1\right]\left[(\eta_m - 1)(\gamma + \eta_f) - 2(\gamma \eta_m - \eta_m)v_f^3\right] \\ + \frac{v_f}{2}(\eta_m + 1)(\gamma - 1)\left[\gamma + \eta_f + (\gamma \eta_m - \eta_f)v_f^3\right]$$

(Equation 7-19):

$$C = 3v_f v_m^2 (\gamma - 1)(\gamma + \eta_f) + \left[\gamma \eta_m + (\gamma - 1)v_f + 1\right]\left[\gamma + \eta_f + (\gamma \eta_m - \eta_f)v_f^3\right]$$

where:

(Equation 7-20):

$$\gamma = \frac{G_f}{G_m}$$

(Equation 7-21):

$$\eta_m = 3 - 4v_m$$

(Equation 7-22):

$$\eta_f = 3 - 4v_f$$

Using G_2^* calculated, the resulting E_2^* and v_{23}^* can be calculated.

It is of interest to note that when the GSCS approximation is applied to those properties for which CCA results are available (see above). For transversely isotropic fibers, the following modifications are necessary (Z. Hashin 1974) and (Z. Hashin 1979):

For k^* k_f is the fiber transverse bulk modulus

For E_1^*, v_{12}^* $E_f = E_{1f}$, $v_f = v_{1f}$ and k_f as above

For G_1^* $G_f = G_{1f}$

For G_2^* $G_f = G_{2f}$, $\eta_f = 1 + 2\dfrac{G_{2f}}{k_f}$

Numerical analysis of the effective elastic properties of the hexagonal array model reveals that the values are extremely close to those predicted by the CCA/GSCS models as given by the above equations. The results are generally in good to excellent agreement with experimental data.

The simple analytical results given here predict effective elastic properties with sufficient engineering accuracy. They are of considerable practical importance for two reasons. First, they permit easy determination of effective properties for a variety of matrix properties, fiber properties, volume fractions, and environmental conditions. Second, they provide the only approach known today for experimental determination of carbon fiber properties.

For purposes of laminate analysis, it is important to consider the plane stress version of the effective stress-strain relations. Let x_3 be normal to the plane of a thin unidirectionally-reinforced lamina.

The plane stress condition is defined by

(Equation 7-23):

$$\bar{\sigma}_{33} = \bar{\sigma}_{13} = \bar{\sigma}_{23} = 0$$

(Equation 7-24):

$$\begin{cases} \bar{\varepsilon}_{11} = \dfrac{1}{E_1^*}\bar{\sigma}_{11} - \dfrac{v_{12}^*}{E_1^*}\bar{\sigma}_{22} \\[3mm] \bar{\varepsilon}_{22} = -\dfrac{v_{12}^*}{E_1^*}\bar{\sigma}_{11} + \dfrac{1}{E_2^*}\bar{\sigma}_{22} \\[3mm] 2\bar{\varepsilon}_{12} = \dfrac{\bar{\sigma}_{12}}{G_1^*} \end{cases}$$

The inversion gives the following equations:

(Equation 7-25):

$$\begin{cases} \bar{\sigma}_{11} = C_{11}^*\bar{\varepsilon}_{11} + C_{12}^*\bar{\varepsilon}_{22} \\ \bar{\sigma}_{22} = C_{12}^*\bar{\varepsilon}_{11} + C_{22}^*\bar{\varepsilon}_{22} \\ \bar{\sigma}_{12} = 2G_2^*\bar{\varepsilon}_{12} \end{cases}$$

where:

(Equation 7-26):

$$\begin{cases} C_{11}^* = \dfrac{E_1^*}{1 - \dfrac{v_{12}^{*2}E_2^*}{E_1}} \\[5mm] C_{12}^* = \dfrac{v_{12}^*E_2^*}{1 - \dfrac{v_{12}^{*2}E_2^*}{E_1}} \\[5mm] C_{22}^* = \dfrac{E_2^*}{1 - \dfrac{v_{12}^{*2}E_2^*}{E_1}} \end{cases}$$

For polymer matrix composites, at the usual 60% fiber volume fraction, the square of

v_{12}^* is close enough to zero to be neglected and the ratio of E_2^*/E_1^* is approximately

0.1 - 0.2. Consequently, the following approximations are often made.

(Equation 7-27):

$$\begin{cases} C_{11}^* \approx E_1^* \\ C_{12}^* \approx v_{12}^*E_2^* \\ C_{22}^* \approx E_2^* \end{cases}$$

7.4.2. *Viscoelastic properties*

The FRP piles are not subjected to sudden changes in stress level. Therefore, the viscoelastic properties are not discussed in this dissertation.

7.5. *Failure Modes and Criteria*

Due to their orthotropic material behavior and multiple possible failure modes, failure analyses of composites are significantly more complex than for isotropic materials. Failure theory is the science of predicting the conditions under which solid materials fail under the action of external loads. The failure of a material is usually classified into brittle failure (fracture) or ductile failure (yield). Depending on the conditions (such as temperature, state of stress, loading rate) most materials can fail in a brittle or ductile manner or both. However, for most practical situations, a material may be classified as either brittle or ductile. Though failure theory has been in development for over 200 years, its level of acceptability is yet to reach that of continuum mechanics.

In mathematical terms, failure theory is expressed in the form of various failure criteria which are valid for specific materials. Failure criteria are functions in stress or strain space which separate "failed" states from "un-failed" states. A precise physical definition of a "failed" state is not easily quantified and several working definitions are in use in the engineering community. Quite often, phenomenological failure criteria of the same form are used to predict brittle failure and ductile yield. Multiple failure criteria are available to predict different failure modes.

7.6. *Failure Modes*

Failure modes can be categorized into several subcategories. The three main failure modes are tension, compression and shear.

7.6.1. Tension Failure Mode

Failure can occur in fibers due to high stresses in fiber direction (fiber failure). Stress concentration around embedded fibers and tension transverse to the fiber direction can also lead to failure (matrix failure). Tensile failures of composite materials is fairly rare, as filament reinforcements are strongest in tension along their primary axis. Tensile loading in an off-axis direction is a different story. Resin and fiber mechanical properties vary widely in tension, so each must be studied for stress or strain limited failure with off-axis loading scenarios.

7.6.2. Compression Failure Mode

Compression in fiber direction can lead to fiber failure including buckling as well as matrix shear failure. It is therefore difficult to model. Strength depends on fiber and matrix properties as well as on the ability of the matrix to support the fibers. Measurements are difficult and dependent on method and specimens. Compression transverse to the fiber direction can lead to a crushing of the matrix and/or the fibers. In addition matrix shear failure and debonding are possible. Compressive failures in composites are probably the hardest to understand or predict. Failures can occur at a very small-scale, such as the compression or buckling of individual fibers. With sandwich panels, skin faces can wrinkle or the panel itself may become unstable. Indeed, incipient failure may occur at some load well below an ultimate failure.

7.6.3.   Shear Failure Mode

Shear failure usually occurs due to stress concentrations at the fiber/matrix level which is not discussed in this dissertation.

7.7. Failure Criteria

Failure criteria compare loading conditions (stress and/or strain values) with defined strength values for the composite material.

The following are the most common failure criteria:

• Maximum Strain & Maximum Stress

• Tsai-Wu

• Tsai-Hill

• Hashin

• Puck

• LaRC

• Cuntze

• Face Sheet Wrinkling

• Core Failure

• Hoffman

Similar to strength of long-fiber composites, the failure of laminae can be understood by the same three failure modes: axial, transverse and shear. A number of failure criteria have been proposed for separate piles subjected to in-plane stress states, with the assumption that coupling stresses are not present.

This dissertation uses maximum stress, Tsai-Wu and Tsai-Hill failure criteria for composite pile study. The failure criteria are described in the following paragraphs.

7.7.1.   Maximum Stress Failure Criteria

Failure will occur when any one of the stress components exceeds the corresponding strength in that direction. All stresses are independent. Stresses occurring in one direction will not affect the strength of the material in the other directions.

This assumes no interaction between the modes of failure, i.e. the critical stress for one mode is unaffected by the stresses tending to cause the other modes. Failure then occurs when one of these critical values, σ_{1u}, σ_{2u} and τ_{12u} is reached. These values refer to the laminar principal axes and can be resolved from the applied stress system by using the equation (Composite Material Handbook (DOD) 2013):

(Equation 7-28):

$$\begin{bmatrix} \sigma_1 \\ \sigma_2 \\ \tau_{12} \end{bmatrix} = [T] \begin{bmatrix} \sigma_x \\ \sigma_y \\ \tau_{xy} \end{bmatrix}$$

where $\quad [T] = \begin{bmatrix} \cos^2\theta & \sin^2\theta & 2\cos\theta\,\sin\theta \\ \sin^2\theta & \cos^2\theta & -2\cos\theta\,\sin\theta \\ -\cos\theta\,\sin\theta & \cos\theta\,\sin\theta & \cos^2\theta - \sin^2\theta \end{bmatrix}$

It follows that under an applied uniaxial tension $\left(\sigma_y = \tau_{xy} = 0\right)$ the critical values of σ_x for each failure mode are:

(Equation 7-29):

$$\sigma_{xu} = \frac{\sigma_{1u}}{\cos^2\theta} \ , \sigma_{xu} = \frac{\sigma_{2u}}{\sin^2\theta} \ , \sigma_{xu} = \frac{\tau_{12u}}{\sin\theta\,\cos\theta}$$

7.7.2.   *Maximum Strain Failure Criteria*

Failure occurs when at least one of the strain components exceeds the ultimate strain. This criterion considers that the composite fails when the strain exceeds the respective allowable, being a simple and direct way to predict failure of composites. Three different conditions of failure are considered in correspondence with a maximum strain in fiber direction, matrix or transversal direction and for shear strains. (Camanho 2002)

(Equation 7-30):

$$
\begin{cases}
\varepsilon_1 \geq \varepsilon_{1T}^u \ \ or \ |\varepsilon_1| \geq \varepsilon_{1C}^u & For \ fiber \\
\varepsilon_2 \geq \varepsilon_{2T}^u \ \ or \ |\varepsilon_2| \geq \varepsilon_{2C}^u & For \ Matrix \\
|\varepsilon_{12}| \geq \varepsilon_{12}^u & For \ Shear
\end{cases}
$$

As described in the following chapters, each material has a strain limit as well. The orthotropic materials have three different strain limits. That means if a strain is within acceptable rage, the same strain may not be acceptable in a different axis. Also, the tensile strain and the compressive strain may be different for orthotropic or isotropic materials.

7.7.3.   Tsai-Hill Failure Criteria

Tsai-Hill failure criteria takes into account interactions between different failure modes. It is based on the von-Mises failure criteria for metals. The Tsai-Hill failure criteria cannot predict different failure modes (Fiber failure, matrix failure, fiber-matrix interface failure, …)

Von Mises Criterion for metals:

(Equation 7-31): $(\sigma_1 - \sigma_2)^2 + (\sigma_2 - \sigma_3)^2 + (\sigma_3 - \sigma_1)^2 = 2\sigma_y^2$

where σ_y is the metal yield stress.

For most of composites in-plane stress states is either $\sigma_3 = 0$ or relatively low. This reduces the Von Miss Criterion to the following:

$$\left(\frac{\sigma_1}{\sigma_y}\right)^2 + \left(\frac{\sigma_2}{\sigma_y}\right)^2 - \frac{\sigma_1\sigma_2}{\sigma_y^2} = 1$$

This is then modified to take into account the anisotropy of composites and the different failure mechanisms to give the following expression:

$$\left(\frac{\sigma_1}{\sigma_{1y}}\right)^2 + \left(\frac{\sigma_2}{\sigma_{2y}}\right)^2 - \frac{\sigma_1\sigma_2}{\sigma_{1y}^2} - \frac{\sigma_1\sigma_2}{\sigma_{2y}^2} + \frac{\sigma_1\sigma_2}{\sigma_{3y}^2} + \left(\frac{\tau_{12}}{\tau_{12y}}\right)^2 = 1$$

The metal yield stresses can be regarded as composite failure stresses and since composites are transversely isotropic $\sigma_{2u} = \sigma_{3u}$ we arrive at the Tsai-Hill criterion for composites:

(Equation 7-32):

$$\left(\frac{\sigma_1}{\sigma_{1u}}\right)^2 + \left(\frac{\sigma_2}{\sigma_{2u}}\right)^2 - \frac{\sigma_1\sigma_2}{\sigma_{1u}^2} + \left(\frac{\tau_{12}}{\tau_{12u}}\right)^2 = 1$$

The maximum stress criterion suggests possible modes of failure whereas the Tsai-Hill criterion does not account for that.

7.7.4. *Tsai-Wu Failure Criteria*

The Tsai–Wu failure criterion is a phenomenological material failure theory which is widely used for anisotropic composite materials which have different strengths in tension and compression. The Tsai-Wu criterion predicts failure when the failure index in a laminate reaches 1. This failure criterion is a specialization of the general quadratic failure criterion proposed by Gol'denblat and Kopnov and can be expressed in the form

(Equation 7-33):

$$F_i \sigma_i + F_{ij} \sigma_i \sigma_j \leq 1$$

where i , j = 1 …..6 and repeated indices indicate summation, and F_i , F_{ij} are experimentally determined material strength parameters. The stresses σ_i are expressed in Voigt notation. If the failure surface is to be closed and convex, the interaction terms f_{ij} must satisfy

(Equation 7-34):

$$F_{ii}F_{jj} - F_{ij}^2 \geq 0$$

which implies that all the F_{ij} terms must be positive.

For orthotropic materials with three planes of symmetry oriented with the coordinate directions, if we assume that $F_{ij} = F_{ji}$ and that there is no coupling between the normal and shear stress terms (and between the shear terms), the general form of the Tsai–Wu failure criterion reduces to

$$F_1 \sigma_1 + F_2 \sigma_2 + F_3 \sigma_3 + F_4 \sigma_4 + F_5 \sigma_5 + F_6 \sigma_6 + F_{11} \sigma_1^2 + F_{22} \sigma_2^2 + F_{33} \sigma_3^2 + F_{44} \sigma_4^2$$
$$+ F_{55} \sigma_5^2 + F_{66} \sigma_6^2 + 2F_{12} \sigma_1 \sigma_2 + 2F_{13} \sigma_1 \sigma_3 + 2F_{23} \sigma_2 \sigma_3 \leq 1$$

Let the failure strength in uniaxial tension and compression in the three directions of anisotropy be $\sigma_{1t}, \sigma_{1c}, \sigma_{2t}, \sigma_{2c}, \sigma_{3t}, \sigma_{3c}$. Also, let us assume that the shear strengths in the three planes of symmetry are $\tau_{23}, \tau_{12}, \tau_{31}$ (and have the same magnitude on a plane even if the signs are different). Then the coefficients of the orthotropic Tsai–Wu failure criterion are:

$$F_1 = \frac{1}{\sigma_{1t}} - \frac{1}{\sigma_{1c}} \; ; F_2 = \frac{1}{\sigma_{2t}} - \frac{1}{\sigma_{2c}} \; ; F_3 = \frac{1}{\sigma_{3t}} - \frac{1}{\sigma_{3c}} \; ; F_4 = F_5 = F_6 = 0$$

$$F_{11} = \frac{1}{\sigma_{1c}\sigma_{1t}} ; F_{22} = \frac{1}{\sigma_{2c}\sigma_{2t}} ; F_{33} = \frac{1}{\sigma_{3c}\sigma_{3t}} ; \; F_{44} = \frac{1}{\tau_{23}^2}; \; F_{55} = \frac{1}{\tau_{31}^2}; \; F_{66} = \frac{1}{\tau_{12}^2};$$

The coefficients F_{12}, F_{13}, F_{23} can be determined using equibiaxial tests. If the failure strengths in equibiaxial tension are $\sigma_1 = \sigma_2 = \sigma_{b12}$, $\sigma_1 = \sigma_3 = \sigma_{b13}$,

$\sigma_2 = \sigma_3 = \sigma_{b23}$ then:

(Equation 7-35):

$$F_{12} = \frac{1}{2\sigma_{b12}^2} \left[1 - \sigma_{b12}(F_1 + F_2) - \sigma_{b12}^2(F_{11} + F_{22}) \right]$$

$$F_{13} = \frac{1}{2\sigma_{b13}^2} \left[1 - \sigma_{b13}(F_1 + F_3) - \sigma_{b13}^2(F_{11} + F_{33}) \right]$$

$$F_{23} = \frac{1}{2\sigma_{b23}^2} \left[1 - \sigma_{b23}(F_2 + F_3) - \sigma_{b23}^2(F_{22} + F_{33}) \right]$$

The near impossibility of performing these equibiaxial tests has led to there being a severe lack of experimental data on the parameters F_{12}, F_{13}, F_{23}. It can be shown that the Tsai-Wu criterion is a particular case of the generalized Hill yield criterion. Tsai-Wu failure criteria takes into account interactions between different failure modes. Differences in tensile and compression strengths are considered in this failure criteria. It cannot predict different failure modes (Fiber failure, matrix failure, fiber-

matrix interface failure, …) Tsai-Wu Failure Criteria requires the definition of interaction parameters (F_{12}, F_{23}, F_{13}). The interaction parameters have to be defined by equibiaxial tests which are nearly impossible to perform. Therefore the interaction parameter are either defined by curve fitting or left to the default values of -1.

7.7.5.   Puck and Cuntze Failure Criteria

Puck and Cuntze failure criteria are is driven by the physics underlying the actual failure modes. They separate fiber-fracture from the several inter-fiber fracture modes. Fiber-fracture can be evaluated using the simple stress criteria. Puck works with action planes in which the composite fails and three inter-fiber fracture modes (Mode A, B and C)
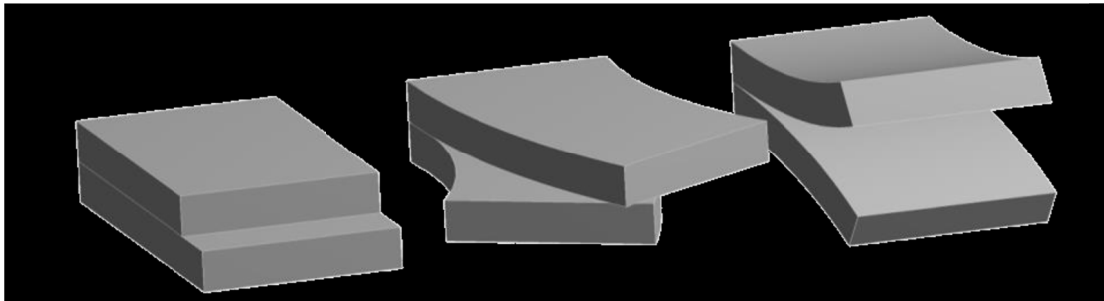
Figure 25 – (left to right) IFF Mode B, C and A (ANSYS Inc. 2016)

7.7.6.   LaRC Failure Criteria

LaRC Failure Criteria is developed by the NASA Langley Research Center. It is a phenomenological criteria which is based on Hashins and Pucks failure criteria. LaRC failure criteria takes into account that a ply has higher transverse tensile and shear strength when it is constrained by plies with different fiber orientations (in-situ effect).

7.7.7. Failure Criteria Terms

e = strain s = stress

1 = material 1 direction

2 = material 2 direction

3 = out-of-plane normal direction

12 = in-plane shear

13 and 23 = out-of-plane shear terms

I = principal I direction

II = principal II direction

III = principal III direction

t = tension, c = compression

7.7.8. Comparison between different Failure Criteria

Table 8 shows the failure more comparison among different criteria.

Table 8 – Failure mode comparison among different criteria

Maximum Strain Failure modes	e1t, e1c, e2t, e2c, e12
Maximum Stress	s1t, s1c, s2t, s2c, s3t, s3c, s12, s23, s13
Tsai-Wu 2D and 3D	tw
Tsai-Hill 2D and 3D	th
Hashin	hf (fiber failure) hm (matrix failure) hd (delamination failure)
Puck (simplified, 2D and 3D)	pf (fiber failure) pmA (matrix tension failure) pmB (matrix compression failure) pmC (matrix shear failure) pd (delamination)
LaRC (2D)	lf (fiber failure) lmt (matrix failure tension) lmc (matrix failure compression)
Cuntze 2D and 3D	cft (fiber tension failure) cfc (fiber compression failure) cmA (matrix tension failure) cmB (matrix compression failure) cmC (matrix wedge shape failure)
Sandwich Failure Wrinkling	wb (wrinkling bottom face) wt (wrinkling top face)
Sandwich Failure Core	cf (core failure)

8. *Structural Analysis of the Models Using ANSYS Workbench*

Before ANSYS workbench, the ANSYS Parametric Design Language (APDL) was used to model structures in ANSYS. Generally, most of the structural analysis software was run on machines that did not have the capability of today's computers. Therefore, nearly all of them were using a programing environment to create and solve the stiffness, load, displacement matrixes to aid in analyzing the structure. With everyday improvement in the computer industry, especially with great improvements in processing speed, memory and graphical capabilities, the software industry is shifting toward graphical data entry. This method makes a better understanding of modeling the structure and reducing the errors drastically. The user can see the structure as it is completed. Besides, mistakes in data entries are detected before the analysis.

Since there are still engineers and designers from previous generations that resist switching to new methods, the APDL is still in use. Obviously, the more modern and user-friendly methods such as ANSYS Workbench will eventually replace the programing methods.

The difference between the APDL and other commercial programing applications is that APDL uses parameters that can be changed during multiple runs. Other similar software does not present this capability. Also the APDL has a variety of FE element types,each being useful for special types of model. For example, SOLID46 is a three-dimensional structural solid that can accommodate 256 layers.

ANSYS Workbench is a very modern and strong tool which combines the strength of APDL with the tools necessary to manage the projects. It was first introduced as ANSYS 12.0 in 2009. The Workbench is modified and improved in each release since then. In 2013 the ANSYS Composite PrepPost (ACP) was added to the program. ANSYS Composite PrepPost (ACP) is an add-on to ANSYS Workbench and is integrated with the standard analysis features. The entire workflow for composite structure can be completed from design to final production as a result. The ACP made it possible to model layered composites, with changing parameters from size to layers and to batch process multiple similar models. This was exactly what was needed to create FE models for this dissertation.

The geometry of the tooling surfaces of a composite structure is the basis for analysis and production. Based on this geometry and a FE mesh, the boundary conditions and composite definitions are applied to the structure in the pre-processing stage. After a completed solution, the post-processing is used to evaluate the performance of the design and laminate. In the case of an insufficient design or material failure, the geometry or laminate has to be modified and the evaluation is repeated. ACP has a pre- and post-processing mode. In the pre-processing mode, all composite definitions can be created and are mapped to the geometry (FE mesh). These composite definitions are transferred to the FE model and the solver input file. In the post-processing mode, after a completed solution and the import of the result file(s), post-processing results (failure, safety, strains and stresses) can be evaluated and visualized. Figure 26 shows the typical ANSYS Workbench using ACP.
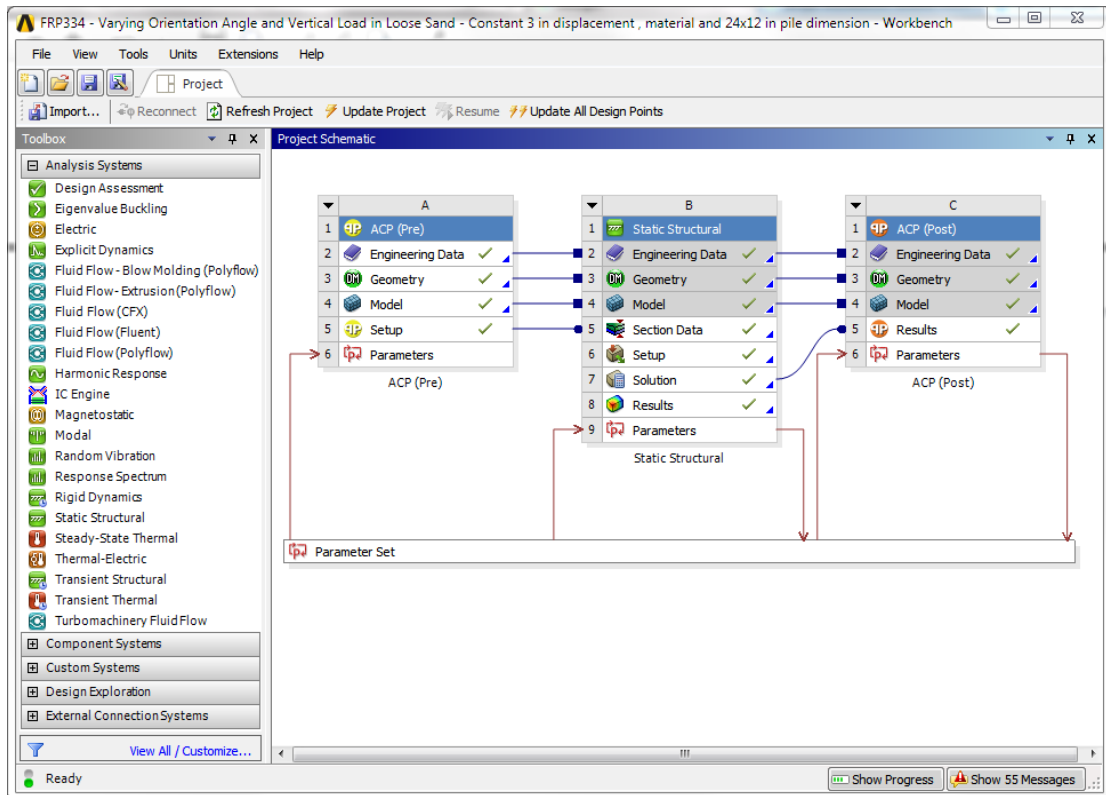
Figure 26 – Typical view of ANSYS Workbench using ACP PrepPost

As shown in the figure the ACP Preprocessing with the header "A" on the left side of project schematic screen creates the stiffness and force matrixes. Then the data is transferred to the Static Structural Processing section in the middle with the header "B". Eventually the processed data is transferred to Post processing section on the right with the header "C".

All three stages are in communication with the "Parameter Set" (PS). This means they get or send the values of the parameters to or from the PS section. This network is specifically designed according to the dissertation requirements.

Figure 27 shows the Post Processing window for one the pile models created for this project.
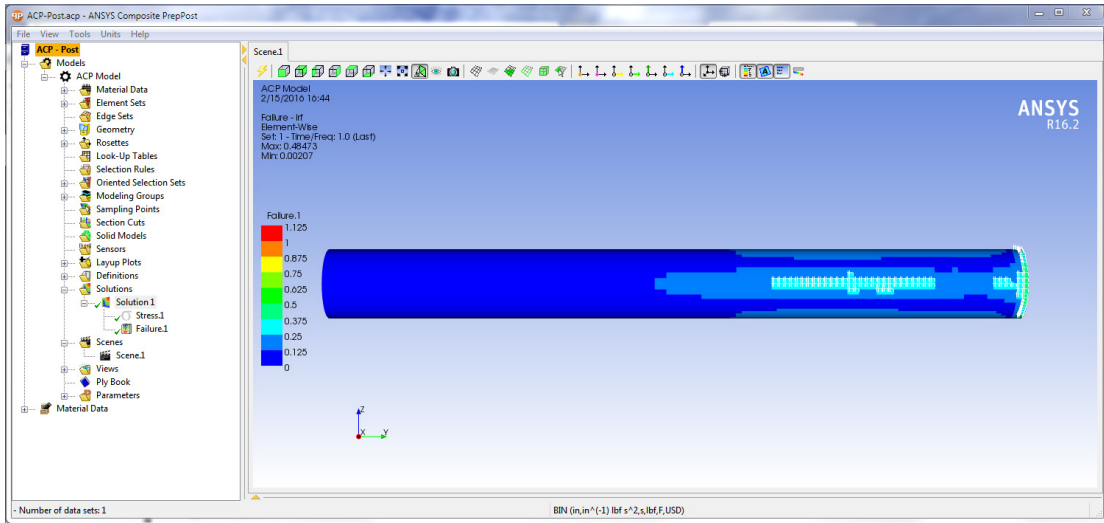
Figure 27 – Typical view of ACP Post Processing

Figure 28 – Typical view of Parameter Set for a FRP pile with varying fiber orientation angle and vertical load

8.1. *Creating the Models*

As described, the FE models are created in ANSYS Workbench. The following steps are taken to generate each one:

8.2. *Non Isotropic Material Definition*

All materials used in this dissertation are layer composite materials. Currently, ANSYS ACP can define orthotropic and elastic materials. It also can define isotropic and nonlinear materials. It cannot define orthotropic and nonlinear materials. After studying the stress strain curves in a variety of composite materials, it was observed that most of the composite materials stay approximately elastic until near fracture. In other words, the yielding either does not happen or happens right before fracture. Therefore, the elastic orthotropic material is a close approximation which can be used to define the materials.

In order to define the orthotropic materials, orthotropic elasticity, Poisson's ratio, shear modulus, stress and strain limits in tension compression and shear, Puck constants are defined each in X, Y and Z directions and, if applied, in XY, YZ and XZ planes.

Figure 29 shows the properties used for the Epoxy E glass UD material.

Other materials are added to the library using the information provided in the Department of Defense Composite Material Handbook (Composite Material Handbook (DOD) 2013) and the Introduction to Composite Material Design Handbook (Barbero 2011)
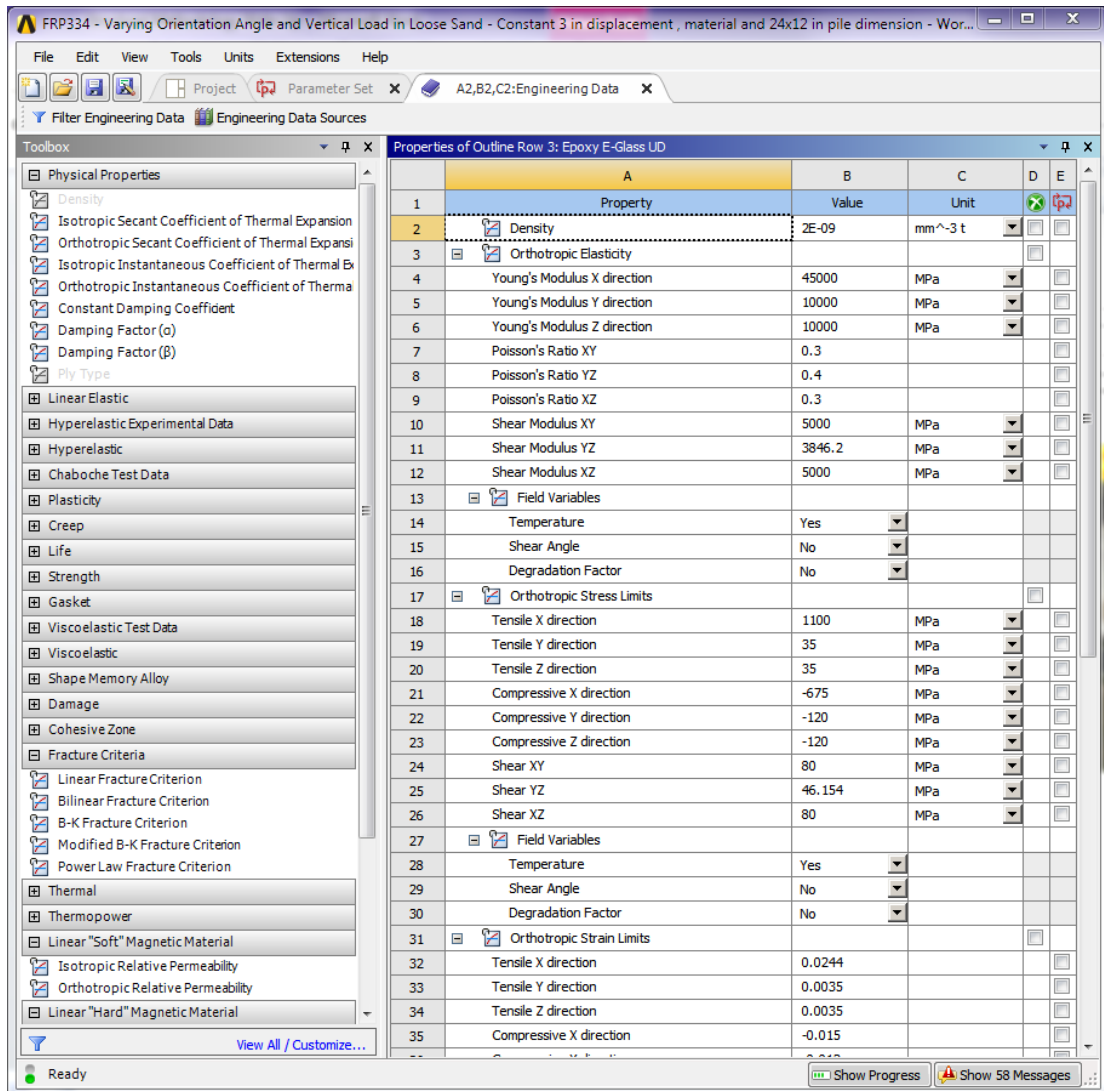
Figure 29 – Typical view of orthotropic material properties

Later in the models, a variety of composite materials such as E-Glass Epoxy, S-Glass Epoxy, E-Glass Polyester, Kevlar 49 Epoxy, E-Glass LY556 (25), E-Glass MY750 (25), E-Glass Epoxy (32), AS4-3501-6, AS4-3501-6 (25), T300-914-C (25), T800-3900-2, IM7-8551-7, IM7-8552, AS4-APC2 and Avimid-K-III are compared. The following table shows the material properties of these materials.

Table 9 – Material properties of the composite materials (Barbero 2011)

Table 1.3: Typical properties of unidirectional composites, obtained from product literature and other sources, with some values estimated for a broad class of materials. The designer is responsible for obtaining actual values.

		E-glass–Epoxy	S-Glass–Epoxy	E-glass–Polyester	Kevlar 49™–Epoxy	E-glass–LY556 [25]	E-glass–MY750 [25]	E-glass–Epoxy [32]
Density [g/cc]	ρ	2.076	1.993	1.85	1.380	-	-	-
Longitudinal Modulus [GPa]	E_1	45	55	37.9	75.8	53.48	45.6	44.7
Transverse Modulus [GPa]	E_2	12	16	11.3	5.5	17.70	16.2	12.7
In-plane Shear Modulus [GPa]	G_{12}	5.5	7.6	3.3	2.07	5.83	5.83	5.8
In-plane Poisson's ratio	ν_{12}	0.19	0.28	0.3	0.34	0.278	0.278	0.297
Transverse Poisson's ratio	ν_{12}	0.31	-	-	-	0.4	0.398	0.410
Longitudinal Tensile Strength [MPa]	F_{1t}	1020	1620	903	1380	1140	1280	-
Transverse Tensile Strength [MPa]	F_{2t}	40	40	40	34.5	35	40	43.4
Longit. Compressive Strength [MPa]	F_{1c}	620	690	357	586.0	800	800	-
Transv. Compressive Strength [MPa]	F_{2c}	140	140	68	138.0	138	145	-
In-plane Shear Strength [MPa]	F_6	60	60	40	44.1	61	73	135.8
Interlaminar Shear Strength [MPa]	F_4	-	-	-	150	-	-	-
Ult. Longit. Tensile Strain [%]	ϵ_{1t}	1.29	1.68	1.64	1.45	2.132	2.807	-
Ult. Transv. Tensile Strain [%]	ϵ_{2t}	-	-	-	-	.197	.246	-
Ult. Longit. Comp. Strain [%]	ϵ_{1c}	-	-	-	-	1.065	1.754	-
Ult. Transv. Comp. Strain [%]	ϵ_{2c}	-	-	-	-	.644	1.2	-
Ultimate Shear Strain [%]	γ_{6u}	-	-	-	-	3.8	4.0	-
Fracture Toughness Mode I [J/m²]	G_{Ic}	-	-	334	-	165	165	360
Fracture Toughness Mode II [J/m²]	G_{IIc}	-	-	456	-	-	-	1400
Longitudinal CTE [10^{-6}/° C]	α_1	3.7	3.5	6.5	-2.0	8.6	8.6	-
Transverse CTE [10^{-6}/° C]	α_2	30	32	22	60	26.4	26.4	-
Stress-free Temperature [° C]	SFT	126	126	25	126	120	120	-
Longitudinal Moisture Expansion	β_1	0	0	0	0.01	-	-	-
Transverse Moisture Expansion	β_2	0.2	0.2	0.2	0.2	-	-	-
Fiber Volume Fraction	V_f	0.6	0.6	0.5	0.6	0.6	0.6	-
Void Content	V_v	-	-	0.02	-	-	-	-
Fiber Misalignment [deg]	α_σ	2.97	2.98	3.53	1.34	-	-	-
Ply Thickness [mm]	t_k	0.144	0.144	0.144	0.144	0.6	0.6	0.144

Table 10 – Material properties of the carbon fiber materials (Barbero 2011)

Table 1.4: Typical properties of unidirectional (carbon-fiber) composites, obtained from product literature and other sources, with some values estimated for broad class of materials. The designer is responsible for obtaining actual values.

		AS4 –3501-6	AS4 –3501-6 [25]	T300 –914-C [25]	T800 –3900-2	IM7 –8551-7	IM7 –8552	AS4 –APC2[a]	Avimid –K-III[b]
Density [g/cc]	ρ	1.58	-	-	-	-	1.55	1.6	-
Longitudinal Modulus [GPa]	E_1	142	126	138	155.8	151	171.4	138	110
Transverse Modulus [GPa]	E_2	10.3	11.0	11.0	8.89	9.0	9.08	10.2	8.3
In-plane Shear Modulus [GPa]	G_{12}	7.2	6.6	5.5	5.14	5.6	5.29	5.7	5.7
In-plane Poisson's ratio	ν_{12}	0.27	0.28	0.28	0.3	0.3	0.32	0.3	-
Transverse Poisson's ratio	ν_{23}	-	0.4	0.4	0.064	0.184	0.4^c	0.3	-
Longitudinal Tensile Strength [MPa]	F_{1t}	1830	1950	1500	2698	-	2326.2	2070	-
Transverse Tensile Strength [MPa]	F_{2t}	57	48	27	-	-	62.3	86	37
Longit. Compressive Strength [MPa]	F_{1c}	1096	1480	900	1691	1200	1200.1	1360	1000
Transv. Compressive Strength [MPa]	F_{2c}	228	200	200	-	-	199.8	186	-
In-plane Shear Strength [MPa]	F_6	71	79	100	186	71	92.3–120	186	63
Interlaminar Shear Strength [MPa]	F_4	-	-	-	-	-	137.2	150	-
Ult. Longit. Tens. Strain [%]	ϵ_{1t}	1.29	1.38	1.087	1.68	1.64	1.62	1.45	-
Ult. Transv. Tens. Strain [%]	ϵ_{2t}	-	0.436	0.245	-	-	-	-	-
Ult. Longit. Comp. Strain [%]	ϵ_{1c}	-	1.175	0.652	-	-	-	-	-
Ult. Transv. Comp. Strain [%]	ϵ_{2c}	-	2.0	0.245	-	-	-	-	-
Ultimate Shear Strain [%]	γ_{6u}	-	2.0	4.0	-	-	3.22	-	-
Fracture Toughness Mode I [J/m²]	G_{1c}	-	220	220	-	-	277	-	-
Fracture Toughness Mode II [J/m²]	G_{11c}	-	-	-	-	-	788	-	-
Longitudinal CTE [$10^{-6}/°$ C]	α_1	-0.9	-1.0	-1.0	-	-	-5.5	0.5	-
Transverse CTE [$10^{-6}/°$ C]	α_2	27	26	26	-	-	25.8	30	-
Stress-free Temperature [° C]	SFT	-	177	120	-	-	176	-	-
Longitudinal Moisture Expansion	β_1	0.0	-	-	0.0095	-	-	-	-
Transverse Moisture Expansion	β_2	0.2	-	-	0.321	-	-	-	-
Fiber Volume Fraction	V_f	0.6	0.6	0.6	-	0.573	0.591	0.61	-
Void Content	V_v	-	-	-	-	0.001	-	-	0.005
Fiber Misalignment [deg]	α_σ	1.70	-	-	1.75	1.27	1.59	2.74	1.52
Ply Thickness [mm]	t_k	0.125	0.8	0.8	0.125	0.125	0.125	0.125	0.125

[a]PEEK matrix. [b]Polyimide matrix; remainder are all epoxy-matrix composites. G_{23}=2.8–5.9 MPa (range reported in the source).

8.3. *Elliptical Sections*

All the sections used in this dissertation have elliptical shapes. As discussed in previous sections, the long and short diameters of the ellipse are defined as parameters. The change in the parameter will provide piles from very elongated ellipse to complete circle.
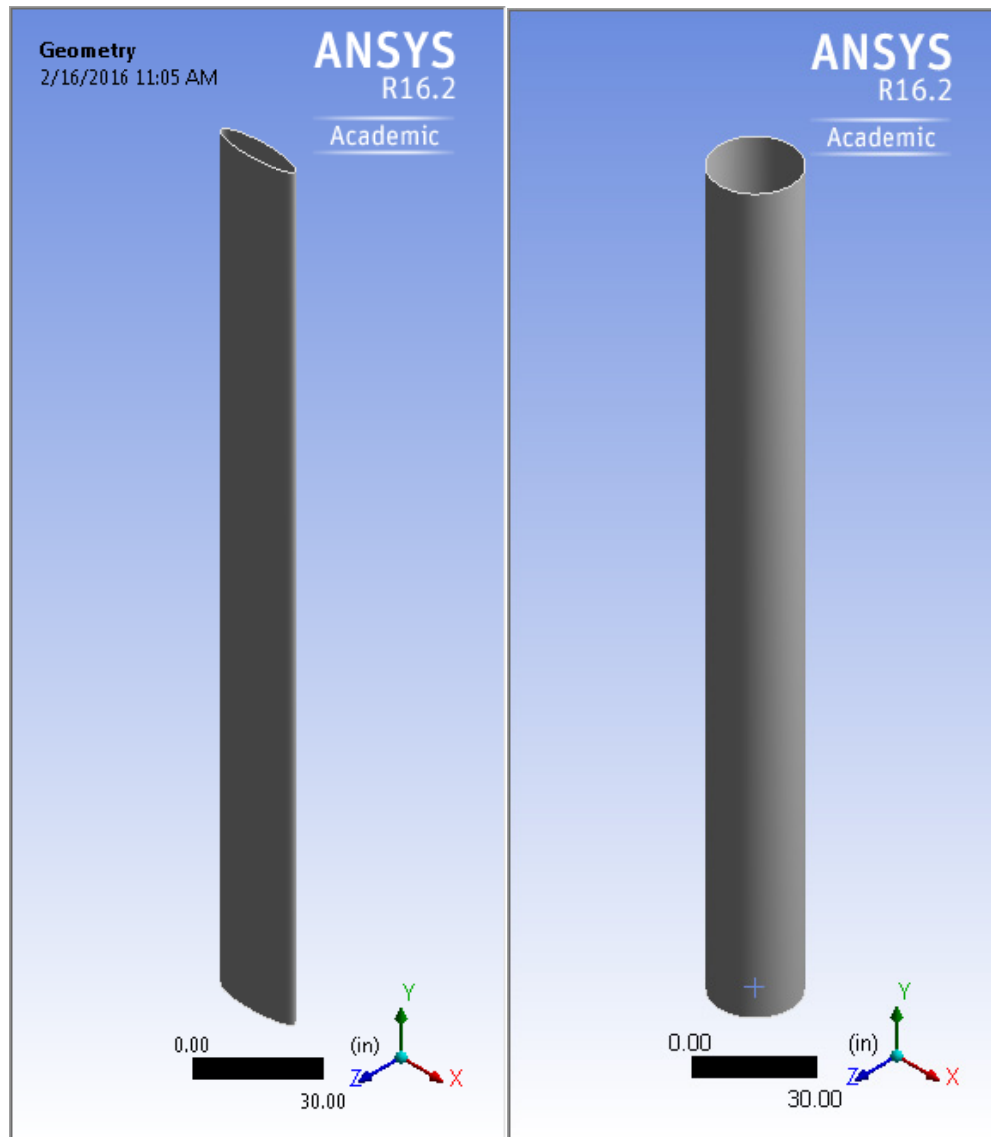
Figure 30 – Pile geometry - Very elongated (left), Complete circle (Right)

8.4. *Numerical Approach*

As described in Section 7.2 (Basic Lamina Properties and Micromechanics), in order to model the composite materials there are three different numerical approaches:

1. Micro-Scale Approach (Fiber Level or Micro Level)

The most detailed approach describes the micro-structure of the composite. This includes fiber shape, location and material properties of reinforcement and matrix.

2. Macro-Scale Approach (Laminate Level)

If only displacements, buckling loads, or vibration frequencies and modes are required, the laminate can be analyzed as a homogeneous shell using a macro-scale approach. In this case the stress distribution cannot be obtained.

3. Meso-Scale Approach (Ply Level or Constituent Level)

Analyzing strains, stresses and failure criteria of the composite laminate requires modeling single layers of a composite design which is built up one by one. This method is called a meso-scale approach. It requires material properties and thicknesses for each layer of the design. ANSYS Composite PrepPost is mainly used to prepare and evaluate composite specific results of a design using the meso-scale approach. The Ply Coordinate System is defined with 3 orthogonal directions.

Direction-1: Parallel to fiber direction (also II-direction, L-direction or x-direction)

Direction-2: Perpendicular to fiber direction (also ⊥ direction, T-direction or y-direction)

Direction-3: Normal to ply (also "out of plane" or z-direction)
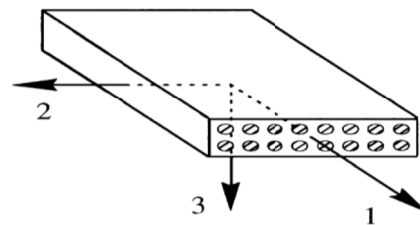
Figure 31 – Composite coordinate system

8.5. *Defining layers*

A composite layer is defined by selecting the following parameters:

- The fabric to be used

- The area where this fabric should be placed

- The layup direction

- The fiber direction

The fabric is defined in the material data and directly takes the material property from that section. The area is set to be the entire surface of the pile. The layup direction is defined by introducing a new directional rosette. The fiber direction in defined, using the layup direction and the orientation angle.

The creation of the FRP depends on various parameters and requires strong knowledge of the desired material. The ACP provided the possibility to even introduce the parametric values instead of fixed values. For example, the fiber orientation can be changed in each model using the "Parameter Set".

The number of layers, type of layers, materials, and many other aspects can be set to be parametric. Then the parameter can be changed to the desired value without introducing a new model.

Figure 32 shows different orientation layers of a composite pile.
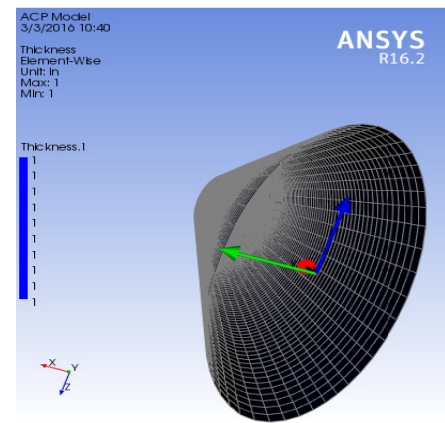
Figure 32 – Created rosette for composite coordinate system
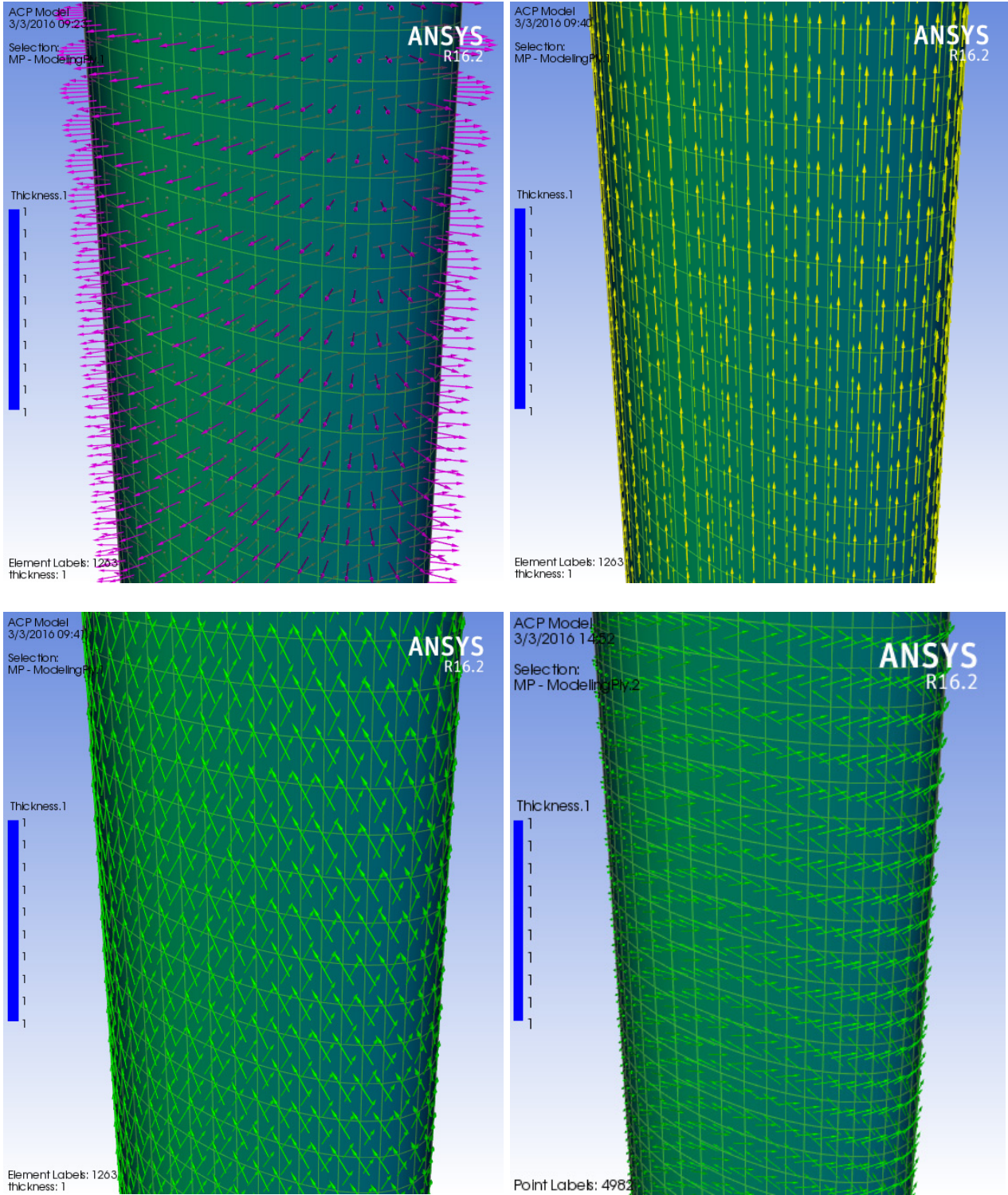
**Figure 33 – Element axis 3 (top left) axis 2 (top right)- axis 1 for 30 degree (bottom left)
and 70 degree (bottom right)**

8.6. *Meshing*

After the geometry is defined, the surface and volume of the model is divided into smaller elements. This process is called meshing. There are several ways to define the mesh. The element type, shape and size can be modified to generate the best optimum meshing. Large size elements can result an inaccurate calculation and very small size elements can increase the calculation time drastically.
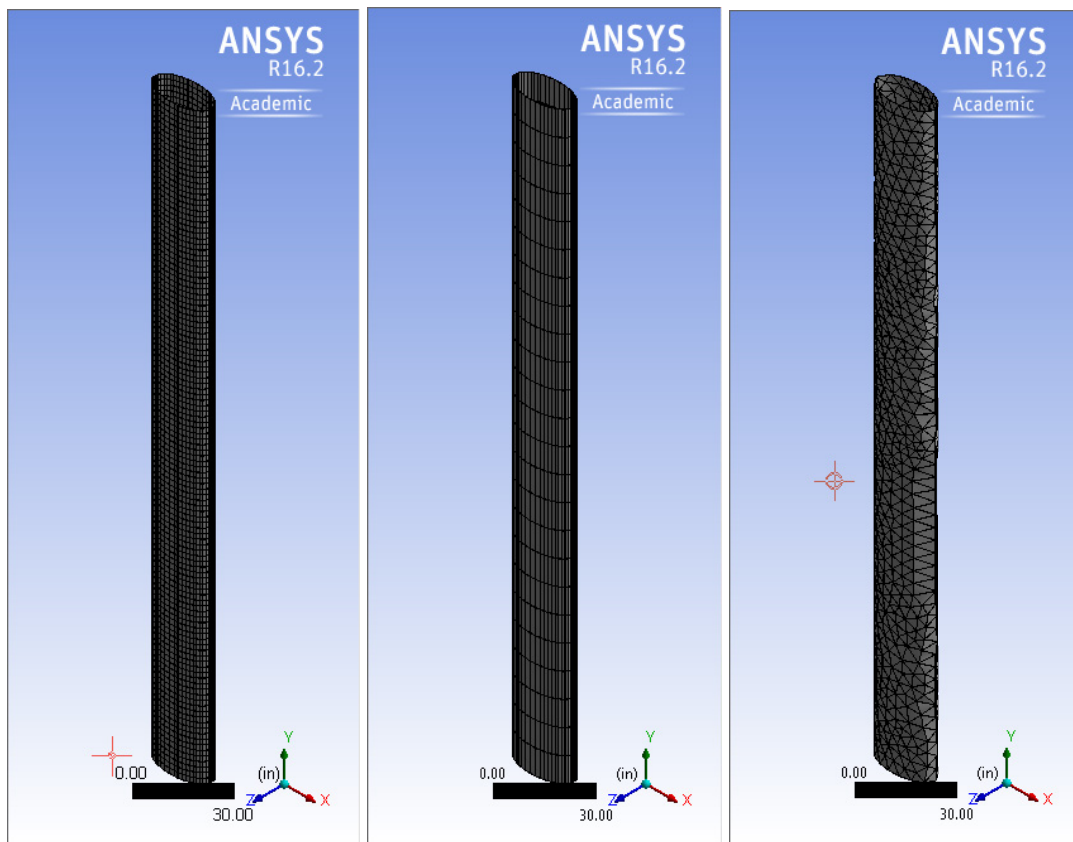
Figure 34 – Meshing methods – used in this dissertation (left) , large size with inaccurate result (middle) , triangular shape with inaccurate sizing (right)

For this dissertation the sweep method is being used. In this method the meshing will start from one end and as it moves toward the other end it sweeps the surface of the model which in this case remains a constant shape. The elements will be quadrilateral

or rectangular. The sizing would also be limited between 1 to 2 inches. The mesh also will be refined if the curvature is less than 5 degree which happens in both ends of the elliptical shape. Figure 34 shows the different meshing options.

8.7. *Concrete Filled Piles*

In order to study the effects of filling the piles with concrete, some modes are created specifically with concrete elements.
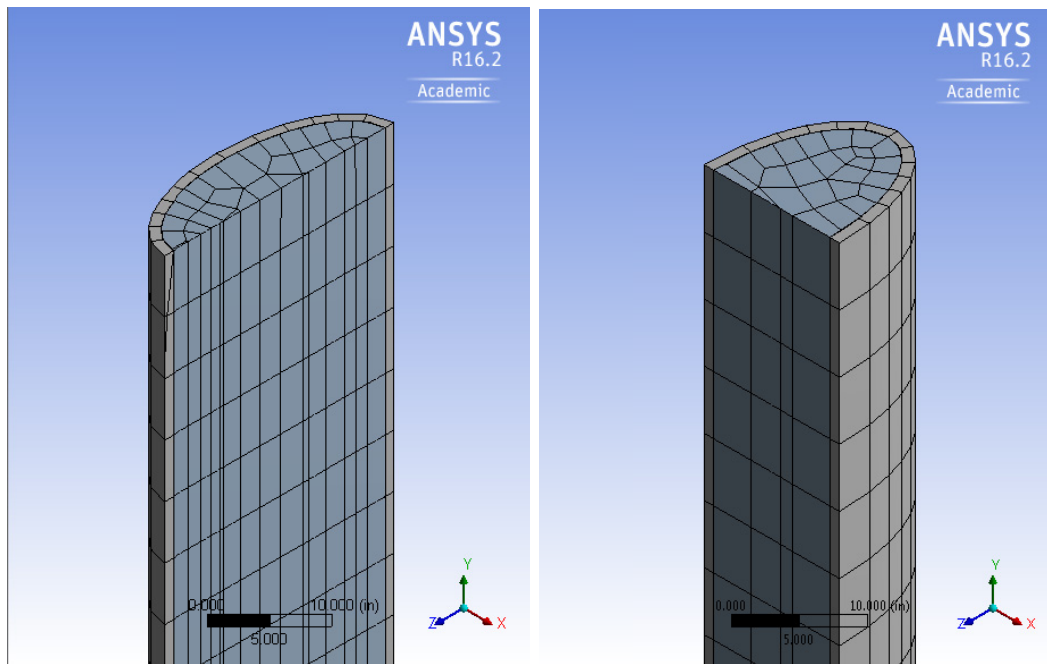
Figure 35 – Pile sections for concrete filled models

8.8. *Forces and Displacement*

Multiple variations and combinations of the loads and displacements are studied. In all cases the vertical load is presented as force in the Y direction. It is applied to the top edge of the pile which will be automatically and evenly distributed at the top portion of the pile.

Figure 36 shows the even distribution of force and displacement.
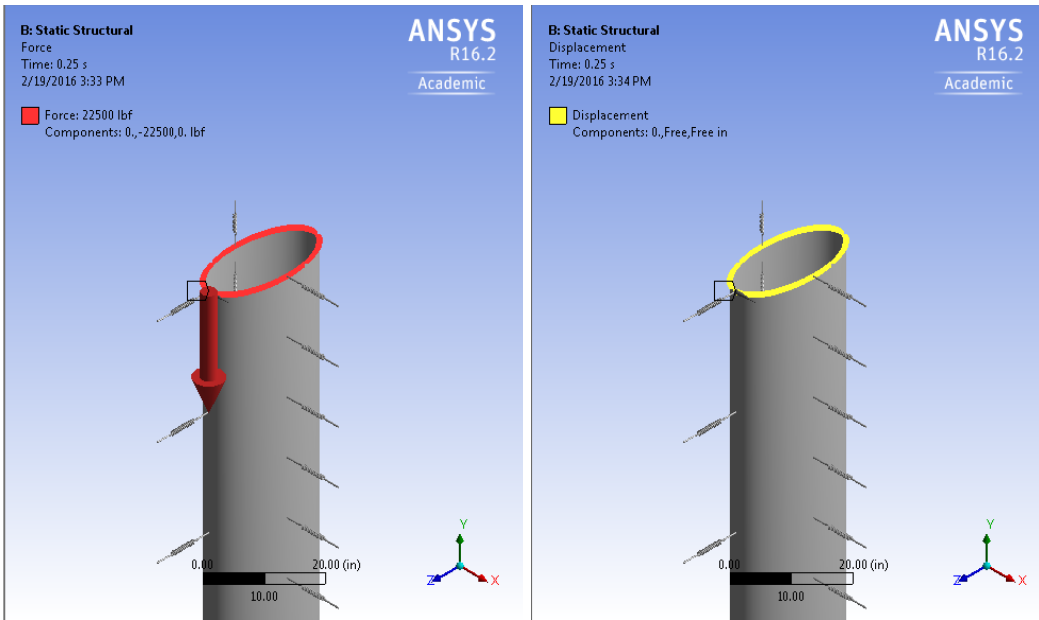
Figure 36 – Even distribution of the forces on the top of the pile

The lateral force is presented as forced displacement. In all of the models the lateral displacement has been limited to 4" and often applied in ½ inch steps. It is described in future chapters that the displacement creates immense loads in denser soil which will cause pile failure. On the other hand, large displacement in soft soils does not apply damaging forces.

8.9. *Supports*

Two kinds of supports are studied on this dissertation. The elastic and nonlinear supports. Each type is described as follows.

8.10. *Elastic Supports*

The elastic supports are defined around the body of the piles. The subgrade modulus is set equal to 50 lbf/in^3 where the soil stiffness is assumed to be constant. In order to

study the effects of soil on FRP piles, in some cases the subgrade modulus is set as a variable parameter from 10 to 100 lbf/in^3.

8.11. *Nonlinear Supports*

The soil around the pile is modeled as soil springs. Figure 37 shows the springs.
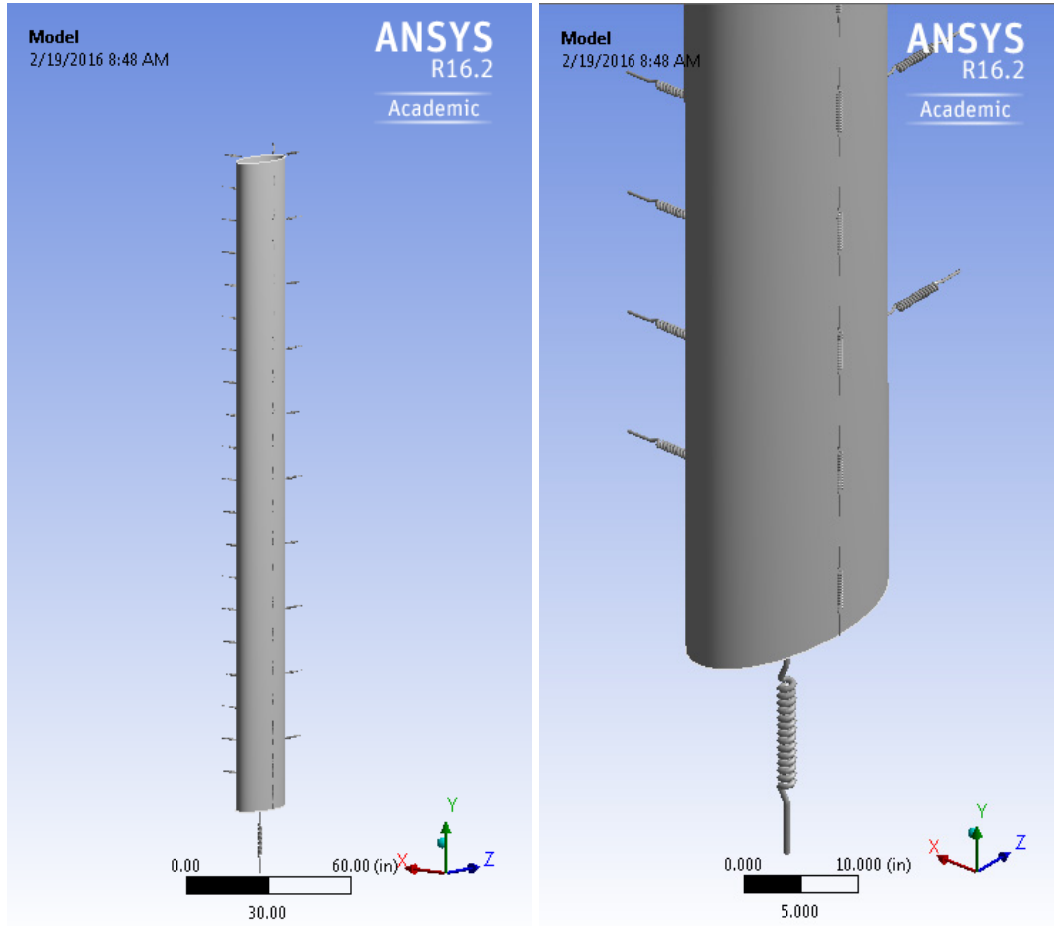
Figure 37 – Soil lateral, slip and end bearing springs

The soil springs are then modeled as nonlinear spring based on Ramberg-Osgood models. Each spring has an area of influence of 12 inch length of the pile body. Therefore, by placing the spring at 12 inch intervals an accurate model of the soil behavior will be modeled.
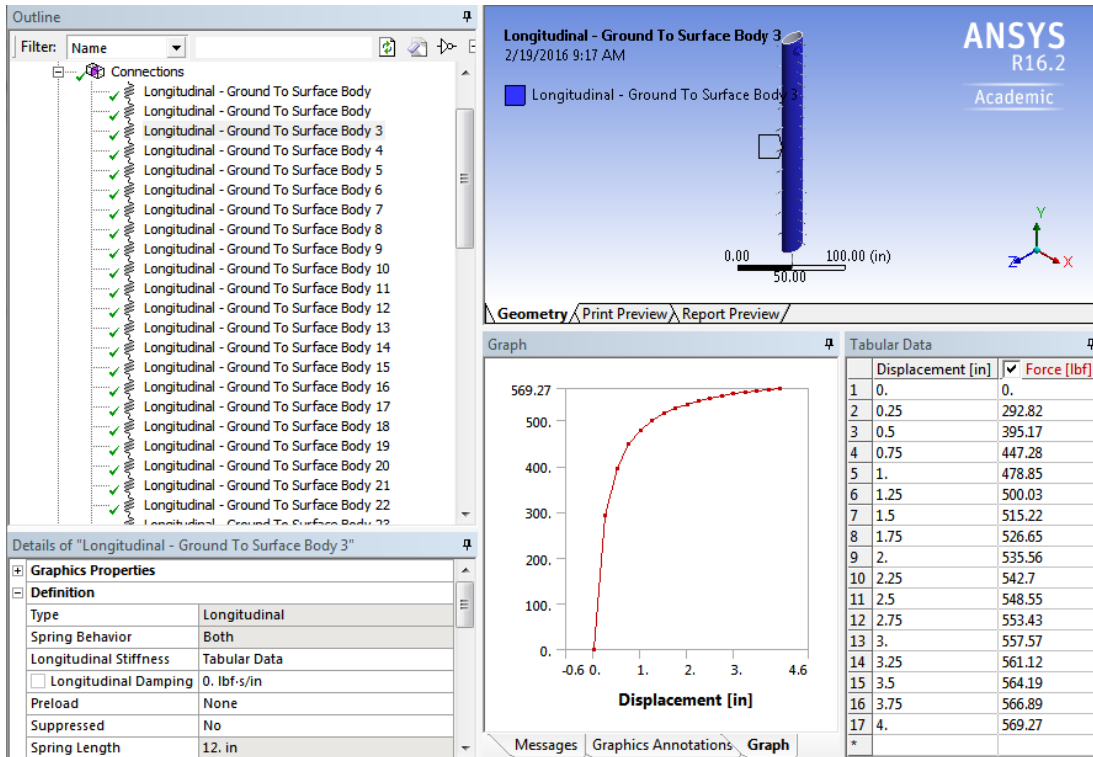
Figure 38 – Lateral Spring model for Soft Clay
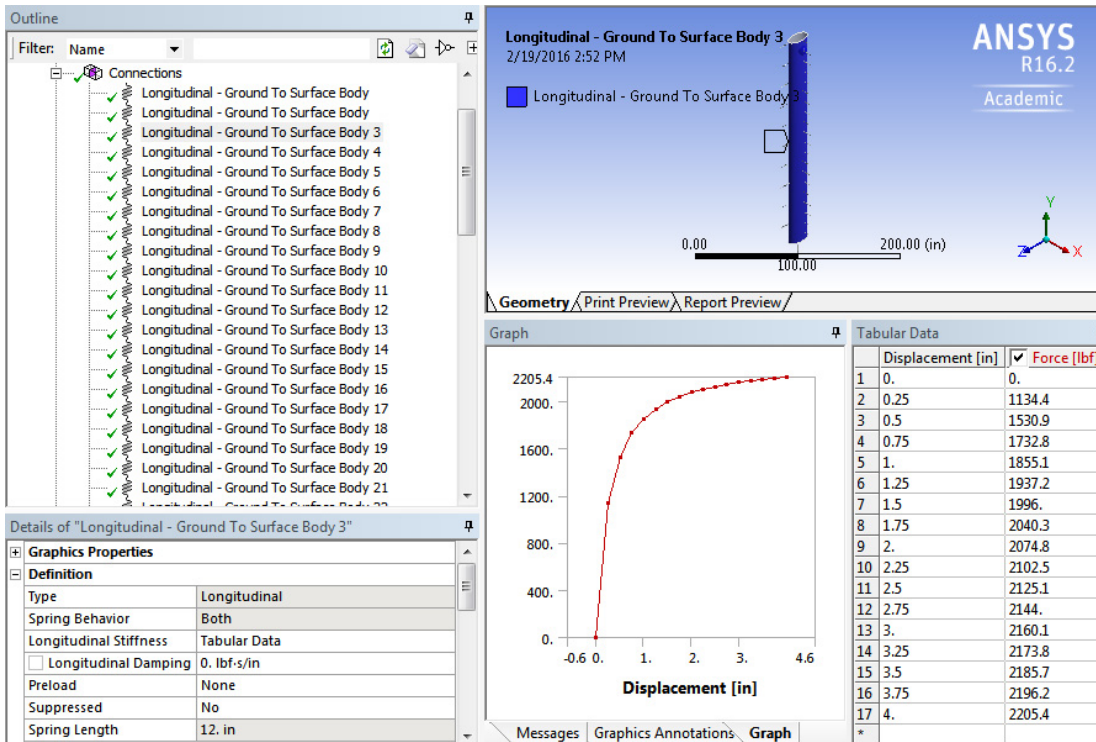
Figure 39 – Lateral soil spring model for Stiff Clay

101
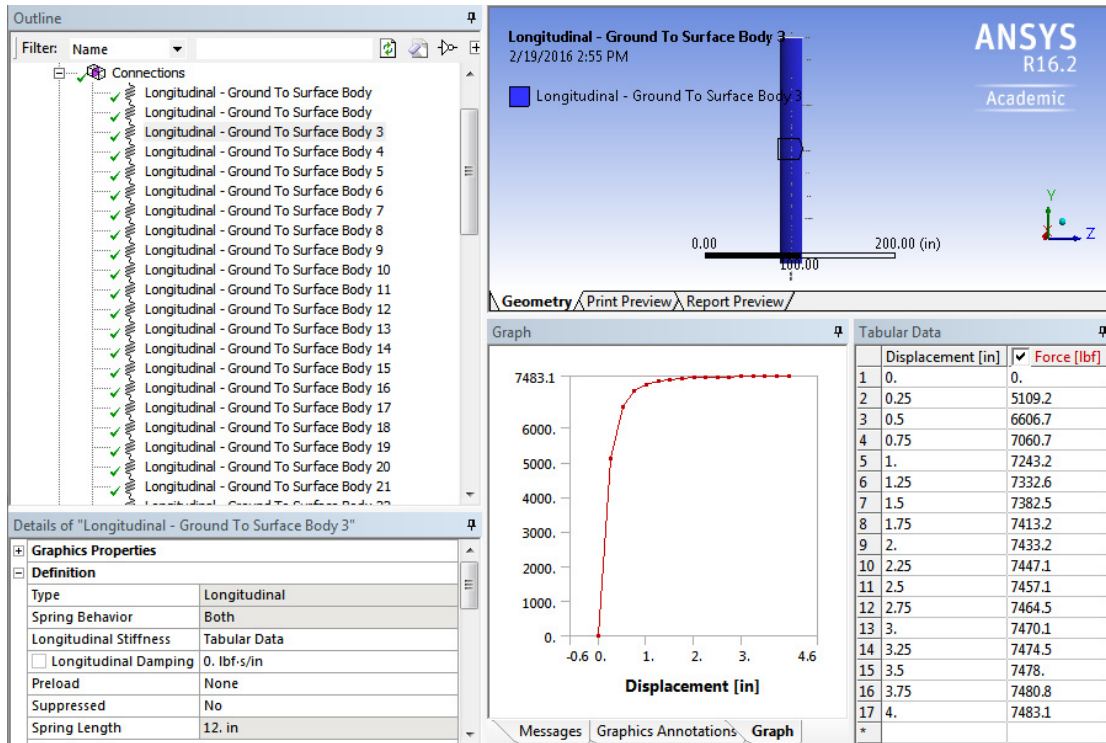
Figure 40 - Lateral soil spring model for Very Stiff Clay
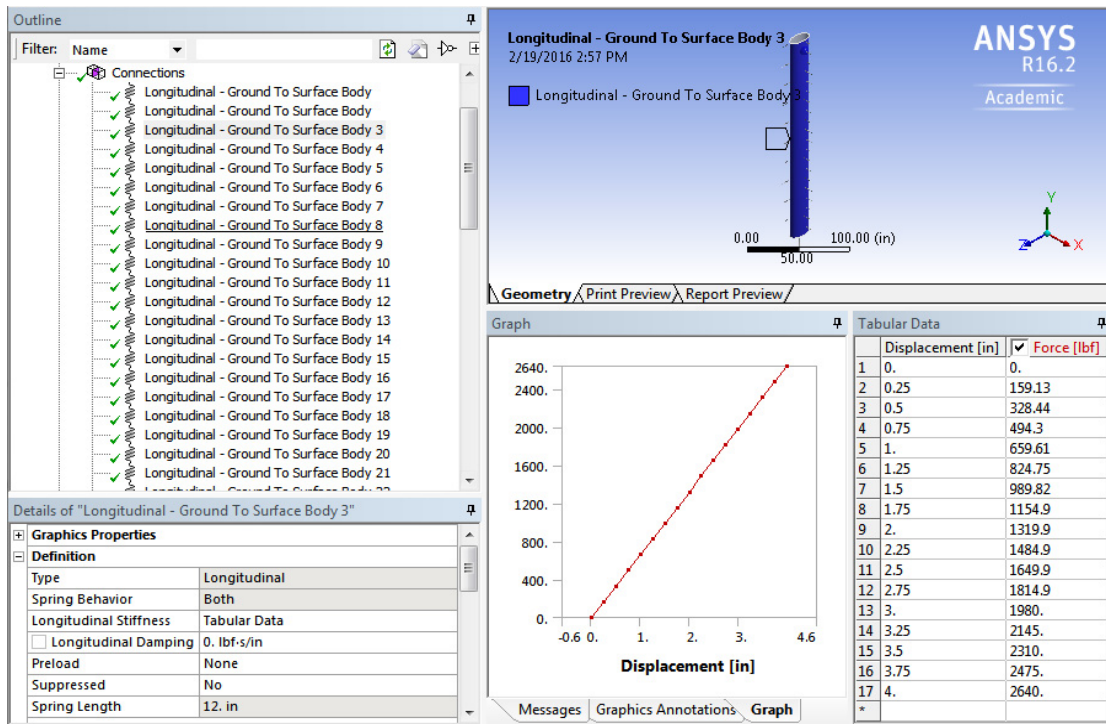
Figure 41 - Lateral soil spring model for Loose Sand
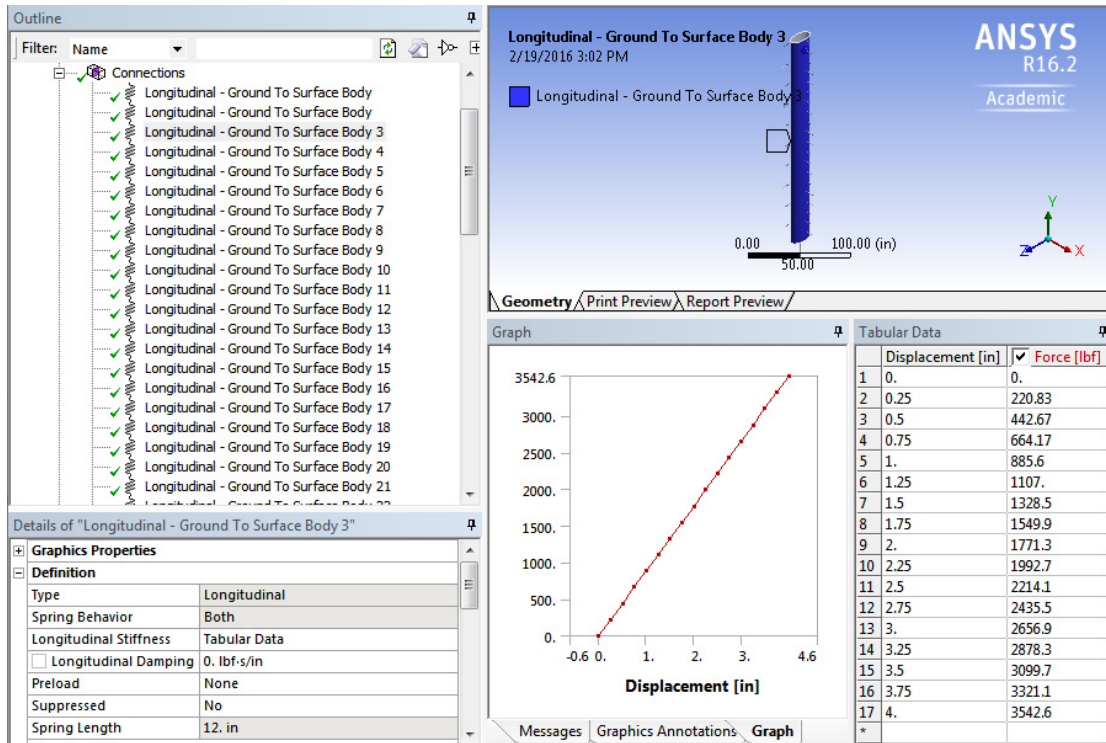
Figure 42 - Lateral soil spring model for Medium Sand
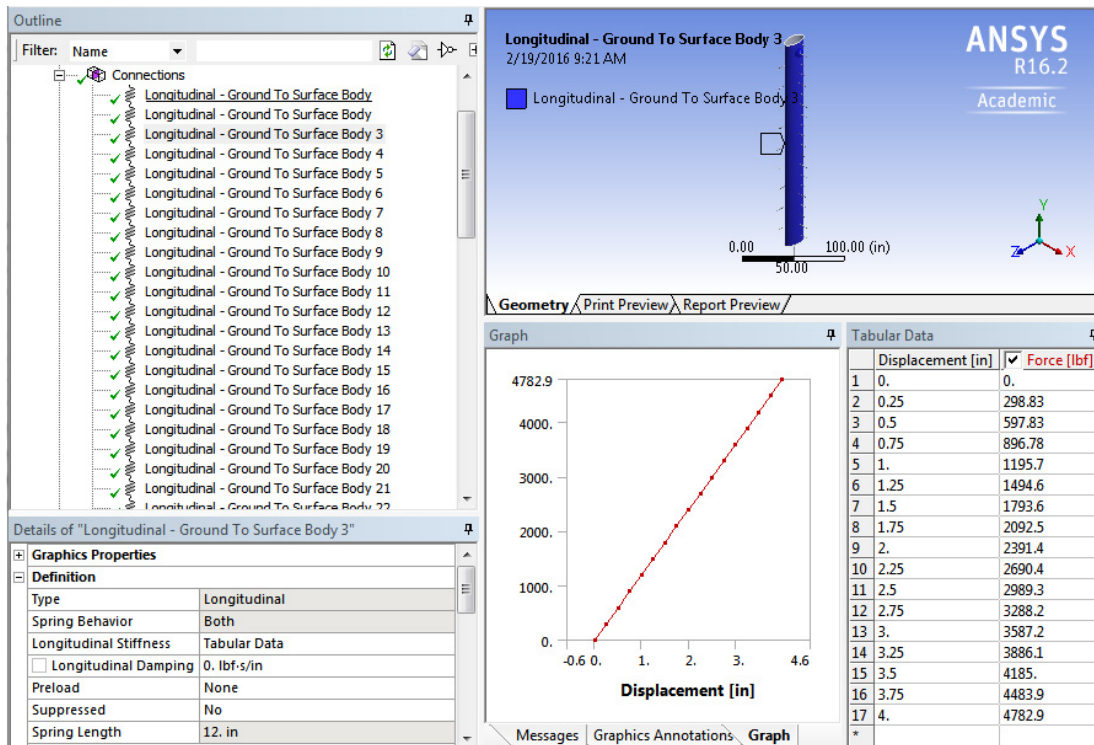
Figure 43 – Lateral soil spring model for Dense Sand

The spring force is evenly distributed on the pile body using the pinball region.

Figure 44 shows the pinball region and the distribution of spring force.
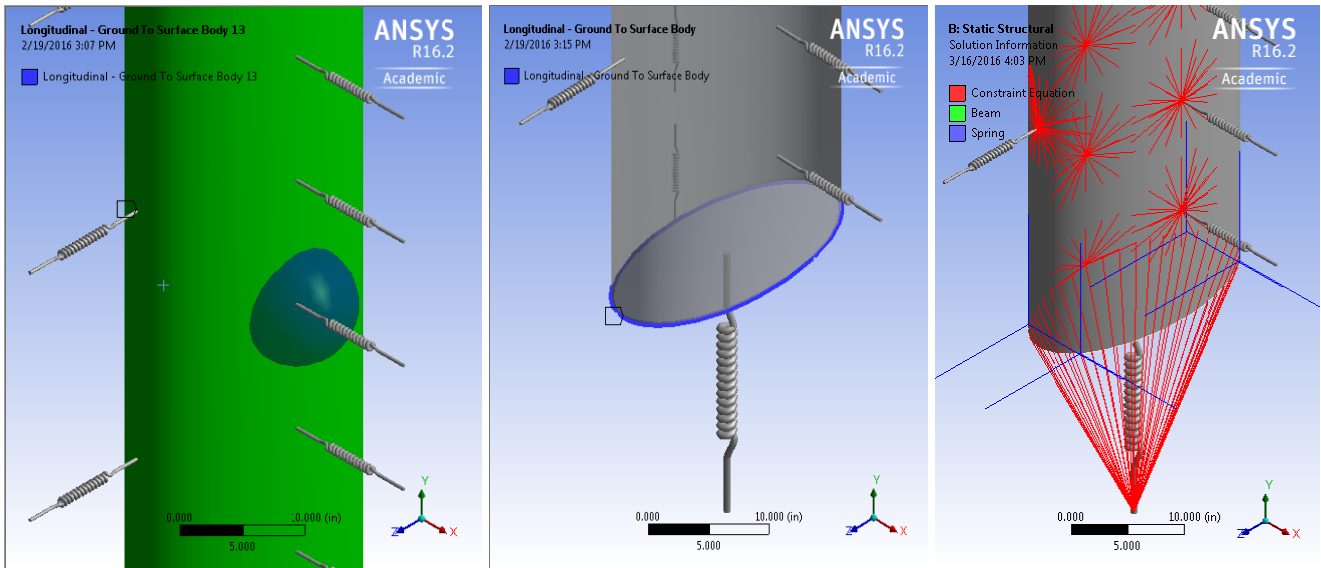
Figure 44 – Pinball region for force distribution

8.12. *Output Results*

The piles are analyzed for the applied loads and displacements. In all cases the maximum principal stress and maximum shear stress are calculated. The ACP post processing unit determines which failure criteria have caused each element to fail. It also calculates the maximum failure ratio for each case. The results are printed in 2D and 3D curves to provide more understanding of how changes in parameters will affect the pile stresses. Figure 45 shows the sample output.
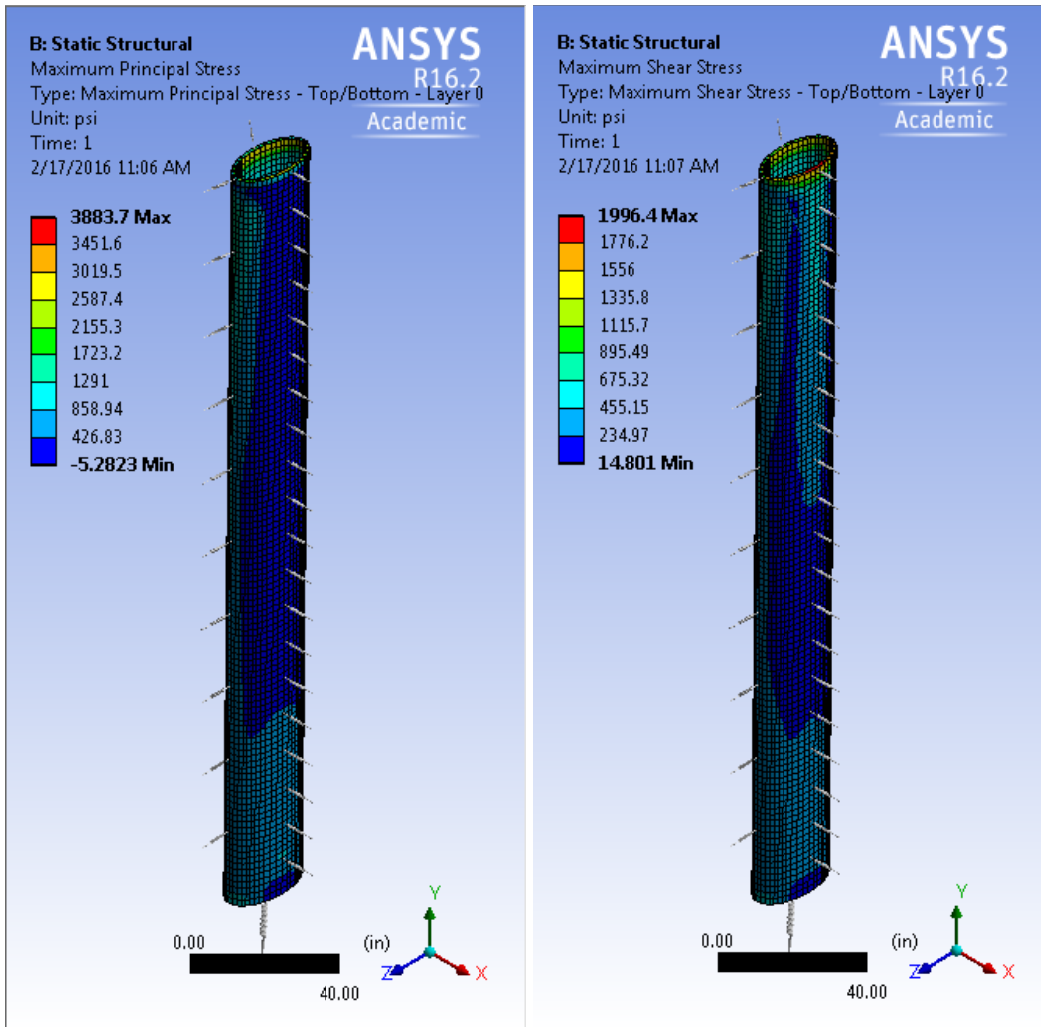
Figure 45 – Maximum principal stress (left) and maximum shear stress (right)

8.13. *Failure criteria*

Figure 46 and

Figure 47 shows the setup of failure criteria. As described previously, the maximum stress, Tsai-Wu and Tsai-Hill criteria are used to define the failure. The failure note "th" indicates those elements have failed under Tsai-Hill criteria.
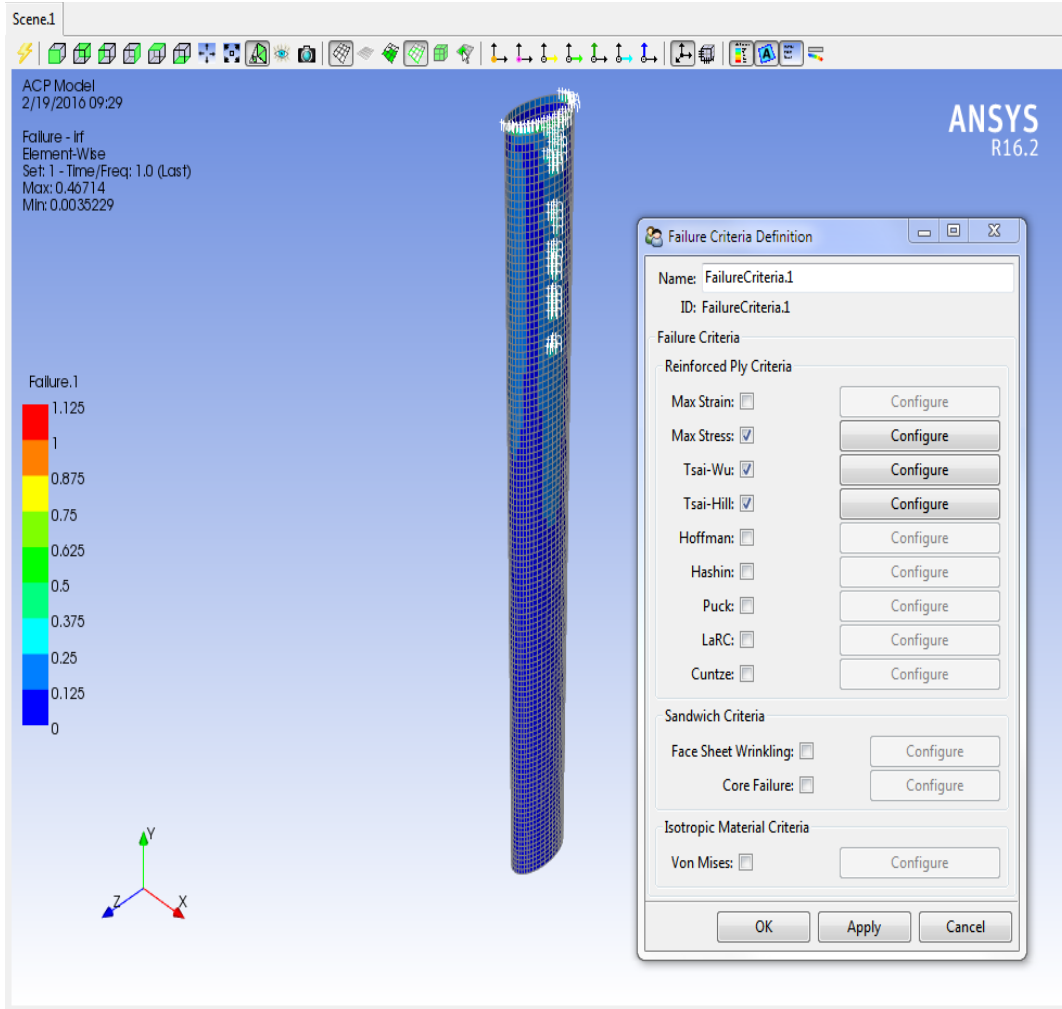
Figure 46 – Governing failure criteria
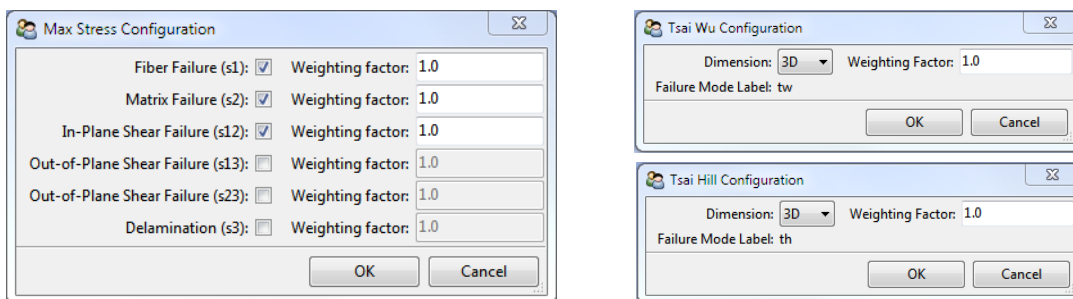
Figure 47 – failure criteria Setup

8.14. *Fiber Orientation Angle*

The fiber orientation angles are defined as positive and negative numbers. Since the filament winding method is used, the absolute values of the angles are equal for all layers. Some models have additional parallel or perpendicular fibers in between usual layers. The layers parallel to the pile axis can be hand laid once each layer is complete. The perpendicular layers can be created using the same winding machine but with very low speed of fiber guide relative to mandrel rotation. (See Figure 16) The filament winding method offers another possible section which has a different orientation angle for each layer. Although this may be very uncommon, different angles can simply be achieved by different horizontal movement of the guide relative to mandrel rotation speed which often stays constant. For the piles with very oval cross section the orientation angle may be affected by pile elliptical cross section. In this dissertation it is assumed that this angle stays constant as desired.

9. Soil Nonlinear Model

9.1. Lateral Soil Resistance

The soil characteristics in tile soil-pile problem can be described by three types of soil resistance-displacement curves: lateral resistance-displacement (p-y) curves; longitudinal load-slip (f-z) curves; and pile tip load-settlement (q-z) curves. The p-y curves represent the relationship between the lateral soil pressure against the pile (force per unit length of pile) and the corresponding lateral pile displacement. The f-z curves describe the relationship between skin friction (force per unit length of pile) and the relative vertical displacement between the pile and the soil. The q-z curves describe the relationship between the bearing stress at the pile tip and the pile tip settlement. The total pile tip force is q times the effective pile tip area. Figure 48 to Figure 53 show typical soil resistance-displacement curves.

All three types of curve assume the soil behavior to be nonlinear and can be developed from basic soil parameters. The modified Ramberg-Osgood model will be used to approximate each of the three types of curve.

Numerical values for these constants are presented in Table 11 to Table 16 for six typical soils. The soil model has three types of nonlinear spring.

The lateral resistance-displacement (p-y) curves are developed using the modified Ramberg-Osgood model). The parameters needed for the modified Ramberg-Osgood equation are the initial lateral stiffness k_h, the ultimate lateral soil resistance p_u and a shape parameter n. These parameters can be obtained using the equations shown in Table 11 to Table 16 headers.

For the design method to be developed in Table 11 to Table 16, the rather

complicated variation of soil properties with depth has also been used. Instead,

simpler expressions for k_h and p_u are used. For cohesive soils (clay), both k_h and

p_u will be assumed to have a constant value for all depths.

(Equation 9-1)

$$k_h = 67\ c_u$$

(Equation 9-2)

$$p_u = 9\ c_u\ B$$

For cohesionless soils (sand), both k_h and p_u will be assumed to vary linearly with

depth.

(Equation 9-3)

$$k_h = n_h x$$

(Equation 9-4)

$$n_h = \frac{J\gamma}{1.35}$$

(Equation 9-5)

$$p_u = \left(3\gamma B k_p\right)x$$

The value n_h is the constant of subgrade reaction. (A. M. Amde August 1984)

As shown in Table 11 to Table 16, the highlighted green columns represent the

simpler solutions compared to the original equation. The following equations

represent the modified Ramberg-Osgood model for lateral resistance.

(Equation 9-6): p-y lateral resistance

$$p = \frac{k_h\, y}{\left(1 + \left|\frac{y}{y_u}\right|^n\right)^{1/n}}$$

in which: $y_u = \frac{p_u}{k_h}$

k_h = Initial Lateral Stiffness

p = Generalized Soil resistance

p_u = Ultimate lateral soil resistance

n = Shape Parameter

y = Generalized displacement

This model offers certain advantages over the other soil models and also includes the

commonly used hyperbola as a special case. The soil lateral resistance has been

calculated for three types of clay and three types of sand. The following tables and

graphs show the calculated values. (A. M. Amde August 1984)

Table 11 – Lateral Resistance calculation for Soft Clay

Blow Count	Unit Weight	Undrained Cohesion	Shape Parameter	Pile Width	Depth from Surface	Ultimate Lateral soil resistance		Simplified Ultimate Lateral Resistance	Initial Lateral Stiffness	Simplified Initial lateral Stiffness	Ultimate Displacement	Generalized Displacement	Generalized Lateral Resistance
N	γ (pcf)	C_u (psf)	n	B (ft)	x (ft)	P_u (klf)	P_u (k/in)	$P_u = 9\, c_u\, B$ (klf)	k_h (ksf)	$k_h = 67c_u$ (ksf)	$y_u = p_u / k_h$ (in)	y (in)	p (klf)
3	100	405	1	2	0	2.4	0.2	7.29	24	27.135	0.2687	0.00	0.00
3	100	405	1	2	1	2.8	0.233	7.29	28.05	27.135	0.2687	0.25	0.29
3	100	405	1	2	2	3.2	0.267	7.29	32.1	27.135	0.2687	0.50	0.40
3	100	405	1	2	3	3.6	0.3	7.29	36.15	27.135	0.2687	0.75	0.45
3	100	405	1	2	4	4	0.333	7.29	40.2	27.135	0.2687	1.00	0.48
3	100	405	1	2	5	4.4	0.367	7.29	44.25	27.135	0.2687	1.25	0.50
3	100	405	1	2	6	4.8	0.4	7.29	48.3	27.135	0.2687	1.50	0.52
3	100	405	1	2	7	5.2	0.433	7.29	52.35	27.135	0.2687	1.75	0.53
3	100	405	1	2	8	5.6	0.467	7.29	56.4	27.135	0.2687	2.00	0.54
3	100	405	1	2	9	6	0.5	7.29	60.45	27.135	0.2687	2.25	0.54
3	100	405	1	2	10	6.4	0.533	7.29	64.5	27.135	0.2687	2.50	0.55
3	100	405	1	2	11	6.8	0.567	7.29	68.55	27.135	0.2687	2.75	0.55
3	100	405	1	2	12	7.2	0.6	7.29	72.6	27.135	0.2687	3.00	0.56
3	100	405	1	2	13	7.2	0.6	7.29	73	27.135	0.2687	3.25	0.56
3	100	405	1	2	14	7.2	0.6	7.29	73	27.135	0.2687	3.50	0.56
3	100	405	1	2	15	7.2	0.6	7.29	73	27.135	0.2687	3.75	0.57
3	100	405	1	2	16	7.2	0.6	7.29	73	27.135	0.2687	4.00	0.57
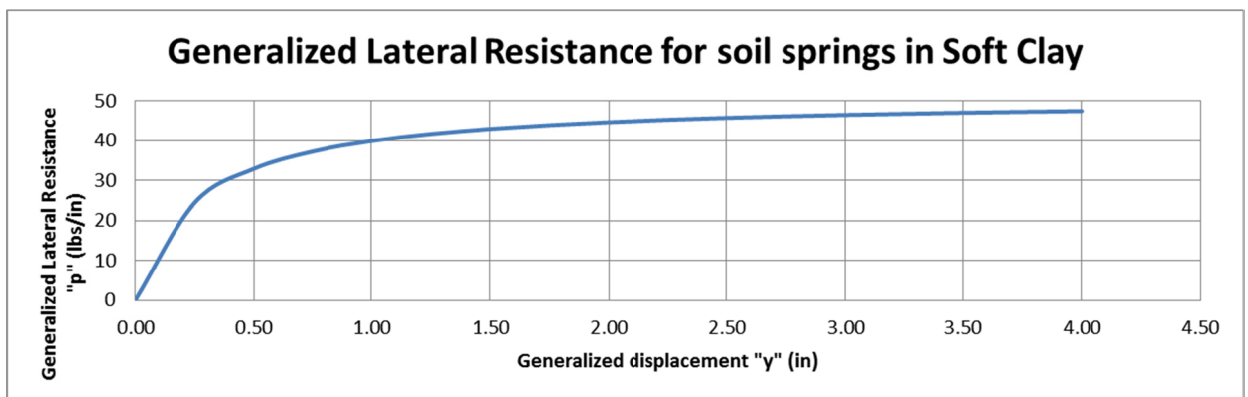
Figure 48 – Lateral Resistance curve for Soft clay

Table 12 – Lateral Resistance calculation for Stiff Clay

Blow Count	Unit Weight	Undrained Cohesion	Shape Parameter	Pile Width	Depth from Surface	Ultimate Lateral soil resistance		Simplified Ultimate Lateral Resistance	Initial Lateral Stiffness	Simplified Initial lateral Stiffness	Ultimate Displacement	Generalized Displacement	Generalized Lateral Resistance
N	γ (pcf)	C_u (psf)	n	B (ft)	x (ft)	P_u (klf)	P_u (k/in)	$P_u = 9\,c_u\,B$ (klf)	k_h (ksf)	$k_h = 67c_u$ (ksf)	$y_u = p_u / k_h$ (in)	y (in)	p (klf)
15	120	1569	1	2	0	9.4	0.783	28.242	190	105.123	0.2687	0.00	0.00
15	120	1569	1	2	1	10.42	0.868	28.242	210.3	105.123	0.2687	0.25	1.13
15	120	1569	1	2	2	11.44	0.953	28.242	230.6	105.123	0.2687	0.50	1.53
15	120	1569	1	2	3	12.46	1.038	28.242	250.9	105.123	0.2687	0.75	1.73
15	120	1569	1	2	4	13.48	1.123	28.242	271.2	105.123	0.2687	1.00	1.86
15	120	1569	1	2	5	14.5	1.208	28.242	291.5	105.123	0.2687	1.25	1.94
15	120	1569	1	2	6	15.52	1.293	28.242	311.8	105.123	0.2687	1.50	2.00
15	120	1569	1	2	7	16.54	1.378	28.242	332.1	105.123	0.2687	1.75	2.04
15	120	1569	1	2	8	17.56	1.463	28.242	352.4	105.123	0.2687	2.00	2.07
15	120	1569	1	2	9	18.58	1.548	28.242	372.7	105.123	0.2687	2.25	2.10
15	120	1569	1	2	10	19.6	1.633	28.242	393	105.123	0.2687	2.50	2.13
15	120	1569	1	2	11	20.62	1.718	28.242	413.3	105.123	0.2687	2.75	2.14
15	120	1569	1	2	12	21.64	1.803	28.242	433.6	105.123	0.2687	3.00	2.16
15	120	1569	1	2	13	22.66	1.888	28.242	453.9	105.123	0.2687	3.25	2.17
15	120	1569	1	2	14	23.68	1.973	28.242	474.2	105.123	0.2687	3.50	2.19
15	120	1569	1	2	15	24.7	2.058	28.242	494.5	105.123	0.2687	3.75	2.20
15	120	1569	1	2	16	25.72	2.143	28.242	514.8	105.123	0.2687	4.00	2.21
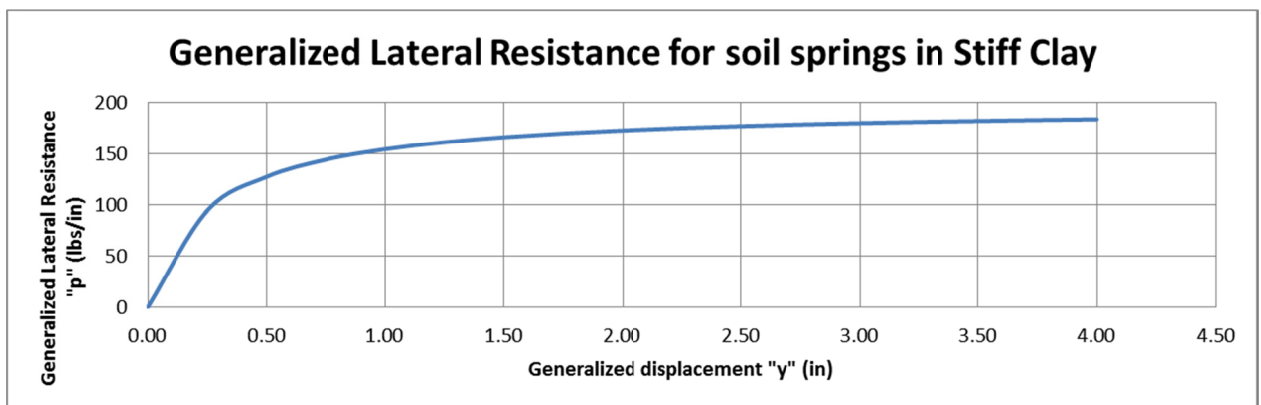
Figure 49 – Lateral Resistance curve for Stiff clay

Table 13 – Lateral Resistance calculation for Very Stiff Clay

Blow Count	Unit Weight	Undrained Cohesion	Shape Parameter	Pile Width	Depth from Surface	Ultimate Lateral soil resistance		Simplified Ultimate Lateral Resistance	Initial Lateral Stiffness	Simplified Initial lateral Stiffness	Ultimate Displacement	Generalized Displacement	Generalized Lateral Resistance
N	γ (pcf)	C_u (psf)	n	B (ft)	x (ft)	P_u (klf)	P_u (k/in)	$P_u = 9$ c_u B (klf)	k_h (ksf)	$k_h =$ $67c_u$ (ksf)	$y_u = p_u/$ k_h (in)	y (in)	p (klf)
50	130	5000	2	2	0	2.4	0.2	90	24	335	0.2687	0.00	0.00
50	130	5000	2	2	1	2.8	0.233	90	28.05	335	0.2687	0.25	5.11
50	130	5000	2	2	2	3.2	0.267	90	32.1	335	0.2687	0.50	6.61
50	130	5000	2	2	3	3.6	0.3	90	36.15	335	0.2687	0.75	7.06
50	130	5000	2	2	4	4	0.333	90	40.2	335	0.2687	1.00	7.24
50	130	5000	2	2	5	4.4	0.367	90	44.25	335	0.2687	1.25	7.33
50	130	5000	2	2	6	4.8	0.4	90	48.3	335	0.2687	1.50	7.38
50	130	5000	2	2	7	5.2	0.433	90	52.35	335	0.2687	1.75	7.41
50	130	5000	2	2	8	5.6	0.467	90	56.4	335	0.2687	2.00	7.43
50	130	5000	2	2	9	6	0.5	90	60.45	335	0.2687	2.25	7.45
50	130	5000	2	2	10	6.4	0.533	90	64.5	335	0.2687	2.50	7.46
50	130	5000	2	2	11	6.8	0.567	90	68.55	335	0.2687	2.75	7.46
50	130	5000	2	2	12	7.2	0.6	90	72.6	335	0.2687	3.00	7.47
50	130	5000	2	2	13	7.2	0.6	90	73	335	0.2687	3.25	7.47
50	130	5000	2	2	14	7.2	0.6	90	73	335	0.2687	3.50	7.48
50	130	5000	2	2	15	7.2	0.6	90	73	335	0.2687	3.75	7.48
50	130	5000	2	2	16	7.2	0.6	90	73	335	0.2687	4.00	7.48
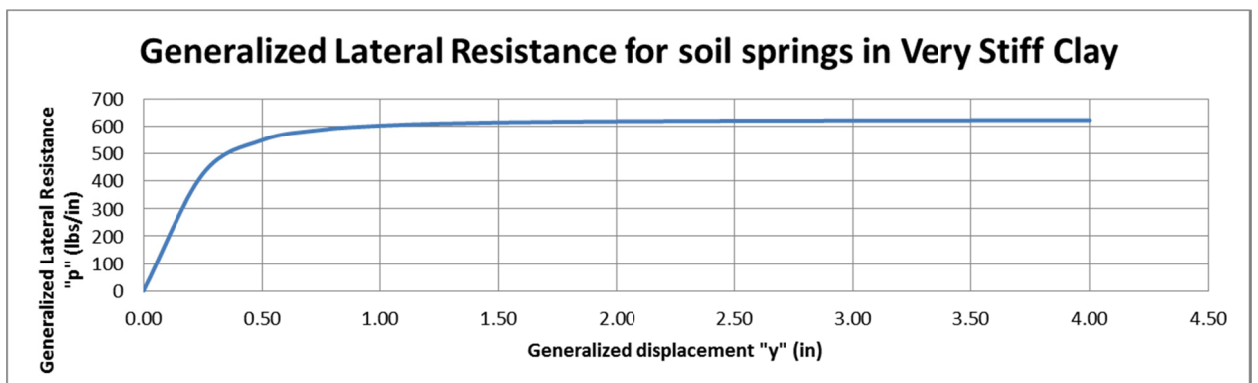
Figure 50 – Lateral Resistance curve for Very Stiff clay

113

Table 14 – Lateral Resistance calculation for Loose Sand

Unit Weight	Angle of Friction	Shape Parameter	Pile Width	Depth from surface	Ultimate Lateral soil resistance	Passive Pressure Coefficient	Simplified Ultimate Lateral Resistance	Initial Lateral Stiffness	Cohesionless soil parametes		Initial lateral Stiffness (Simplified)	Ultimate Displacement	Generalized Displacement	Generalized Lateral Resistance
γ (pcf)	φ (deg)	n	B (ft)	x (ft)	P_u (klf)	kp	$P_u = (3\,\gamma\,B\,k_p)\times$ (klf)	k_h (ksf)	J	$n_h = J\,\gamma\,/1.35$	$k_h = n_h\,x$ (ksf)	$y_u = p_u/k_h$ (in)	y (in)	p (klf)
110	30	3	2	0	0.0058	3.00	0	0.16	200	16,296	0	0.1215	0.00	0.00
110	30	3	2	1	0.72	3.00	2	16	200	16,296	16	0.1215	0.25	0.16
110	30	3	2	2	1.72	3.00	4	32	200	16,296	33	0.1215	0.50	0.33
110	30	3	2	3	3	3.00	6	48	200	16,296	49	0.1215	0.75	0.49
110	30	3	2	4	4.56	3.00	8	64	200	16,296	65	0.1215	1.00	0.66
110	30	3	2	5	6.4	3.00	10	80	200	16,296	81	0.1215	1.25	0.82
110	30	3	2	6	8.52	3.00	12	96	200	16,296	98	0.1215	1.50	0.99
110	30	3	2	7	10.92	3.00	14	112	200	16,296	114	0.1215	1.75	1.15
110	30	3	2	8	13.6	3.00	16	128	200	16,296	130	0.1215	2.00	1.32
110	30	3	2	9	16.56	3.00	18	144	200	16,296	147	0.1215	2.25	1.48
110	30	3	2	10	19.8	3.00	20	160	200	16,296	163	0.1215	2.50	1.65
110	30	3	2	11	23.32	3.00	22	176	200	16,296	179	0.1215	2.75	1.81
110	30	3	2	12	27.12	3.00	24	192	200	16,296	196	0.1215	3.00	1.98
110	30	3	2	13	31.2	3.00	26	208	200	16,296	212	0.1215	3.25	2.14
110	30	3	2	14	35.56	3.00	28	224	200	16,296	228	0.1215	3.50	2.31
110	30	3	2	15	40.2	3.00	30	240	200	16,296	244	0.1215	3.75	2.47
110	30	3	2	16	45.12	3.00	32	256	200	16,296	261	0.1215	4.00	2.64

Generalized Lateral Resistance for soil springs in Loose Sand
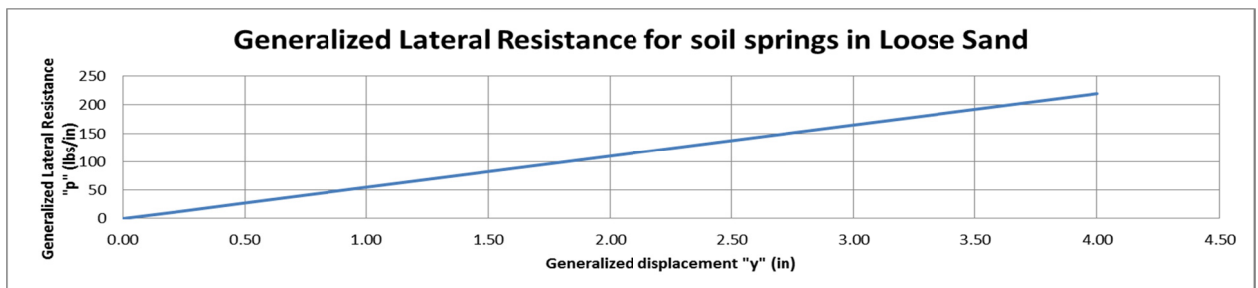
Figure 51 – Lateral Resistance curve for Loose Sand

Table 15 – Lateral Resistance calculation for Medium Sand

Unit Weight γ (pcf)	Angle of Friction φ (deg)	Shape Parameter n	Pile Width B (ft)	Depth from surface x (ft)	Ultimate Lateral soil resistance P_u (klf)	Passive Pressure Coefficient kp	Simplified Ultimate Lateral Resistance $P_u = (3\gamma B k_p) x$ (klf)	Initial Lateral Stiffness k_h (ksf)	Cohesionless soil parametes J	$n_h = J\gamma/1.35$	Initial lateral Stiffness (Simplified) $k_h = n_h x$ (ksf)	Ultimate Displacement $y_u = p_u/k_h$ (in)	Generalized Displacement y (in)	Generalized Lateral Resistance p (klf)
120	35	3	2	0	0.0082	3.69	0	0.53	600	53,333	1	0.0498	0.00	0.00
120	35	3	2	1	1.13	3.69	3	53	600	53,333	53	0.0498	0.25	0.22
120	35	3	2	2	2.88	3.69	5	106	600	53,333	107	0.0498	0.50	0.44
120	35	3	2	3	5.25	3.69	8	159	600	53,333	160	0.0498	0.75	0.66
120	35	3	2	4	8.24	3.69	11	212	600	53,333	213	0.0498	1.00	0.89
120	35	3	2	5	11.85	3.69	13	265	600	53,333	267	0.0498	1.25	1.11
120	35	3	2	6	16.08	3.69	16	318	600	53,333	320	0.0498	1.50	1.33
120	35	3	2	7	20.93	3.69	19	371	600	53,333	373	0.0498	1.75	1.55
120	35	3	2	8	26.4	3.69	21	424	600	53,333	427	0.0498	2.00	1.77
120	35	3	2	9	32.49	3.69	24	477	600	53,333	480	0.0498	2.25	1.99
120	35	3	2	10	39.2	3.69	27	530	600	53,333	533	0.0498	2.50	2.21
120	35	3	2	11	46.53	3.69	29	583	600	53,333	587	0.0498	2.75	2.44
120	35	3	2	12	54.48	3.69	32	636	600	53,333	640	0.0498	3.00	2.66
120	35	3	2	13	63.05	3.69	35	689	600	53,333	693	0.0498	3.25	2.88
120	35	3	2	14	72.24	3.69	37	742	600	53,333	747	0.0498	3.50	3.10
120	35	3	2	15	82.05	3.69	40	795	600	53,333	800	0.0498	3.75	3.32
120	35	3	2	16	92.48	3.69	43	848	600	53,333	853	0.0498	4.00	3.54

Figure 52 – Lateral Resistance curve for Medium Sand

Table 16 – Lateral Resistance calculation for Dense Sand

Unit Weight γ (pcf)	Angle of Friction φ (deg)	Shape Parameter n	Pile Width B (ft)	Depth from surface x (ft)	Ultimate Lateral soil resistance P_u (klf)	Passive Pressure Coefficient kp	Simplified Ultimate Lateral Resistance $P_u = (3\,\gamma\,B\,k_p) \times$ (klf)	Initial Lateral Stiffness k_h (ksf)	Cohesionless soil parametes J	$n_h = J\,\gamma\,/1.35$	Initial lateral Stiffness (Simplified) $k_h = n_h\,x$ (ksf)	Ultimate Displacement $y_u = p_u\,/\,k_h$ (in)	Generalized Displacement y (in)	Generalized Lateral Resistance p (klf)
130	40	3	2	0	0.0115	4.60	0	1.4	1500	144,444	1	0.0248	0.00	0.00
130	40	3	2	1	1.65	4.60	4	140	1500	144,444	144	0.0248	0.25	0.30
130	40	3	2	2	4.32	4.60	7	280	1500	144,444	289	0.0248	0.50	0.60
130	40	3	2	3	8.01	4.60	11	420	1500	144,444	433	0.0248	0.75	0.90
130	40	3	2	4	12.72	4.60	14	560	1500	144,444	578	0.0248	1.00	1.20
130	40	3	2	5	18.45	4.60	18	700	1500	144,444	722	0.0248	1.25	1.49
130	40	3	2	6	25.2	4.60	22	840	1500	144,444	867	0.0248	1.50	1.79
130	40	3	2	7	32.97	4.60	25	980	1500	144,444	1,011	0.0248	1.75	2.09
130	40	3	2	8	41.76	4.60	29	1120	1500	144,444	1,156	0.0248	2.00	2.39
130	40	3	2	9	51.57	4.60	32	1260	1500	144,444	1,300	0.0248	2.25	2.69
130	40	3	2	10	62.4	4.60	36	1400	1500	144,444	1,444	0.0248	2.50	2.99
130	40	3	2	11	74.25	4.60	39	1540	1500	144,444	1,589	0.0248	2.75	3.29
130	40	3	2	12	87.12	4.60	43	1680	1500	144,444	1,733	0.0248	3.00	3.59
130	40	3	2	13	101.01	4.60	47	1820	1500	144,444	1,878	0.0248	3.25	3.89
130	40	3	2	14	115.92	4.60	50	1960	1500	144,444	2,022	0.0248	3.50	4.19
130	40	3	2	15	131.85	4.60	54	2100	1500	144,444	2,167	0.0248	3.75	4.48
130	40	3	2	16	148.8	4.60	57	2240	1500	144,444	2,311	0.0248	4.00	4.78
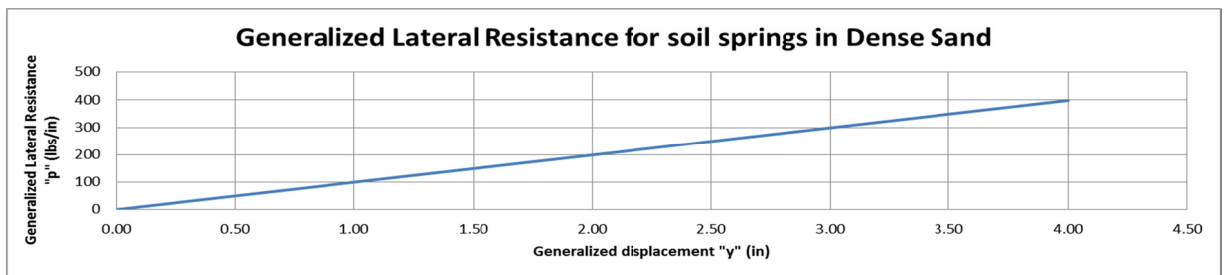
Figure 53 – Lateral Resistance curve for Dense Sand

The load-slip (f-z) and pile tip load-settlement (q-z) curves are developed using the modified Ramberg-Osgood model).

9.2. *Vertical Slip Resistance*

The parameters needed for the f-z curve are the initial vertical stiffness k_v , the maximum shear stress f_{max}, and the shape parameter n. These parameters are shown in the header of Table 17 to Table 22.

A similar approach has been taken for slip resistance. The following equations represent the modified Ramberg-Osgood model.

The factor $\alpha = 1.0$ is used to obtain the soil/pile adhesion, given the soil cohesion.

(Equation 9-7): f-z Vertical Slip Resistance

$$f = \frac{k_v\, z}{\left(1 + \left|\frac{z}{z_u}\right|^n\right)^{1/n}}$$

in which: $z_u = \frac{f_{max}}{k_v}$

k_v = Initial Slip resistance, q= Generalized Soil resistance

f_{max} = Ultimate soil Slip resistance

n = Shape Parameter

z = Generalized displacement

9.3. *Vertical Bearing Resistance*

The parameters needed for the q-z curve are the initial point stiffness k_q , the maximum bearing stress q_{max}, and the shape parameter n. These parameters are shown on header of Table 23 to Table 28.

The following equations represent the modified Ramberg-Osgood model:

(Equation 9-8): f-z Vertical End Bearing Resistance

$$q = \frac{k_q \, z}{\left(1 + \left|\frac{z}{z_u}\right|^n\right)^{1/n}}$$

in which: $\quad z_u = \frac{q_{max}}{k_q}$

k_q = Initial Point Stiffness, q= Generalized Soil resistance

q_{max} = Ultimate soil Bearing resistance

n = Shape Parameter

z = Generalized displacement

Table 17 – Vertical Slip Resistance calculation for Soft Clay

Blow Count	Shape Parameter	Gross Permiter of pile	Undrained Cohesion of Clay	Shear Strength Reduction Factor	Adhesion of soil and pile	Maximum Shear Stress	Simplified Maximum Shear Stress	Relative Displacement to develop f_{max}	Initial Vertical Stiffness	Simplified Initial Vertical Stiffness		Generalized Displacement	Generalized Slip Resistance
N	n	l_g (ft)	$C_u =$ 97 N+114 (psf)	α	$C_a =$ αC_a (psf)	$f_{max} =$ $min(l_g c_u$, $l_g c_a)$ (klf)	f_{max} (klf)	z_c (in)	$k_v = 10$ f_{max} / z_c (ksf)	k_v (ksf)	$z_u =$ f_{max}/k_v (in)	z (in)	q (klf)
3	1	5	405	1	405	1.96	1.34	0.25	939.6	640	0.0251	0.00	0.00
3	1	5	405	1	405	1.96	1.34	0.25	939.6	640	0.0251	0.25	1.22
3	1	5	405	1	405	1.96	1.34	0.25	939.6	640	0.0251	0.50	1.28
3	1	5	405	1	405	1.96	1.34	0.25	939.6	640	0.0251	0.75	1.30
3	1	5	405	1	405	1.96	1.34	0.25	939.6	640	0.0251	1.00	1.31
3	1	5	405	1	405	1.96	1.34	0.25	939.6	640	0.0251	1.25	1.31
3	1	5	405	1	405	1.96	1.34	0.25	939.6	640	0.0251	1.50	1.32
3	1	5	405	1	405	1.96	1.34	0.25	939.6	640	0.0251	1.75	1.32
3	1	5	405	1	405	1.96	1.34	0.25	939.6	640	0.0251	2.00	1.32
3	1	5	405	1	405	1.96	1.34	0.25	939.6	640	0.0251	2.25	1.33
3	1	5	405	1	405	1.96	1.34	0.25	939.6	640	0.0251	2.50	1.33
3	1	5	405	1	405	1.96	1.34	0.25	939.6	640	0.0251	2.75	1.33
3	1	5	405	1	405	1.96	1.34	0.25	939.6	640	0.0251	3.00	1.33
3	1	5	405	1	405	1.96	1.34	0.25	939.6	640	0.0251	3.25	1.33
3	1	5	405	1	405	1.96	1.34	0.25	939.6	640	0.0251	3.50	1.33
3	1	5	405	1	405	1.96	1.34	0.25	939.6	640	0.0251	3.75	1.33
3	1	5	405	1	405	1.96	1.34	0.25	939.6	640	0.0251	4.00	1.33
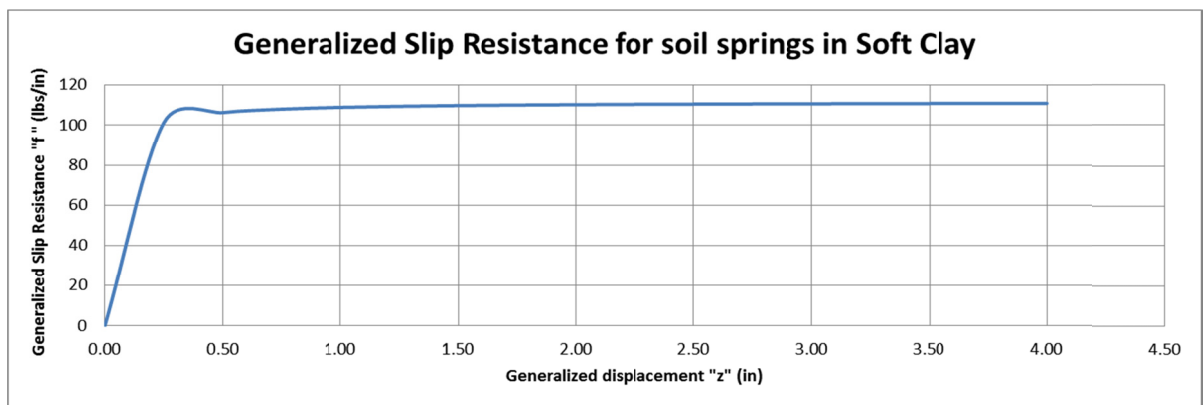
Figure 54 – Vertical Slip Resistance curve for Soft Clay

Table 18 – Vertical Slip Resistance calculation for Stiff Clay

Blow Count	Shape Parameter	Gross Perimeter of pile	Undrained Cohesion of Clay	Shear Strength Reduction Factor	Adhesion of soil and pile	Maximum Shear Stress	Simplified Maximum Shear Stress	Relative Displacement to develop f_{max}	Initial Vertical Stiffness	Simplified Initial Vertical Stiffness		Generalized Displacement	Generalized Slip Resistance
N	n	l_g (ft)	$C_u = 97 N+114$ (psf)	α	$C_a = \alpha C_a$ (psf)	$f_{max} = min(l_g c_u, l_g c_a)$ (klf)	f_{max} (klf)	z_c (in)	$k_v = 10 f_{max}/z_c$ (ksf)	k_v (ksf)	$z_u = f_{max}/k_v$ (in)	z (in)	q (klf)
15	1	5	1569	1	1569	7.58	3.86	0.25	3640.1	1850	0.0250	0.00	0.00
15	1	5	1569	1	1569	7.58	3.86	0.25	3640.1	1850	0.0250	0.25	3.51
15	1	5	1569	1	1569	7.58	3.86	0.25	3640.1	1850	0.0250	0.50	3.68
15	1	5	1569	1	1569	7.58	3.86	0.25	3640.1	1850	0.0250	0.75	3.74
15	1	5	1569	1	1569	7.58	3.86	0.25	3640.1	1850	0.0250	1.00	3.77
15	1	5	1569	1	1569	7.58	3.86	0.25	3640.1	1850	0.0250	1.25	3.78
15	1	5	1569	1	1569	7.58	3.86	0.25	3640.1	1850	0.0250	1.50	3.80
15	1	5	1569	1	1569	7.58	3.86	0.25	3640.1	1850	0.0250	1.75	3.81
15	1	5	1569	1	1569	7.58	3.86	0.25	3640.1	1850	0.0250	2.00	3.81
15	1	5	1569	1	1569	7.58	3.86	0.25	3640.1	1850	0.0250	2.25	3.82
15	1	5	1569	1	1569	7.58	3.86	0.25	3640.1	1850	0.0250	2.50	3.82
15	1	5	1569	1	1569	7.58	3.86	0.25	3640.1	1850	0.0250	2.75	3.83
15	1	5	1569	1	1569	7.58	3.86	0.25	3640.1	1850	0.0250	3.00	3.83
15	1	5	1569	1	1569	7.58	3.86	0.25	3640.1	1850	0.0250	3.25	3.83
15	1	5	1569	1	1569	7.58	3.86	0.25	3640.1	1850	0.0250	3.50	3.83
15	1	5	1569	1	1569	7.58	3.86	0.25	3640.1	1850	0.0250	3.75	3.83
15	1	5	1569	1	1569	7.58	3.86	0.25	3640.1	1850	0.0250	4.00	3.84
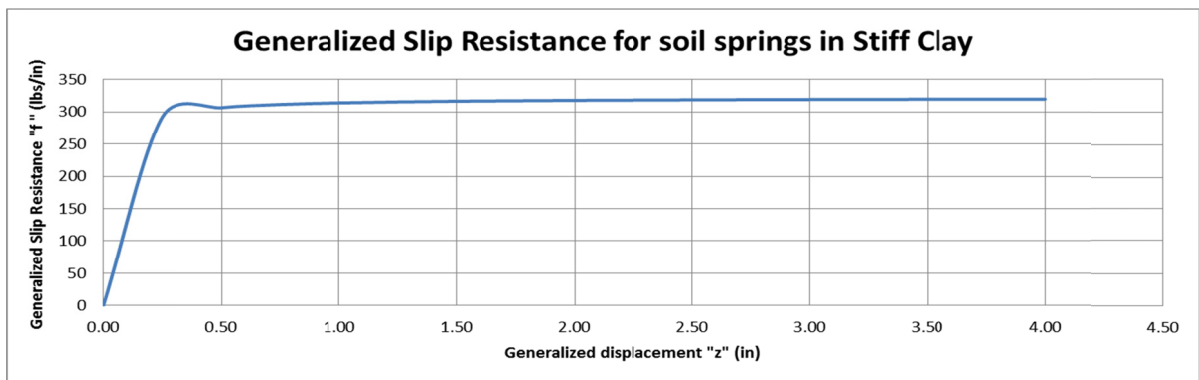
Figure 55 – Vertical Slip Resistance curve for Stiff Clay

Table 19 – Vertical Slip Resistance calculation for Very Stiff Clay

Blow Count	Shape Parameter	Gross Perimeter of pile	Undrained Cohesion of Clay	Shear Strength Reduction Factor	Adhesion of soil and pile	Maximum Shear Stress	Simplified Maximum Shear Stress	Relative Displacement to develop f_{max}	Initial Vertical Stiffness	Simplified Initial Vertical Stiffness		Generalized Displacement	Generalized Slip Resistance
N	n	l_g (ft)	$C_u =$ 97 N+114 (psf)	α	$C_a =$ αC_a (psf)	$f_{max} =$ $min(l_g c_u, l_g c_a)$ (klf)	f_{max} (klf)	z_c (in)	$k_v = 10$ f_{max} / z_c (ksf)	k_v (ksf)	$z_u =$ f_{max}/k_v (in)	z (in)	q (klf)
50	1	5	4964	1	4964	23.99	6.22	0.25	11516.5	2960	0.0252	0.00	0.00
50	1	5	4964	1	4964	23.99	6.22	0.25	11516.5	2960	0.0252	0.25	5.65
50	1	5	4964	1	4964	23.99	6.22	0.25	11516.5	2960	0.0252	0.50	5.92
50	1	5	4964	1	4964	23.99	6.22	0.25	11516.5	2960	0.0252	0.75	6.02
50	1	5	4964	1	4964	23.99	6.22	0.25	11516.5	2960	0.0252	1.00	6.07
50	1	5	4964	1	4964	23.99	6.22	0.25	11516.5	2960	0.0252	1.25	6.10
50	1	5	4964	1	4964	23.99	6.22	0.25	11516.5	2960	0.0252	1.50	6.12
50	1	5	4964	1	4964	23.99	6.22	0.25	11516.5	2960	0.0252	1.75	6.13
50	1	5	4964	1	4964	23.99	6.22	0.25	11516.5	2960	0.0252	2.00	6.14
50	1	5	4964	1	4964	23.99	6.22	0.25	11516.5	2960	0.0252	2.25	6.15
50	1	5	4964	1	4964	23.99	6.22	0.25	11516.5	2960	0.0252	2.50	6.16
50	1	5	4964	1	4964	23.99	6.22	0.25	11516.5	2960	0.0252	2.75	6.16
50	1	5	4964	1	4964	23.99	6.22	0.25	11516.5	2960	0.0252	3.00	6.17
50	1	5	4964	1	4964	23.99	6.22	0.25	11516.5	2960	0.0252	3.25	6.17
50	1	5	4964	1	4964	23.99	6.22	0.25	11516.5	2960	0.0252	3.50	6.18
50	1	5	4964	1	4964	23.99	6.22	0.25	11516.5	2960	0.0252	3.75	6.18
50	1	5	4964	1	4964	23.99	6.22	0.25	11516.5	2960	0.0252	4.00	6.18
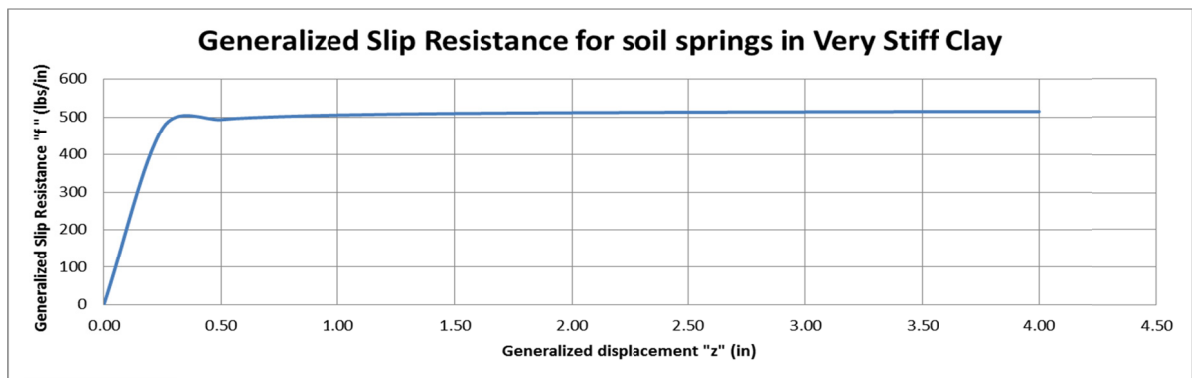
Figure 56 – Vertical Slip Resistance curve for Very Stiff Clay

Table 20 – Vertical Slip Resistance calculation for Loose Sand

Blow Count	Shape Parameter	Gross Permiter of pile	Maximum Shear Stress	Simplified Maximum Shear Stress	Relative Displacement to develop f_{max}	Initial Vertical Stiffness	Simplified Initial Vertical Stiffness		Generalized Displacement	Generalized Slip Resistance
N	n	l_g (ft)	$f_{max} = 0.04\ N\ l_g$ (klf)	f_{max} (klf)	z_c (in)	$k_v = 10\ f_{max} / z_c$ (ksf)	k_v (ksf)	$z_u = f_{max}/k_v$ (in)	z (in)	q (klf)
5	1	5	0.97	0.50	0.4	290.0	150	0.0400	0.00	0.00
5	1	5	0.97	0.50	0.4	290.0	150	0.0400	0.25	0.43
5	1	5	0.97	0.50	0.4	290.0	150	0.0400	0.50	0.46
5	1	5	0.97	0.50	0.4	290.0	150	0.0400	0.75	0.47
5	1	5	0.97	0.50	0.4	290.0	150	0.0400	1.00	0.48
5	1	5	0.97	0.50	0.4	290.0	150	0.0400	1.25	0.48
5	1	5	0.97	0.50	0.4	290.0	150	0.0400	1.50	0.49
5	1	5	0.97	0.50	0.4	290.0	150	0.0400	1.75	0.49
5	1	5	0.97	0.50	0.4	290.0	150	0.0400	2.00	0.49
5	1	5	0.97	0.50	0.4	290.0	150	0.0400	2.25	0.49
5	1	5	0.97	0.50	0.4	290.0	150	0.0400	2.50	0.49
5	1	5	0.97	0.50	0.4	290.0	150	0.0400	2.75	0.49
5	1	5	0.97	0.50	0.4	290.0	150	0.0400	3.00	0.49
5	1	5	0.97	0.50	0.4	290.0	150	0.0400	3.25	0.49
5	1	5	0.97	0.50	0.4	290.0	150	0.0400	3.50	0.49
5	1	5	0.97	0.50	0.4	290.0	150	0.0400	3.75	0.49
5	1	5	0.97	0.50	0.4	290.0	150	0.0400	4.00	0.50
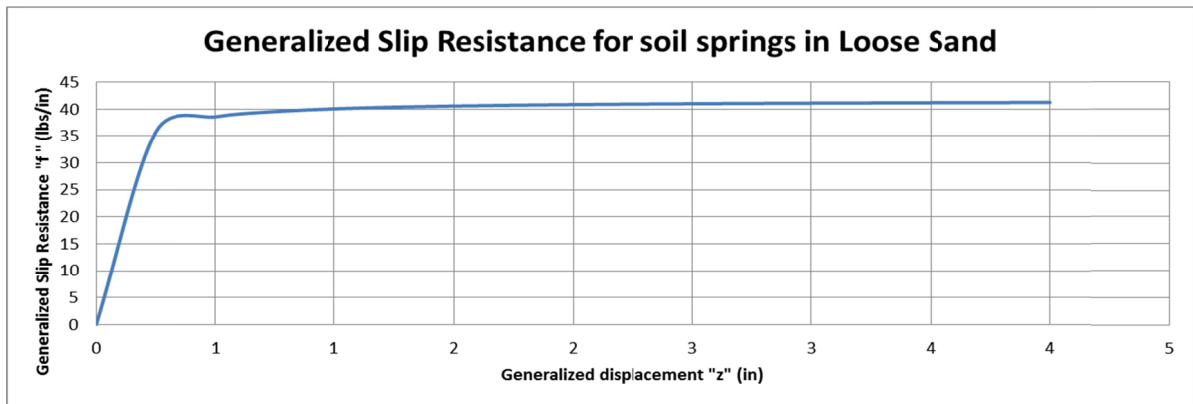
Figure 57 – Vertical Slip Resistance curve for Loose Sand

Table 21 – Vertical Slip Resistance calculation for Medium Sand

Blow Count	Shape Parameter	Gross Permiter of pile	Maximum Shear Stress	Simplified Maximum Shear Stress	Relative Displacement to develop f_{max}	Initial Vertical Stiffness	Simplified Initial Vertical Stiffness		Generalized Displacement	Generalized Slip Resistance
N	n	l_g (ft)	$f_{max} = 0.04\,N\,l_g$ (klf)	f_{max} (klf)	z_c (in)	$k_v = 10\,f_{max} / z_c$ (ksf)	k_v (ksf)	$z_u = f_{max}/k_v$ (in)	z (in)	q (klf)
15	1	5	2.90	1.50	0.4	870.0	450	0.0400	0.00	0.00
15	1	5	2.90	1.50	0.4	870.0	450	0.0400	0.25	1.29
15	1	5	2.90	1.50	0.4	870.0	450	0.0400	0.50	1.39
15	1	5	2.90	1.50	0.4	870.0	450	0.0400	0.75	1.42
15	1	5	2.90	1.50	0.4	870.0	450	0.0400	1.00	1.44
15	1	5	2.90	1.50	0.4	870.0	450	0.0400	1.25	1.45
15	1	5	2.90	1.50	0.4	870.0	450	0.0400	1.50	1.46
15	1	5	2.90	1.50	0.4	870.0	450	0.0400	1.75	1.47
15	1	5	2.90	1.50	0.4	870.0	450	0.0400	2.00	1.47
15	1	5	2.90	1.50	0.4	870.0	450	0.0400	2.25	1.47
15	1	5	2.90	1.50	0.4	870.0	450	0.0400	2.50	1.48
15	1	5	2.90	1.50	0.4	870.0	450	0.0400	2.75	1.48
15	1	5	2.90	1.50	0.4	870.0	450	0.0400	3.00	1.48
15	1	5	2.90	1.50	0.4	870.0	450	0.0400	3.25	1.48
15	1	5	2.90	1.50	0.4	870.0	450	0.0400	3.50	1.48
15	1	5	2.90	1.50	0.4	870.0	450	0.0400	3.75	1.48
15	1	5	2.90	1.50	0.4	870.0	450	0.0400	4.00	1.49
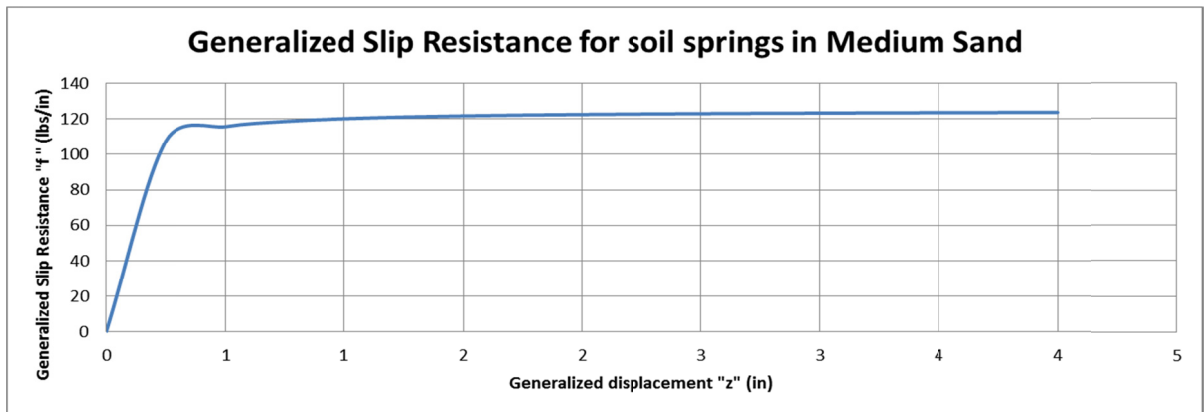
Figure 58 – Vertical Slip Resistance curve for Medium Sand

Table 22 – Vertical Slip Resistance calculation for Dense Sand

Blow Count	Shape Parameter	Gross Permiter of pile	Maximum Shear Stress	Simplified Maximum Shear Stress	Relative Displacement to develop f_{max}	Initial Vertical Stiffness	Simplified Initial Vertical Stiffness		Generalized Displacement	Generalized Slip Resistance
N	n	l_g (ft)	$f_{max} = 0.04\, N\, l_g$ (klf)	f_{max} (klf)	z_c (in)	$k_v = 10\, f_{max} / z_c$ (ksf)	k_v (ksf)	$z_u = f_{max}/k_v$ (in)	z (in)	q (klf)
30	1	5	5.80	3.00	0.4	1740.0	900	0.0400	0.00	0.00
30	1	5	5.80	3.00	0.4	1740.0	900	0.0400	0.25	2.59
30	1	5	5.80	3.00	0.4	1740.0	900	0.0400	0.50	2.78
30	1	5	5.80	3.00	0.4	1740.0	900	0.0400	0.75	2.85
30	1	5	5.80	3.00	0.4	1740.0	900	0.0400	1.00	2.88
30	1	5	5.80	3.00	0.4	1740.0	900	0.0400	1.25	2.91
30	1	5	5.80	3.00	0.4	1740.0	900	0.0400	1.50	2.92
30	1	5	5.80	3.00	0.4	1740.0	900	0.0400	1.75	2.93
30	1	5	5.80	3.00	0.4	1740.0	900	0.0400	2.00	2.94
30	1	5	5.80	3.00	0.4	1740.0	900	0.0400	2.25	2.95
30	1	5	5.80	3.00	0.4	1740.0	900	0.0400	2.50	2.95
30	1	5	5.80	3.00	0.4	1740.0	900	0.0400	2.75	2.96
30	1	5	5.80	3.00	0.4	1740.0	900	0.0400	3.00	2.96
30	1	5	5.80	3.00	0.4	1740.0	900	0.0400	3.25	2.96
30	1	5	5.80	3.00	0.4	1740.0	900	0.0400	3.50	2.97
30	1	5	5.80	3.00	0.4	1740.0	900	0.0400	3.75	2.97
30	1	5	5.80	3.00	0.4	1740.0	900	0.0400	4.00	2.97
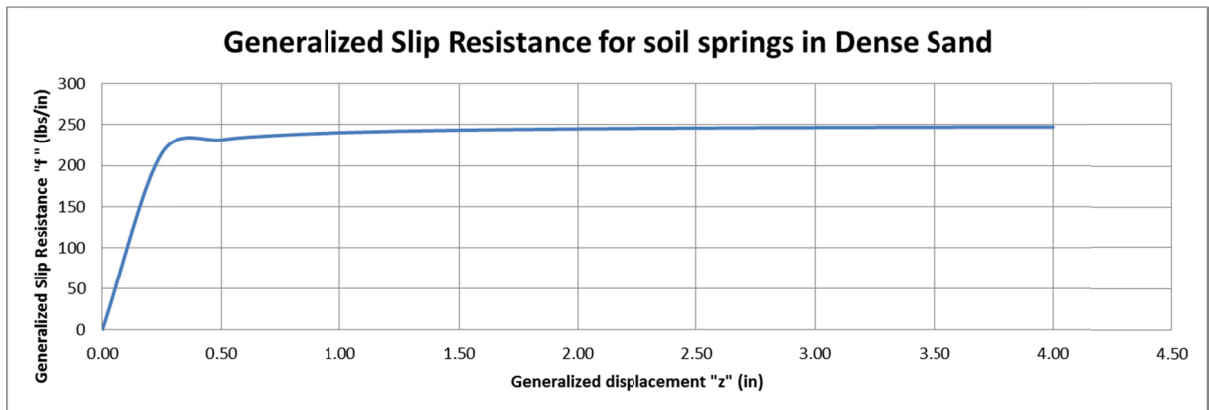
Figure 59 – Vertical Slip Resistance curve for Dense Sand

Table 23 – Vertical End Bearing Resistance calculation for Soft Clay

Blow Count	Shape Parameter	Undrained Cohesion of Clay	Maximum Bearing Stress	Simplified Maximum Bearing Stress	Relative Displacement to develop q_{max}	Initial Point Stiffness	Simplified Initial Point Stiffness		Generalized displacement	Generalized Resistance
N	n	$C_u = 97$ N+114 (psf)	q_{max} =9 c_u (ksf)	q_{max} (ksf)	z_c (in)	k_q= 10 q_{max} / z_c (kcf)	k_q (ksf)	z_u = q_{max}/k_q (in)	z (in)	q (klf)
3	1	405	4	3.60	0.25	1749.6	1700	0.0254	0.00	0.00
3	1	405	4	3.60	0.25	1749.6	1700	0.0254	0.25	3.27
3	1	405	4	3.60	0.25	1749.6	1700	0.0254	0.50	3.43
3	1	405	4	3.60	0.25	1749.6	1700	0.0254	0.75	3.48
3	1	405	4	3.60	0.25	1749.6	1700	0.0254	1.00	3.51
3	1	405	4	3.60	0.25	1749.6	1700	0.0254	1.25	3.53
3	1	405	4	3.60	0.25	1749.6	1700	0.0254	1.50	3.54
3	1	405	4	3.60	0.25	1749.6	1700	0.0254	1.75	3.55
3	1	405	4	3.60	0.25	1749.6	1700	0.0254	2.00	3.55
3	1	405	4	3.60	0.25	1749.6	1700	0.0254	2.25	3.56
3	1	405	4	3.60	0.25	1749.6	1700	0.0254	2.50	3.56
3	1	405	4	3.60	0.25	1749.6	1700	0.0254	2.75	3.57
3	1	405	4	3.60	0.25	1749.6	1700	0.0254	3.00	3.57
3	1	405	4	3.60	0.25	1749.6	1700	0.0254	3.25	3.57
3	1	405	4	3.60	0.25	1749.6	1700	0.0254	3.50	3.57
3	1	405	4	3.60	0.25	1749.6	1700	0.0254	3.75	3.58
3	1	405	4	3.60	0.25	1749.6	1700	0.0254	4.00	3.58
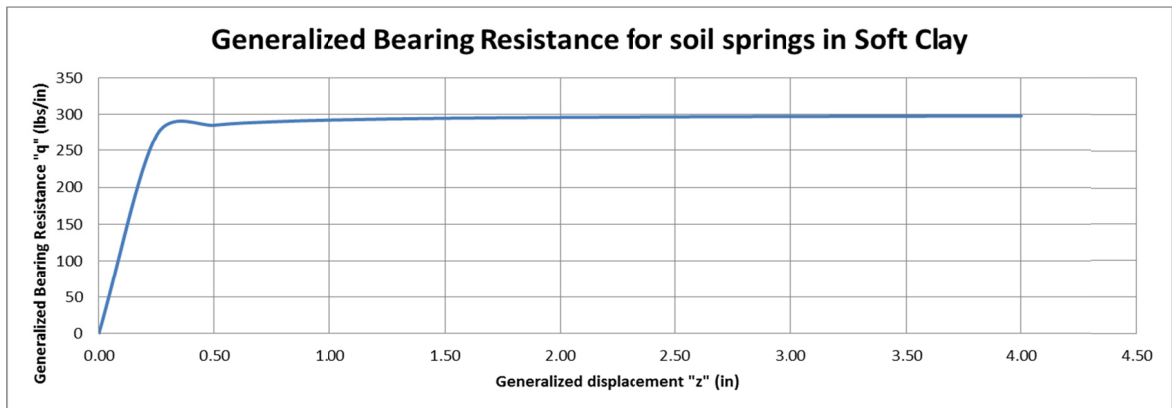
Figure 60 – Vertical End Bearing Resistance curve for Soft Clay

Table 24 – Vertical End Bearing Resistance calculation for Stiff Clay

Blow Count	Shape Parameter	Undrained Cohesion of Clay	Maximum Bearing Stress	Simplified Maximum Bearing Stress	Relative Displacement to develop q_{max}	Initial Point Stiffness	Simplified Initial Point Stiffness		Generalized displacement	Generalized Resistance
N	n	$C_u = 97$ N+114 (psf)	$q_{max} = 9$ c_u (ksf)	q_{max} (ksf)	z_c (in)	$k_q = 10\, q_{max}/z_c$ (kcf)	k_q (ksf)	$z_u = q_{max}/k_q$ (in)	z (in)	q (klf)
15	1	1569	14	14.00	0.25	6778.1	6700	0.0251	0.00	0.00
15	1	1569	14	14.00	0.25	6778.1	6700	0.0251	0.25	12.72
15	1	1569	14	14.00	0.25	6778.1	6700	0.0251	0.50	13.33
15	1	1569	14	14.00	0.25	6778.1	6700	0.0251	0.75	13.55
15	1	1569	14	14.00	0.25	6778.1	6700	0.0251	1.00	13.66
15	1	1569	14	14.00	0.25	6778.1	6700	0.0251	1.25	13.72
15	1	1569	14	14.00	0.25	6778.1	6700	0.0251	1.50	13.77
15	1	1569	14	14.00	0.25	6778.1	6700	0.0251	1.75	13.80
15	1	1569	14	14.00	0.25	6778.1	6700	0.0251	2.00	13.83
15	1	1569	14	14.00	0.25	6778.1	6700	0.0251	2.25	13.85
15	1	1569	14	14.00	0.25	6778.1	6700	0.0251	2.50	13.86
15	1	1569	14	14.00	0.25	6778.1	6700	0.0251	2.75	13.87
15	1	1569	14	14.00	0.25	6778.1	6700	0.0251	3.00	13.88
15	1	1569	14	14.00	0.25	6778.1	6700	0.0251	3.25	13.89
15	1	1569	14	14.00	0.25	6778.1	6700	0.0251	3.50	13.90
15	1	1569	14	14.00	0.25	6778.1	6700	0.0251	3.75	13.91
15	1	1569	14	14.00	0.25	6778.1	6700	0.0251	4.00	13.91
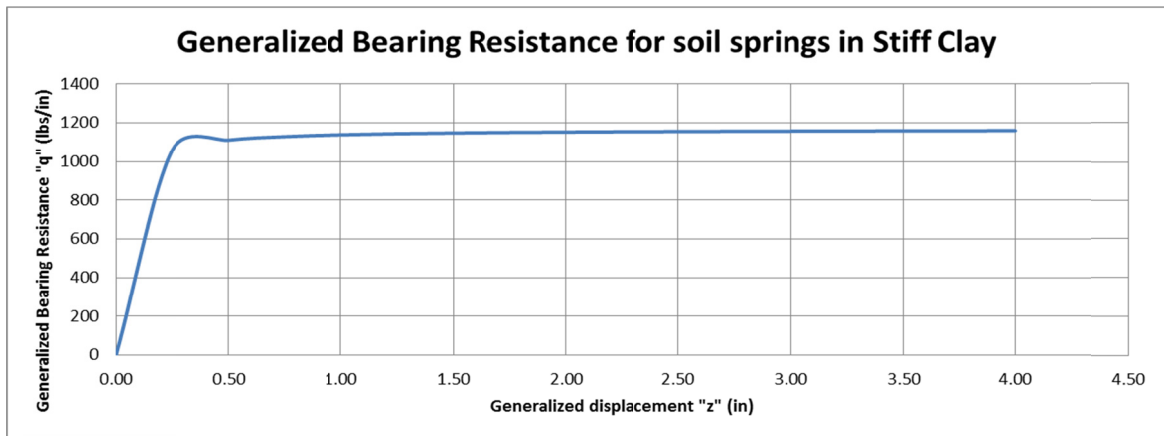
Figure 61 – Vertical End Bearing Resistance curve for Stiff Clay

126

Table 25 – Vertical End Bearing Resistance calculation for Very Stiff Clay

Blow Count	Shape Parameter	Undrained Cohesion of Clay	Maximum Bearing Stress	Simplified Maximum Bearing Stress	Relative Displacement to develop q_{max}	Initial Point Stiffness	Simplified Initial Point Stiffness		Generalized displacement	Generalized Resistance
N	n	$C_u = 97$ $N+114$ (psf)	$q_{max} = 9$ c_u (ksf)	q_{max} (ksf)	z_c (in)	$k_q = 10\, q_{max} / z_c$ (kcf)	k_q (ksf)	$z_u = q_{max}/k_q$ (in)	z (in)	q (klf)
50	1	4964	45	45.00	0.25	21444.5	21000	0.0257	0.00	0.00
50	1	4964	45	45.00	0.25	21444.5	21000	0.0257	0.25	40.80
50	1	4964	45	45.00	0.25	21444.5	21000	0.0257	0.50	42.80
50	1	4964	45	45.00	0.25	21444.5	21000	0.0257	0.75	43.51
50	1	4964	45	45.00	0.25	21444.5	21000	0.0257	1.00	43.87
50	1	4964	45	45.00	0.25	21444.5	21000	0.0257	1.25	44.09
50	1	4964	45	45.00	0.25	21444.5	21000	0.0257	1.50	44.24
50	1	4964	45	45.00	0.25	21444.5	21000	0.0257	1.75	44.35
50	1	4964	45	45.00	0.25	21444.5	21000	0.0257	2.00	44.43
50	1	4964	45	45.00	0.25	21444.5	21000	0.0257	2.25	44.49
50	1	4964	45	45.00	0.25	21444.5	21000	0.0257	2.50	44.54
50	1	4964	45	45.00	0.25	21444.5	21000	0.0257	2.75	44.58
50	1	4964	45	45.00	0.25	21444.5	21000	0.0257	3.00	44.62
50	1	4964	45	45.00	0.25	21444.5	21000	0.0257	3.25	44.65
50	1	4964	45	45.00	0.25	21444.5	21000	0.0257	3.50	44.67
50	1	4964	45	45.00	0.25	21444.5	21000	0.0257	3.75	44.69
50	1	4964	45	45.00	0.25	21444.5	21000	0.0257	4.00	44.71
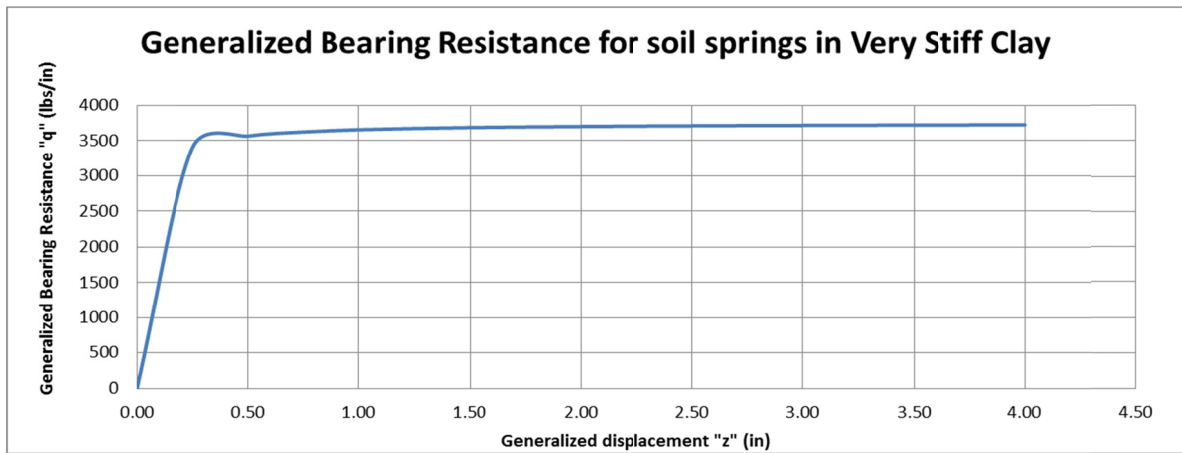
Figure 62 – Vertical End Bearing Resistance curve for Very Stiff Clay

Table 26 – Vertical End Bearing Resistance calculation for Loose Sand

Blow Count	Shape Parameter	Corrected Standard Penetration at depth of pile tip	Maximum Bearing Stress	Simplified Maximum Bearing Stress	Relative Displacement to develop q_{max}	Initial Point Stiffness	Simplified Initial Point Stiffness		Generalized displacement	Generalized Resistance
N	n	N_{corr}	$q_{max} = 8$ N_{corr} (ksf)	q_{max} (ksf)	z_c (in)	$k_q = 10\, q_{max} /$ z_c (kcf)	k_q (ksf)	$z_u =$ q_{max}/k_q (in)	z (in)	q (klf)
5	1	5	40	40.00	0.4	12000.0	12000	0.0400	0.00	0.00
5	1	5	40	40.00	0.4	12000.0	12000	0.0400	0.25	34.48
5	1	5	40	40.00	0.4	12000.0	12000	0.0400	0.50	37.04
5	1	5	40	40.00	0.4	12000.0	12000	0.0400	0.75	37.97
5	1	5	40	40.00	0.4	12000.0	12000	0.0400	1.00	38.46
5	1	5	40	40.00	0.4	12000.0	12000	0.0400	1.25	38.76
5	1	5	40	40.00	0.4	12000.0	12000	0.0400	1.50	38.96
5	1	5	40	40.00	0.4	12000.0	12000	0.0400	1.75	39.11
5	1	5	40	40.00	0.4	12000.0	12000	0.0400	2.00	39.22
5	1	5	40	40.00	0.4	12000.0	12000	0.0400	2.25	39.30
5	1	5	40	40.00	0.4	12000.0	12000	0.0400	2.50	39.37
5	1	5	40	40.00	0.4	12000.0	12000	0.0400	2.75	39.43
5	1	5	40	40.00	0.4	12000.0	12000	0.0400	3.00	39.47
5	1	5	40	40.00	0.4	12000.0	12000	0.0400	3.25	39.51
5	1	5	40	40.00	0.4	12000.0	12000	0.0400	3.50	39.55
5	1	5	40	40.00	0.4	12000.0	12000	0.0400	3.75	39.58
5	1	5	40	40.00	0.4	12000.0	12000	0.0400	4.00	39.60
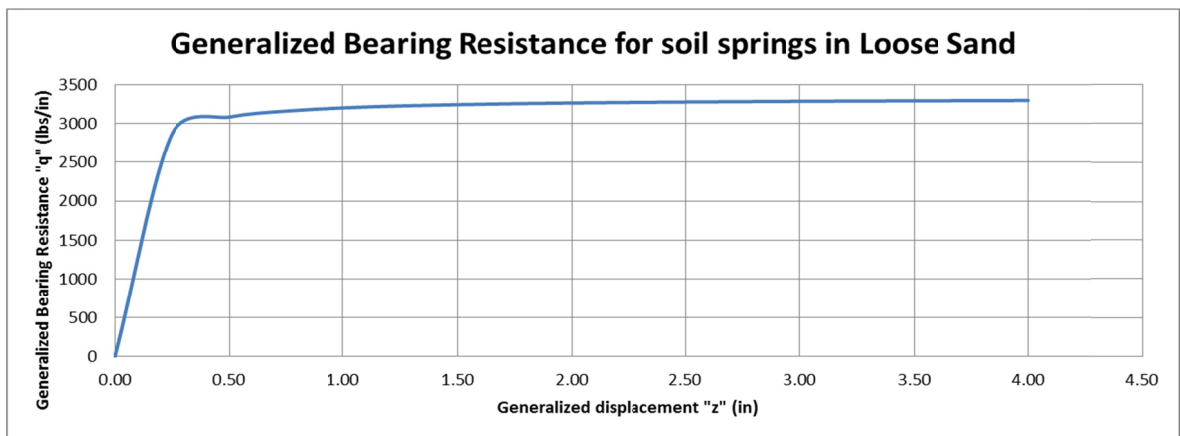
Figure 63 – Vertical End Bearing Resistance curve for Loose Sand

Table 27 – Vertical End Bearing Resistance calculation for Medium Sand

Blow Count	Shape Parameter	Corrected Standard Penetration at depth of pile tip	Maximum Bearing Stress	Simplified Maximum Bearing Stress	Relative Displacement to develop q_{max}	Initial Point Stiffness	Simplified Initial Point Stiffness		Generalized displacement	Generalized Resistance
N	n	N_{corr}	$q_{max} = 8$ N_{corr} (ksf)	q_{max} (ksf)	z_c (in)	$k_q = 10\, q_{max}\, /$ z_c (kcf)	k_q (ksf)	$z_u =$ q_{max}/k_q (in)	z (in)	q (klf)
15	1	15	120	120.00	0.4	36000.0	36000	0.0400	0.00	0.00
15	1	15	120	120.00	0.4	36000.0	36000	0.0400	0.25	103.45
15	1	15	120	120.00	0.4	36000.0	36000	0.0400	0.50	111.11
15	1	15	120	120.00	0.4	36000.0	36000	0.0400	0.75	113.92
15	1	15	120	120.00	0.4	36000.0	36000	0.0400	1.00	115.38
15	1	15	120	120.00	0.4	36000.0	36000	0.0400	1.25	116.28
15	1	15	120	120.00	0.4	36000.0	36000	0.0400	1.50	116.88
15	1	15	120	120.00	0.4	36000.0	36000	0.0400	1.75	117.32
15	1	15	120	120.00	0.4	36000.0	36000	0.0400	2.00	117.65
15	1	15	120	120.00	0.4	36000.0	36000	0.0400	2.25	117.90
15	1	15	120	120.00	0.4	36000.0	36000	0.0400	2.50	118.11
15	1	15	120	120.00	0.4	36000.0	36000	0.0400	2.75	118.28
15	1	15	120	120.00	0.4	36000.0	36000	0.0400	3.00	118.42
15	1	15	120	120.00	0.4	36000.0	36000	0.0400	3.25	118.54
15	1	15	120	120.00	0.4	36000.0	36000	0.0400	3.50	118.64
15	1	15	120	120.00	0.4	36000.0	36000	0.0400	3.75	118.73
15	1	15	120	120.00	0.4	36000.0	36000	0.0400	4.00	118.81
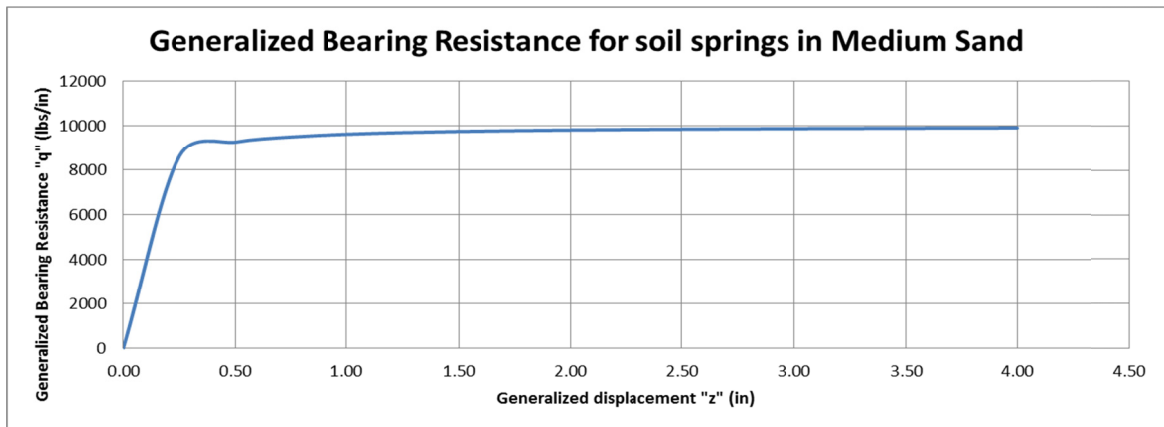
Figure 64 – Vertical End Bearing Resistance curve for Medium Sand

Table 28 – Vertical End Bearing Resistance calculation for Dense Sand

Blow Count	Shape Parameter	Corrected Standard Penetration at depth of pile tip	Maximum Bearing Stress	Simplified Maximum Bearing Stress	Relative Displacement to develop q_{max}	Initial Point Stiffness	Simplified Initial Point Stiffness		Generalized displacement	Generalized Resistance
N	n	N_{corr}	$q_{max} = 8\ N_{corr}$ (ksf)	q_{max} (ksf)	z_c (in)	$k_q = 10\ q_{max} / z_c$ (kcf)	k_q (ksf)	$z_u = q_{max}/k_q$ (in)	z (in)	q (klf)
30	1	23	180	180.00	0.4	54000.0	55000	0.0393	0.00	0.00
30	1	23	180	180.00	0.4	54000.0	55000	0.0393	0.25	155.56
30	1	23	180	180.00	0.4	54000.0	55000	0.0393	0.50	166.89
30	1	23	180	180.00	0.4	54000.0	55000	0.0393	0.75	171.04
30	1	23	180	180.00	0.4	54000.0	55000	0.0393	1.00	173.20
30	1	23	180	180.00	0.4	54000.0	55000	0.0393	1.25	174.52
30	1	23	180	180.00	0.4	54000.0	55000	0.0393	1.50	175.41
30	1	23	180	180.00	0.4	54000.0	55000	0.0393	1.75	176.05
30	1	23	180	180.00	0.4	54000.0	55000	0.0393	2.00	176.53
30	1	23	180	180.00	0.4	54000.0	55000	0.0393	2.25	176.91
30	1	23	180	180.00	0.4	54000.0	55000	0.0393	2.50	177.22
30	1	23	180	180.00	0.4	54000.0	55000	0.0393	2.75	177.47
30	1	23	180	180.00	0.4	54000.0	55000	0.0393	3.00	177.67
30	1	23	180	180.00	0.4	54000.0	55000	0.0393	3.25	177.85
30	1	23	180	180.00	0.4	54000.0	55000	0.0393	3.50	178.00
30	1	23	180	180.00	0.4	54000.0	55000	0.0393	3.75	178.13
30	1	23	180	180.00	0.4	54000.0	55000	0.0393	4.00	178.25
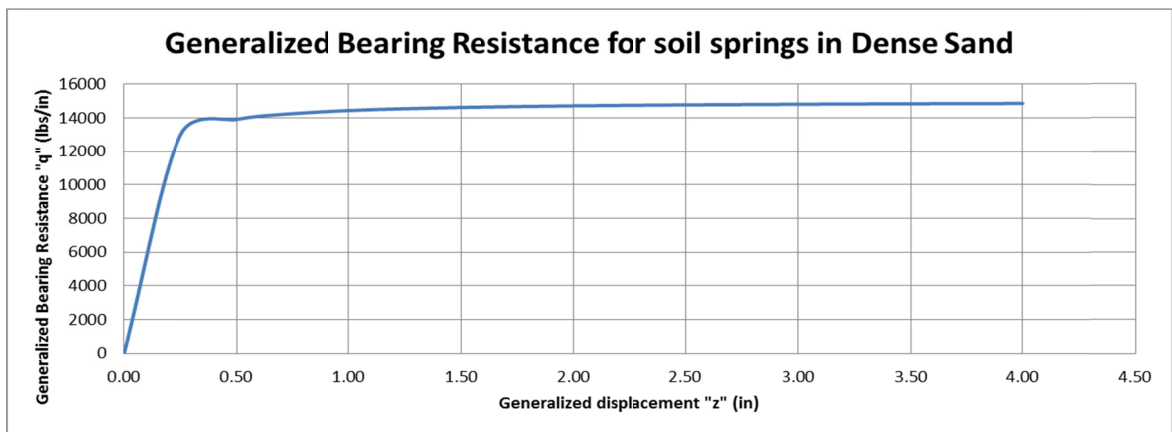
Figure 65 – Vertical End Bearing Resistance curve for Dense Sand

130

10. FRP Pile models

In order to study the behavior of the piles, 14,310 different FE models of the piles have been created. The total data volume of the created models exceeds 1.5 TB. The results generated 1,341 charts. In each series of the models, two variables are changed. The maximum principal stress and maximum shear stress are calculated for changing variables. A 3D chart is drawn in which the vertical Z axis is the maximum principal or shear stress and the other two perpendicular horizontal X and Y axes represent each variables. Then the 3D chart is transformed to 2D curves by slicing the chart according to each axis. These two pairs of charts show the stress changes in the pile while each variable changes.

Another set of charts is created using the ACP post-processing tool. The failure ratio is calculated on each pile and the failure criteria are set to maximum stress, Tsai-Wu and Tsai-Hill controls. The ratios above 1.0 represent failure of the pile by either criterion. So, all points below the failure ratio of 1.0 are considered acceptable.

The failure ratio curves also define the lowest values which are the optimum points. This is useful when there is no limitation for the pile and the engineer or designer wants to find the most economical combination.

Table 29 shows the summary of pile models and the variables used on each series. The FE models are named FRP and then the series three-digit numbers. Pile model series FRP100 and FRP200 have elastic supports. FRP300 series represents models with nonlinear supports. FRP400 series is created for comparison between the circular and elliptical sections.

Table 29 – FRP pile variables

Model Name	Design points	Z Dia (in)	X Dia (in)	Fiber Orient. Angle (deg)	Number of layers	Horz. Disp. (in)	Horz. X Load (Kips)	Vert. Load (Kips)	Concrete Fill	Material	Subg. Mod. (lbf/in3) or type	Max Prn. Str.	Max Shr. Str.	Failure Ratio	Total Disp.
				Inputs									Outputs Charts		
FRP101	99	24	Var.	Var.	10	1		10		Ep. Gl. UD	50	3	3	3	
FRP102	99	Var.	24	Var.	10	1		10		Ep. Gl. UD	50	3	3	3	
FRP103	99	24	Var.	Var.	10		10	10		Ep. Gl. UD	50	3	3	3	3
FRP104	99	Var.	24	Var.	10		10	10		Ep. Gl. UD	50	3	3	3	3
FRP111	121	Var.	Var.	15, -15	10	1		10		Ep. Gl. UD	50	3	3	3	
FRP112	121	Var.	Var.	30, -30	10	1		10		Ep. Gl. UD	50	3	3	3	
FRP113	121	Var.	Var.	45, -45	10	1		10		Ep. Gl. UD	50	3	3	3	
FRP114	121	Var.	Var.	60, -60	10	1		10		Ep. Gl. UD	50	3	3	3	
FRP115	121	Var.	Var.	75, -75	10	1		10		Ep. Gl. UD	50	3	3	3	
FRP121	121	Var.	Var.	15, -15	10		10	10		Ep. Gl. UD	50	3	3	3	3
FRP122	121	Var.	Var.	30, -30	10		10	10		Ep. Gl. UD	50	3	3	3	3
FRP123	121	Var.	Var.	45, -45	10		10	10		Ep. Gl. UD	50	3	3	3	3
FRP124	121	Var.	Var.	60, -60	10		10	10		Ep. Gl. UD	50	3	3	3	3
FRP125	121	Var.	Var.	75, -75	10		10	10		Ep. Gl. UD	50	3	3	3	3
FRP131	110	24	Var.	15, -15	Var.		10	10		Ep. Gl. UD	50	3	3	3	3
FRP132	110	24	Var.	30, -30	Var.		10	10		Ep. Gl. UD	50	3	3	3	3
FRP133	110	24	Var.	45, -45	Var.		10	10		Ep. Gl. UD	50	3	3	3	3
FRP134	110	24	Var.	60, -60	Var.		10	10		Ep. Gl. UD	50	3	3	3	3
FRP135	110	24	Var.	75, -75	Var.		10	10		Ep. Gl. UD	50	3	3	3	3
FRP141	90	24	4	Var.	Var.		10	10		Ep. Gl. UD	50	3	3	3	3
FRP142	90	24	8	Var.	Var.		10	10		Ep. Gl. UD	50	3	3	3	3
FRP143	90	24	12	Var.	Var.		10	10		Ep. Gl. UD	50	3	3	3	3
FRP144	90	24	16	Var.	Var.		10	10		Ep. Gl. UD	50	3	3	3	3
FRP145	90	24	20	Var.	Var.		10	10		Ep. Gl. UD	50	3	3	3	3
FRP146	90	24	24	Var.	Var.		10	10		Ep. Gl. UD	50	3	3	3	3

Table 29 – FRP pile variables (continued)

Model Name	Design points	Z Dia (in)	X Dia (in)	Fiber Orient. Angle (deg)	Number of layers	Horz. Disp. (in)	Horz. X Load (Kips)	Vert. Load (Kips)	Concrete Fill	Material	Subg. Mod. (lbf/in3) or type	Max Prn. Str.	Max Shr. Str.	Failure Ratio	Total Disp.
												Outputs Charts			
FRP151	110	24	Var.	15, -15	Var.	1		10		Ep. Gl. UD	50	3	3	3	
FRP152	110	24	Var.	30, -30	Var.	1		10		Ep. Gl. UD	50	3	3	3	
FRP153	110	24	Var.	45, -45	Var.	1		10		Ep. Gl. UD	50	3	3	3	
FRP154	110	24	Var.	60, -60	Var.	1		10		Ep. Gl. UD	50	3	3	3	
FRP155	110	24	Var.	75, -75	Var.	1		10		Ep. Gl. UD	50	3	3	3	
FRP161	90	24	4	Var.	Var.	1		10		Ep. Gl. UD	50	3	3	3	
FRP162	90	24	8	Var.	Var.	1		10		Ep. Gl. UD	50	3	3	3	
FRP163	90	24	12	Var.	Var.	1		10		Ep. Gl. UD	50	3	3	3	
FRP164	90	24	16	Var.	Var.	1		10		Ep. Gl. UD	50	3	3	3	
FRP165	90	24	20	Var.	Var.	1		10		Ep. Gl. UD	50	3	3	3	
FRP166	90	24	24	Var.	Var.	1		10		Ep. Gl. UD	50	3	3	3	
FRP171	99	24	Var.	Var.	10	1		10	Y	Ep. Gl. UD	50	3	3	3	
FRP172	99	Var.	24	Var.	10	1		10	Y	Ep. Gl. UD	50	3	3	3	
FRP173	99	24	Var.	Var.	10		10	10	Y	Ep. Gl. UD	50	3	3	3	3
FRP174	99	Var.	24	Var.	10		10	10	Y	Ep. Gl. UD	50	3	3	3	3
FRP175	99	24	Var.	Var.	10			100	Y	Ep. Gl. UD					
FRP176	99	24	Var.	Var.	10			100		Ep. GL UD					
FRP181	110	24	Var.	15, -15	20		10	10		Ep. Gl. UD	Var.	3	3	3	3
FRP182	110	24	Var.	30, -30	20		10	10		Ep. Gl. UD	Var.	3	3	3	3
FRP183	110	24	Var.	45, -45	20		10	10		Ep. Gl. UD	Var.	3	3	3	3
FRP184	110	24	Var.	60, -60	20		10	10		Ep. Gl. UD	Var.	3	3	3	3
FRP185	110	24	Var.	75, -75	20		10	10		Ep. Gl. UD	Var.	3	3	3	3
FRP191	110	24	Var.	15, -15	20		10	10	Y	Ep. Gl. UD	Var.	3	3	3	3
FRP192	110	24	Var.	30, -30	20		10	10	Y	Ep. Gl. UD	Var.	3	3	3	3
FRP193	110	24	Var.	45, -45	20		10	10	Y	Ep. Gl. UD	Var.	3	3	3	3
FRP194	110	24	Var.	60, -60	20		10	10	Y	Ep. Gl. UD	Var.	3	3	3	3
FRP195	110	24	Var.	75, -75	20		10	10	Y	Ep. Gl. UD	Var.	3	3	3	3

Table 29 – FRP pile variables (continued)

Model Name	Design points	Z Dia (in)	X Dia (in)	Fiber Orient. Angle (deg)	Number of layers	Horz. Disp. (in)	Horz. X Load (Kips)	Vert. Load (Kips)	Concrete Fill	Material	Subg. Mod. (lbf/in3) or type	Max Prn. Str.	Max Shr. Str.	Failure Ratio	Total Disp.
											Inputs → Outputs Charts				
FRP201	77	24	Var.	15, -15	20		10	10		Var. Built in	50	3	3	3	3
FRP202	77	24	Var.	30, -30	20		10	10		Var. Built in	50	3	3	3	3
FRP203	77	24	Var.	45, -45	20		10	10		Var. Built in	50	3	3	3	3
FRP204	77	24	Var.	60, -60	20		10	10		Var. Built in	50	3	3	3	3
FRP205	77	24	Var.	75, -75	20		10	10		Var. Built in	50	3	3	3	3
FRP211	165	24	Var.	15, -15	20	2		10		Var. Manual	50	2	2	2	
FRP212	165	24	Var.	30, -30	20	2		10		Var. Manual	50	2	2	2	
FRP213	165	24	Var.	45, -45	20	2		10		Var. Manual	50	2	2	2	
FRP214	165	24	Var.	60, -60	20	2		10		Var. Manual	50	2	2	2	
FRP215	165	24	Var.	75, -75	20	2		10		Var. Manual	50	2	2	2	
FRP221	99	24	12	15, -15	20	Var.		Var.		Ep. Gl. UD	50	3	3	3	
FRP222	99	24	12	30, -30	20	Var.		Var.		Ep. Gl. UD	50	3	3	3	
FRP223	99	24	12	45, -45	20	Var.		Var.		Ep. Gl. UD	50	3	3	3	
FRP224	99	24	12	60, -60	20	Var.		Var.		Ep. Gl. UD	50	3	3	3	
FRP225	99	24	12	75, -75	20	Var.		Var.		Ep. Gl. UD	50	3	3	3	
FRP231	120	24	12	15, -15	20	Var.		10		Var. Manual	50	3	3	3	
FRP232	120	24	12	30, -30	20	Var.		10		Var. Manual	50	3	3	3	
FRP233	120	24	12	45, -45	20	Var.		10		Var. Manual	50	3	3	3	
FRP234	120	24	12	60, -60	20	Var.		10		Var. Manual	50	3	3	3	
FRP235	120	24	12	75, -75	20	Var.		10		Var. Manual	50	3	3	3	

Table 29 – FRP pile variables (continued)

Model Name	Design points	Z Dia (in)	X Dia (in)	Fiber Orient. Angle (deg)	Number of layers	Horz. Disp. (in)	Horz. X Load (Kips)	Vert. Load (Kips)	Concrete Fill	Material	Subg. Mod. (lbf/in3) or type	Max Prn. Str.	Max Shr. Str.	Failure Ratio	Total Disp.
								Inputs					Outputs Charts		
FRP241	75	24	12	Var.	10	Var.		20		Ep. Gl. UD	50	3	3	3	
FRP242	75	24	12	Var.	10	Var.		40		Ep. Gl. UD	50	3	3	3	
FRP243	75	24	12	Var.	10	Var.		60		Ep. Gl. UD	50	3	3	3	
FRP244	75	24	12	Var.	10	Var.		80		Ep. Gl. UD	50	3	3	3	
FRP245	75	24	12	Var.	10	Var.		100		Ep. Gl. UD	50	3	3	3	
FRP251	100	24	12	Var.	10	0		Var.		Ep. Gl. UD	50	3	3	3	
FRP252	100	24	12	Var.	10	1		Var.		Ep. Gl. UD	50	3	3	3	
FRP253	100	24	12	Var.	10	2		Var.		Ep. Gl. UD	50	3	3	3	
FRP254	100	24	12	Var.	10	3		Var.		Ep. Gl. UD	50	3	3	3	
FRP255	100	24	12	Var.	10	4		Var.		Ep. Gl. UD	50	3	3	3	
FRP261	75	24	12	Var.+ 0	20	Var.		20		Ep. Gl. UD	50	3	3	3	
FRP262	75	24	12	Var.+ 0	20	Var.		40		Ep. Gl. UD	50	3	3	3	
FRP263	75	24	12	Var.+ 0	20	Var.		60		Ep. Gl. UD	50	3	3	3	
FRP264	75	24	12	Var.+ 0	20	Var.		80		Ep. Gl. UD	50	3	3	3	
FRP265	75	24	12	Var.+ 0	20	Var.		100		Ep. Gl. UD	50	3	3	3	
FRP271	100	24	12	Var.+ 0	20	0		Var.		Ep. Gl. UD	50	3	3	3	
FRP272	100	24	12	Var.+ 0	20	1		Var.		Ep. Gl. UD	50	3	3	3	
FRP273	100	24	12	Var.+ 0	20	2		Var.		Ep. Gl. UD	50	3	3	3	
FRP274	100	24	12	Var.+ 0	20	3		Var.		Ep. Gl. UD	50	3	3	3	
FRP275	100	24	12	Var.+ 0	20	4		Var.		Ep. Gl. UD	50	3	3	3	
FRP281	75	24	12	Var.+ 90	20	Var.		20		Ep. Gl. UD	50	3	3	3	
FRP282	75	24	12	Var.+ 90	20	Var.		40		Ep. Gl. UD	50	3	3	3	
FRP283	75	24	12	Var.+ 90	20	Var.		60		Ep. Gl. UD	50	3	3	3	
FRP284	75	24	12	Var.+ 90	20	Var.		80		Ep. Gl. UD	50	3	3	3	
FRP285	75	24	12	Var.+ 90	20	Var.		100		Ep. Gl. UD	50	3	3	3	

Table 29 – FRP pile variables (continued)

Model Name	Design points	Z Dia (in)	X Dia (in)	Fiber Orient. Angle (deg)	Number of layers	Horz. Disp. (in)	Horz. X Load (Kips)	Vert. Load (Kips)	Concrete Fill	Material	Subg. Mod. (lbf/in3) or type	Max Prn. Str.	Max Shr. Str.	Failure Ratio	Total Disp.
FRP301	100	24	12	Var.	10	0		Var.		Ep. Gl. UD	Soft Clay	3	3	3	
FRP302	100	24	12	Var.	10	1		Var.		Ep. Gl. UD	Soft Clay	3	3	3	
FRP303	100	24	12	Var.	10	2		Var.		Ep. Gl. UD	Soft Clay	3	3	3	
FRP304	100	24	12	Var.	10	3		Var.		Ep. Gl. UD	Soft Clay	3	3	3	
FRP305	100	24	12	Var.	10	4		Var.		Ep. Gl. UD	Soft Clay	3	3	3	
FRP311	100	24	12	Var.	10	0		Var.		Ep. Gl. UD	Stiff Clay	3	3	3	
FRP312	100	24	12	Var.	10	1		Var.		Ep. Gl. UD	Stiff Clay	3	3	3	
FRP313	100	24	12	Var.	10	2		Var.		Ep. Gl. UD	Stiff Clay	3	3	3	
FRP314	100	24	12	Var.	10	3		Var.		Ep. Gl. UD	Stiff Clay	3	3	3	
FRP315	100	24	12	Var.	10	4		Var.		Ep. Gl. UD	Stiff Clay	3	3	3	
FRP321	100	24	12	Var.	10	0		Var.		Ep. Gl. UD	V. S. Clay	3	3	3	
FRP322	100	24	12	Var.	10	1		Var.		Ep. Gl. UD	V. S. Clay	3	3	3	
FRP323	100	24	12	Var.	10	2		Var.		Ep. Gl. UD	V. S. Clay	3	3	3	
FRP324	100	24	12	Var.	10	3		Var.		Ep. Gl. UD	V. S. Clay	3	3	3	
FRP325	100	24	12	Var.	10	4		Var.		Ep. Gl. UD	V. S. Clay	3	3	3	

Table 29 – FRP pile variables (continued)

Model Name	Design points	Z Dia (in)	X Dia (in)	Fiber Orient. Angle (deg)	Number of layers	Horz. Disp. (in)	Horz. X Load (Kips)	Vert. Load (Kips)	Concrete Fill	Material	Subg. Mod. (lbf/in3) or type	Max Prn. Str.	Max Shr. Str.	Failure Ratio	Total Disp.
											Inputs			**Outputs Charts**	
FRP331	100	24	12	Var.	10	0		Var.		Ep. Gl. UD	Loose Sand	3	3	3	
FRP332	100	24	12	Var.	10	1		Var.		Ep. Gl. UD	Loose Sand	3	3	3	
FRP333	100	24	12	Var.	10	2		Var.		Ep. Gl. UD	Loose Sand	3	3	3	
FRP334	100	24	12	Var.	10	3		Var.		Ep. Gl. UD	Loose Sand	3	3	3	
FRP335	100	24	12	Var.	10	4		Var.		Ep. Gl. UD	Loose Sand	3	3	3	
FRP341	100	24	12	Var.	10	0		Var.		Ep. Gl. UD	Med. Sand	3	3	3	
FRP342	100	24	12	Var.	10	1		Var.		Ep. Gl. UD	Med. Sand	3	3	3	
FRP343	100	24	12	Var.	10	2		Var.		Ep. Gl. UD	Med. Sand	3	3	3	
FRP344	100	24	12	Var.	10	3		Var.		Ep. Gl. UD	Med. Sand	3	3	3	
FRP345	100	24	12	Var.	10	4		Var.		Ep. Gl. UD	Med. Sand	3	3	3	
FRP351	100	24	12	Var.	10	0		Var.		Ep. Gl. UD	Den. Sand	3	3	3	
FRP352	100	24	12	Var.	10	1		Var.		Ep. Gl. UD	Den. Sand	3	3	3	
FRP353	100	24	12	Var.	10	2		Var.		Ep. Gl. UD	Den. Sand	3	3	3	
FRP354	100	24	12	Var.	10	3		Var.		Ep. Gl. UD	Den. Sand	3	3	3	
FRP355	100	24	12	Var.	10	4		Var.		Ep. Gl. UD	Den. Sand	3	3	3	

Table 29 – FRP pile variables (continued)

Model Name	Design points	Z Dia (in)	X Dia (in)	Fiber Orient. Angle (deg)	Number of layers	Horz. Disp. (in)	Horz. X Load (Kips)	Vert. Load (Kips)	Concrete Fill	Material	Subg. Mod. (lbf/in3) or type	Max Prn. Str.	Max Shr. Str.	Failure Ratio	Total Disp.
		Inputs										Outputs Charts			
FRP401	100	24	24	Var	10	4		Var.		Ep. Gl. UD	50	3	3	3	
FRP402	100	28	20	Var	10	4		Var.		Ep. Gl. UD	50	3	3	3	
FRP403	100	32	14	Var	10	4		Var.		Ep. Gl. UD	50	3	3	3	
FRP404	100	36	7	Var	10	4		Var.		Ep. Gl. UD	50	3	3	3	
FRP411	100	24	24	Var	10	4		Var.		Ep. Gl. UD	Stiff Clay	3	3	3	
FRP412	100	28	20	Var	10	4		Var.		Ep. Gl. UD	Stiff Clay	3	3	3	
FRP413	100	32	14	Var	10	4		Var.		Ep. Gl. UD	Stiff Clay	3	3	3	
FRP414	100	36	7	Var	10	4		Var.		Ep. Gl. UD	Stiff Clay	3	3	3	
FRP421	100	24	24	Var	10	4		Var.		Ep. Gl. UD	Med. Sand	3	3	3	
FRP422	100	28	20	Var	10	4		Var.		Ep. Gl. UD	Med. Sand	3	3	3	
FRP423	100	32	14	Var	10	4		Var.		Ep. Gl. UD	Med. Sand	3	3	3	
FRP424	100	36	7	Var	10	4		Var.		Ep. Gl. UD	Med. Sand	3	3	3	
FRP431	100	24	Var.	45, -45				Var.		Ep. Gl. UD	Stiff Clay	3	3	3	
FRP441	100	24	Var.	45, -45				Var.		Ep. Gl. UD	Med. Sand	3	3	3	
Total	14,310											412	412	412	105
												Totally 1341 charts			

138

11. FRP Pile Behavior

As described in earlier chapters, in each sets of models two variables have been studied. Since the stress is assigned to the vertical axis of a 3D chart, in fact there can be a maximum of two variables to be assigned to the other two axes. Table 30 represents the variables used in each series of FRP models. The following pages show the graphs for each case. In each group only one case is represented.

Table 30 –Variables of FRP Finite Element models

Model Name	Z Dia (in)	X Dia (in)	Fiber Orient. Angle (deg)	Number of layers	Horz. Disp. (in)	Horz. X Load (Kips)	Vert. Load (Kips)	Concrete Fill	Material	Subg. Mod. (lbf/in3) or type
FRP101 and 103		Var.	Var.							
FRP102 and 104	Var.		Var.							
FRP111 to 115	Var.	Var.								
FRP121 to 125	Var.	Var.								
FRP131 to 135		Var.		Var.						
FRP141 to 146				Var.						
FRP151 to 155		Var.		Var.						
FRP161 to 166			Var.	Var.						
FRP171 and 173		Var.	Var.					Y		
FRP172 and 174	Var.		Var.					Y		
FRP181 to 185		Var.								Var.
FRP191 to 195		Var.						Y		Var.
FRP201 to 205		Var.							Var.	
FRP211 to 215		Var.							Var.	
FRP221 to 225					Var.		Var.			
FRP231 to 235					Var.				Var.	
FRP241 to 245			Var.		Var.					
FRP251 to 255			Var.				Var.			
FRP261 to 265			Var.+ 0		Var.					
FRP271 to 275			Var.+ 0				Var.			
FRP281 to 285			Var.+ 90		Var.					
FRP301 to 305			Var.				Var.			Soft Clay
FRP311 to 315			Var.				Var.			Stiff Clay
FRP321 to 325			Var.				Var.			V. S. Clay
FRP331 to 335			Var.				Var.			Loose Sand
FRP341 to 345			Var.				Var.			Med. Sand
FRP351 to 355			Var.				Var.			Den. Sand
FRP401 to 441	Var.	Var.	Var.				Var.			Var.

11.1. *FRP 101 to 104 with Constant Displacement and Varying Fiber Orientation and Pile Dimensions*
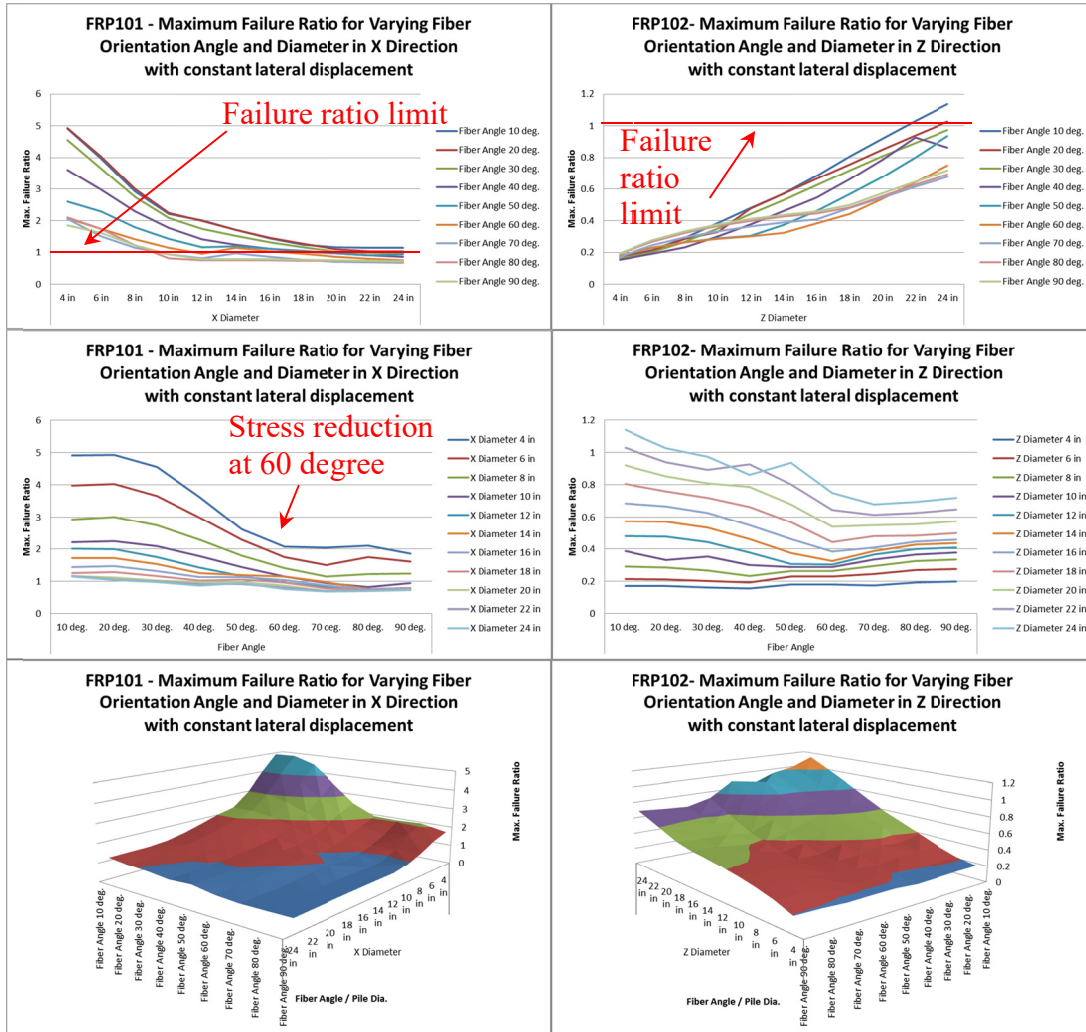
Figure 66 – Stress curves for varying fiber orientation and pile dimensions

As shown in Figure 66, pile stress will decrease with an increase in fiber orientation. It is also observed that beyond a 60 degree orientation, the failure ratio decreases considerably.

Figure 67 compares the principal stress in a 24x6 section with 10- and 60-degree

fiber orientation. The stress is reduced in piles with higher fiber orientation angle.
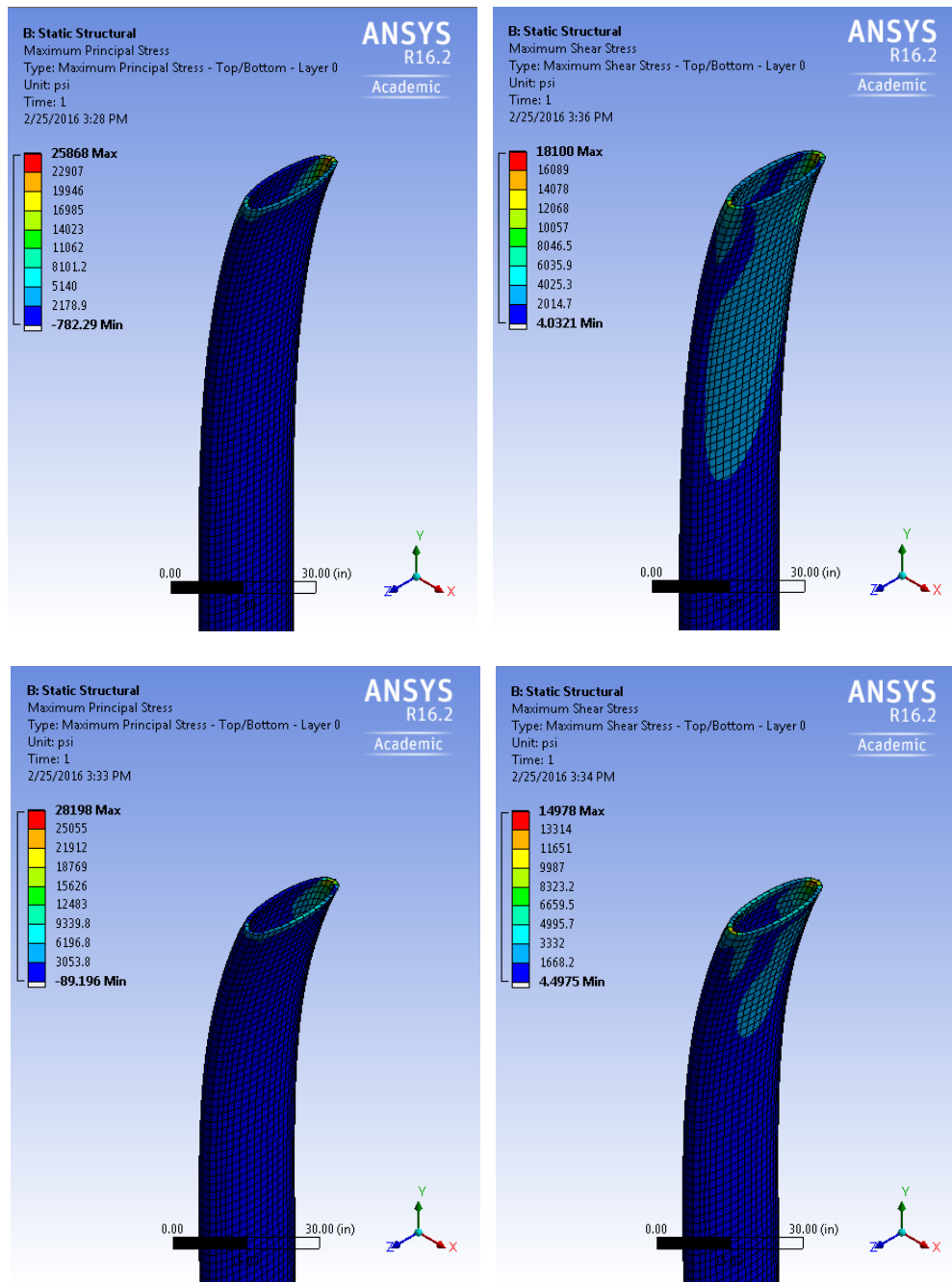
Figure 67 – Principal and shear stress for 24"x6" section with 10 deg. (up) and 60 deg. (down)

11.2. *FRP 111 to 115 with Constant Top of the Pile Displacement and Constant Vertical Force and Varying Pile Dimensions*
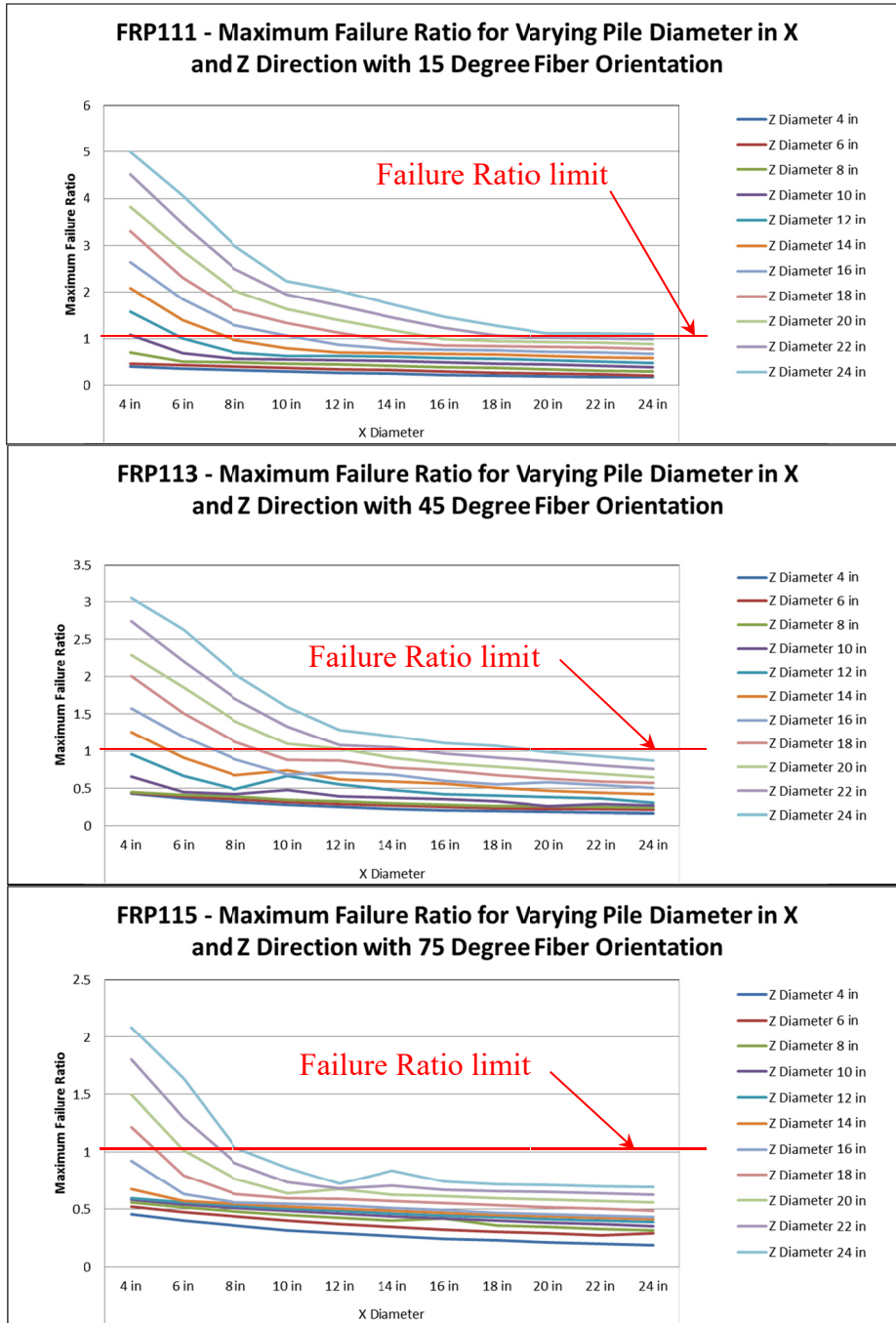
Figure 68 – Failure Ratio curves for varying fiber orientation and pile dimensions

As shown in Figure 68, pile the failure ratio will decrease with an increase in fiber orientation. It is also observed that with increase in pile dimension the failure ratio decreases. Figure 69 compares the principal stress in a 24x12 and 24x24 (round) section with 45-degree fiber orientation. As expected, the stress is reduced in the round section.
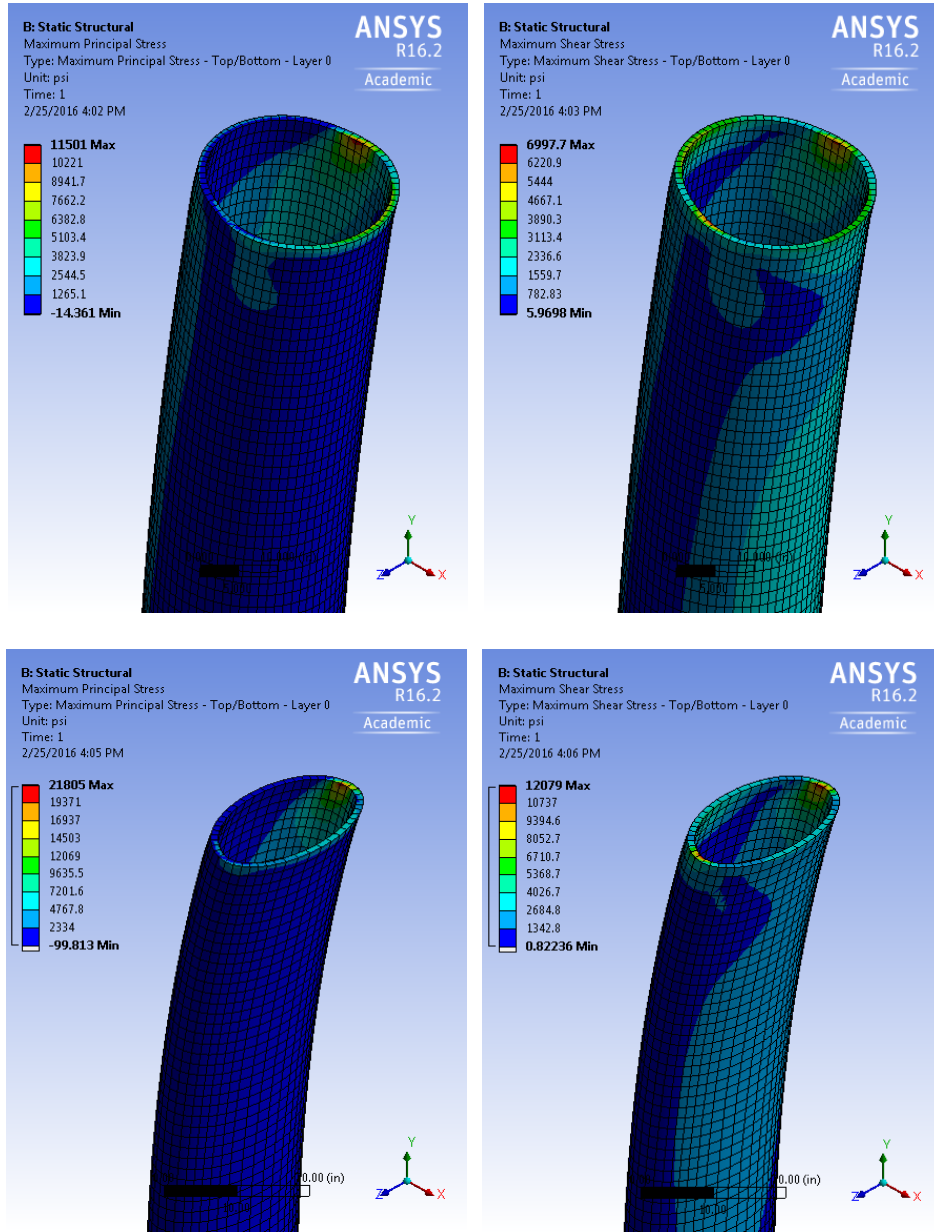
Figure 69 – Principal and shear stress for round (up) 24" and 24"x12"section (down)

11.3. *FRP 121 to 125 with Constant Lateral Force and Varying Pile Dimensions*
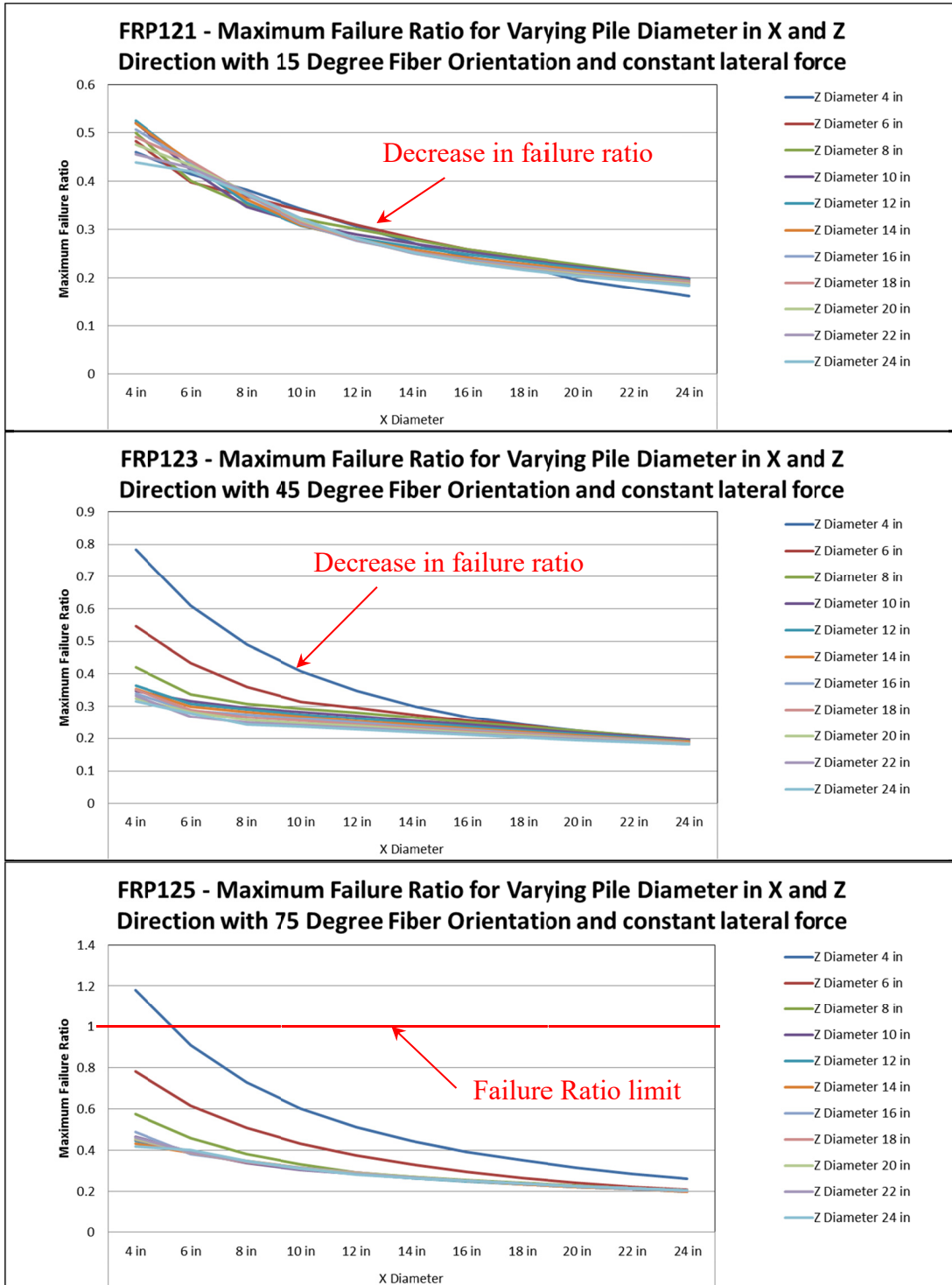
Figure 70 – Failure Ratio curves for varying fiber orientation and pile dimensions

As shown in Figure 70, it is also observed that with an increase in pile X and Z dimension the failure ratio decreases.

Figure 71Figure 69 compares the principal stress in piles with different orientation angles. The stress decreases when the shorter diameter is more than half of the longer diameter of the elliptical cross section. This happens regardless of orientation angle.

Figure 71 – Principal stress for 15 (up), 45 (middle) and 75 (down) degree fiber orientation

11.4. *FRP 131 to 145 with Constant Top of the Pile Horizontal and Vertical Force and Varying Number of Composite Layers*
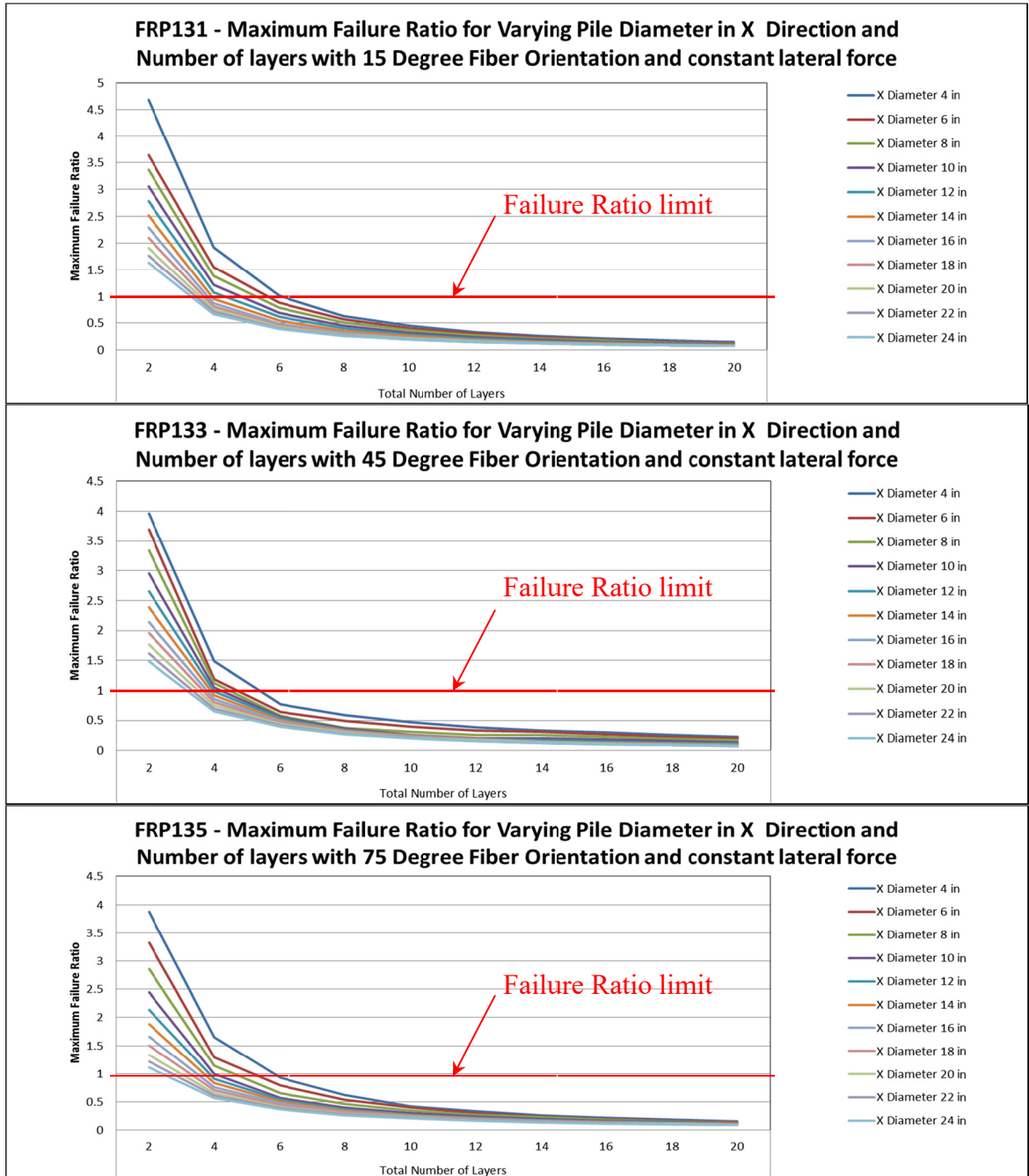
Figure 72 – Failure Ratio curves for varying fiber orientation and number of composite layers

As shown in Figure 72Figure 68 and as expected, pile failure ratio will decrease with an increase in the number of fiber layers. The ratio falls drastically when the number of layers is small.

Figure 73 represents the changes in principal stress, shear and failure ratio for varying layer orientation and number of layers. It shows the stress remains approximately constant with changing orientation angles but drastically decreases when the number of layers increases.
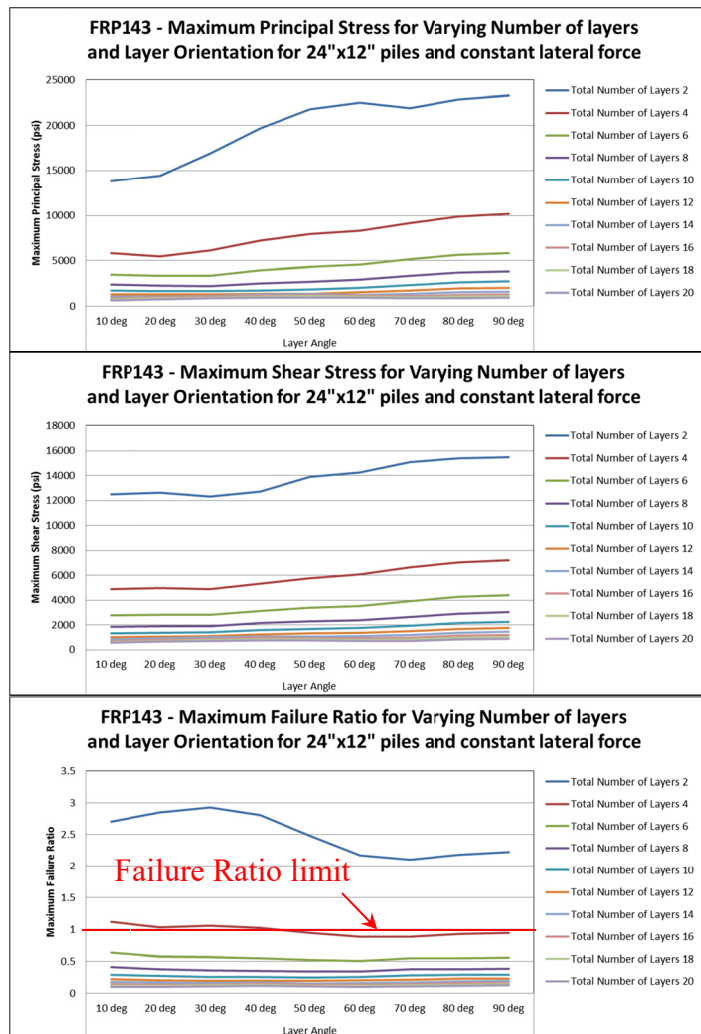
Figure 73 – Principal stress, shear and Failure Ratio curve for 24"x12" section

Figure 74Figure 69 compares the principal and shear stresses in a 24x12 section with a 40-degree fiber orientation. As expected, the stress is reduced as the layers are increased.
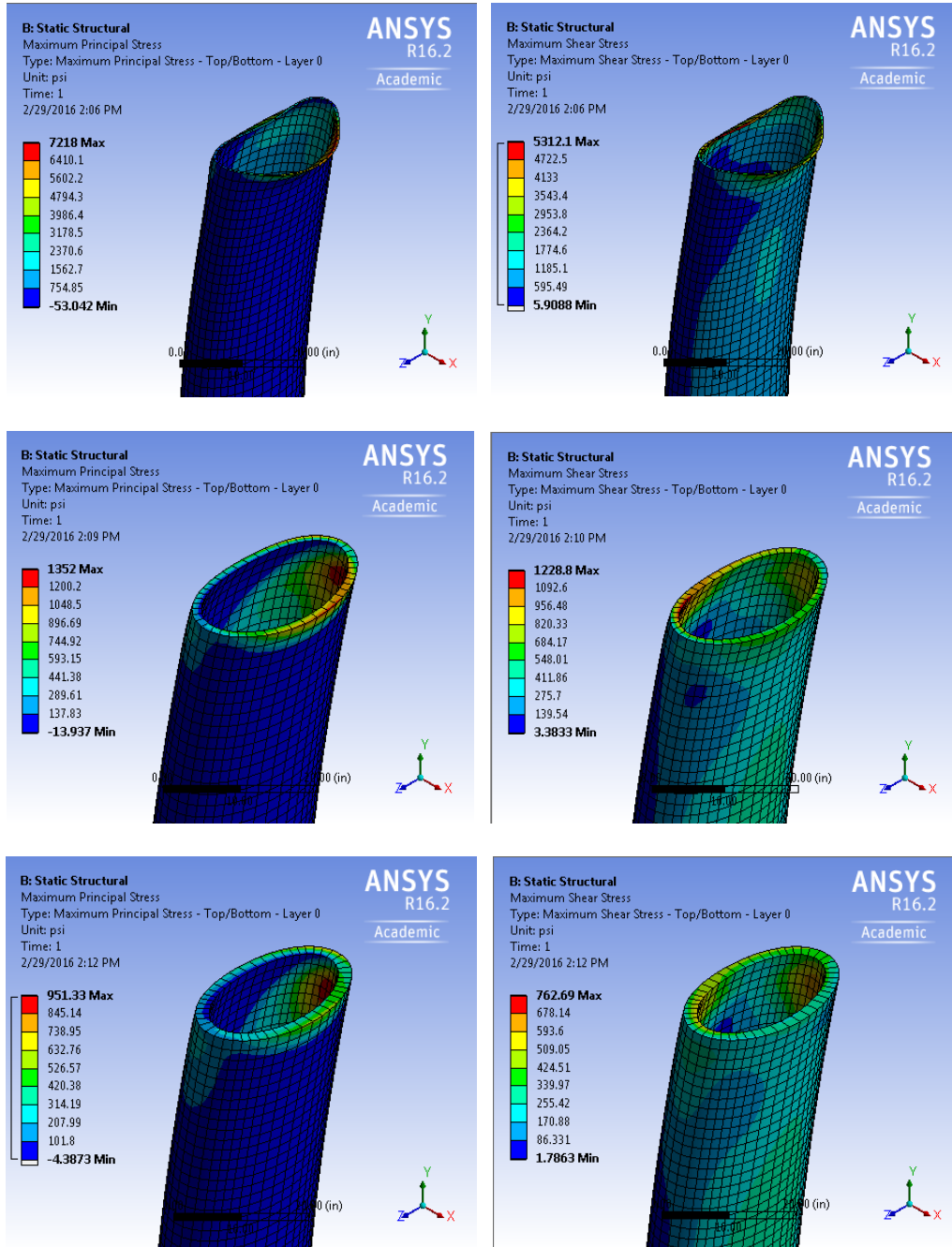
Figure 74 – Principal and shear stress for 4 (up) 12 (middle) and 20 (down) layers

11.5. *FRP 171 to 174 Concrete Filled Piles with Constant Displacement and Varying Fiber Orientation and Pile Dimensions*
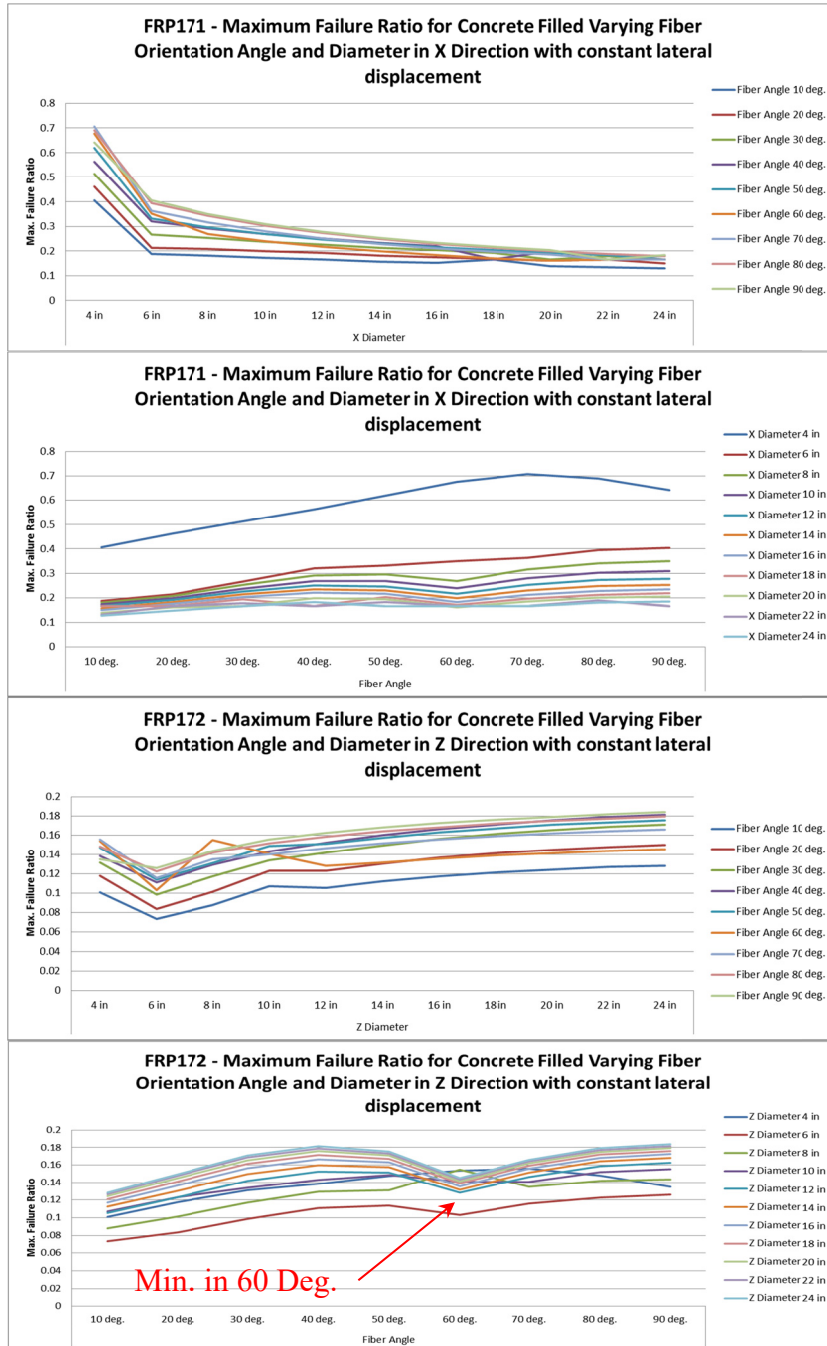
Figure 75 – Stress curves for varying fiber orientation and pile dimensions

As shown in Figure 75Figure 66, the failure ratio is changing for narrow sections but remains relatively constant for rounder sections. It is also observed that piles with a 60-degree fiber orientation have a lower failure ratio. Figure 76Figure 67 compares the principal stress in a 24"x12" section filled with concrete with 10- and 60-degree fiber orientation. The stress is reduced in piles with a 60-degree fiber orientation angle.
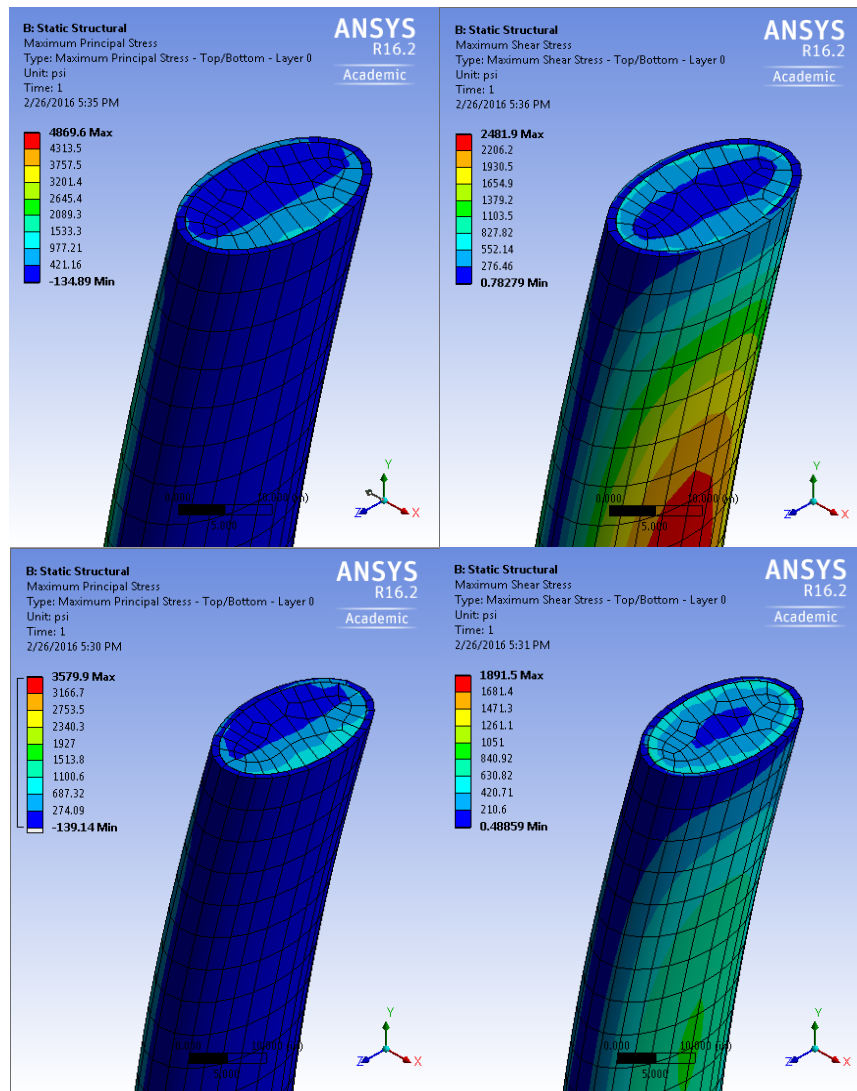
Figure 76 – Principal and shear stress for 24"x12" section with 10 deg. (up) and 60 deg. (down)

11.6. *FRP 201 to 215 with Constant Displacement and Vertical Load and Varying Composite Material*
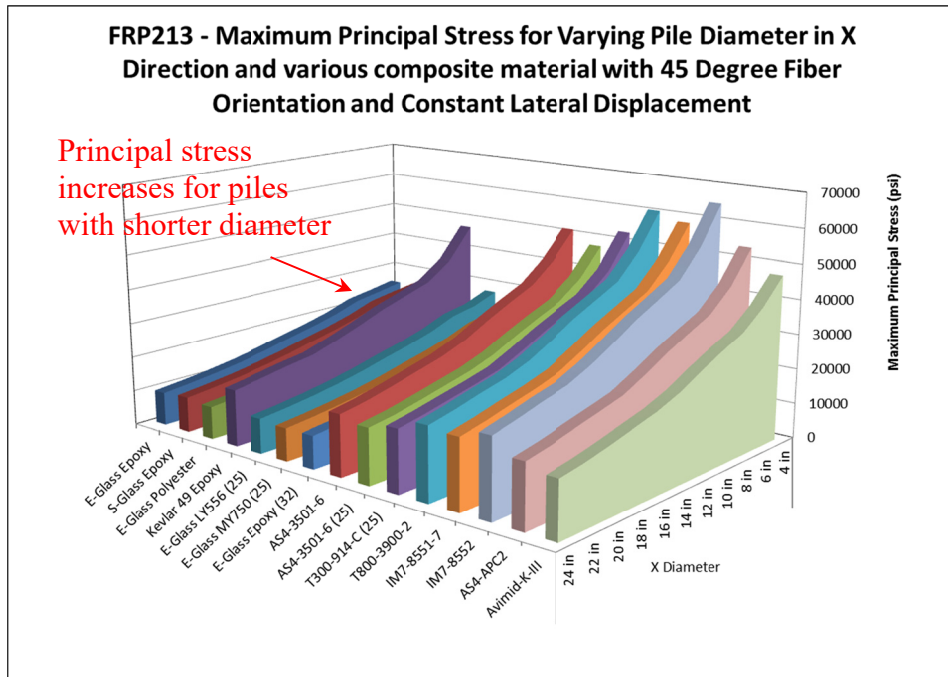
Figure 77 – Principal Stress curves for varying composite materials
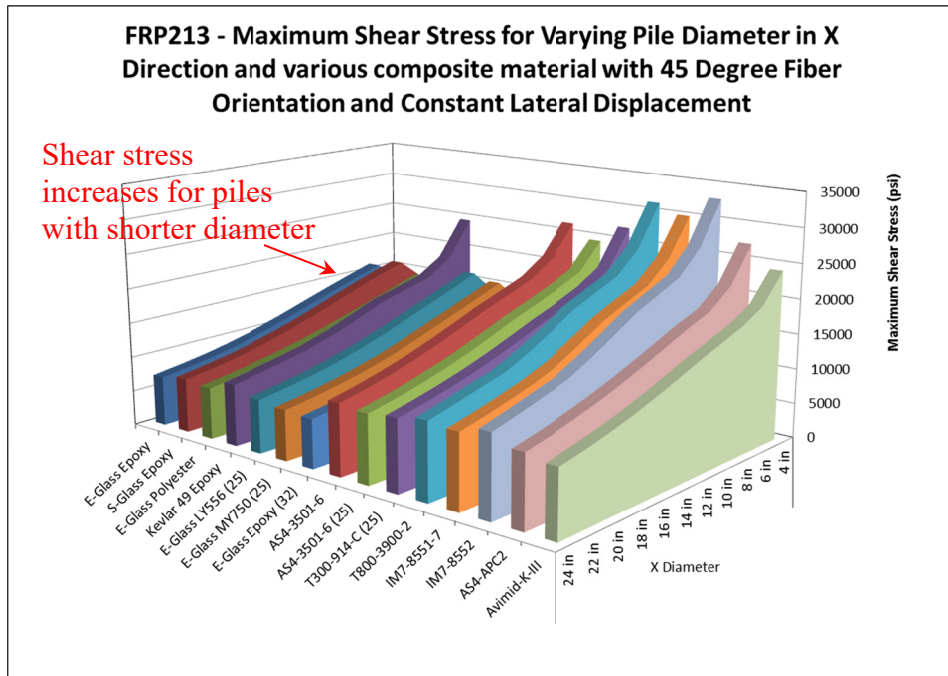
Figure 78 – Principal Stress curves for varying composite materials
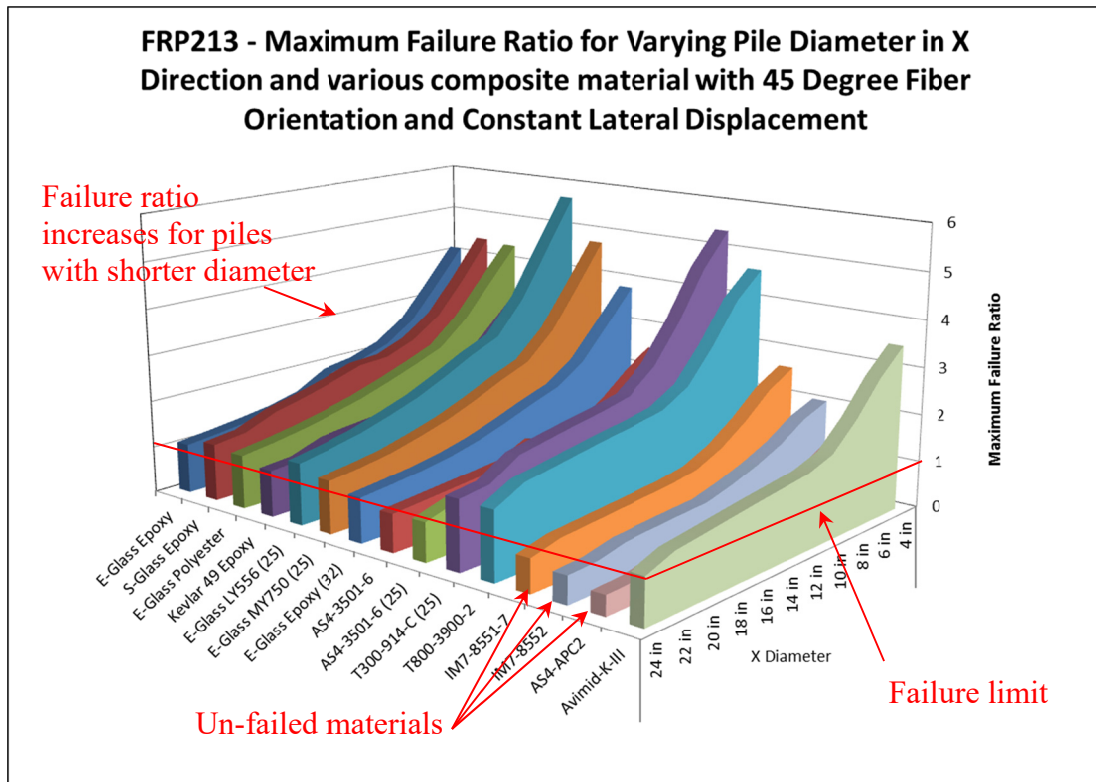
Figure 79 – Principal Stress curves for varying composite materials

As shown in Figure 77 to Figure 79 , pile stress varies drastically with the type of composite material. It is also observed that the stress is reduced with closer to round sections. In another word the more oval shape, the higher will be the principal and shear stresses.

It also shows how in similar condition some materials may work while others fail.

Figure 80 compares the stress contour lines of 20 layer 24"x12" sections made with E-Glass Epoxy and Kevlar 49 the two common type and composites.
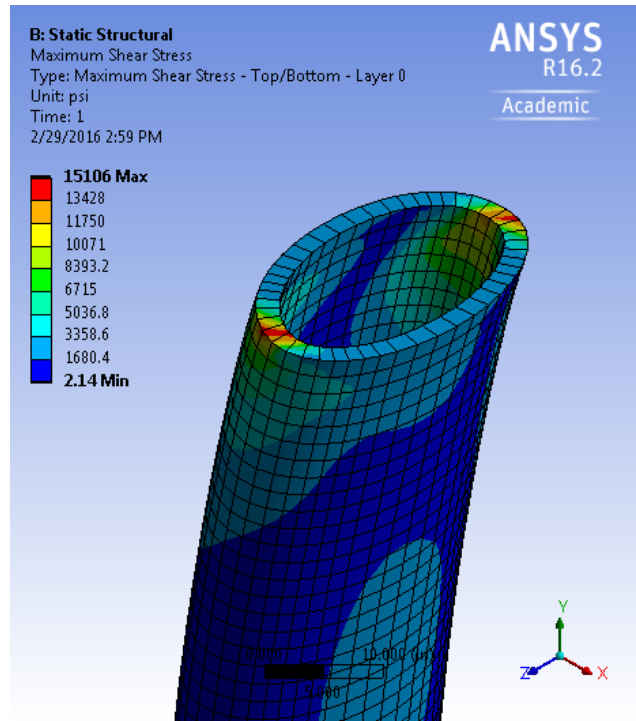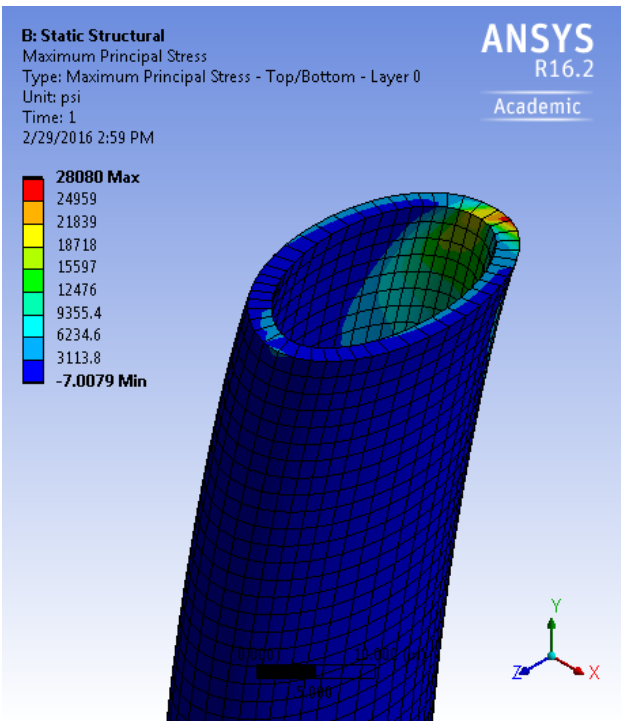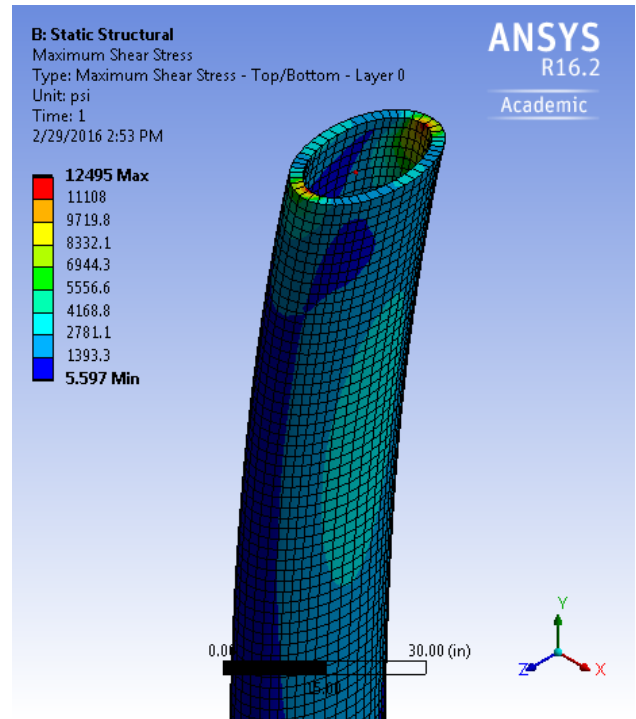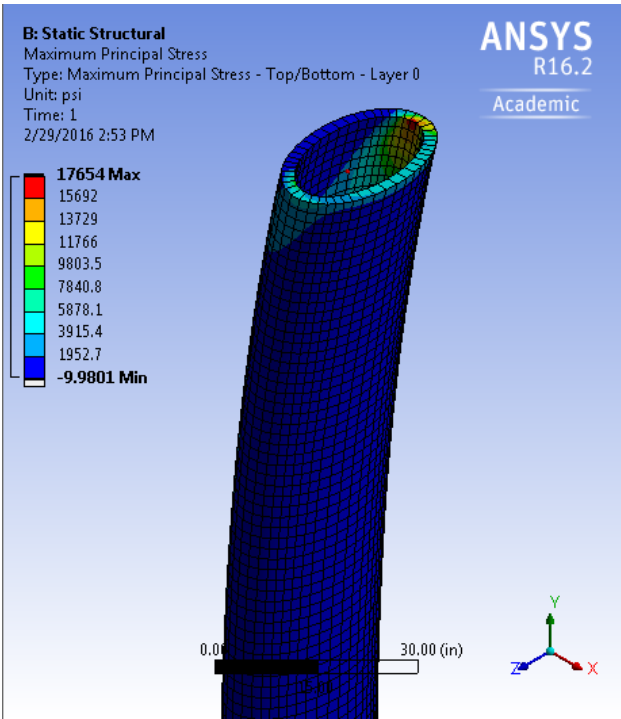
Figure 80 – Principal and shear stress for E-Glass Epoxy (up) and Kevlar 49 (down)

11.7. *FRP 231 to 235 with Constant Vertical Load and Constant Dimensions and Varying Composite Material and Displacement*

Figure 81 – Principal Stress curves for varying composite materials

Figure 82 – Principal Stress curves for varying composite materials
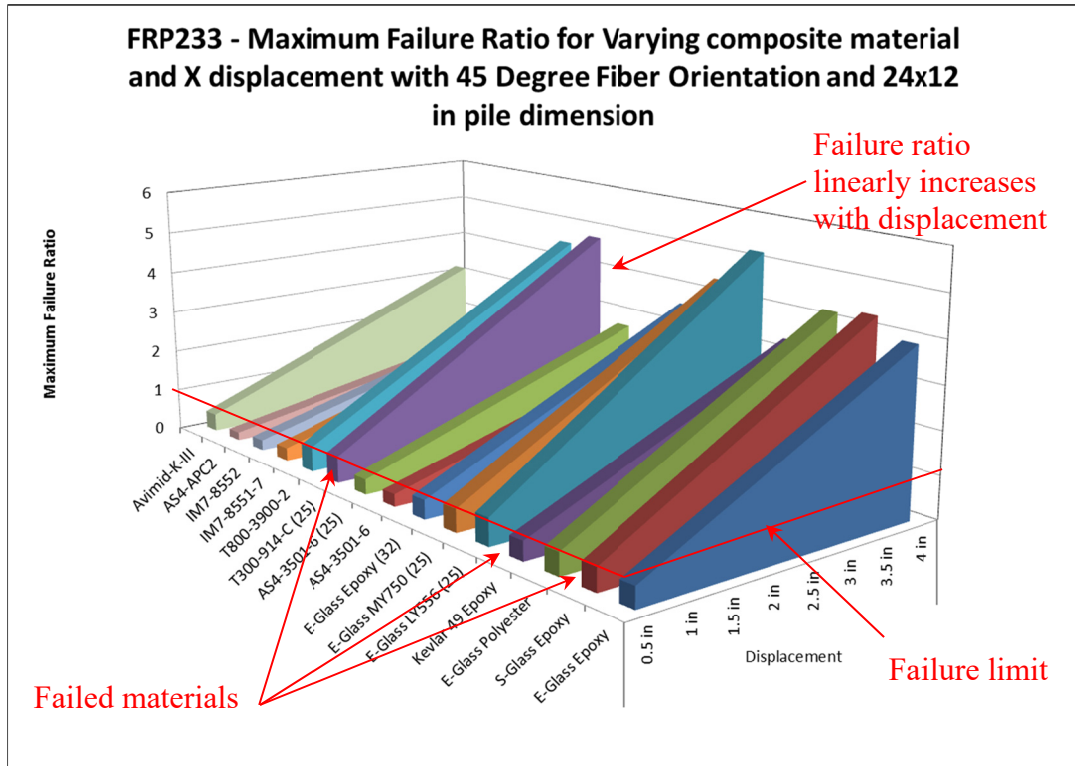
Figure 83 – Principal Stress curves for varying composite materials

As shown in Figure 81 to Figure 83, pile stress varies drastically with the type of composite material. It is also observed that the stress is proportional to the applied displacement. In another word the more displacement, the higher will be the principal and shear stresses.

11.8. *FRP 241 to 245 with Constant Displacement and Varying Fiber Orientation and Pile Dimensions*

This case appears to be the most important case. It summarizes the conclusions made in other previously described case. It shows that the piles stress changes linear with displacement and no linear with orientation angle. Figure 84 shows 30 to 40 degree fiber orientation angle produces the most principal and shear stress in a 24"x12" section. This is different from failure mode which will be discussed in next page.
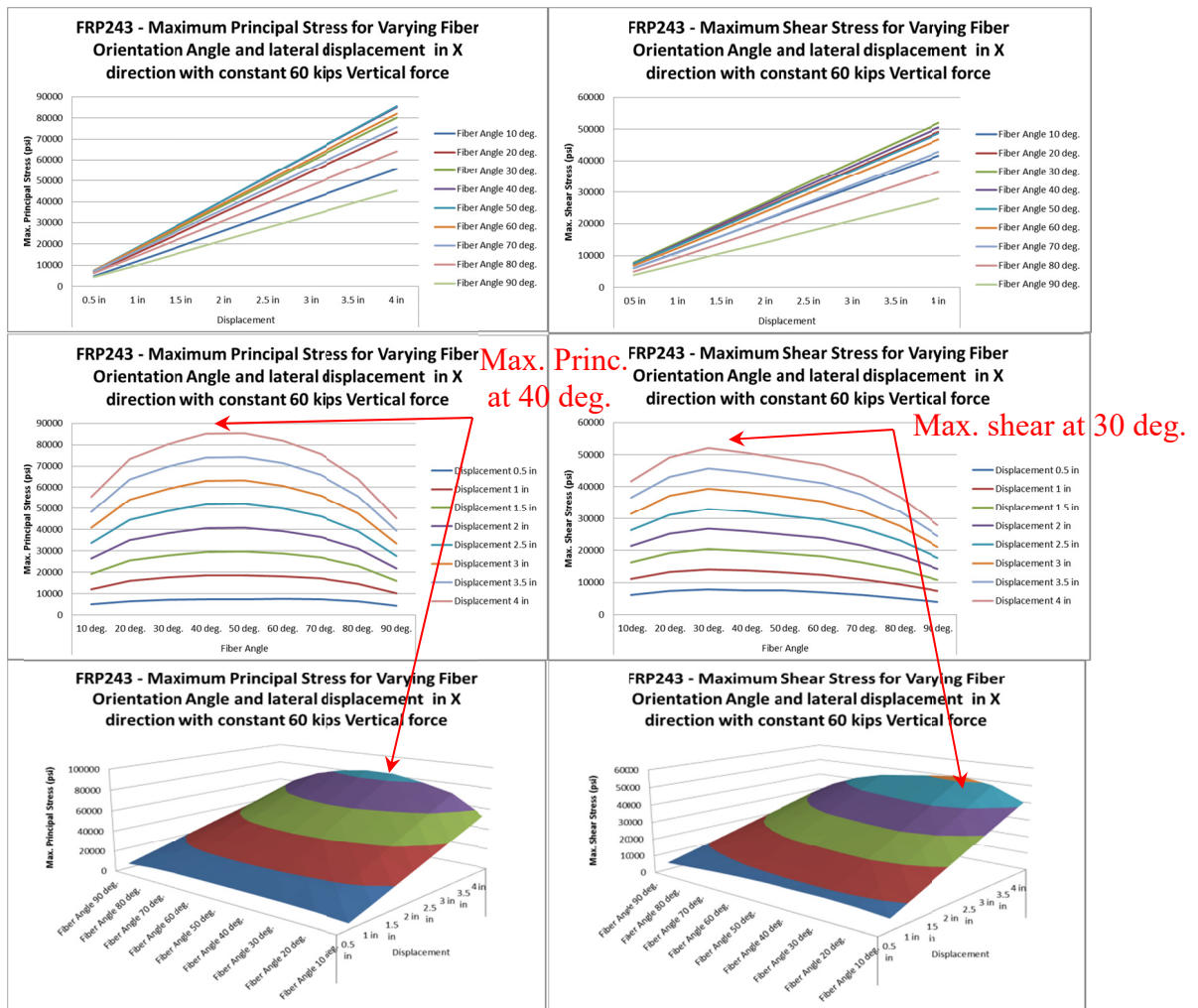
Figure 84 – Principal and shear Stress curves for varying fiber orientation and pile displacement
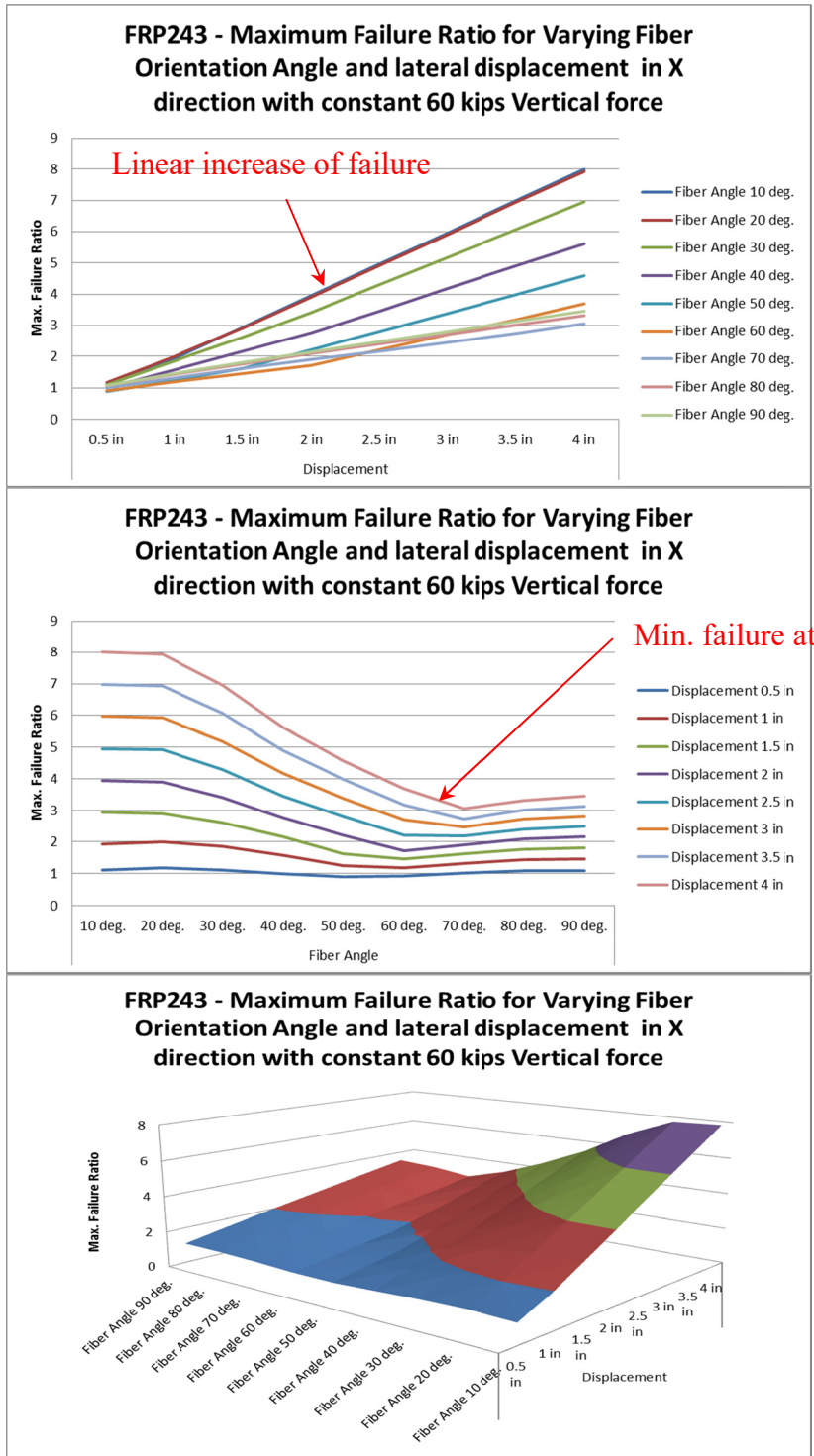
Figure 85 – Failure Ratio for a 24"x12" composite section

Figure 85 shows the pile capacity will be maximum, with 70 degree fiber orientation.

The pile capacity depends on many failure criteria.

Figure 86 compares the failure criteria in a 24"x12" section with 20 and 70 degree

fiber orientation. Failure is reduced in piles with higher fiber orientation angle.
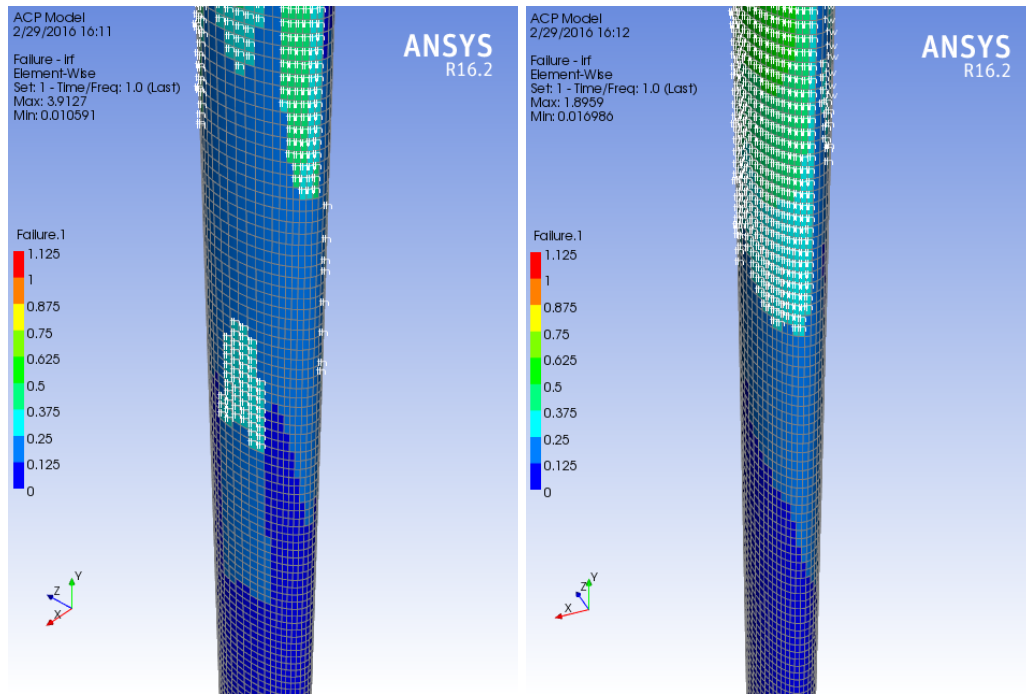
Figure 86 – Failure of elements in 24"x12" section with 20 deg. (left) and 70 deg. (right)

11.9. *FRP 261 to 265 with Constant Displacement and Varying Fiber Orientation and Pile Dimensions with Additional Parallel Fibers*
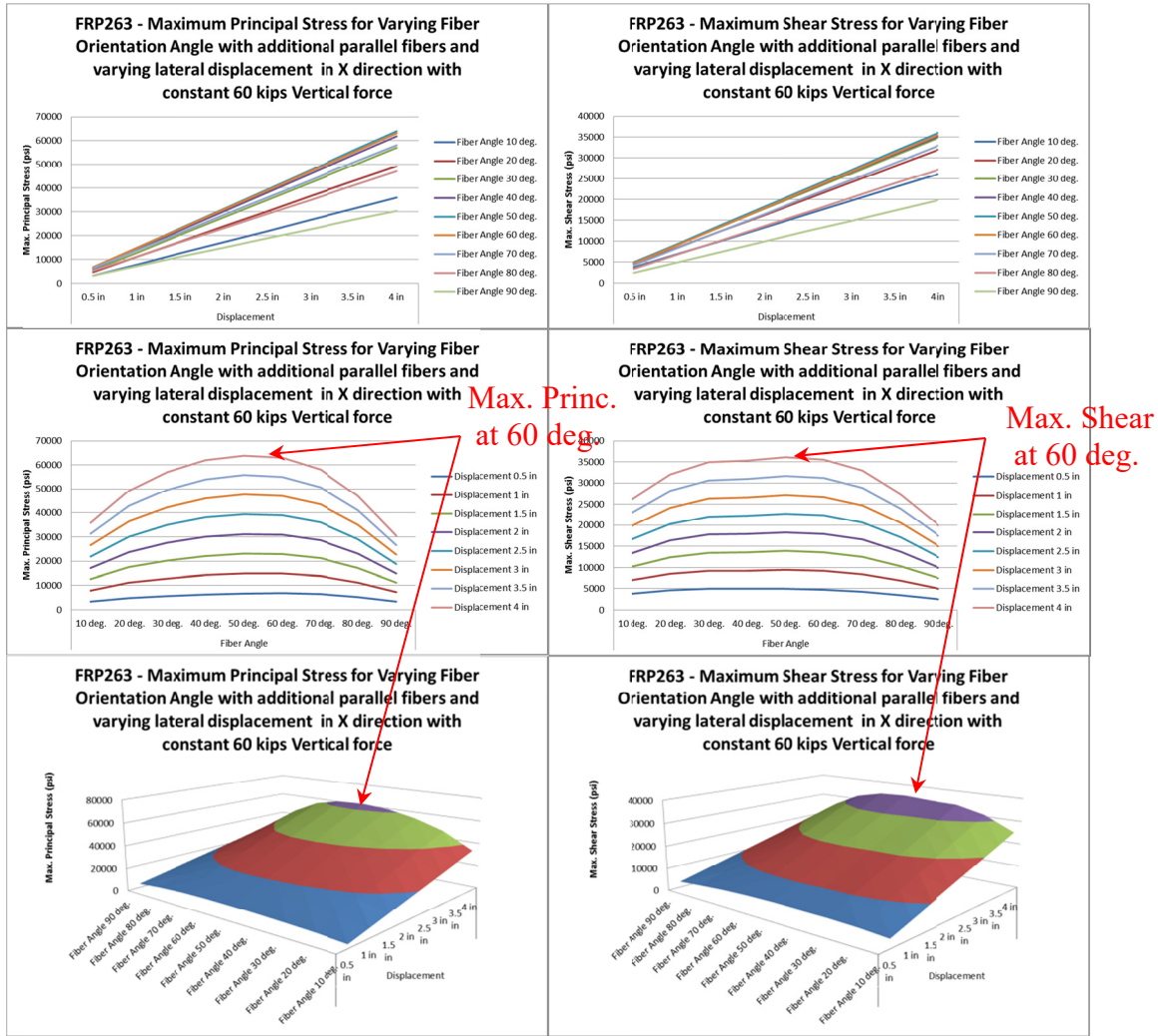
Figure 87 – Principal and shear Stress curves for varying fiber orientation and pile displacement for composites with additional parallel to axis fibers
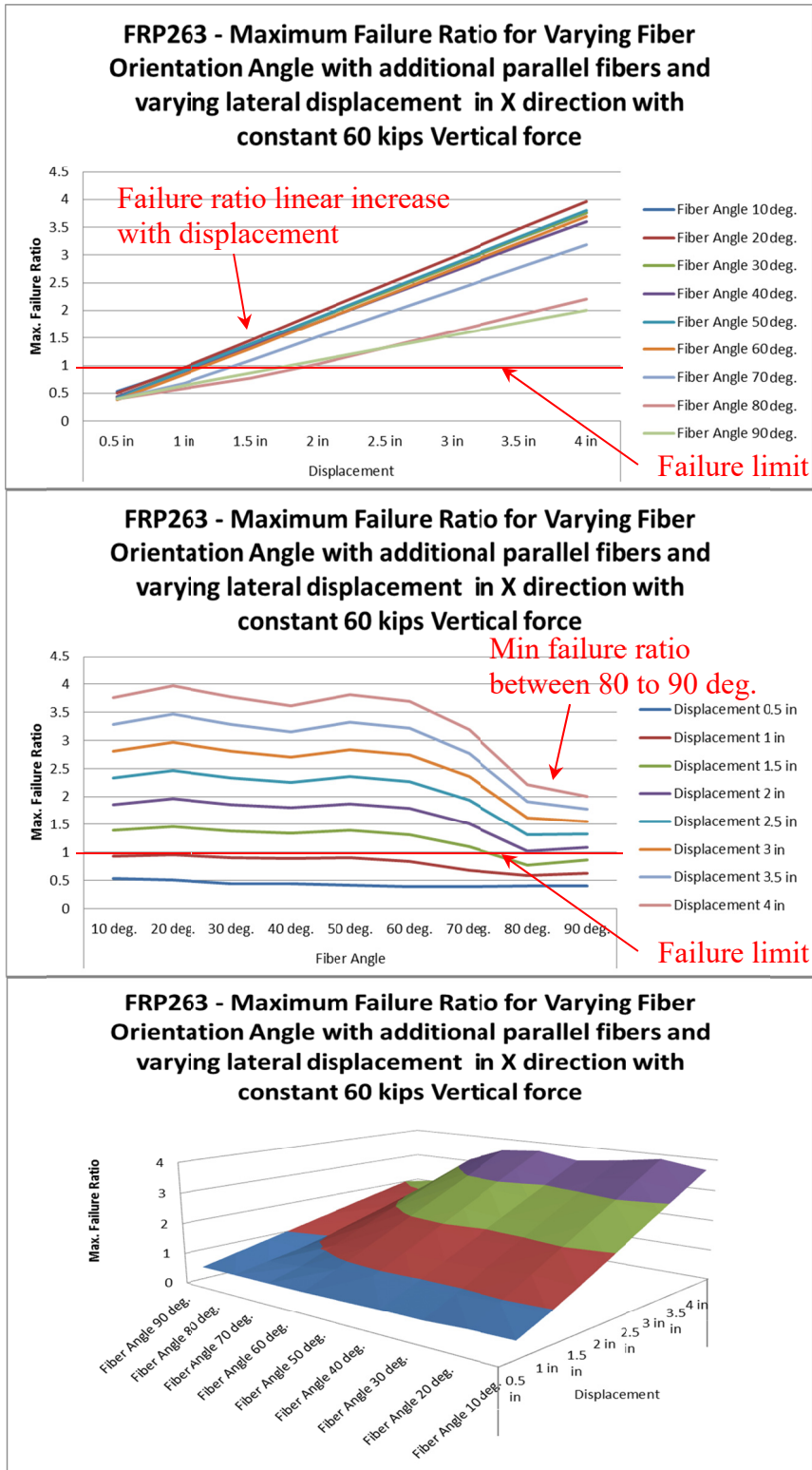
Figure 88 – Failure Ratio for a 24"x12" composite section with additional parallel fibers

160

Figure 88 shows the decrease in Failure Ratio around 80 to 90 degrees. This

obviously happens because additional layers are included with 0 degree fibers. When

rests of the layers are closer to 90 degree a balance in forces and shear of the element

reduces the failure in elements. When all of the layers are approximately in the same

direction the element shear stress limit may be lower than the applied shear. This will

result the failure in the element.

Figure 89 compares the failure criteria in a 24"x12" section with 20 and 90 degree

fiber orientation. Failure is reduced in piles with higher fiber orientation angle.
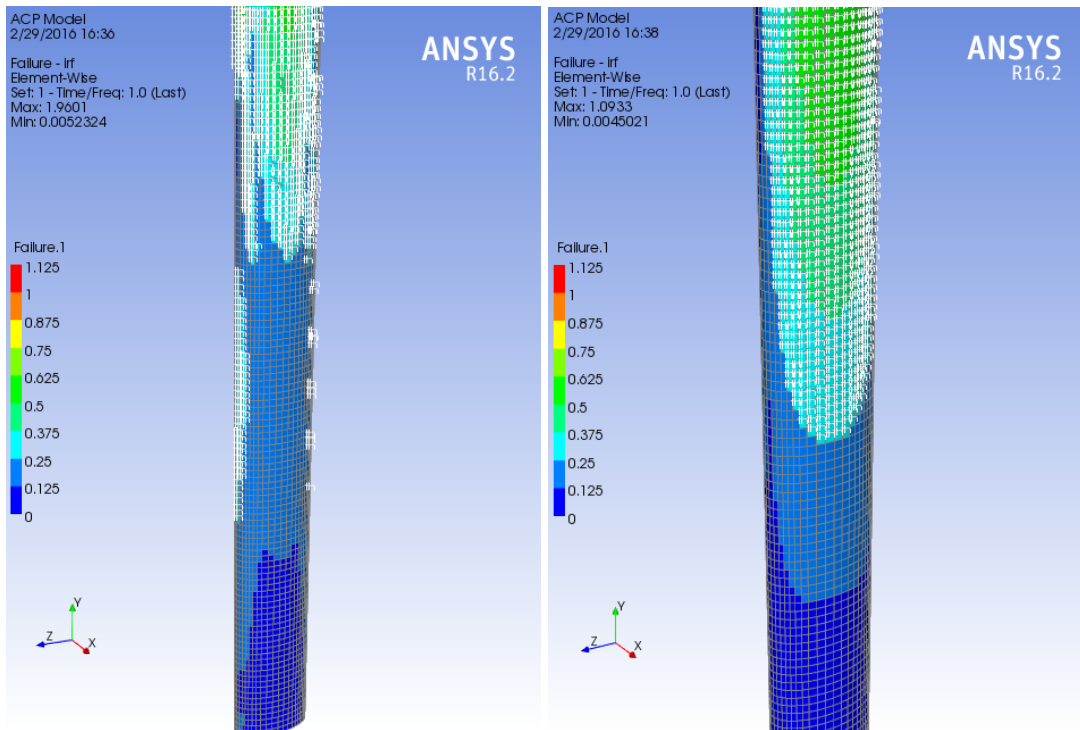
Figure 89 – Failure of elements in 24"x12" section with 90 deg. (left) and 20 deg. (right)

11.10. *FRP 281 to 285 with Constant Displacement and Varying Fiber Orientation and Pile Dimensions with Additional Perpendicular Fibers*
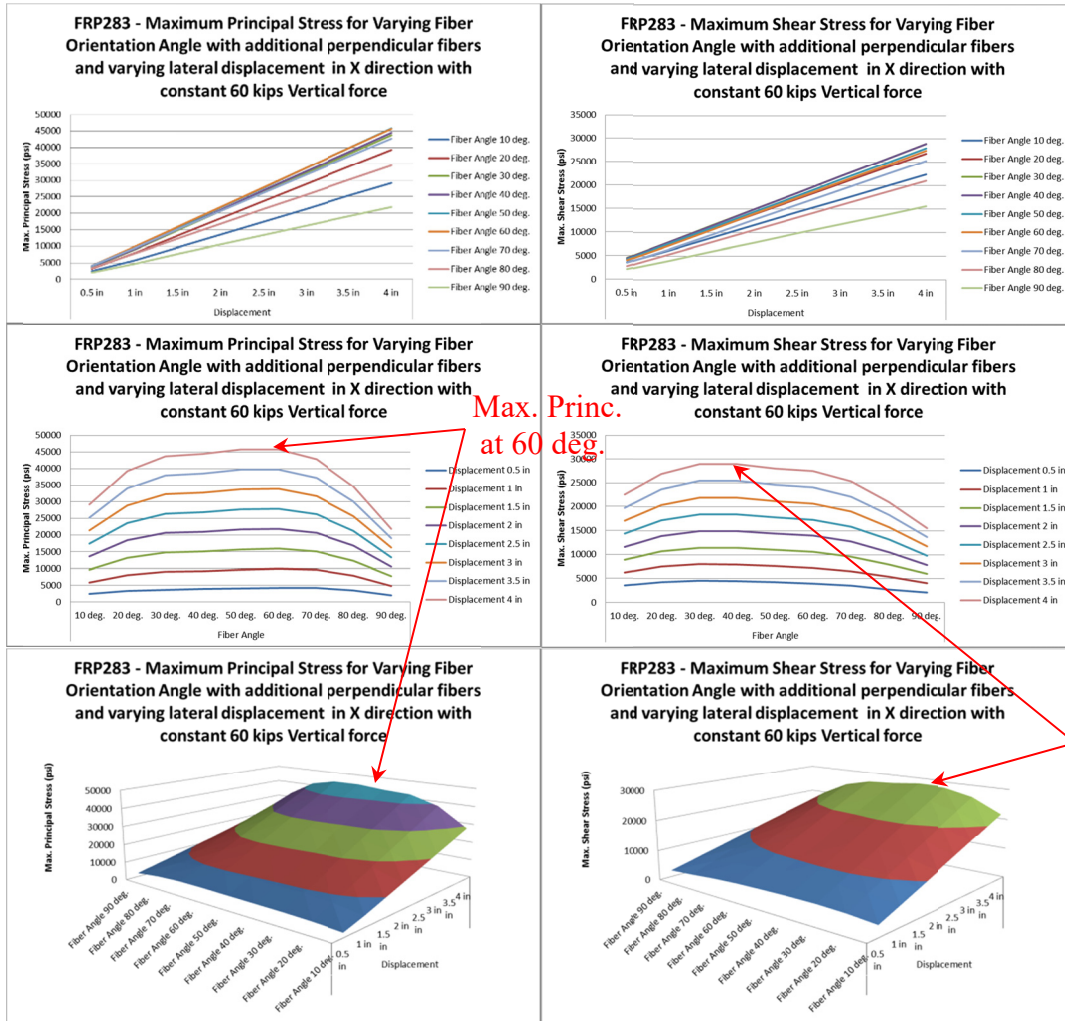
Figure 90 – Principal and shear Stress curves for varying fiber orientation and pile displacement for composites with additional perpendicular to axis fibers
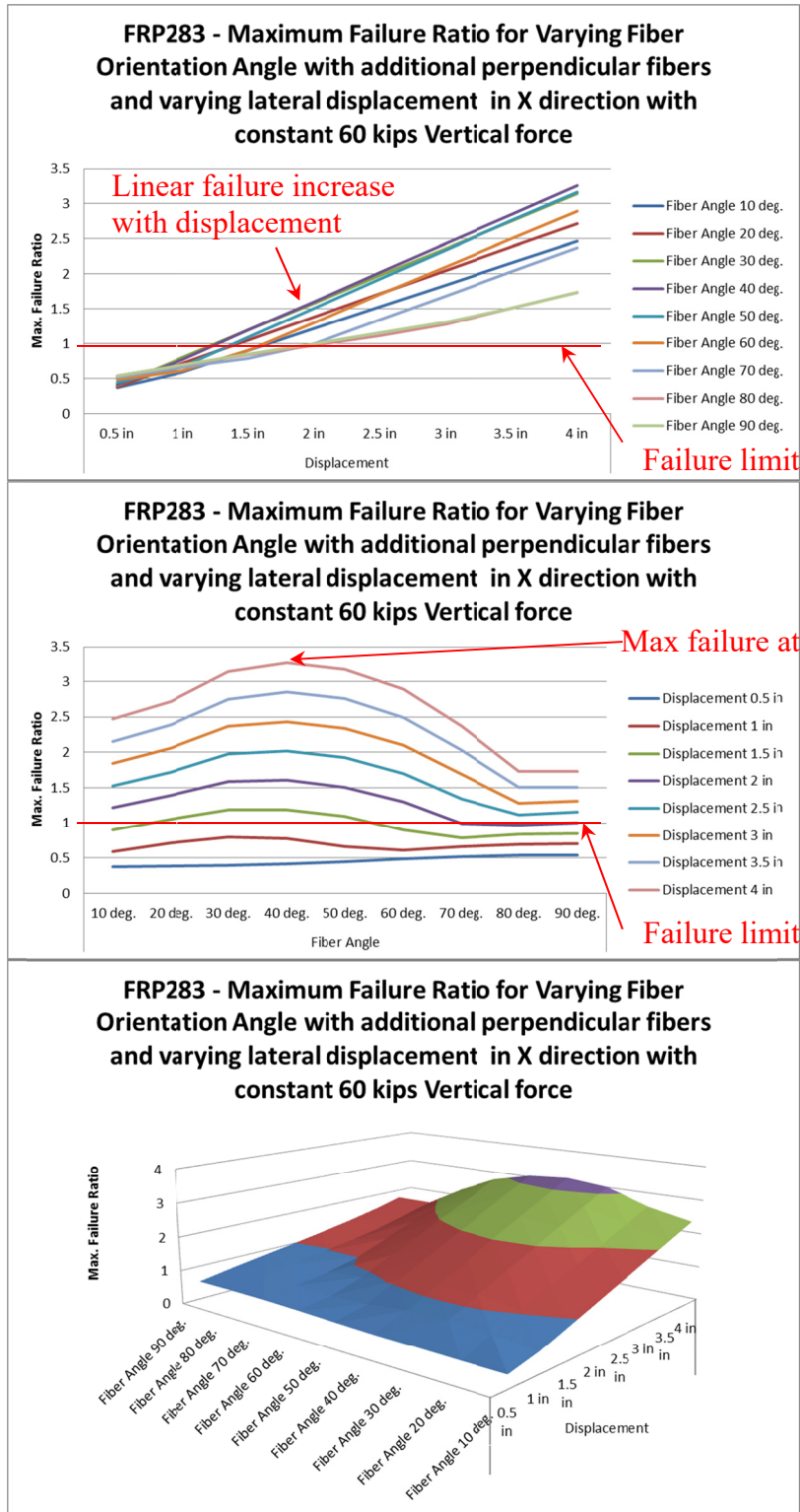
Figure 91 – Failure Ratio for a 24"x12" composite section with additional perpendicular fibers

Figure 91 shows the decrease in Failure Ratio around 80 to 90 degrees. This obviously happens because additional layers are included with 90 degree fibers. When rests of the layers are closer to 90 degree a balance in forces and shear of the element reduces the failure in elements. When all of the layers are approximately in the same direction the element shear stress limit may be lower than the applied shear. This will result the failure in the element.

Figure 92 compares the failure criteria in a 24"x12" section with 40 and 90 degree fiber orientation. Failure is reduced in piles with higher fiber orientation angle.
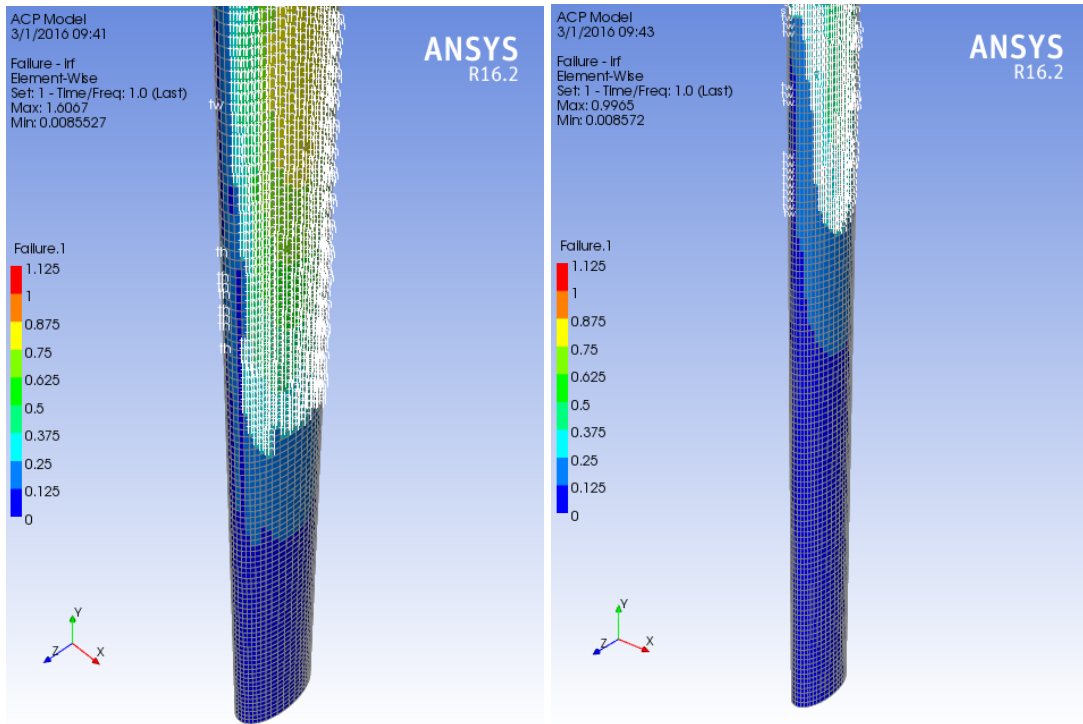
Figure 92 – Failure of elements in 24"x12" section with 40 deg. (left) and 90 deg. (right)

11.11. *FRP 301 to 305 with Constant Displacement and Varying Fiber Orientation with Nonlinear Soft Clay Soil*
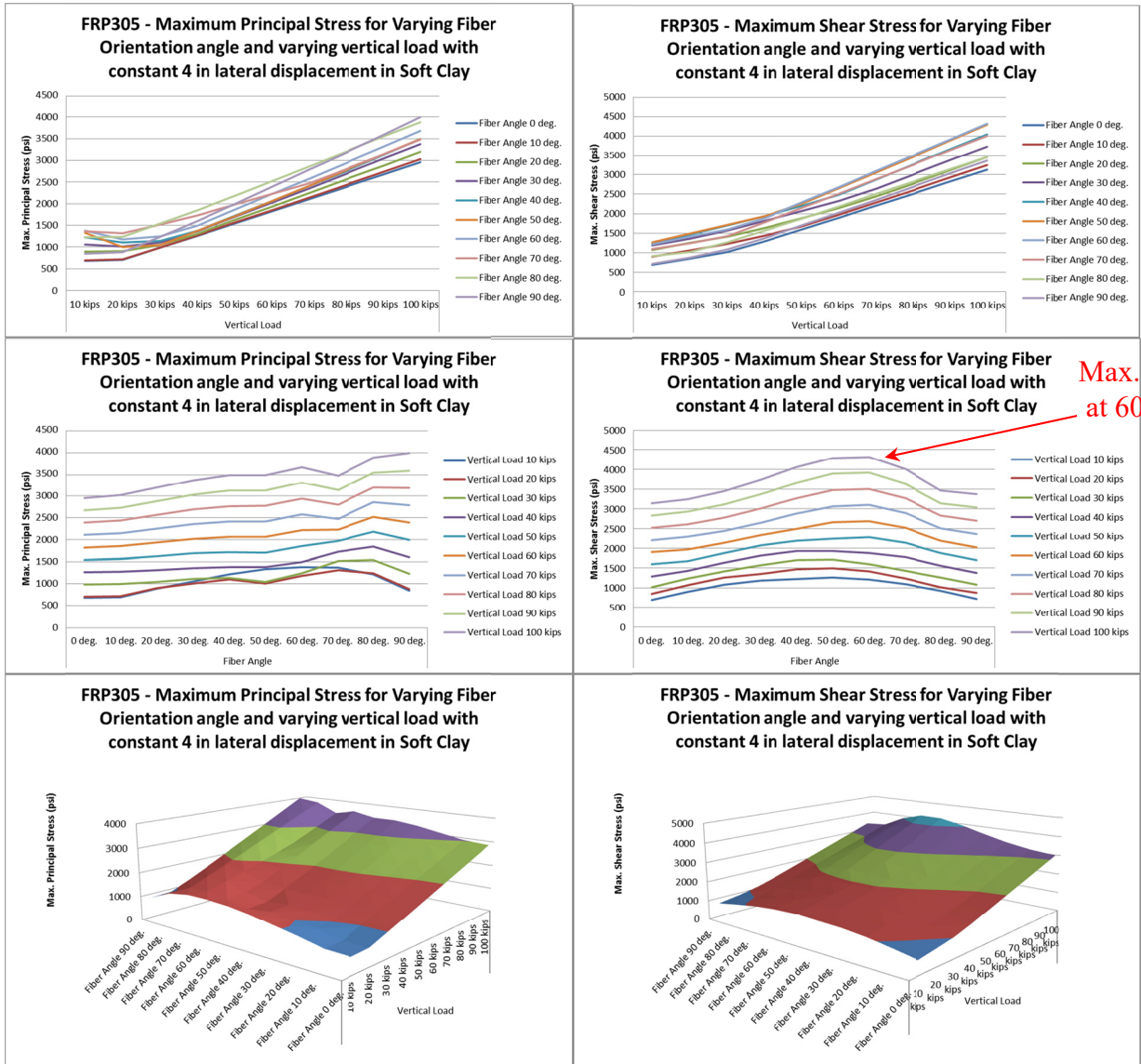
Figure 93 – Principal and shear stress curves for varying fiber orientation and pile vertical load for composites with nonlinear soft clay soil
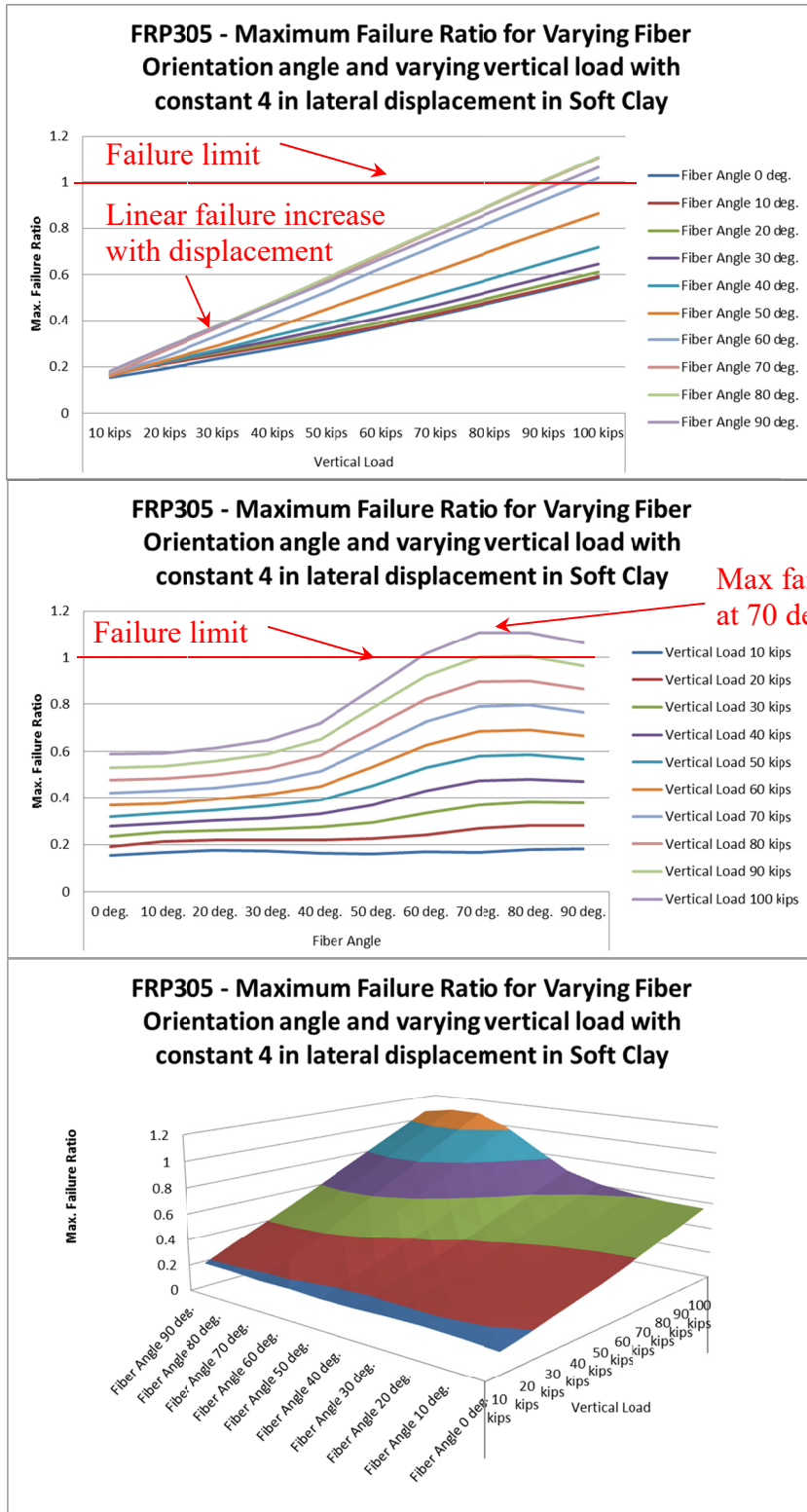
Figure 94 – Failure Ratio for a 24"x12" composite section with nonlinear soft clay

Figure 94 shows the increase in Failure Ratio around 80 to 90 degrees. Figure 95 compares the stresses in a 24"x12" section with 10 and 80 degree fiber orientation. Stress is increased in piles with higher fiber orientation angle.
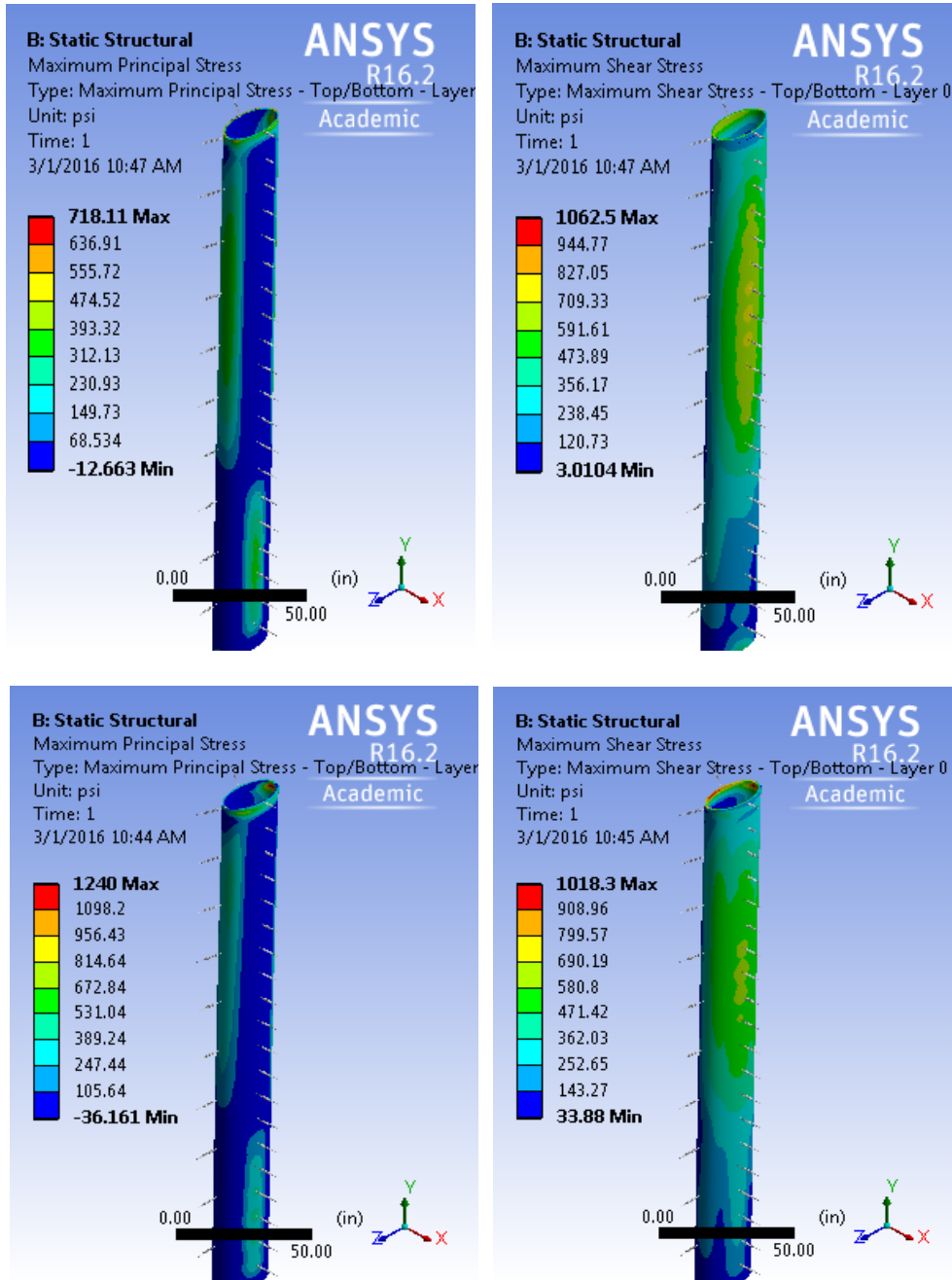
Figure 95 – Principal and shear stress contour line of 24"x12" section with 10 deg. (up) and 80 deg. (down) with soft clay soil

11.12. *FRP 311 to 315 with Constant Displacement and Varying fiber Orientation with Nonlinear Stiff Clay Soil*
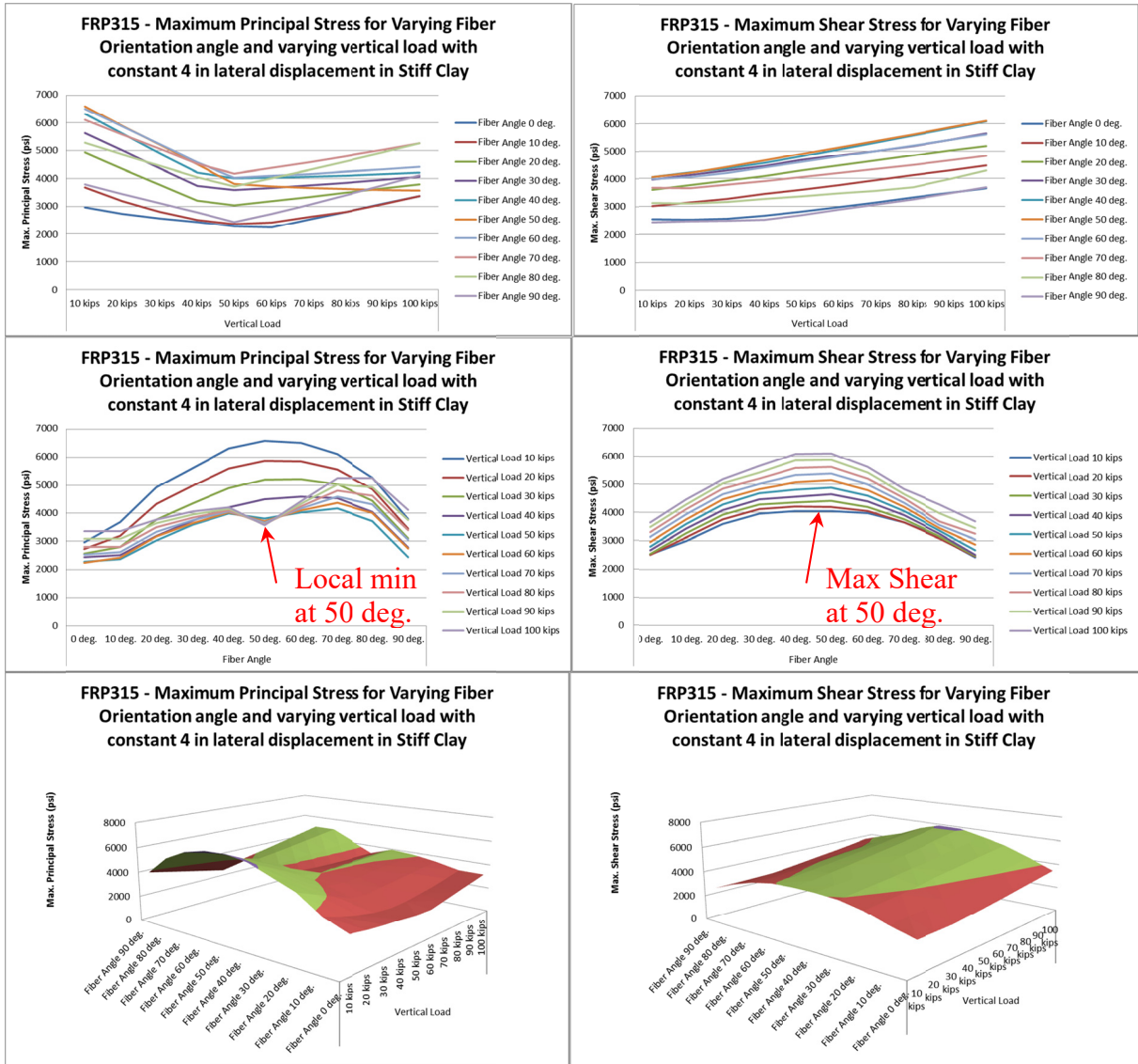
Figure 96 – Principal and shear stress curves for varying fiber orientation and pile vertical load for composites with nonlinear stiff clay soil
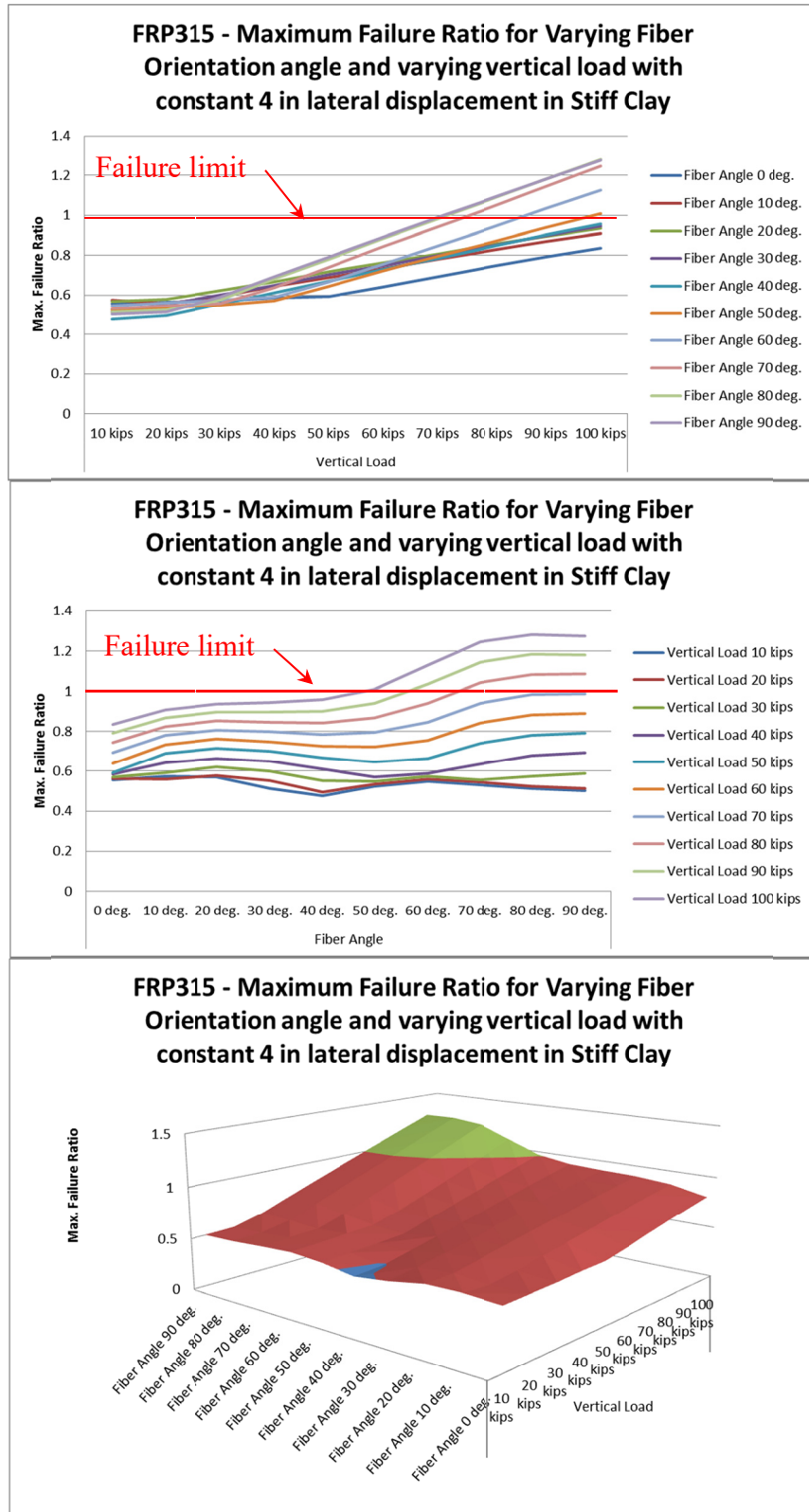
Figure 97 – Failure Ratio for a 24"x12" composite section with nonlinear stiff clay

Figure 97 shows the increase in Failure Ratio around 80 to 90 degrees. Figure 98 compares the stresses in a 24"x12" section with 10 and 80 degree fiber orientation. Stress is increased in piles with higher fiber orientation angle.
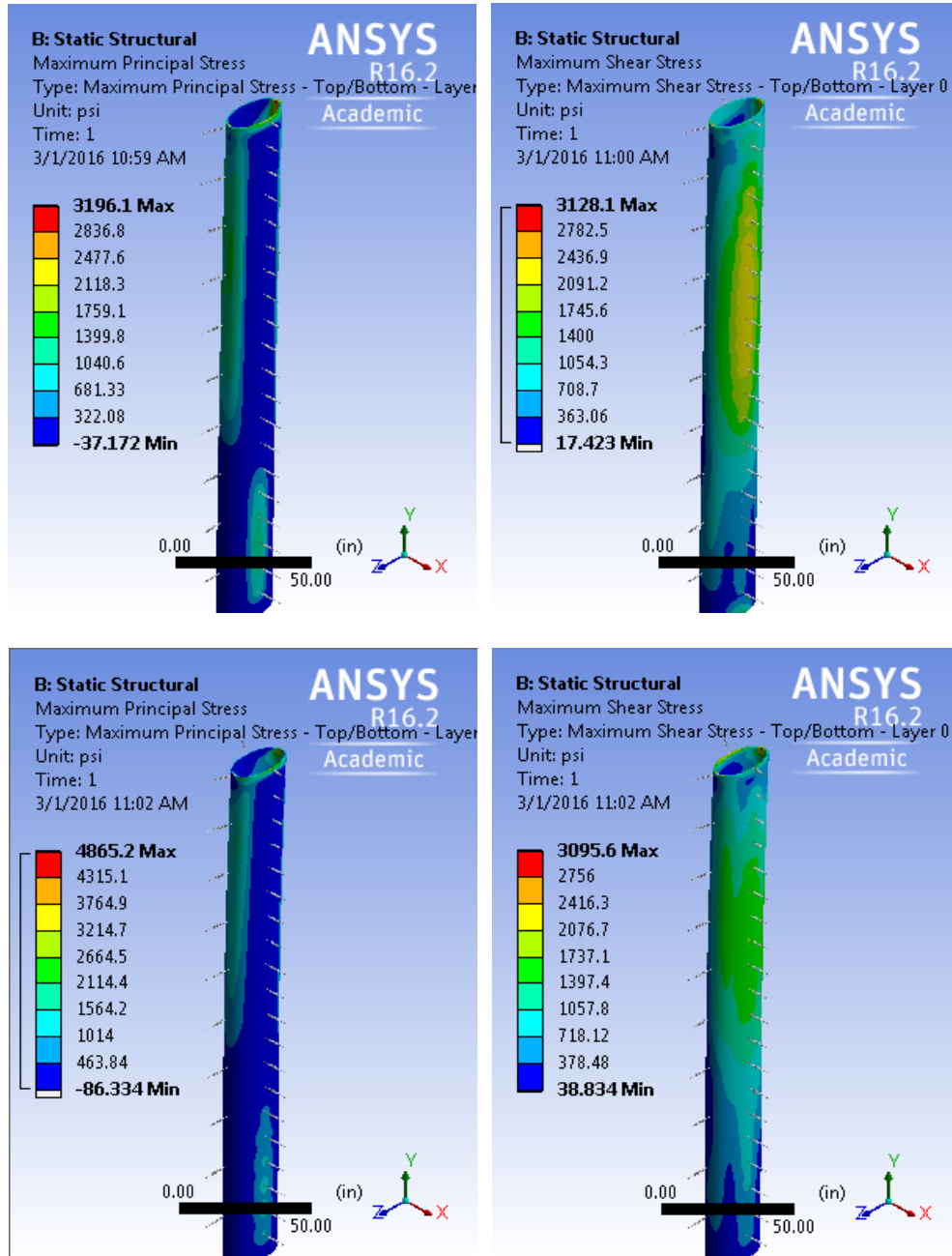
Figure 98 – Principal and shear stress contour line of 24"x12" section with 10 deg. (up) and 80 deg. (down) with stiff clay soil

11.13. *FRP 321 to 325 with Constant Displacement and Varying Fiber Orientation with Nonlinear Very Stiff Clay Soil*
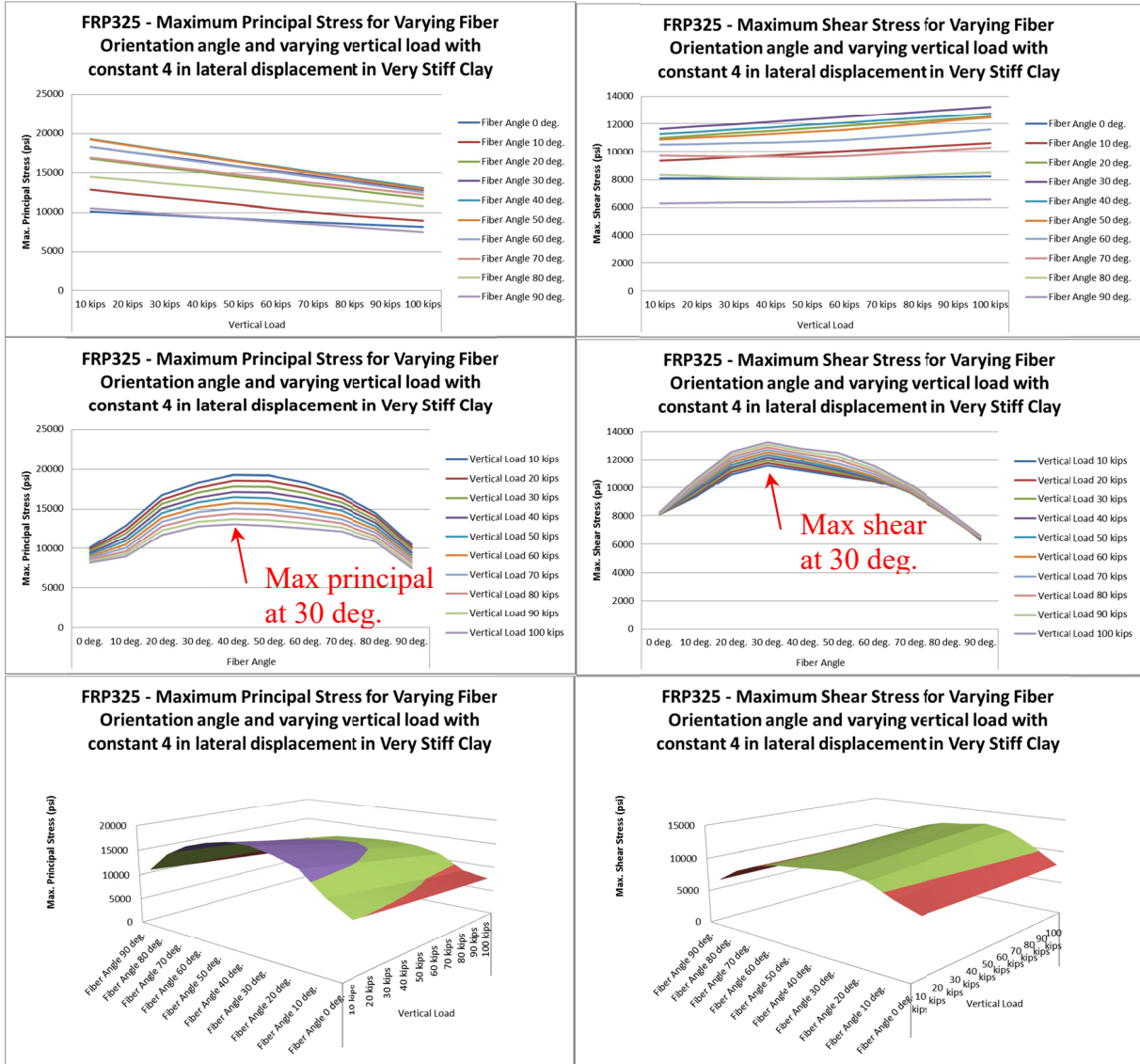
Figure 99 – Principal and shear stress curves for varying fiber orientation and pile vertical load for composites with nonlinear very stiff clay soil
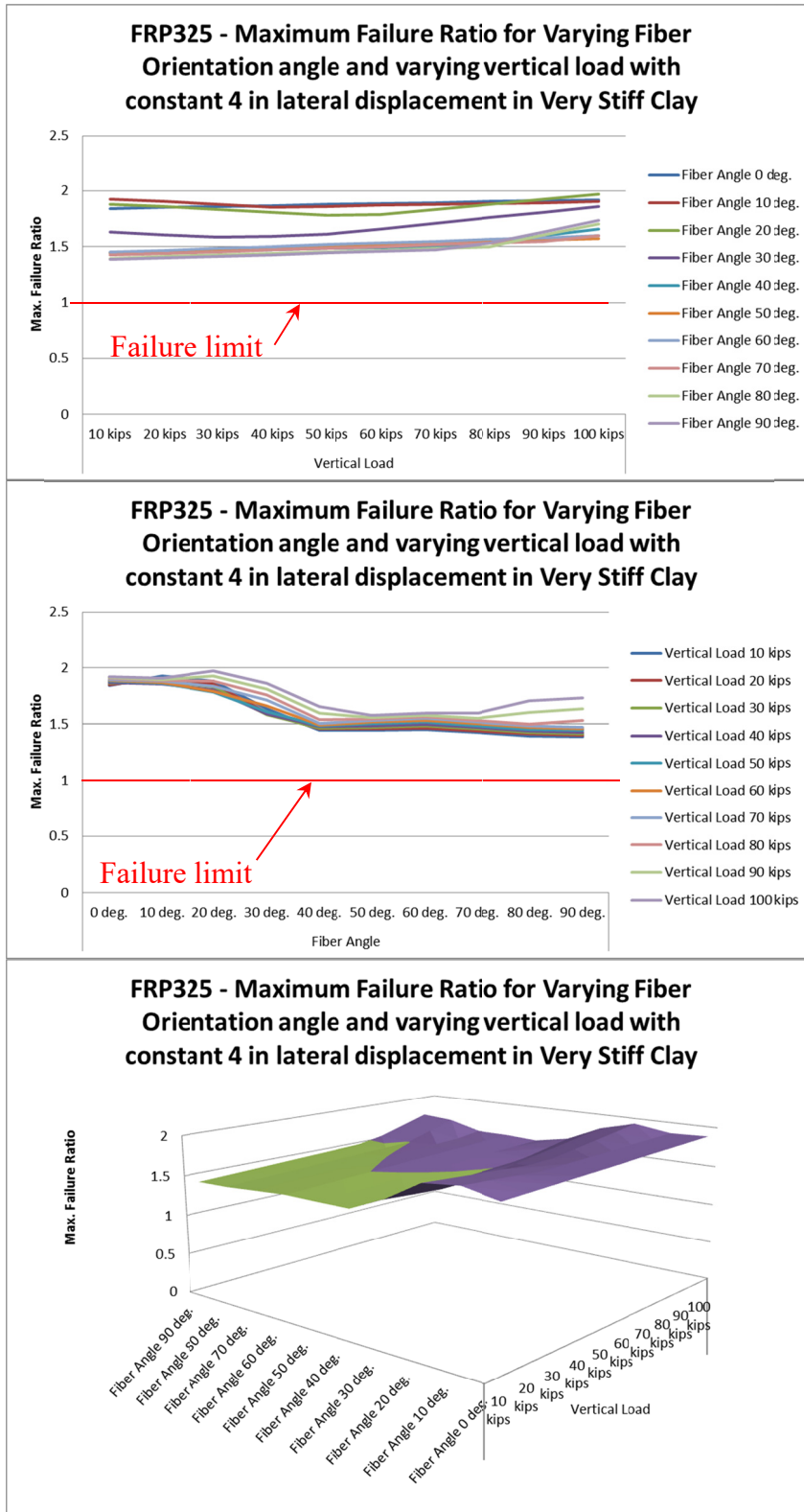
Figure 100 – Failure Ratio for a 24"x12" composite section with nonlinear very stiff clay

Figure 100 shows Failure Ratio remains almost constant with changes in fiber orientation angle. Figure 101 compares the stresses in a 24"x12" section with 10 and 80 degree fiber orientation. Stress remains approximately constant.
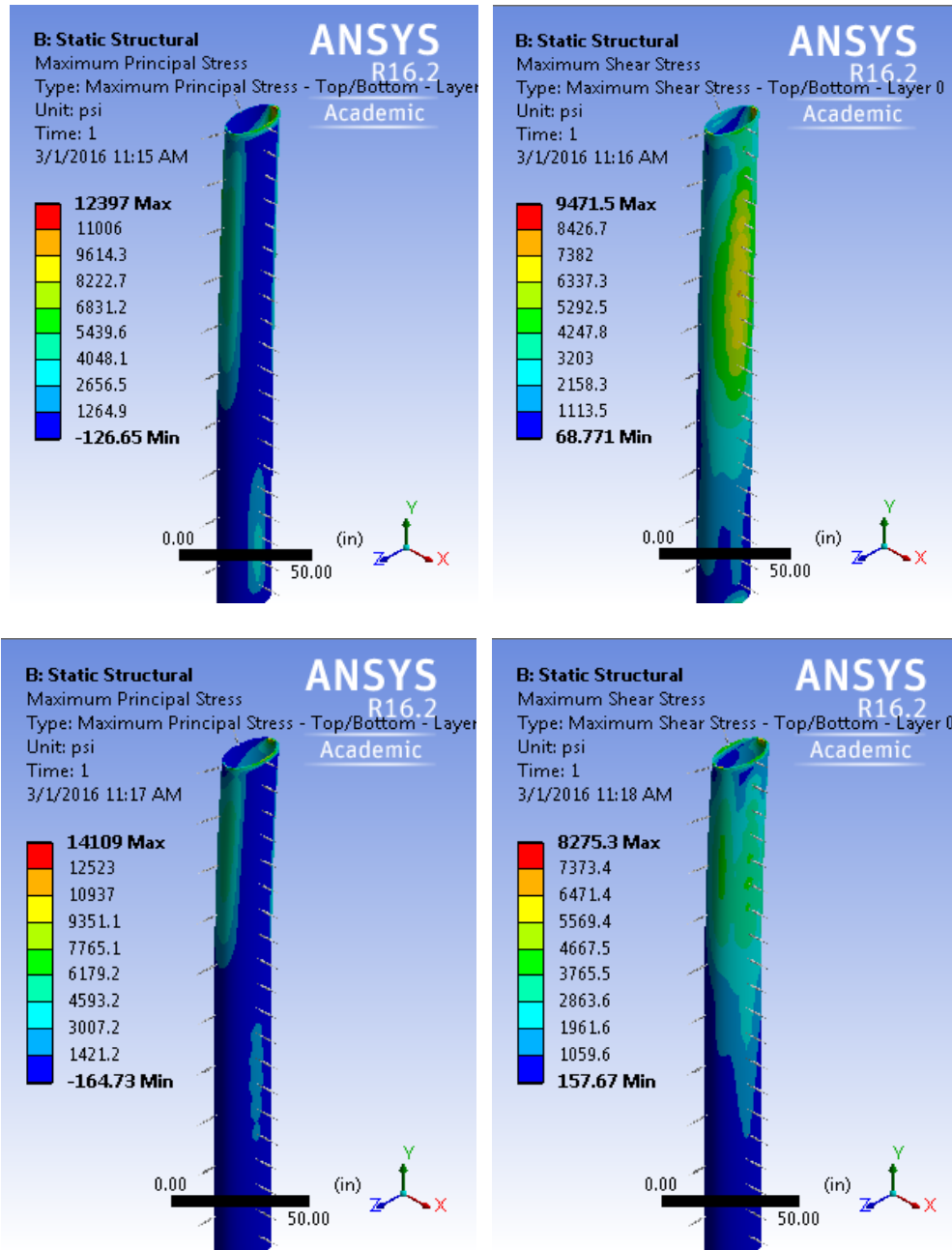
Figure 101 – Principal and shear stress contour line of 24"x12" section with 10 deg. (up) and 80 deg. (down) with very stiff clay soil

11.14. *FRP 331 to 335 with Constant Displacement and Varying Fiber Orientation with Nonlinear Loose Sand Soil*
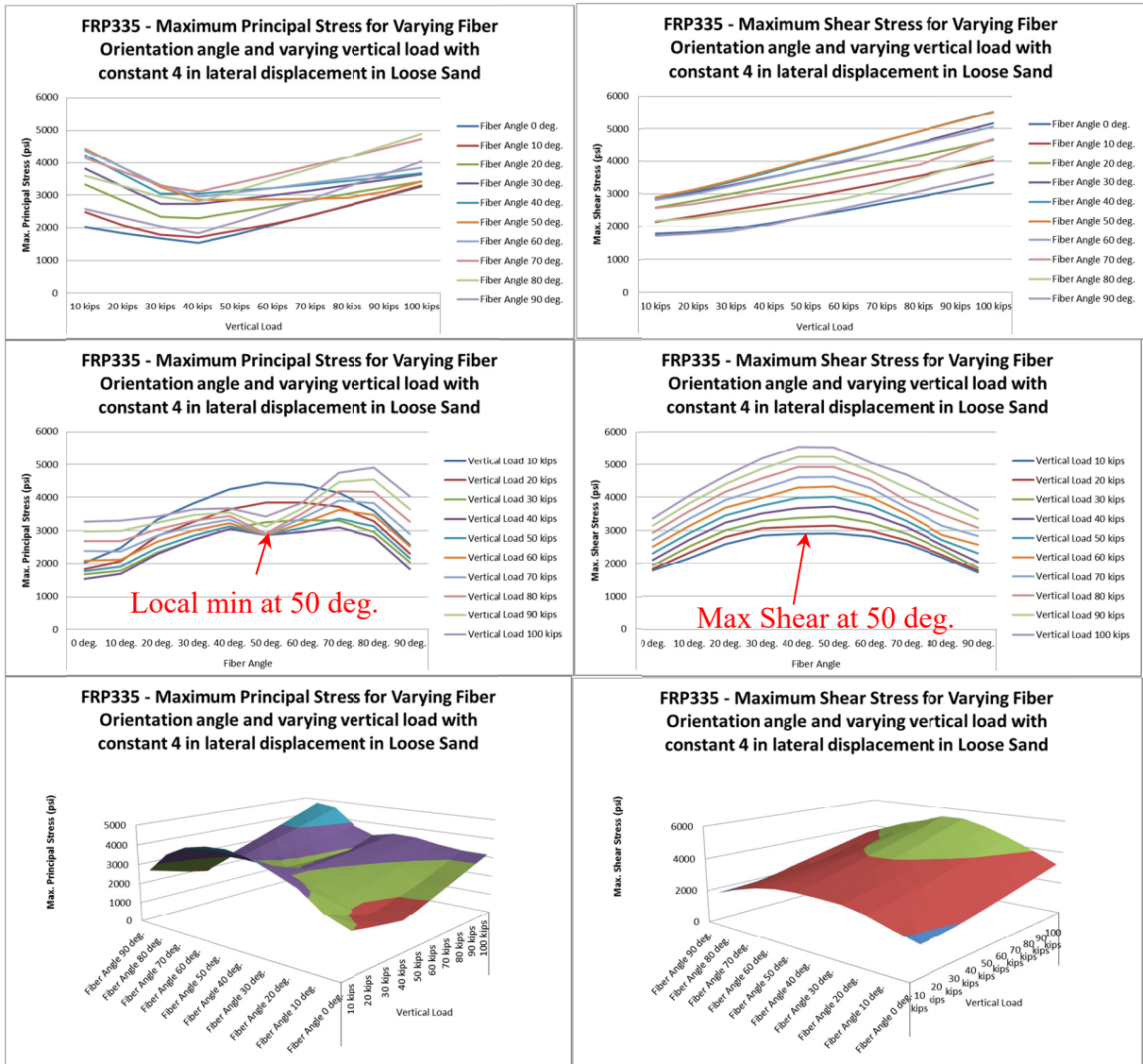
Figure 102 – Principal and shear stress curves for varying fiber orientation and pile vertical load for composites with nonlinear loose sand soil
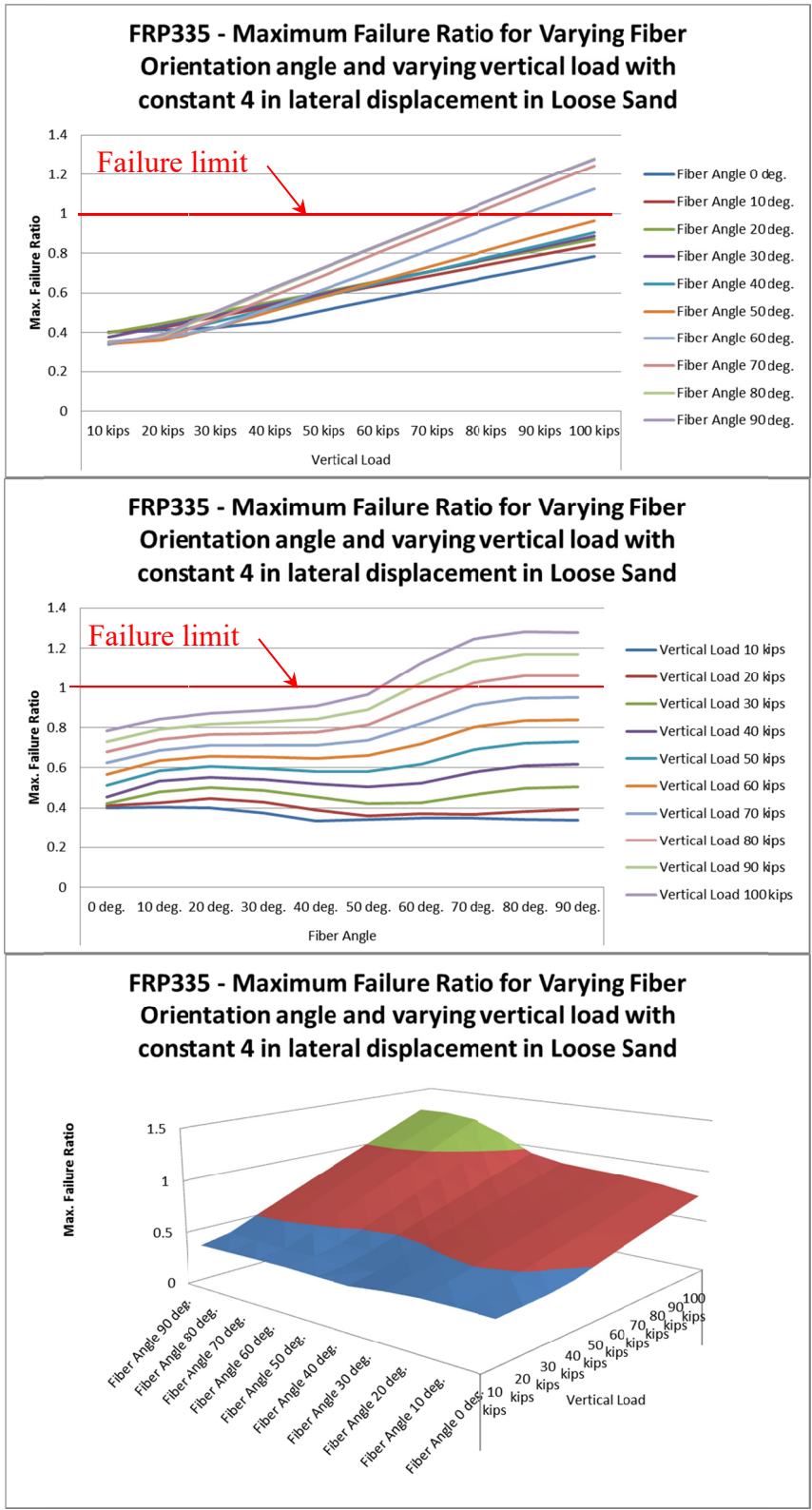
Figure 103 – Failure Ratio for a 24"x12" composite section with nonlinear loose sand

Figure 103 shows Failure Ratio increases with increase in fiber orientation angle.
Figure 104 compares the stresses in a 24"x12" section with 10 and 80 degree fiber
orientation. Stress increases with higher orientation angle.
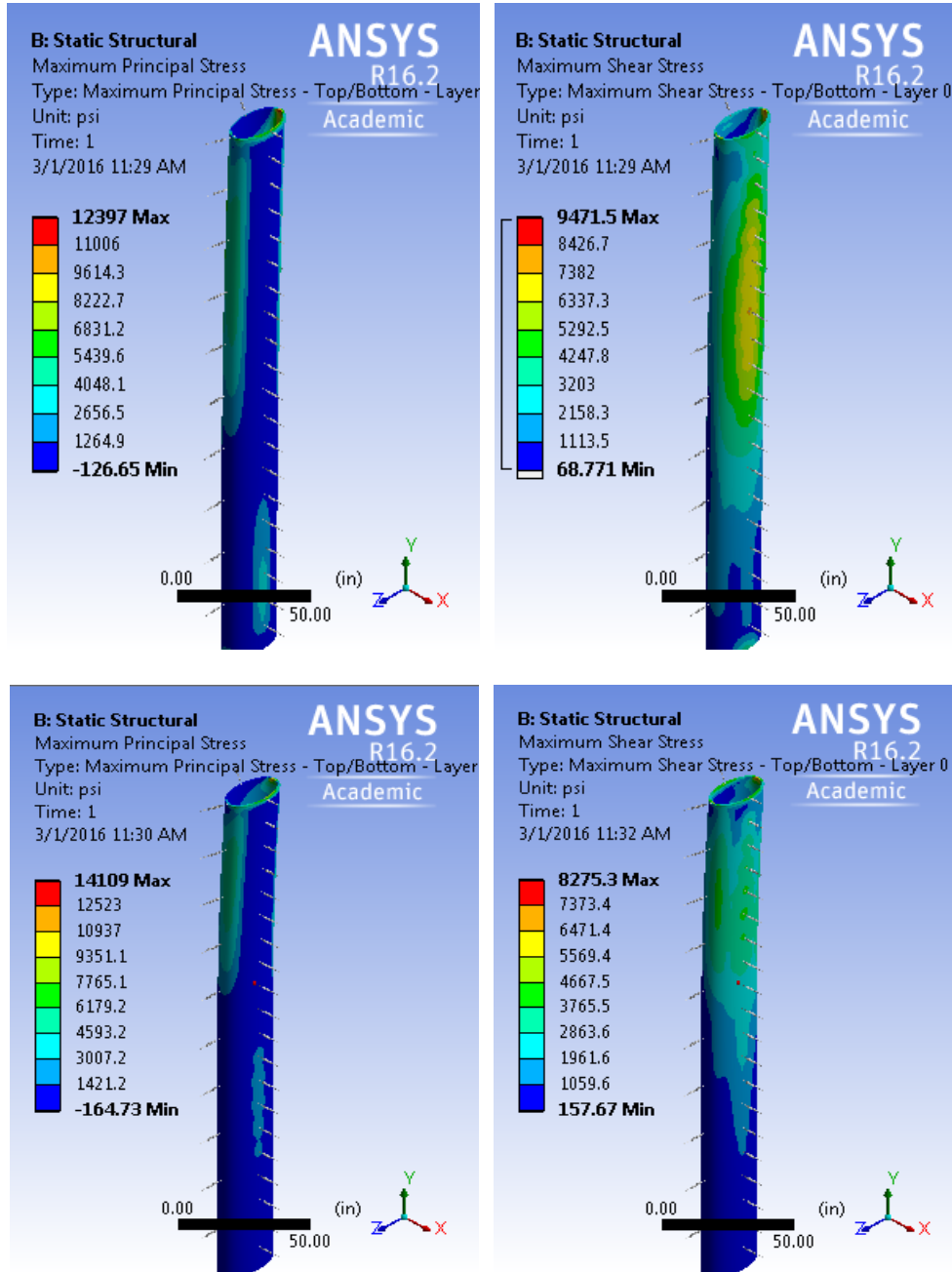
**Figure 104 – Principal and shear stress contour line of 24"x12" section with 10 deg. (up)
and 80 deg. (down) with loose sand soil**

11.15. *FRP 341 to 345 with Constant Displacement and Varying Fiber Orientation With Nonlinear Medium Sand Soil*
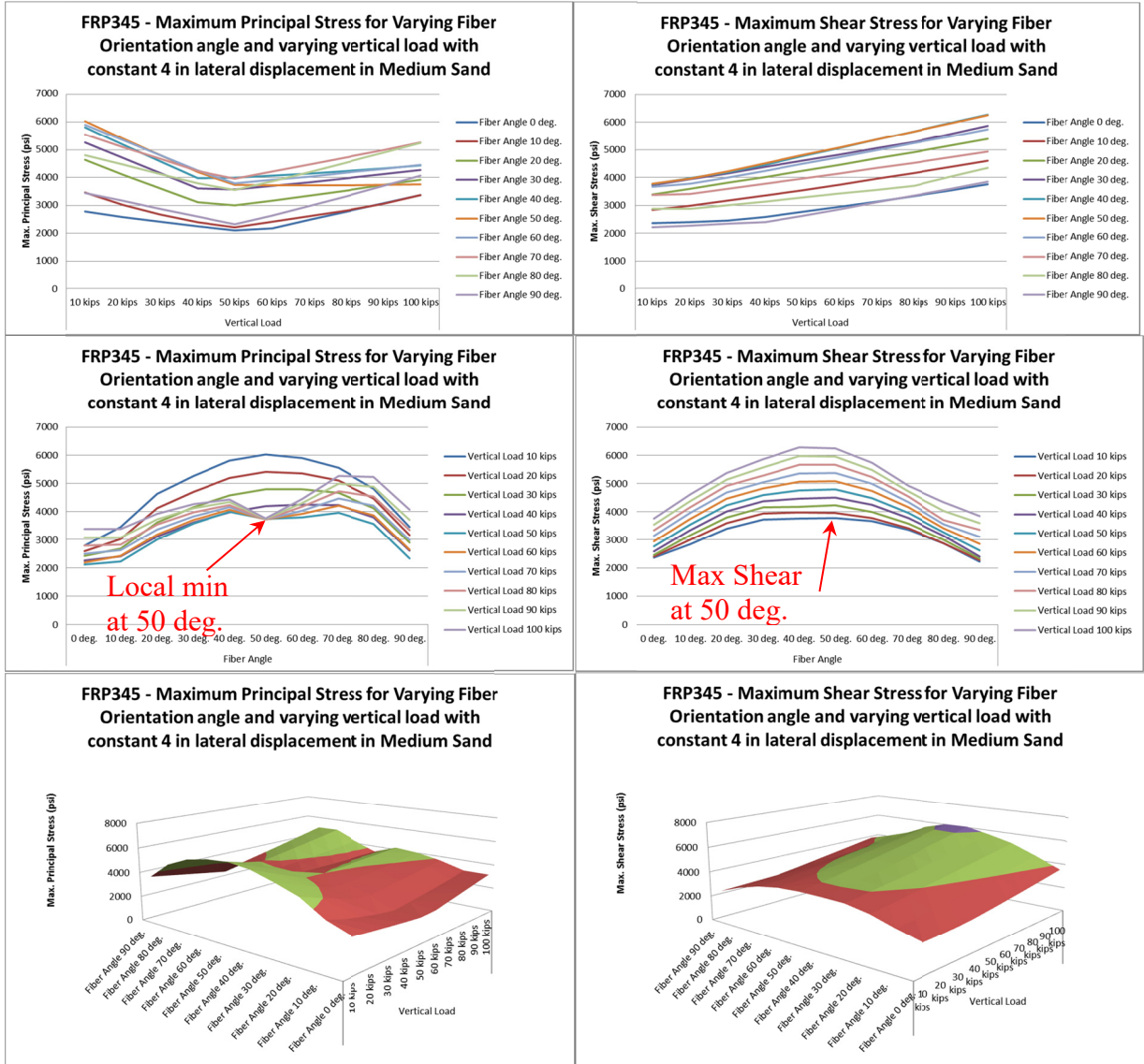
Figure 105 – Principal and shear stress curves for varying fiber orientation and pile vertical load for composites with nonlinear medium sand soil
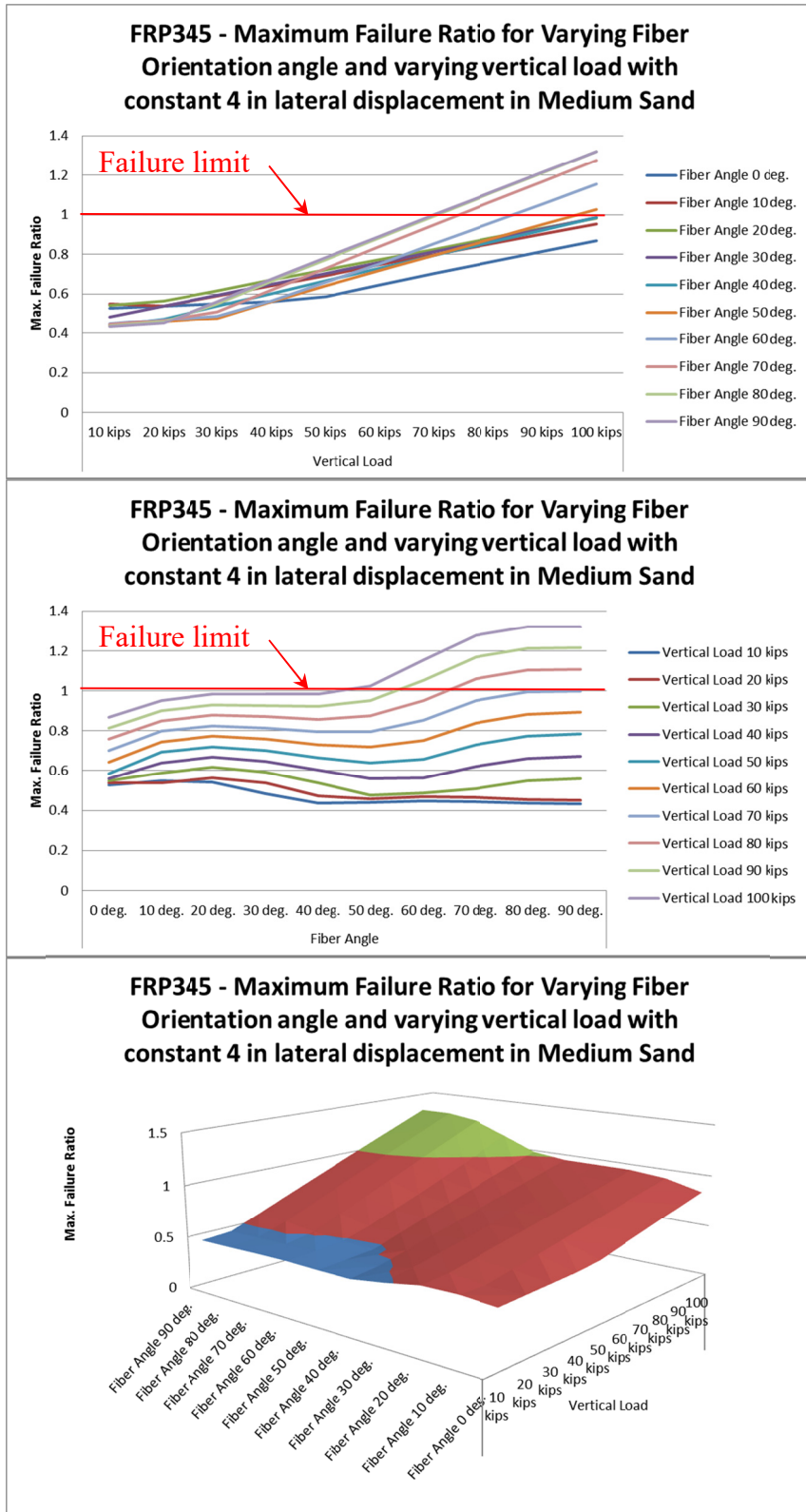
Figure 106 – Failure Ratio for a 24"x12" composite section with nonlinear medium sand

Figure 106 shows Failure Ratio increases with increase in fiber orientation angle.

Figure 107 compares the stresses in a 24"x12" section with 10 and 80 degree fiber

orientation. Stress increases with higher orientation angle.
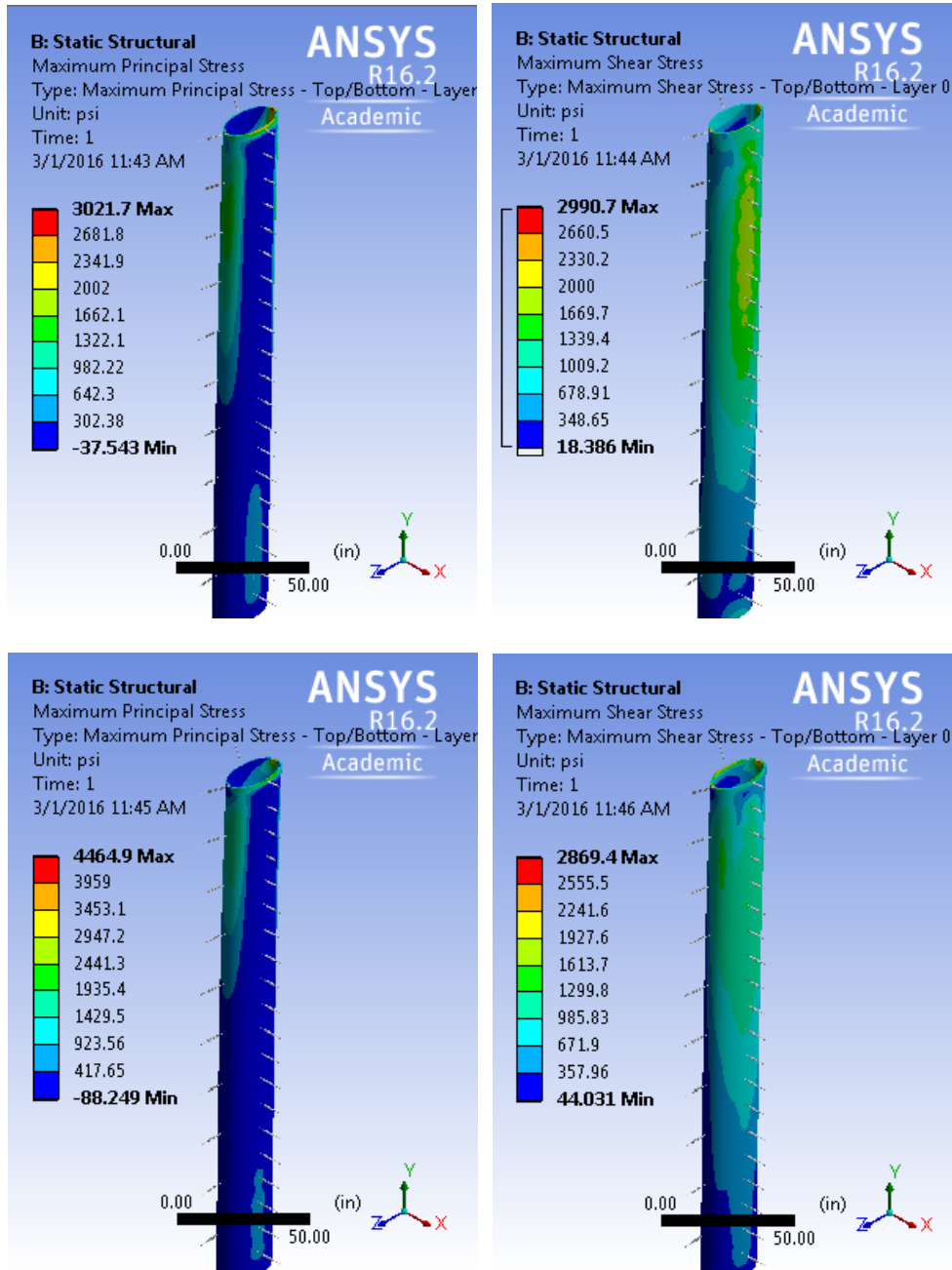
Figure 107 – Principal and shear stress contour line of 24"x12" section with 10 deg. (up) and 80 deg. (down) with medium sand soil

11.16. *FRP 351 to 355 with Constant Displacement and Varying Fiber Orientation with Nonlinear Dense Sand Soil*
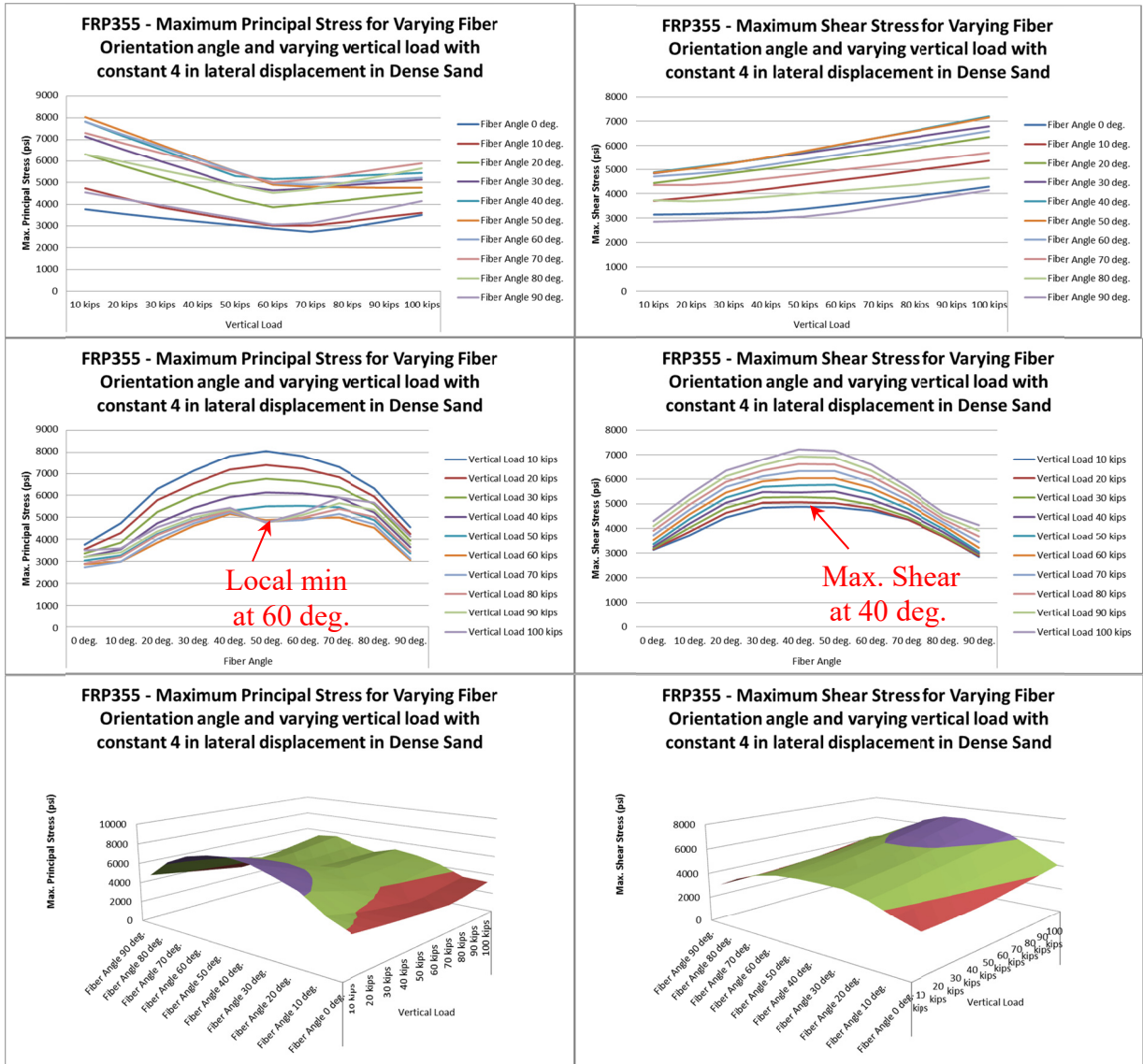
Figure 108 – Principal and shear stress curves for varying fiber orientation and pile vertical load for composites with nonlinear dense sand soil
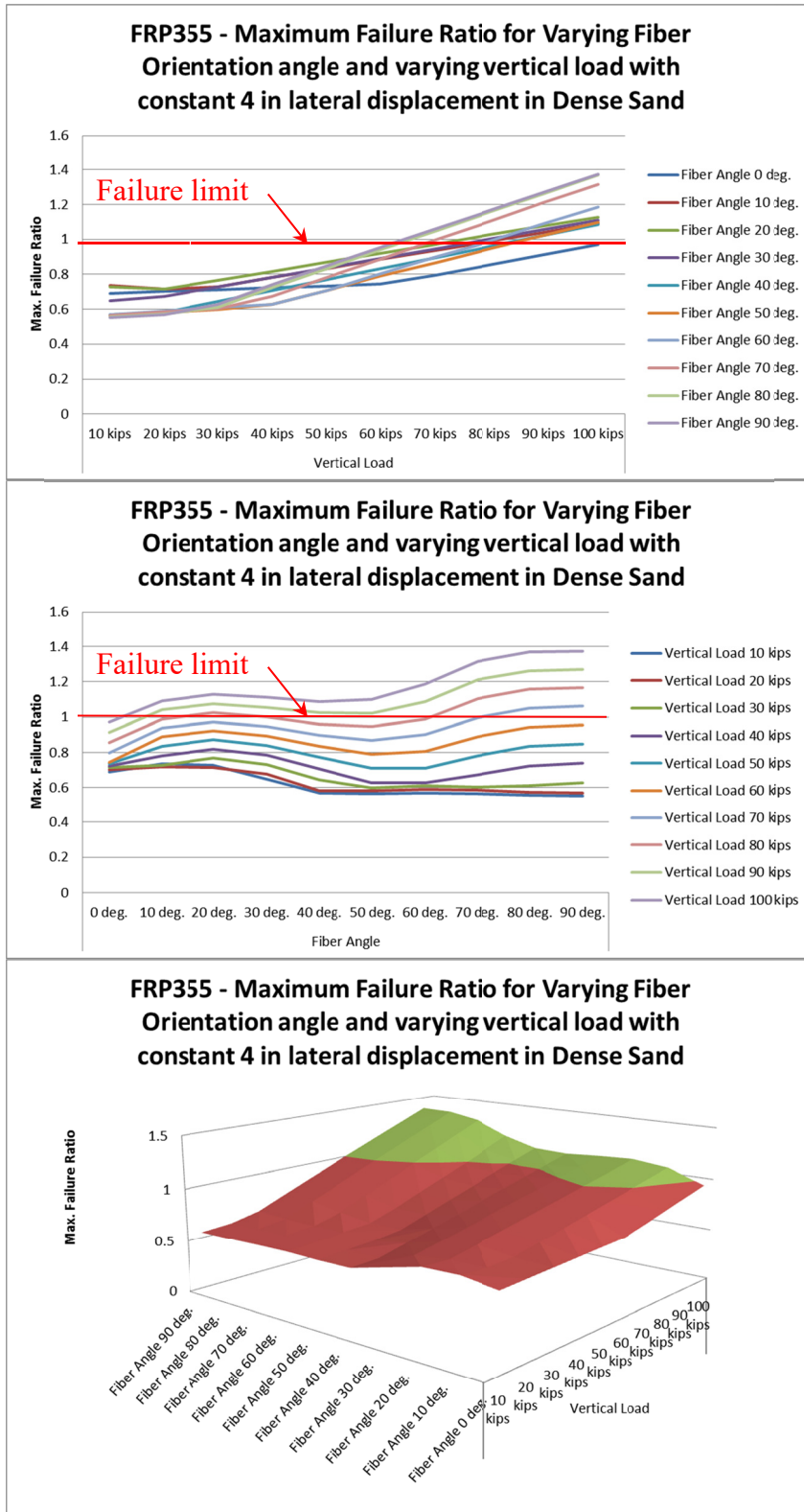
Figure 109 – Failure Ratio for a 24"x12" composite section with nonlinear dense sand

181

Figure 109 shows Failure Ratio increases with increase in fiber orientation angle.
Figure 110 compares the stresses in a 24"x12" section with 10 and 80 degree fiber
orientation. Stress increases with higher orientation angle.
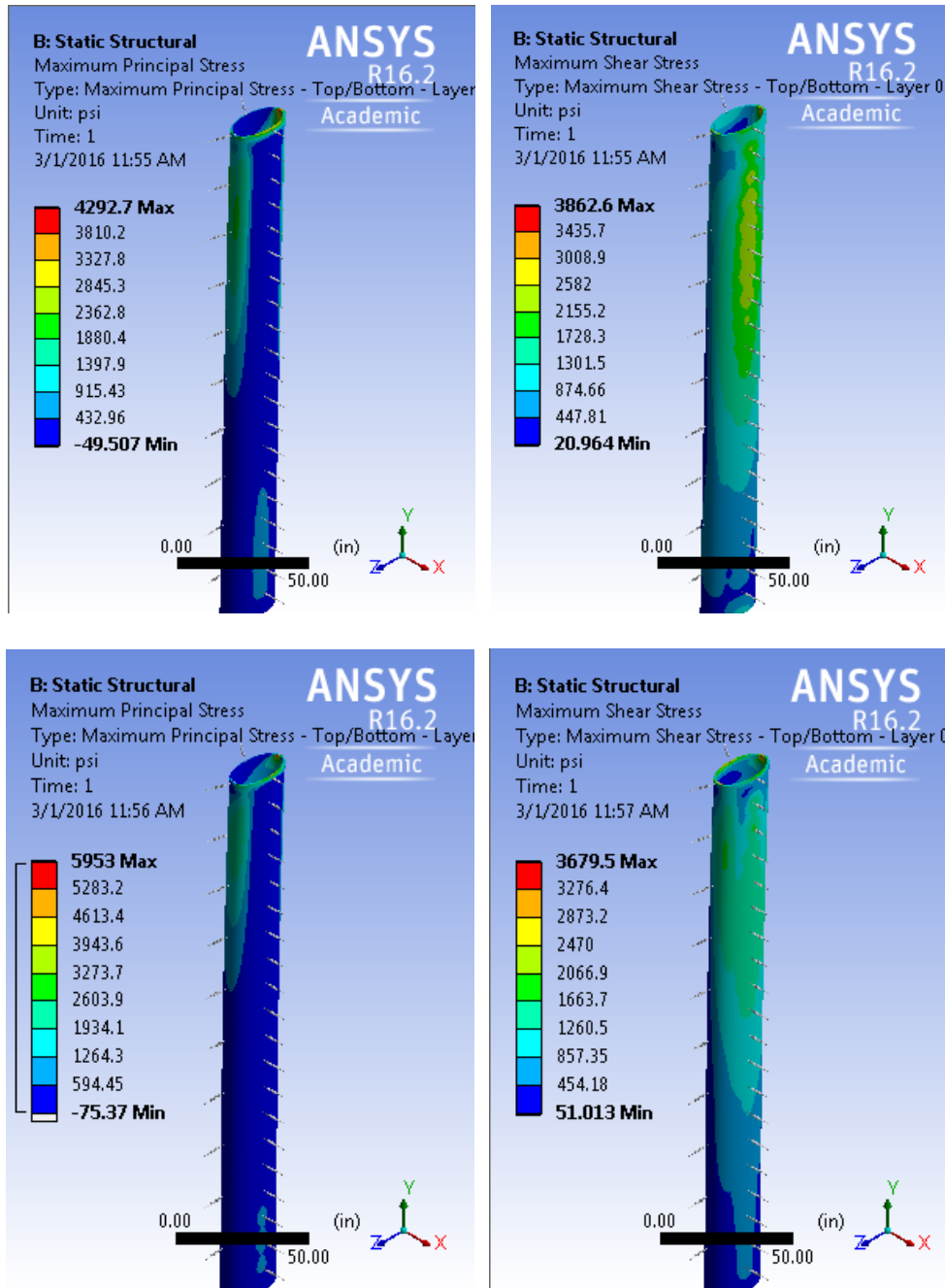
Figure 110 – Principal and shear stress contour line of 24"x12" section with 10 deg. (up) and 80 deg. (down) with dense sand soil

12. *Comparing Results of Different Cases*

The following section is dedicated to compare the result of different cases. The comparison is focused in several parameters as well as shape, concrete fill and soil type.

12.1. *Circular and Equivalent Elliptical Piles Comparison*

In the next series of the models a 24" circular pile is compared to elliptical piles with equal perimeter. The sections with equal perimeter are assumed to have same material and same cost of production. Table 31 shows the sections have same perimeter. The ellipse perimeter is calculated using the following equation (Circumference of Ellipse 2016):
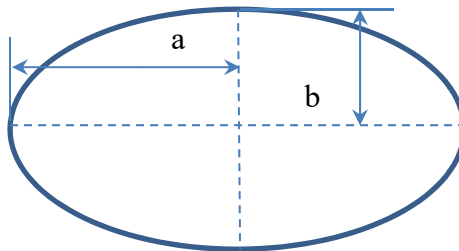
Figure 111 – Ellipse shorter and longer diameters

(Equation 12-1):

$$P \approx \pi(a + b)\left(1 + \frac{3h}{10 + \sqrt{4 - 3h}}\right)$$

in which,

$$h = \frac{(a - b)^2}{(a + b)^2}$$

The equation does not calculate the exact perimeter. It calculates the perimeter with relatively good precision. There is no exact formula for ellipse perimeter. All

183

suggested formula can calculate approximate values. (Equation 12-1):(Equation 12-1)

appear to be the most common equation.

The ellipse surface is calculated from

A simpler following equation:

(Equation 12-2):

$$S = \pi ab$$

Table 31 calculates the perimeter and surface are for four elliptical sections. The short

diameters of the sections are defined to have equal perimeter in all sections.

Table 31 – Sections with equal perimeter

a (in)	b (in)	2a (in)	2b (in)	h	P (in)	S (in^2)
12.00	12.00	24.00	24.00	0	75.398	452.38
14.00	9.83	28.00	19.66	0.03063	75.399	432.31
16.00	7.16	32.00	14.32	0.145644	75.399	359.94
18.00	3.48	36.00	6.96	0.45721	75.399	196.64

Figure 112 to Figure 117 show increase in the stress level and the Failure Ratio

resulted by more elongated sections in Stiff Clay soil. It is expected to have more

stress since the displacement is fixed 4 inches and the pile projection area is

increased.
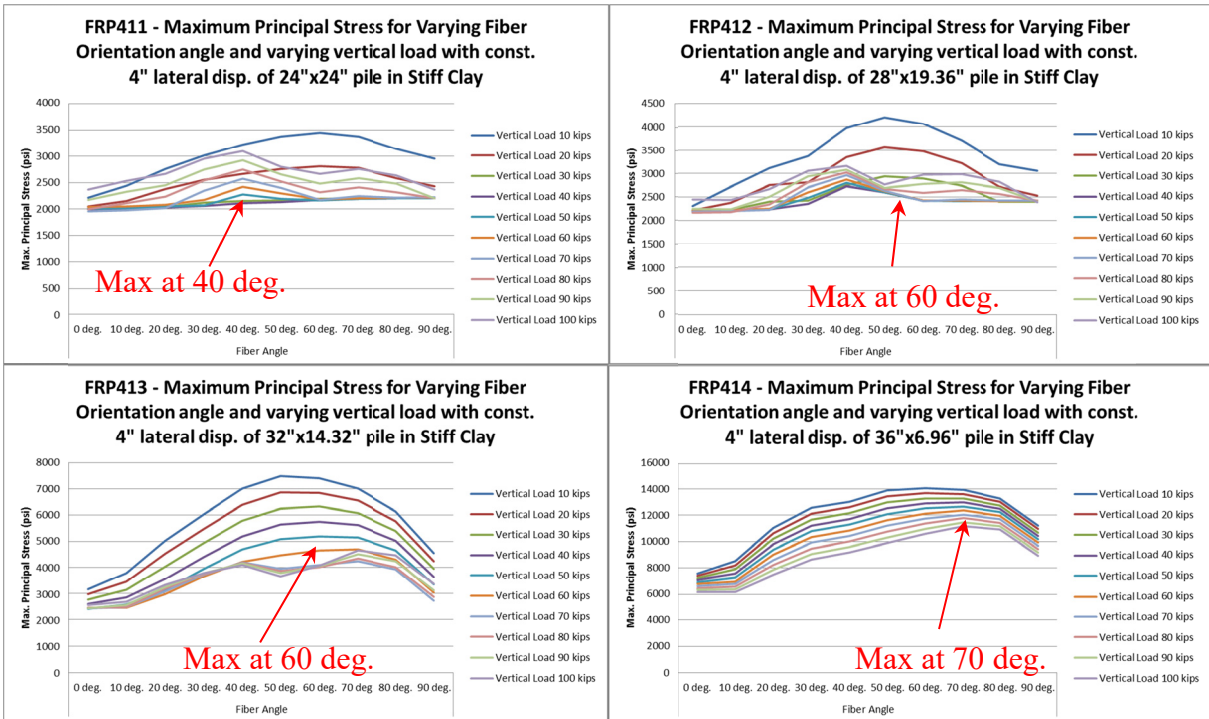
Figure 112 – Increase in principal stress as a result of changing the shape from circle to elongated ellipse in stiff clay
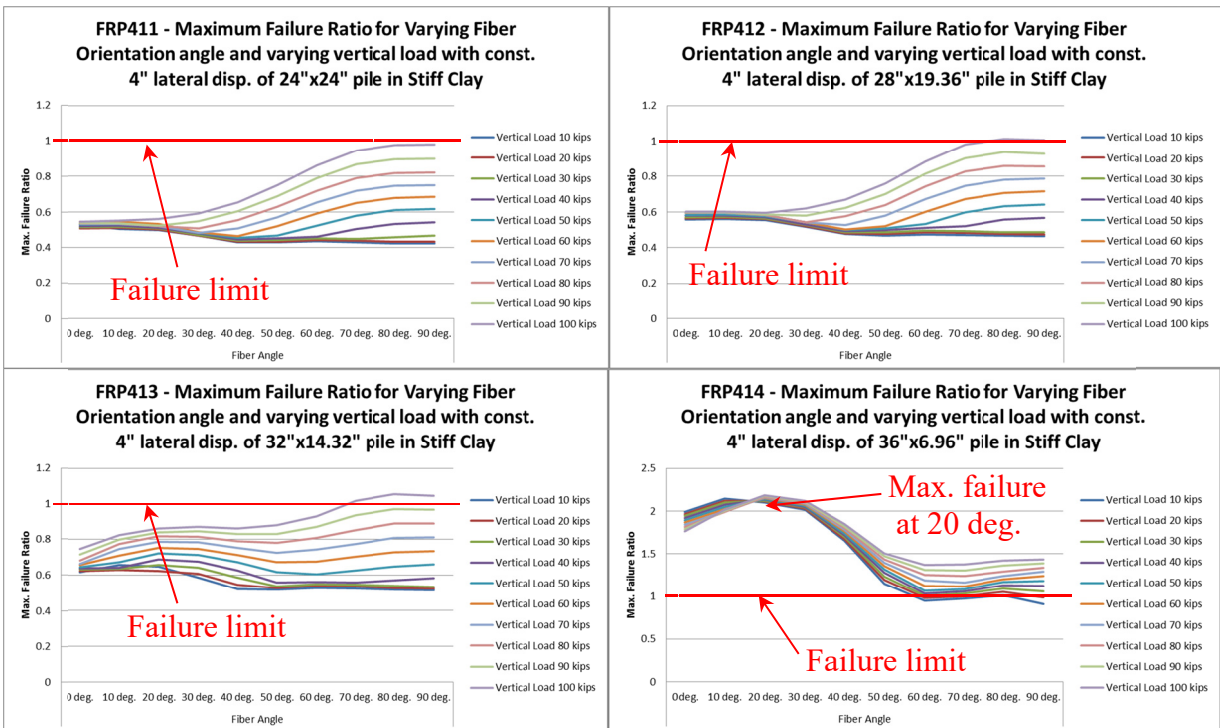
Figure 113 - Increase in failure ratio as a result of changing the shape from circle to elongated ellipse in stiff clay

185
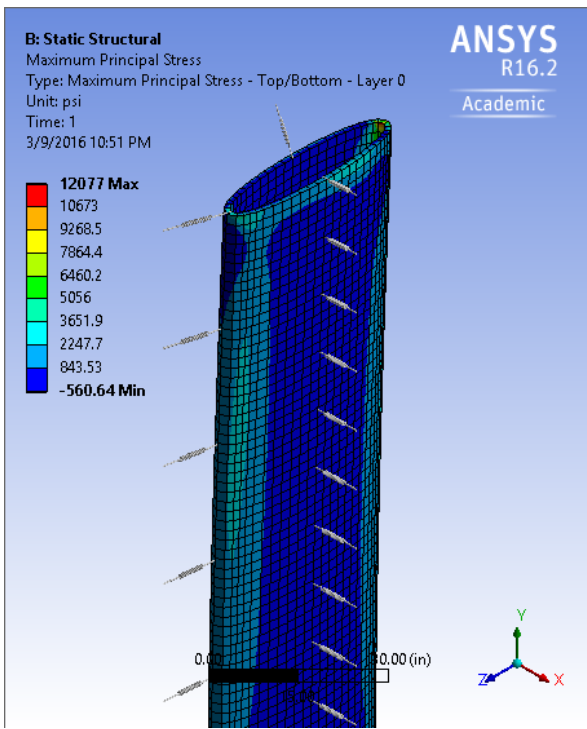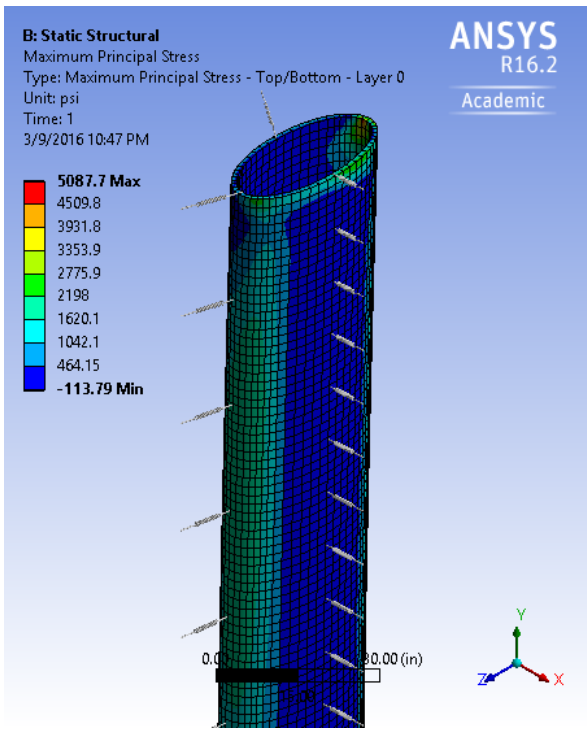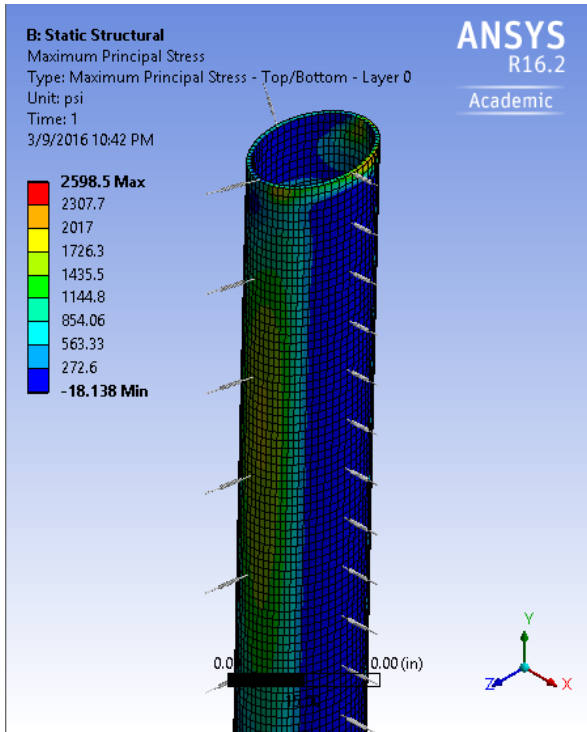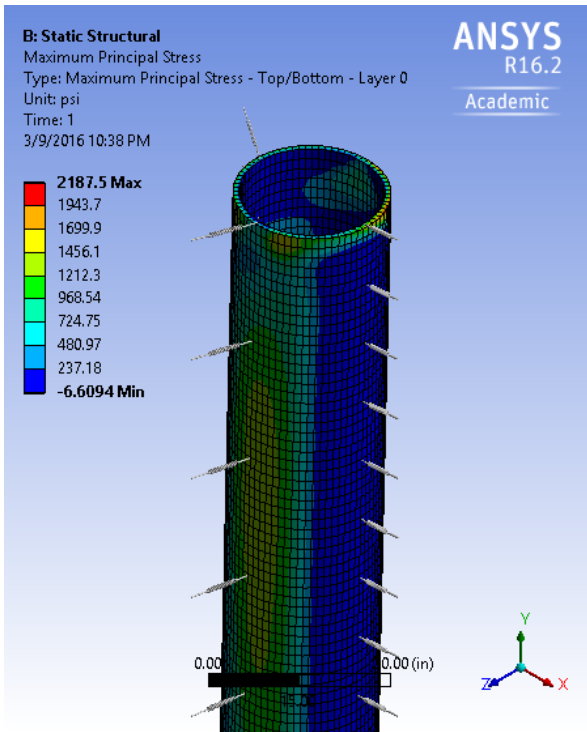
Figure 114 – Principal stress for piles with 50 degree fiber orientation and 50 kips vertical load in stiff clay
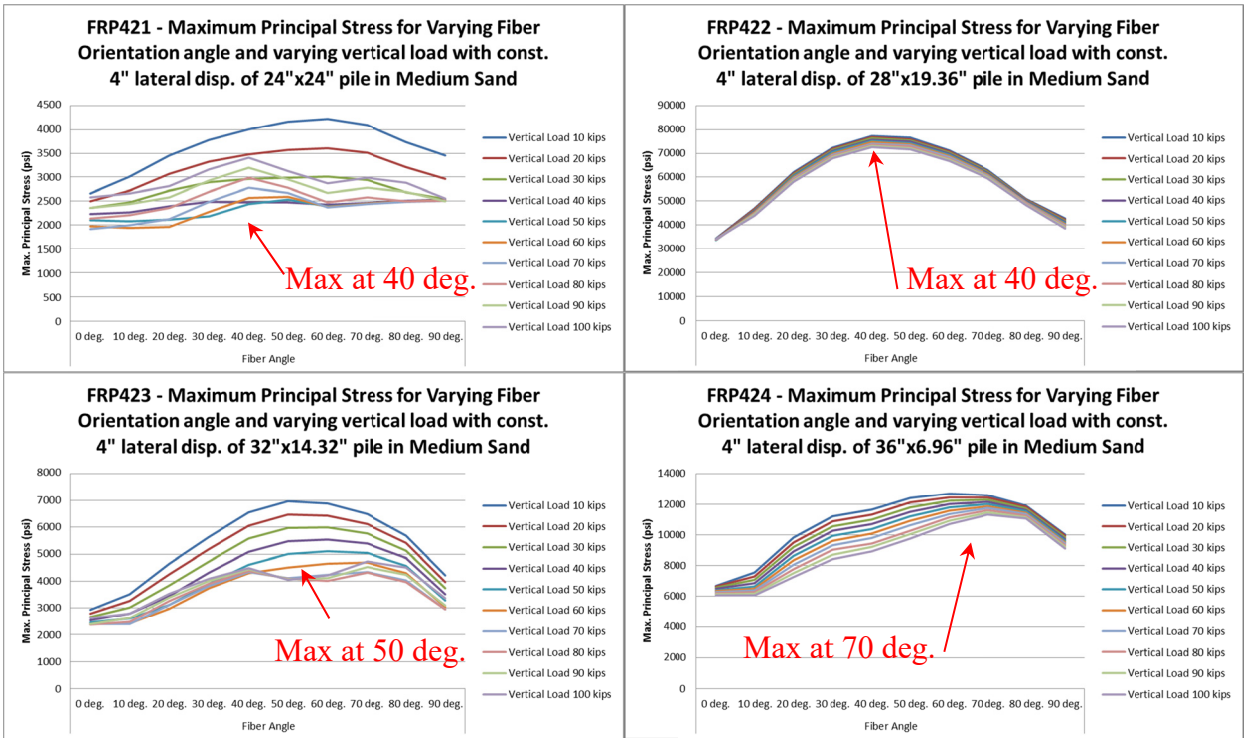
Figure 115 - Increase in principal stress as a result of changing the shape from circle to elongated ellipse in medium sand
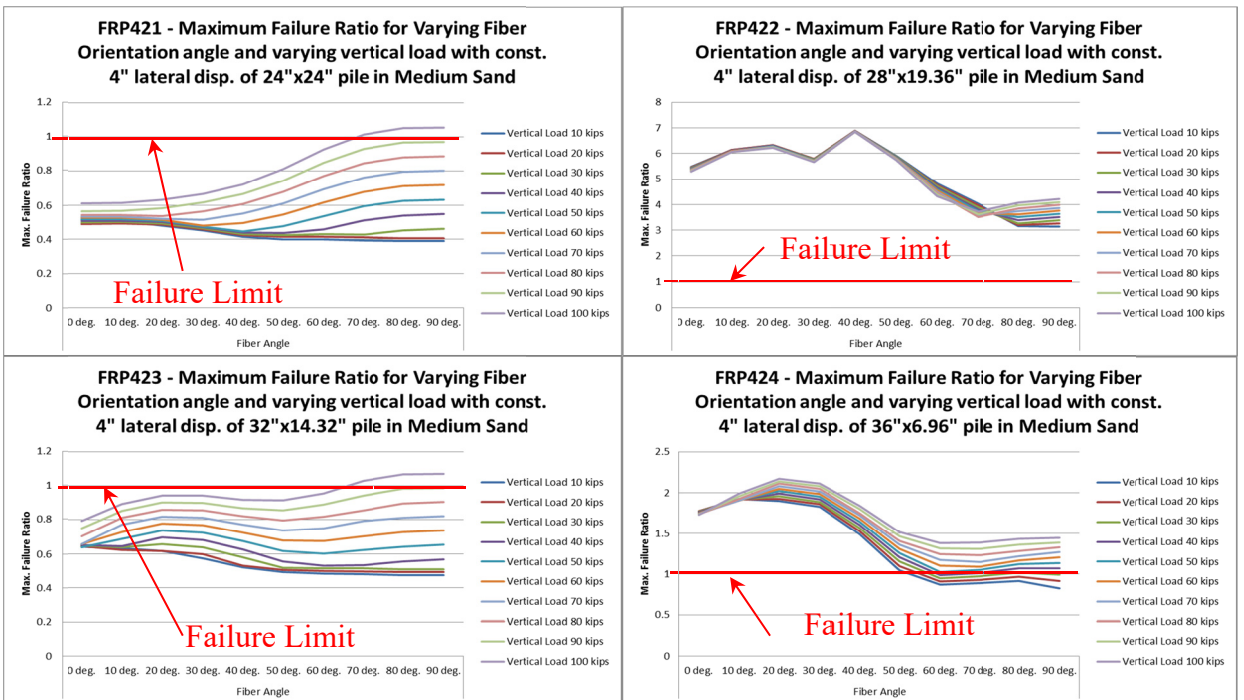
Figure 116 - Increase in failure ratio as a result of changing the shape from circle to elongated ellipse in medium sand

187
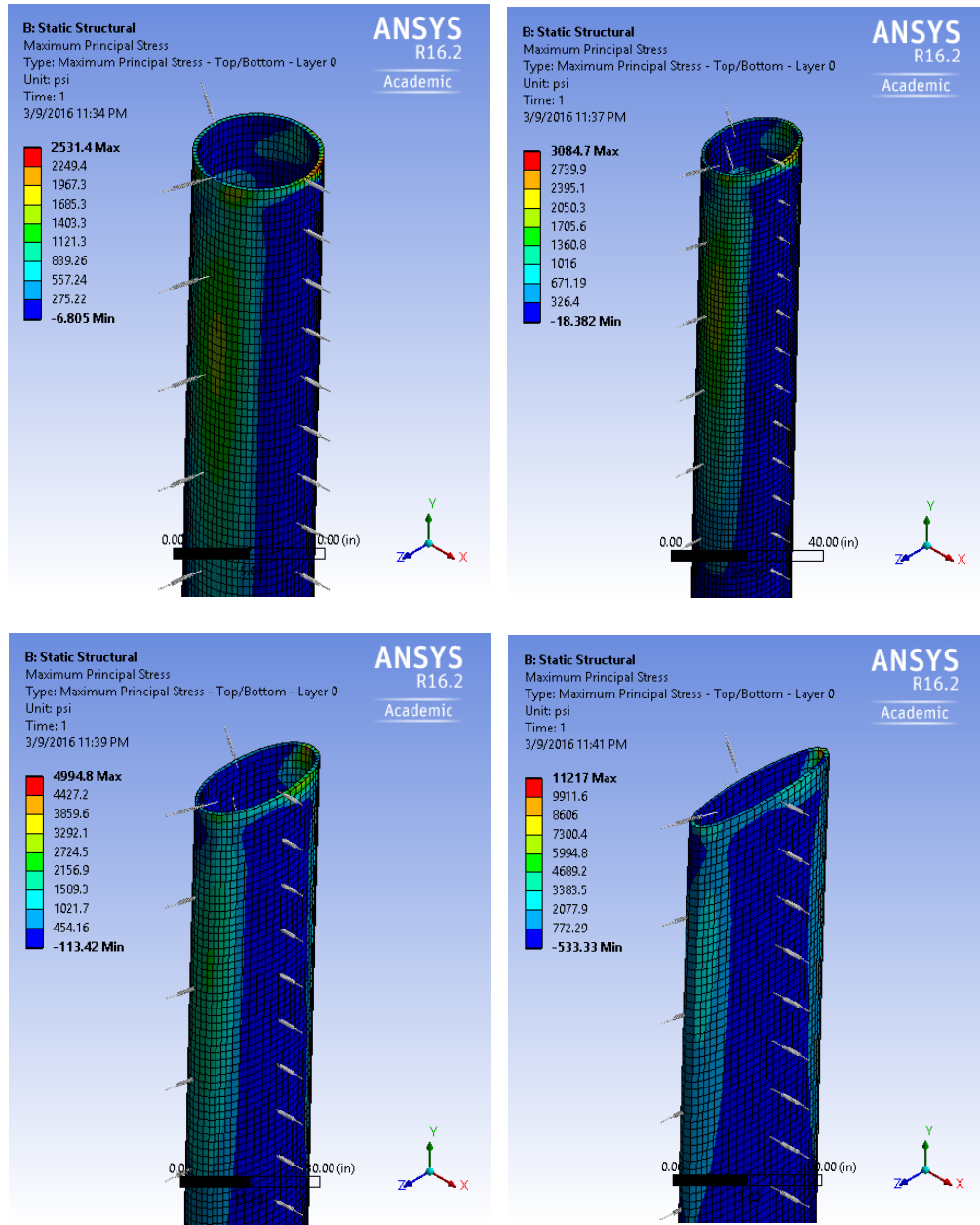
Figure 117 - Principal stress for piles with 50 degree fiber orientation and 50 kips vertical load in medium sand

As described earlier the stress and failure ratio increases in both type of soil due to increase in pile width and therefore the soil spring stiffness. In order to eliminate this problem the long diameter of the ellipse should be kept constant as it is done in earlier models.

12.2. *Hollow and concrete filled piles comparison*

Cases FRP171 to 174 are similar to cases FRP101 to 104 with the exception that

FRP171 to 174 have concrete core. The principal stress and failure ratio are compared

in two cases.
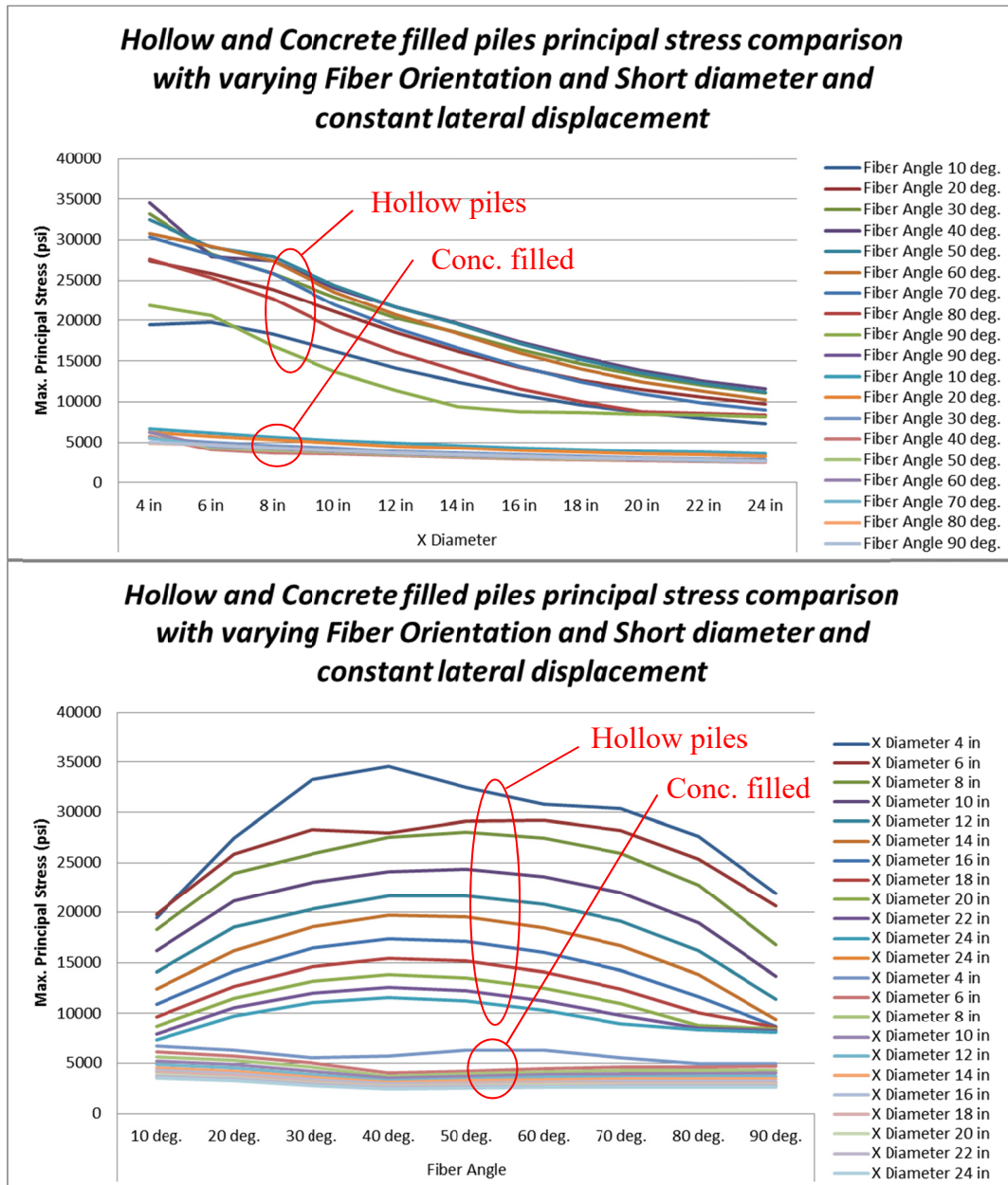
Figure 118 – Concrete fill effects on principal stresses

Figure 119 - Concrete fill effects on failure ratio
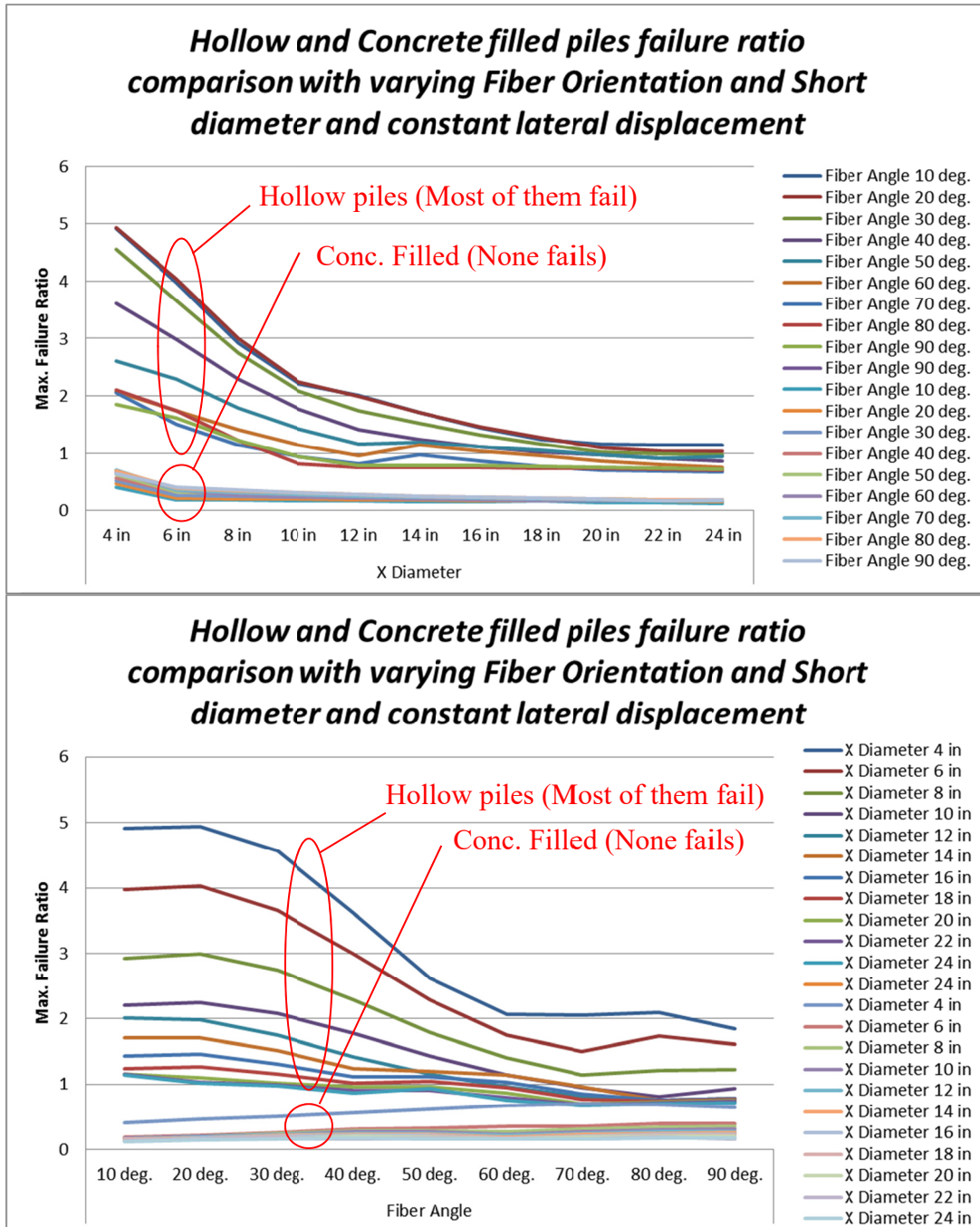
Figure 118 and Figure 119 show that the filling the pile with concrete has considerable effect on pile loading capacity and failure. Pile capacity considerably increases when filled with concrete.

Figure 120 shows the displacements in pile with and without concrete fill. Obviously to eliminate the vertical flexibility of the hollow piles under IABs, the piles should be filled with concrete. Since this dissertation focusses on the FRP piles both cases are studied.
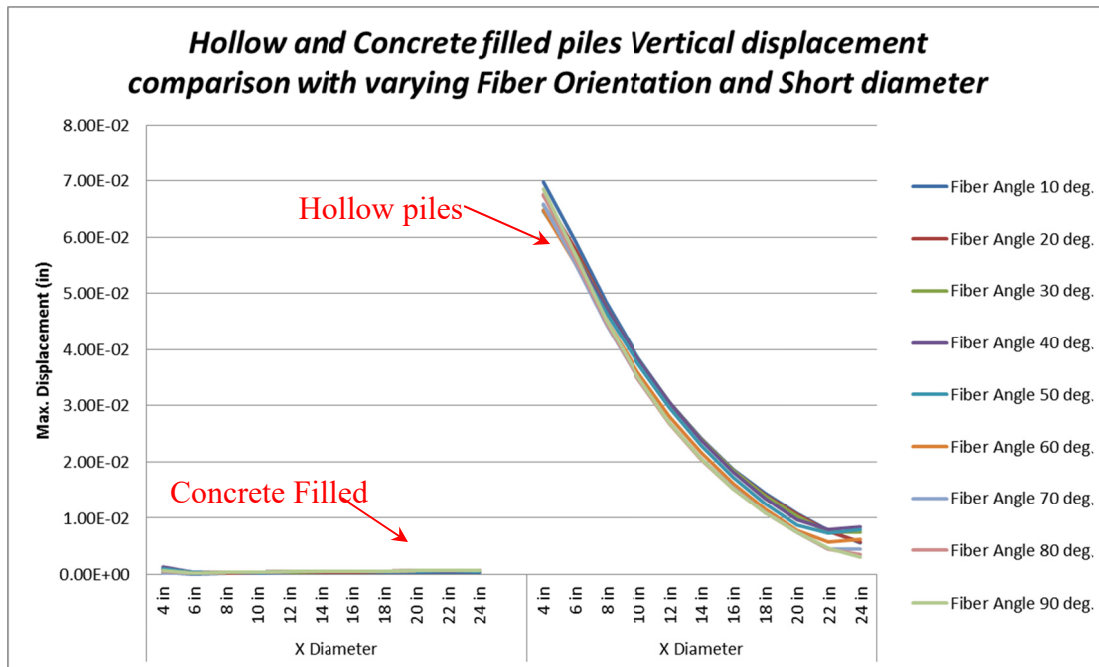
Figure 120 – Concrete Filled (left) and Hollow (right) piles displacement

In order to show the difference in vertical displacement of the pile, the models are subjected to vertical loads only. The graph also shows with increase in pile short diameter, the pile cross section area is increased which results less displacement in the piles. The orientation angle of the composite has minimal effect on the displacement.

12.3. *Soil Type*

Soil type is certainly an important factor in pile behavior. Softer soil material allows more area of the pile to transfer the lateral load to the soil. Therefore the stress is reduced in the pile material. On the other hand rigid soil causes great stresses in the top portion of the pile leading to failure of the composite material.
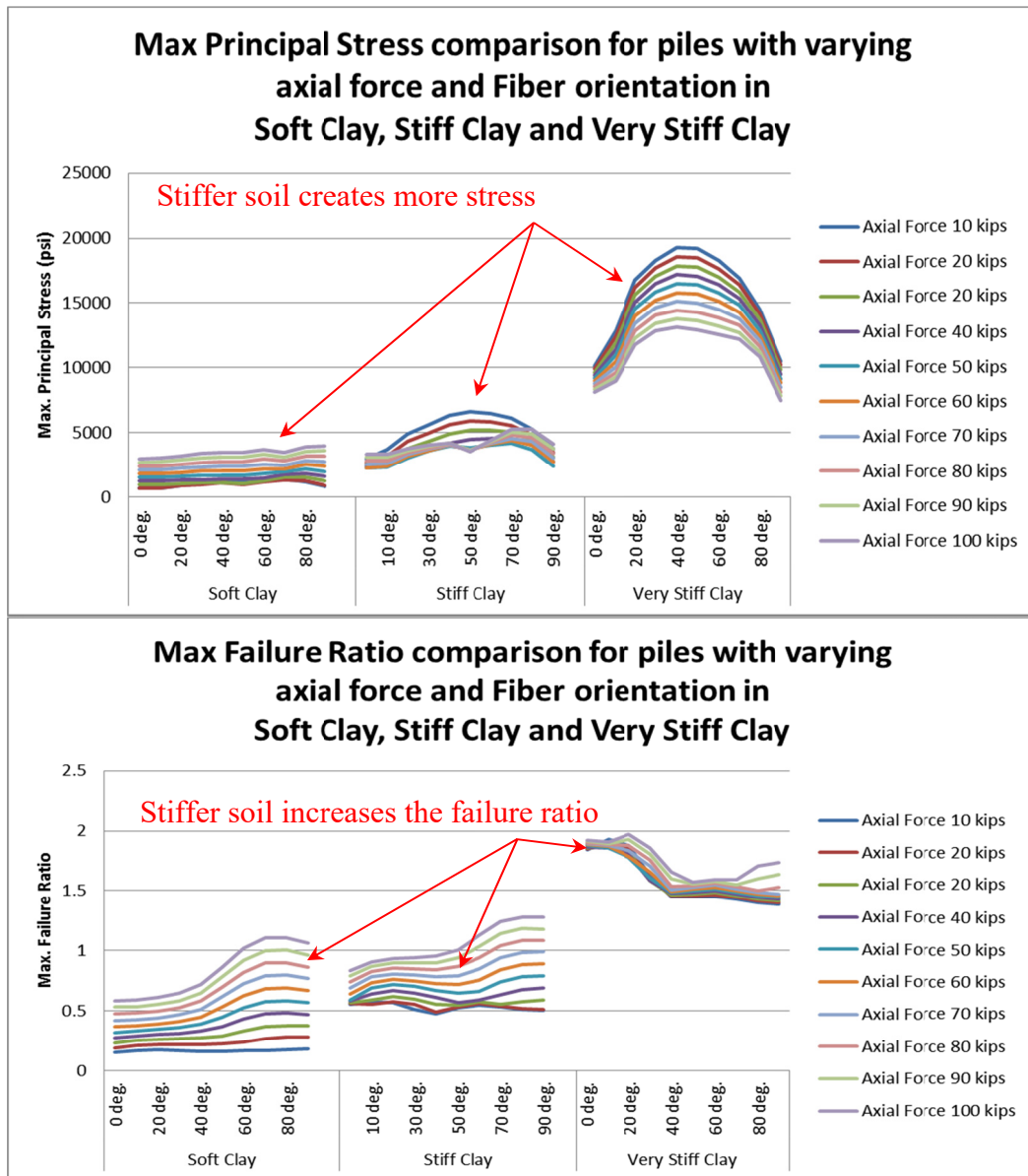
Figure 121 – Principal Stress and Failure Ratio comparison in different Clays
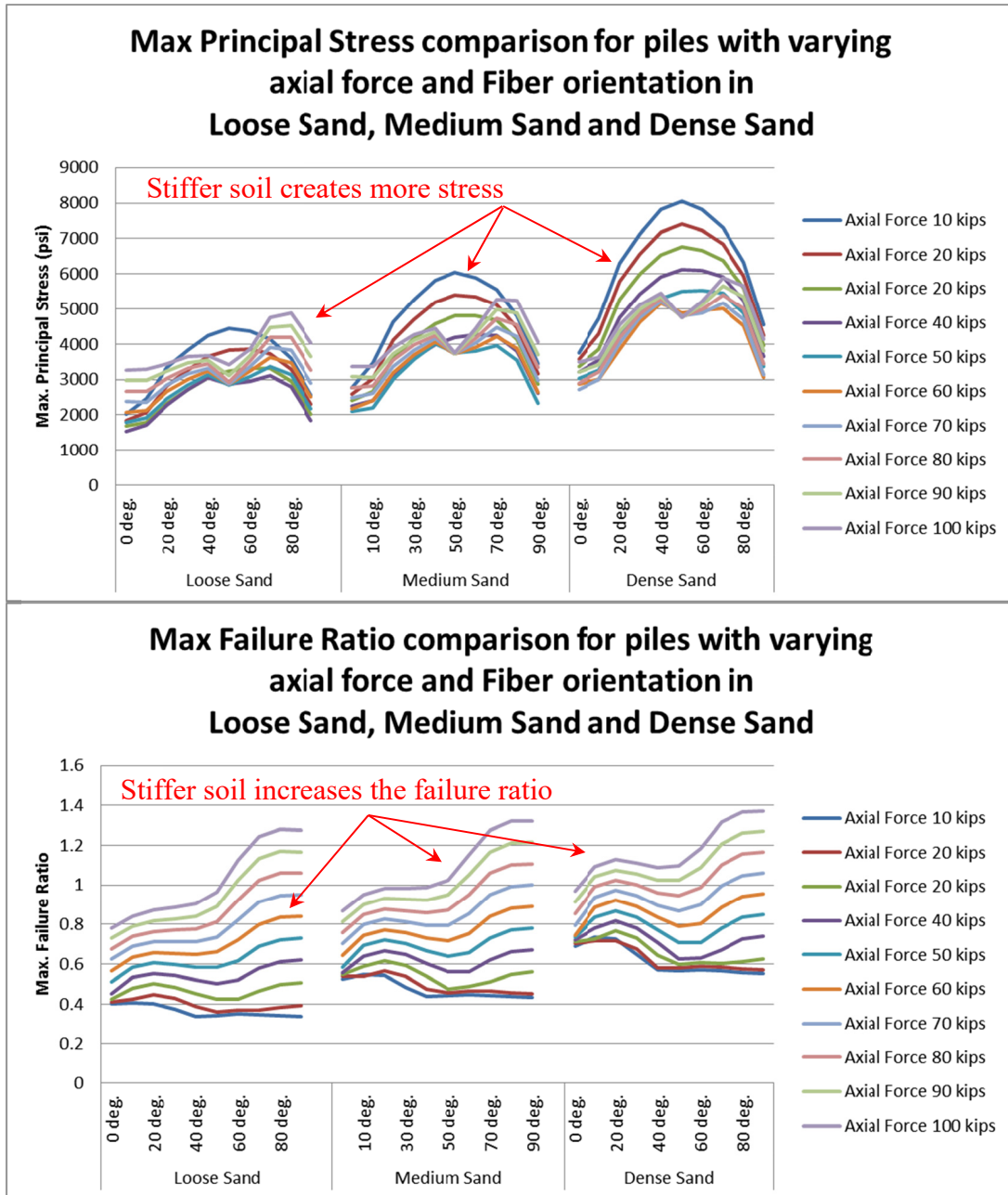
Figure 122 – Principal Stress and Failure Ratio comparison in different Sands

Figure 121 and Figure 122 compare the stress and failure ratios in different soils. As expected stiffer and denser soil results more stress and failure.

Stiff soils also are not suitable for IABs. Since the abutments of bridge displace on the pile cap, softer material allows the displacement to take place easier. Generally

193

piles do not require high bearing capacity of the soil under the pile cap. Therefore, when soft soil is encountered at the bridge foundation, it would be a good sign to build IAB. Deep piles can take big axial loads while the soft soil on top allows lateral displacement.

13. Conclusions

This dissertation studies FRP piles with elliptical cross section. The elliptical cross section is the best and most economical cross section for the piles under Integral Abutment Bridges. Several parameters can affect the file behavior. The known parameters are listed as layer orientation, number of layers, ellipse eccentricity, concrete fill, composite material and soil stiffness.

In order to study the behavior of the pile, various models were created. In each model two variables are set as parameters. The maximum principal stress and maximum shear stress as well as pile failure are defined by changing each parameter. The result is shown in 3D and 2D curves. The study of the curves concluded the following results:

- Stiffer soil creates more stress and results in earlier failure in the composite material. This makes softer soils ideal for IAB structures. In softer soils, stresses generated by horizontal displacement are better absorbed and distributed in pile body.

- Piles filled with concrete have considerably lower stress compared to hollow piles. In another words, concrete fill drastically reduces the stress in the composite and transfers the stress from the composite to the concrete.

- Piles filled with concrete have considerable lower vertical displacement compared to hollow piles. Orientation angles of the fibers have minimal effects on the vertical displacement.

- Among different sections with similar perimeter the circle cross section has the lowest failure since it has the lease width of soil profile. This does not

mean that the elliptical sections are not the best choice. It means increasing the pile width will simply increase the soil profile and therefore increase the soil resistance unwantedly. The desired lower stiffness can be achieved by a smaller diameter in the directions of load. This makes the circular section the worst section among all the elliptical sections.

- For piles with constant displacement and varying fiber orientation and pile dimension, the pile stress will decrease with an increase in fiber orientation. It is also observed that beyond a 60-degree fiber orientation the failure ratio decreases considerably.

- For piles with constant top of pile displacement and constant vertical force and varying pile dimensions, pile failure ratio will decrease with an increase in fiber orientation. It is also observed that with an increase in pile dimension the failure ratio decreases.

- For piles with constant lateral force and varying pile dimensions, pile failure ratio will be at a maximum in 45-degree fiber orientation. The stress decreases when the shorter diameter is more than half of the longer diameter of the elliptical cross section. This happens regardless of orientation angle.
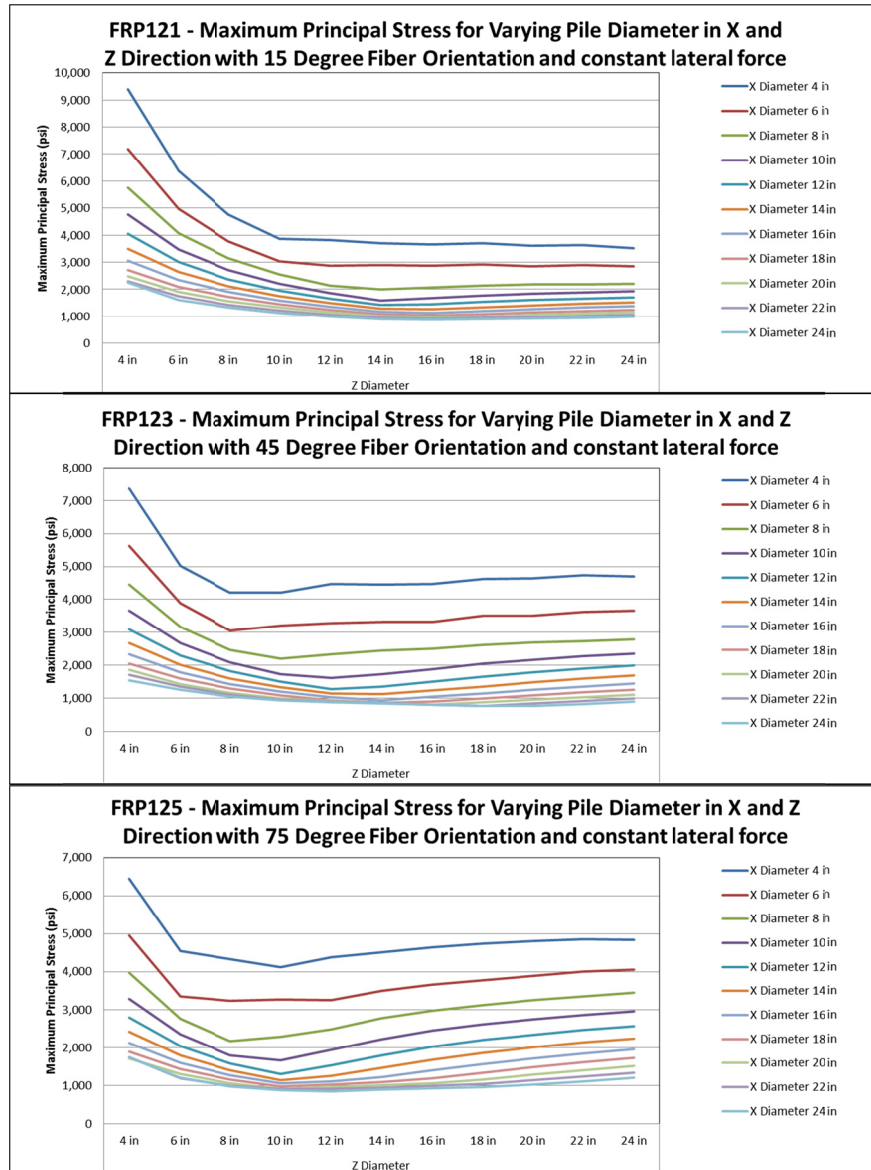
- For piles with constant top of pile horizontal and vertical force and varying number of composite layers, pile failure ratio will decrease with an increase in number of layers. The ratio falls drastically when the number of layers is small.

- For concrete filled piles with constant displacement and varying fiber orientation and pile dimensions, the failure ratio varies for oval sections but

remains relatively constant for rounder sections. Piles with a 60-degree fiber orientation have a lower failure ratio. The stress is reduced in piles with a 60-fiber orientation angle.

- For piles with constant displacement and vertical load and varying composite material, pile stress varies drastically with the type of composite material. The stress is reduced with the closer to round sections for all types of material.

- For piles with constant displacement and varying fiber orientation and pile dimensions, the piles stress changes linearly with displacement and nonlinearly with orientation angle. Pile capacity will be maximum with a 70-degree fiber orientation.

- For piles with constant displacement and varying fiber orientation and pile dimensions with additional parallel fibers, failure ratio decreases around 80 to 90 degrees. Failure is reduced in piles with higher fiber orientation angle.

- For piles with constant displacement and varying fiber orientation and pile dimensions with additional perpendicular fibers, failure ratio also decreases around 80 to 90 degrees. Failure is reduced in piles with a greater fiber orientation angle.

- For piles with constant displacement and varying fiber orientation with nonlinear soft clay, the failure ratio increases around 80 to 90 degrees.

- For piles with constant displacement and varying fiber orientation with nonlinear stiff clay, similar to soft clay, the failure ratio increases around 80 to 90 degrees.

- For piles with constant displacement and varying fiber orientation with nonlinear very stiff clay, the failure ratio remains constant.

- For piles with constant displacement and varying fiber orientation with nonlinear loose sand, the failure ratio increases with an increase in fiber orientation angle.

- For piles with constant displacement and varying fiber orientation with nonlinear medium sand, the failure ratio increases with an increase in fiber orientation angle.

- For piles with constant displacement and varying fiber orientation with nonlinear dense sand, the failure ratio slightly increases with an increase in fiber orientation angle.

- As expected, in all cases the stress increases with an increase in displacement and load. Just like any other structure the stress is proportional to the displacement and forces. Composite material may not behave equally in all directions, but the stress always is proportional to the applied loads. If for example the load is doubled, the stress will be doubled, which can bring pile to failure.

- Piles with more layers of composite fibers have less stress when subjected to displacement and vertical loads. This makes sense since the moment of inertia of the thin section is increased by increasing the thickness of the pile body.

This concludes the study on FRP piles with elliptical cross sections. As mentioned, the composite material is relatively new to the bridge industry and requires years of

experiment and data collection. When concrete was introduced to the construction industry there were many unknown aspects. This combined with a higher cost of production and poor initial quality of concrete may have appeared undesirable in the early stages. Today, the composite industry is in its early stages. There will certainly be improvements to the quality, better strength and more economically feasible materials. Designers and engineers will start using composite once it becomes more common. More usage will bring more study and more study will lead to more standards, codification and regulations.

Composite will eventually replace concrete and steel since it is much lighter and stronger than traditional materials. It is also durable especially in harsh and corrosive environments. Its weaknesses are high cost and low resistance to heat and UV radiation. Currently there is no code or proven design method for composites. Handbooks and design guides have been recently developed, but no national code is available at this time as it is for concrete, timber and steel. Production is limited and often less economically feasible. Where concrete was in the nineteen century, the composite industry is now.

Among all bridges, the IAB bridges have a small percentage of usage. FRP piles in IAB structures are rare. FRP piles with elliptical cross sections are even rarer. There has been very little or no study on elliptical cross sections. This dissertation introduced a new method to build elliptical shapes with less expensive cost and faster production method. It highlighted a new approach to FRP piles and demonstrated the behavior of FRP piles with elliptical cross sections.

13.1. *Future work*

Currently there is almost no research on the elliptical cross sections. All the study is either on circular piles or on other sections such as rectangular or H sections. This dissertation opens a new door for future research on piles with either elliptical or any other cross section that can be built with the filament winding method. For the first time a new method of manufacturing of the piles with the filament winding method is introduced in this dissertation. This provides a faster and more economical solution for making the FRP piles that are well suited for Integral Abutment Bridges. The future study on FRP piles could focus in the following agenda:

- Dynamic loads on the piles

- Isotropic composite material

- New composite materials

- New soil pile interaction and soil spring models

- Pile groups

- Hybrid composite piles made of steel core and composite shell

- Hexagonal, Octagonal and Oval cross sections, which are not commonly made in composite industry

- Other failure criteria such as Hoffman, Hashin, Puck, LaRC and Cuntze

- Sandwich criteria such as face sheet wrinkling and core failure

- Pile body local buckling

The suggested future work is only part of what appears to be an interesting area today. Obviously new agenda may emerge as further study is performed on FRP piles.

14. *Appendices*

The following sheets are the sample data for FRP305 design point number 4. This is

one of the 14,310 models created for this dissertation.

14.1. *Solver output*

```
ANSYS Academic Research


 *--------------------------------------------------------------------*
 |                                                                    |
 |   W E L C O M E   T O   T H E   A N S Y S (R)   P R O G R A M     |
 |                                                                    |
 *--------------------------------------------------------------------*




 ******************************************************************
 *            ANSYS Release 16.2     LEGAL NOTICES              *
 ******************************************************************
 *                                                              *
 * Copyright 2015 SAS IP, Inc.  All rights reserved.           *
 * Unauthorized use, distribution or duplication is            *
 * prohibited.                                                 *
 *                                                              *
 * Ansys is a registered trademark of ANSYS, Inc. or its       *
 * subsidiaries in the United States or other countries.       *
 * See the ANSYS, Inc. online documentation or the ANSYS, Inc. *
 * documentation CD or online help for the complete Legal      *
 * Notice.                                                     *
 *                                                              *
 ******************************************************************
 *                                                              *
 * THIS ANSYS SOFTWARE PRODUCT AND PROGRAM DOCUMENTATION        *
 * INCLUDE TRADE SECRETS AND CONFIDENTIAL AND PROPRIETARY       *
 * PRODUCTS OF ANSYS, INC., ITS SUBSIDIARIES, OR LICENSORS.     *
 * The software products and documentation are furnished by     *
 * ANSYS, Inc. or its subsidiaries under a software license     *
 * agreement that contains provisions concerning               *
 * non-disclosure, copying, length and nature of use,          *
 * compliance with exporting laws, warranties, disclaimers,    *
 * limitations of liability, and remedies, and other           *
 * provisions.  The software products and documentation may be *
```

Release 16.2

Point Releases and Patches installed:

ANSYS, Inc. Products Release 16.2
ANSYS Mechanical Products Release 16.2
ANSYS Customization Files for User Programmable Features Release 16.2
ANSYS Autodyn Release 16.2
ANSYS LS-DYNA Release 16.2
ANSYS CFX (includes ANSYS CFD-Post) Release 16.2
ANSYS Fluent (includes ANSYS CFD-Post) Release 16.2
ANSYS TurboGrid Release 16.2
ANSYS Polyflow (includes ANSYS CFD-Post) Release 16.2
ANSYS CFD-Post only Release 16.2
ANSYS ICEM CFD Release 16.2
ANSYS Composite PrepPost Release 16.2
ANSYS Icepak (includes ANSYS CFD-Post) Release 16.2
ANSYS, Inc. License Manager Release 16.2

        ***** ANSYS COMMAND LINE ARGUMENTS *****
 BATCH MODE REQUESTED (-b)   = NOLIST
 INPUT FILE COPY MODE (-c)   = COPY
 SHARED MEMORY PARALLEL REQUESTED
   SINGLE PROCESS WITH   2 THREADS REQUESTED
   TOTAL OF   2 CORES REQUESTED
 DESIGNXPLORER REQUESTED

```
   START-UP FILE MODE          = NOREAD
   STOP FILE MODE              = NOREAD


 RELEASE= Release 16.2          BUILD= 16.2      UP20150629   VERSION=WINDOWS x64
 CURRENT JOBNAME=file  13:19:49  FEB 20, 2016 CP=      0.812



   PARAMETER _DS_PROGRESS =      999.0000000


  /INPUT FILE= ds.dat  LINE=         0



 DO NOT WRITE ELEMENT RESULTS INTO DATABASE

 *GET  _WALLSTRT  FROM  ACTI  ITEM=TIME WALL  VALUE=  13.3302778

 TITLE=
 FRP305 - Varying Orientation Angle and Vertical Load in Soft Clay - Constant 4

  ACT Extensions:

 SET PARAMETER DIMENSIONS ON  _WB_PROJECTSCRATCH_DIR
  TYPE=STRI  DIMENSIONS=      248          1          1

  PARAMETER _WB_PROJECTSCRATCH_DIR(1) = E:\FRP\_ProjectScratch\ScrEB4D\

  SET PARAMETER DIMENSIONS ON  _WB_SOLVERFILES_DIR
   TYPE=STRI  DIMENSIONS=      248          1          1

  PARAMETER _WB_SOLVERFILES_DIR(1) = E:\FRP\FRP305 - Varying Orientation Angle and
Vertical Load in Soft Clay - Constant 4 in displacement , material and 24x12 in pile
dimension_files\dp4\SYS\MECH\

  SET PARAMETER DIMENSIONS ON  _WB_USERFILES_DIR
   TYPE=STRI  DIMENSIONS=      248          1          1

  PARAMETER _WB_USERFILES_DIR(1) = E:\FRP\FRP305 - Varying Orientation Angle and
Vertical Load in Soft Clay - Constant 4 in displacement , material and 24x12 in pile
dimension_files\user_files\
  --- Data in consistent BIN units. See Solving Units in the help system for more

  U.S. CUSTOMARY INCH UNITS SPECIFIED FOR INTERNAL
   LENGTH      = INCHES (IN)
   MASS        = LBF-S**2/IN
   TIME        = SECONDS (SEC)
   TEMPERATURE = FAHRENHEIT
   TOFFSET     = 460.0
```

```
 FORCE      = LBF
 HEAT       = IN-LBF
 PRESSURE   = PSI (LBF/IN**2)
 ENERGY     = IN-LBF
 POWER      = IN-LBF/SEC


INPUT  UNITS ARE ALSO SET TO BIN

*** ANSYS - ENGINEERING ANALYSIS SYSTEM  RELEASE Release 16.2     16.2     ***
ANSYS Academic Research
00427805  VERSION=WINDOWS x64   13:19:49  FEB 20, 2016 CP=      0.859


FRP305 - Varying Orientation Angle and Vertical Load in Soft Clay - Constant 4




          ***** ANSYS ANALYSIS DEFINITION (PREP7) *****
*********** Nodes for the whole assembly ***********
*********** Elements for Body 1 "Surface Body" ***********
*********** Send User Defined Coordinate System(s) ***********
*********** Set Reference Temperature ***********
*********** Send Materials ***********
*********** Send Sheet Properties ***********
*********** Sending Coordinate Systems for External Layered Section***********
*********** Sending Materials for External Layered Section***********
*********** Send External Layered Section Properties ***********
*********** Define Force Using Surface Effect Elements ***********
*********** Create Remote Point "Internal Remote Point 4" ***********
*********** Create Remote Point "Internal Remote Point 6" ***********
*********** Create Remote Point "Internal Remote Point 7" ***********
*********** Create Remote Point "Internal Remote Point 9" ***********
*********** Create Remote Point "Internal Remote Point 11" ***********
*********** Create Remote Point "Internal Remote Point 13" ***********
*********** Create Remote Point "Internal Remote Point 15" ***********
*********** Create Remote Point "Internal Remote Point 17" ***********
*********** Create Remote Point "Internal Remote Point 19" ***********
*********** Create Remote Point "Internal Remote Point 21" ***********
*********** Create Remote Point "Internal Remote Point 23" ***********
*********** Create Remote Point "Internal Remote Point 25" ***********
*********** Create Remote Point "Internal Remote Point 27" ***********
*********** Create Remote Point "Internal Remote Point 29" ***********
*********** Create Remote Point "Internal Remote Point 31" ***********
*********** Create Remote Point "Internal Remote Point 33" ***********
*********** Create Remote Point "Internal Remote Point 35" ***********
*********** Create Remote Point "Internal Remote Point 37" ***********
*********** Create Remote Point "Internal Remote Point 39" ***********
*********** Create Remote Point "Internal Remote Point 41" ***********
*********** Create Remote Point "Internal Remote Point 43" ***********
```

```
*********** Create Remote Point "Internal Remote Point 45" ***********
*********** Create Remote Point "Internal Remote Point 47" ***********
*********** Create Remote Point "Internal Remote Point 49" ***********
*********** Create Remote Point "Internal Remote Point 51" ***********
*********** Create Remote Point "Internal Remote Point 53" ***********
*********** Create Remote Point "Internal Remote Point 55" ***********
*********** Create Remote Point "Internal Remote Point 57" ***********
*********** Create Remote Point "Internal Remote Point 59" ***********
*********** Create Remote Point "Internal Remote Point 61" ***********
*********** Create Remote Point "Internal Remote Point 63" ***********
*********** Create Remote Point "Internal Remote Point 65" ***********
*********** Create Remote Point "Internal Remote Point 67" ***********
*********** Create Remote Point "Internal Remote Point 69" ***********
*********** Create Remote Point "Internal Remote Point 71" ***********
*********** Create Remote Point "Internal Remote Point 73" ***********
*********** Create Remote Point "Internal Remote Point 75" ***********
*********** Create Remote Point "Internal Remote Point 77" ***********
*********** Create Remote Point "Internal Remote Point 79" ***********
*********** Create Remote Point "Internal Remote Point 81" ***********
*********** Create Remote Point "Internal Remote Point 83" ***********
*********** Create Remote Point "Internal Remote Point 85" ***********
*********** Create Remote Point "Internal Remote Point 87" ***********
*********** Create Remote Point "Internal Remote Point 89" ***********
*********** Create Remote Point "Internal Remote Point 91" ***********
*********** Create Remote Point "Internal Remote Point 93" ***********
*********** Create Remote Point "Internal Remote Point 95" ***********
*********** Create Remote Point "Internal Remote Point 97" ***********
*********** Create Remote Point "Internal Remote Point 99" ***********
*********** Create Remote Point "Internal Remote Point 101" ***********
*********** Create Remote Point "Internal Remote Point 103" ***********
*********** Create Remote Point "Internal Remote Point 105" ***********
*********** Create Spring Connection "Longitudinal - Ground To Surface Body" **
            Real Constant Set For Above Spring Connection Is 110
*********** Create Spring Connection "Longitudinal - Ground To Surface Body" **
            Real Constant Set For Above Spring Connection Is 111
*********** Create Spring Connection "Longitudinal - Ground To Surface Body 3"
            Real Constant Set For Above Spring Connection Is 112
*********** Create Spring Connection "Longitudinal - Ground To Surface Body 4"
            Real Constant Set For Above Spring Connection Is 113
*********** Create Spring Connection "Longitudinal - Ground To Surface Body 5"
            Real Constant Set For Above Spring Connection Is 114
*********** Create Spring Connection "Longitudinal - Ground To Surface Body 6"
            Real Constant Set For Above Spring Connection Is 115
*********** Create Spring Connection "Longitudinal - Ground To Surface Body 7"
            Real Constant Set For Above Spring Connection Is 116
*********** Create Spring Connection "Longitudinal - Ground To Surface Body 8"
            Real Constant Set For Above Spring Connection Is 117
*********** Create Spring Connection "Longitudinal - Ground To Surface Body 9"
```

```
            Real Constant Set For Above Spring Connection Is 118
*********** Create Spring Connection "Longitudinal - Ground To Surface Body 10"
            Real Constant Set For Above Spring Connection Is 119
*********** Create Spring Connection "Longitudinal - Ground To Surface Body 11"
            Real Constant Set For Above Spring Connection Is 120
*********** Create Spring Connection "Longitudinal - Ground To Surface Body 12"
            Real Constant Set For Above Spring Connection Is 121
*********** Create Spring Connection "Longitudinal - Ground To Surface Body 13"
            Real Constant Set For Above Spring Connection Is 122
*********** Create Spring Connection "Longitudinal - Ground To Surface Body 14"
            Real Constant Set For Above Spring Connection Is 123
*********** Create Spring Connection "Longitudinal - Ground To Surface Body 15"
            Real Constant Set For Above Spring Connection Is 124
*********** Create Spring Connection "Longitudinal - Ground To Surface Body 16"
            Real Constant Set For Above Spring Connection Is 125
*********** Create Spring Connection "Longitudinal - Ground To Surface Body 17"
            Real Constant Set For Above Spring Connection Is 126
*********** Create Spring Connection "Longitudinal - Ground To Surface Body 18"
            Real Constant Set For Above Spring Connection Is 127
*********** Create Spring Connection "Longitudinal - Ground To Surface Body 19"
            Real Constant Set For Above Spring Connection Is 128
*********** Create Spring Connection "Longitudinal - Ground To Surface Body 20"
            Real Constant Set For Above Spring Connection Is 129
*********** Create Spring Connection "Longitudinal - Ground To Surface Body 21"
            Real Constant Set For Above Spring Connection Is 130
*********** Create Spring Connection "Longitudinal - Ground To Surface Body 22"
            Real Constant Set For Above Spring Connection Is 131
*********** Create Spring Connection "Longitudinal - Ground To Surface Body 23"
            Real Constant Set For Above Spring Connection Is 132
*********** Create Spring Connection "Longitudinal - Ground To Surface Body 24"
            Real Constant Set For Above Spring Connection Is 133
*********** Create Spring Connection "Longitudinal - Ground To Surface Body 25"
            Real Constant Set For Above Spring Connection Is 134
*********** Create Spring Connection "Longitudinal - Ground To Surface Body 26"
            Real Constant Set For Above Spring Connection Is 135
*********** Create Spring Connection "Longitudinal - Ground To Surface Body 27"
            Real Constant Set For Above Spring Connection Is 136
*********** Create Spring Connection "Longitudinal - Ground To Surface Body 28"
            Real Constant Set For Above Spring Connection Is 137
*********** Create Spring Connection "Longitudinal - Ground To Surface Body 29"
            Real Constant Set For Above Spring Connection Is 138
*********** Create Spring Connection "Longitudinal - Ground To Surface Body 30"
            Real Constant Set For Above Spring Connection Is 139
*********** Create Spring Connection "Longitudinal - Ground To Surface Body 31"
            Real Constant Set For Above Spring Connection Is 140
*********** Create Spring Connection "Longitudinal - Ground To Surface Body 32"
            Real Constant Set For Above Spring Connection Is 141
*********** Create Spring Connection "Longitudinal - Ground To Surface Body 33"
```

```
              Real Constant Set For Above Spring Connection Is 142
*********** Create Spring Connection "Longitudinal - Ground To Surface Body 34"
              Real Constant Set For Above Spring Connection Is 143
*********** Create Spring Connection "Longitudinal - Ground To Surface Body 35"
              Real Constant Set For Above Spring Connection Is 144
*********** Create Spring Connection "Longitudinal - Ground To Surface Body 36"
              Real Constant Set For Above Spring Connection Is 145
*********** Create Spring Connection "Longitudinal - Ground To Surface Body 37"
              Real Constant Set For Above Spring Connection Is 146
*********** Create Spring Connection "Longitudinal - Ground To Surface Body 38"
              Real Constant Set For Above Spring Connection Is 147
*********** Create Spring Connection "Longitudinal - Ground To Surface Body 39"
              Real Constant Set For Above Spring Connection Is 148
*********** Create Spring Connection "Longitudinal - Ground To Surface Body 40"
              Real Constant Set For Above Spring Connection Is 149
*********** Create Spring Connection "Longitudinal - Ground To Surface Body 41"
              Real Constant Set For Above Spring Connection Is 150
*********** Create Spring Connection "Longitudinal - Ground To Surface Body 42"
              Real Constant Set For Above Spring Connection Is 151
*********** Create Spring Connection "Longitudinal - Ground To Surface Body 43"
              Real Constant Set For Above Spring Connection Is 152
*********** Create Spring Connection "Longitudinal - Ground To Surface Body 44"
              Real Constant Set For Above Spring Connection Is 153
*********** Create Spring Connection "Longitudinal - Ground To Surface Body 45"
              Real Constant Set For Above Spring Connection Is 154
*********** Create Spring Connection "Longitudinal - Ground To Surface Body 46"
              Real Constant Set For Above Spring Connection Is 155
*********** Create Spring Connection "Longitudinal - Ground To Surface Body 47"
              Real Constant Set For Above Spring Connection Is 156
*********** Create Spring Connection "Longitudinal - Ground To Surface Body 48"
              Real Constant Set For Above Spring Connection Is 157
*********** Create Spring Connection "Longitudinal - Ground To Surface Body 49"
              Real Constant Set For Above Spring Connection Is 158
*********** Create Spring Connection "Longitudinal - Ground To Surface Body 50"
              Real Constant Set For Above Spring Connection Is 159
*********** Create Spring Connection "Longitudinal - Ground To Surface Body 51"
              Real Constant Set For Above Spring Connection Is 160
*********** Create Spring Connection "Longitudinal - Ground To Surface Body 52"
              Real Constant Set For Above Spring Connection Is 161
*********** Construct Weak Springs, Prototype 1 ***********
*********** Create Displacement Tables and Functions ******


***** ROUTINE COMPLETED *****  CP =          1.109


--- Number of total nodes = 5740
--- Number of contact elements = 1320
```

```
--- Number of spring elements = 24
--- Number of bearing elements = 0
--- Number of solid elements = 5566
--- Number of total elements = 7060

*GET  _WALLBSOL  FROM  ACTI   ITEM=TIME WALL   VALUE=  13.3302778
*****************************************************************************
***********************    SOLUTION    *******************************
*****************************************************************************


*****  ANSYS SOLUTION ROUTINE  *****


PERFORM A STATIC ANALYSIS
 THIS WILL BE A NEW ANALYSIS


USE SPARSE MATRIX DIRECT SOLVER


CONTACT INFORMATION PRINTOUT LEVEL        1


NLDIAG: Nonlinear diagnostics CONT option is set to ON.
        Writing frequency : each ITERATION.


DEFINE RESTART CONTROL FOR LOADSTEP LAST
AT FREQUENCY OF LAST AND NUMBER FOR OVERWRITE IS     0


DELETE RESTART FILES OF ENDSTEP
**************************************************
****************** SOLVE FOR LS 1 ****************


SELECT       FOR ITEM=TYPE COMPONENT=
 IN RANGE        5 TO          5 STEP          1

        46  ELEMENTS (OF      7060  DEFINED) SELECTED BY  ESEL  COMMAND.


SELECT      ALL NODES HAVING ANY ELEMENT IN ELEMENT SET.

      46 NODES (OF     5740  DEFINED) SELECTED FROM
      46 SELECTED ELEMENTS BY NSLE COMMAND.


SPECIFIED SURFACE LOAD PRES FOR ALL SELECTED ELEMENTS  LKEY = 1   KVAL = 1
     SET ACCORDING TO TABLE PARAMETER = _LOADVARI123X


SPECIFIED SURFACE LOAD PRES FOR ALL SELECTED ELEMENTS  LKEY = 2   KVAL = 1
     SET ACCORDING TO TABLE PARAMETER = _LOADVARI123Y


SPECIFIED SURFACE LOAD PRES FOR ALL SELECTED ELEMENTS  LKEY = 3   KVAL = 1
     SET ACCORDING TO TABLE PARAMETER = _LOADVARI123Z
```

208

```
ALL SELECT   FOR ITEM=NODE COMPONENT=
 IN RANGE          1 TO       5740 STEP           1

     5740  NODES (OF       5740  DEFINED) SELECTED BY NSEL  COMMAND.


ALL SELECT   FOR ITEM=ELEM COMPONENT=
 IN RANGE          1 TO       7219 STEP           1

     7060  ELEMENTS (OF       7060  DEFINED) SELECTED BY  ESEL  COMMAND.
*** Set Displacements ***
CMBLOCK read of NODE component _CM116UX_XP  completed


SELECT        COMPONENT _CM116UX_XP


SPECIFIED CONSTRAINT UX   FOR SELECTED NODES          1 TO     5740 BY          1
SET ACCORDING TO TABLE PARAMETER = _LOADVARI116XP


ALL SELECT   FOR ITEM=NODE COMPONENT=
 IN RANGE          1 TO       5740 STEP           1

     5740  NODES (OF       5740  DEFINED) SELECTED BY NSEL  COMMAND.


PRINTOUT RESUMED BY /GOP


USE AUTOMATIC TIME STEPPING THIS LOAD STEP


USE      1 SUBSTEPS INITIALLY THIS LOAD STEP FOR ALL  DEGREES OF FREEDOM
FOR AUTOMATIC TIME STEPPING:
  USE     10 SUBSTEPS AS A MAXIMUM
  USE      1 SUBSTEPS AS A MINIMUM


TIME=  1.0000


ERASE THE CURRENT DATABASE OUTPUT CONTROL TABLE.



WRITE ALL  ITEMS TO THE DATABASE WITH A FREQUENCY OF NONE
  FOR ALL APPLICABLE ENTITIES

WRITE NSOL ITEMS TO THE DATABASE WITH A FREQUENCY OF ALL
  FOR ALL APPLICABLE ENTITIES

WRITE RSOL ITEMS TO THE DATABASE WITH A FREQUENCY OF ALL
  FOR ALL APPLICABLE ENTITIES

WRITE STRS ITEMS TO THE DATABASE WITH A FREQUENCY OF ALL
  FOR ALL APPLICABLE ENTITIES
```

WRITE EPEL ITEMS TO THE DATABASE WITH A FREQUENCY OF ALL
   FOR ALL APPLICABLE ENTITIES

WRITE EPPL ITEMS TO THE DATABASE WITH A FREQUENCY OF ALL
   FOR ALL APPLICABLE ENTITIES

PRINTOUT RESUMED BY /GOP

WRITE MISC ITEMS TO THE DATABASE WITH A FREQUENCY OF ALL
   FOR THE ENTITIES DEFINED BY COMPONENT _ELMISC

NONLINEAR STABILIZATION CONTROL:
KEY=OFF

*GET ANSINTER_ FROM ACTI ITEM=INT   VALUE= 0.00000000

*IF ANSINTER_   (=   0.00000   ) NE
     0   (=   0.00000   ) THEN

*ENDIF

***** ANSYS SOLVE   COMMAND *****

*** WARNING ***   CP =   1.141   TIME= 13:19:49
Element shape checking is currently inactive. Issue SHPP,ON or
SHPP,WARN to reactivate, if desired.

*** NOTE ***   CP =   1.141   TIME= 13:19:49
The model data was checked and warning messages were found.
 Please review output or errors file (
E:\FRP_ProjectScratch\ScrEB4D\file.err) for these warning messages.

*** SELECTION OF ELEMENT TECHNOLOGIES FOR APPLICABLE ELEMENTS ***
      --- GIVE SUGGESTIONS AND RESET THE KEY OPTIONS ---

ELEMENT TYPE   1 IS SHELL181. IT IS ASSOCIATED WITH ELASTOPLASTIC
MATERIALS ONLY. KEYOPT(8) IS ALREADY SET AS SUGGESTED. KEYOPT(3)=2
IS SUGGESTED FOR HIGHER ACCURACY OF MEMBRANE STRESSES; OTHERWISE,
KEYOPT(3)=0 IS SUGGESTED. KEYOPT(3) CAN NOT BE RESET HERE. PLEASE RESET
IT MANUALLY IF NECESSARY.

*** ANSYS - ENGINEERING ANALYSIS SYSTEM RELEASE Release 16.2   16.2   ***
ANSYS Academic Research
00427805 VERSION=WINDOWS x64   13:19:49 FEB 20, 2016 CP=   1.172

S O L U T I O N   O P T I O N S

```
PROBLEM DIMENSIONALITY. . . . . . . . . . . . . .3-D
DEGREES OF FREEDOM. . . . . . UX   UY   UZ   ROTX ROTY ROTZ
ANALYSIS TYPE . . . . . . . . . . . . . . . . . .STATIC (STEADY-STATE)
OFFSET TEMPERATURE FROM ABSOLUTE ZERO . . . . .  459.67
EQUATION SOLVER OPTION. . . . . . . . . . . . . .SPARSE
NEWTON-RAPHSON OPTION . . . . . . . . . . . . . .PROGRAM CHOSEN
GLOBALLY ASSEMBLED MATRIX . . . . . . . . . . . .SYMMETRIC
```

```
*** NOTE ***                          CP =      1.172   TIME= 13:19:49
Poisson's ratio PR input has been converted to NU input.


*** WARNING ***                       CP =      1.172   TIME= 13:19:49
Material number 110 (used by element 5567 ) should normally have at
least one MP or one TB type command associated with it.  Output of
energy by material may not be available.


*** NOTE ***                          CP =      1.203   TIME= 13:19:49
The step data was checked and warning messages were found.
 Please review output or errors file (
E:\FRP\_ProjectScratch\ScrEB4D\file.err ) for these warning messages.


*** NOTE ***                          CP =      1.203   TIME= 13:19:49
This nonlinear analysis defaults to using the full Newton-Raphson
solution procedure.  This can be modified using the NROPT command.


*** NOTE ***                          CP =      1.203   TIME= 13:19:49
Internal nodes from 5741 to 5792 are created.
52 internal nodes are used for handling degrees of freedom on pilot
nodes of rigid target surfaces.
```

L O A D   S T E P   O P T I O N S

```
LOAD STEP NUMBER. . . . . . . . . . . . . . . .      1
TIME AT END OF THE LOAD STEP. . . . . . . . . . 1.0000
AUTOMATIC TIME STEPPING . . . . . . . . . . . .     ON
    INITIAL NUMBER OF SUBSTEPS . . . . . . . . .     1
    MAXIMUM NUMBER OF SUBSTEPS . . . . . . . . .    10
    MINIMUM NUMBER OF SUBSTEPS . . . . . . . . .     1
MAXIMUM NUMBER OF EQUILIBRIUM ITERATIONS. . . .    15
STEP CHANGE BOUNDARY CONDITIONS . . . . . . . .    NO
TERMINATE ANALYSIS IF NOT CONVERGED . . . . . .YES (EXIT)
```

```
   CONVERGENCE CONTROLS. . . . . . . . . . . . . .USE DEFAULTS
   PRINT OUTPUT CONTROLS . . . . . . . . . . . .NO PRINTOUT
   DATABASE OUTPUT CONTROLS
      ITEM     FREQUENCY   COMPONENT
       ALL        NONE
      NSOL         ALL
      RSOL         ALL
      STRS         ALL
      EPEL         ALL
      EPPL         ALL
      MISC         ALL       _ELMISC


 SOLUTION MONITORING INFO IS WRITTEN TO FILE=
file.mntr



 *WARNING*: Some MPC/Lagrange based elements (e.g.5856) in real constant
 set 6 overlap with other MPC/Lagrange based elements (e.g.7187) in
 real constant set 108 which can cause overconstraint.

 *** NOTE ***                          CP =       1.484   TIME= 13:19:49
 It is highly recommended to use the auto contact setting option by
 issuing CNCHECK,AUTO command for this problem in order to achieve
 better convergence.

 *** NOTE ***                          CP =       1.484   TIME= 13:19:49
 Rigid-constraint surface identified by real constant set 6 and contact
 element type 6 has been set up.  The degrees of freedom of the rigid
 surface are driven by the pilot node 5614 which connects to other
 element 5567.  Internal MPC will be built.
 The used degrees of freedom set is  UX   UY   UZ   ROTX ROTY ROTZ
 *WARNING*: Certain contact elements (for example 5862&7194) overlap
 each other.
 ****************************************


 *** NOTE ***                          CP =       1.484   TIME= 13:19:49
 Force-distributed-surface identified by real constant set 8 and
 contact element type 8 has been set up.  The pilot node 5616 is used
 to apply the force which connects to other element 5568.  Internal MPC
 will be built.
 The used degrees of freedom set is  UX   UY   UZ   ROTX ROTY ROTZ
 ****************************************


 *** NOTE ***                          CP =       1.484   TIME= 13:19:49
```

Force-distributed-surface identified by real constant set 10 and
contact element type 10 has been set up. The pilot node 5618 is used
to apply the force which connects to other element 5581. Internal MPC
will be built.
The used degrees of freedom set is UX   UY   UZ   ROTX ROTY ROTZ
****

*** NOTE ***   CP =   1.484   TIME= 13:19:49
Force-distributed-surface identified by real constant set 12 and
contact element type 12 has been set up. The pilot node 5620 is used
to apply the force which connects to other element 5585. Internal MPC
will be built.
The used degrees of freedom set is UX   UY   UZ   ROTX ROTY ROTZ
****

*** NOTE ***   CP =   1.484   TIME= 13:19:49
Force-distributed-surface identified by real constant set 14 and
contact element type 14 has been set up. The pilot node 5622 is used
to apply the force which connects to other element 5589. Internal MPC
will be built.
The used degrees of freedom set is UX   UY   UZ   ROTX ROTY ROTZ
****

*** NOTE ***   CP =   1.484   TIME= 13:19:49
Force-distributed-surface identified by real constant set 16 and
contact element type 16 has been set up. The pilot node 5624 is used
to apply the force which connects to other element 5593. Internal MPC
will be built.
The used degrees of freedom set is UX   UY   UZ   ROTX ROTY ROTZ
****

*** NOTE ***   CP =   1.484   TIME= 13:19:49
Force-distributed-surface identified by real constant set 18 and
contact element type 18 has been set up. The pilot node 5626 is used
to apply the force which connects to other element 5597. Internal MPC
will be built.
The used degrees of freedom set is UX   UY   UZ   ROTX ROTY ROTZ
****

*** NOTE ***   CP =   1.484   TIME= 13:19:49
Force-distributed-surface identified by real constant set 20 and
contact element type 20 has been set up. The pilot node 5628 is used
to apply the force which connects to other element 5601. Internal MPC

213

will be built.
The used degrees of freedom set is UX   UY   UZ   ROTX ROTY ROTZ
****

*** NOTE ***   CP =   1.484   TIME= 13:19:49
Force-distributed-surface identified by real constant set 22 and
contact element type 22 has been set up. The pilot node 5630 is used
to apply the force which connects to other element 5605. Internal MPC
will be built.
The used degrees of freedom set is UX   UY   UZ   ROTX ROTY ROTZ
****

*** NOTE ***   CP =   1.484   TIME= 13:19:49
Force-distributed-surface identified by real constant set 24 and
contact element type 24 has been set up. The pilot node 5632 is used
to apply the force which connects to other element 5609. Internal MPC
will be built.
The used degrees of freedom set is UX   UY   UZ   ROTX ROTY ROTZ
****

*** NOTE ***   CP =   1.484   TIME= 13:19:49
Force-distributed-surface identified by real constant set 26 and
contact element type 26 has been set up. The pilot node 5634 is used
to apply the force which connects to other element 5613. Internal MPC
will be built.
The used degrees of freedom set is UX   UY   UZ   ROTX ROTY ROTZ
****

*** NOTE ***   CP =   1.484   TIME= 13:19:49
Force-distributed-surface identified by real constant set 28 and
contact element type 28 has been set up. The pilot node 5636 is used
to apply the force which connects to other element 5617. Internal MPC
will be built.
The used degrees of freedom set is UX   UY   UZ   ROTX ROTY ROTZ
****

*** NOTE ***   CP =   1.484   TIME= 13:19:49
Force-distributed-surface identified by real constant set 30 and
contact element type 30 has been set up. The pilot node 5638 is used
to apply the force which connects to other element 5621. Internal MPC
will be built.
The used degrees of freedom set is UX   UY   UZ   ROTX ROTY ROTZ
****

214

```
*** NOTE ***                            CP =       1.484   TIME= 13:19:49
Force-distributed-surface identified by real constant set 32 and
contact element type 32 has been set up.  The pilot node 5640 is used
to apply the force which connects to other element 5625.  Internal MPC
will be built.
The used degrees of freedom set is  UX   UY   UZ   ROTX ROTY ROTZ
****************************************


*** NOTE ***                            CP =       1.484   TIME= 13:19:49
Force-distributed-surface identified by real constant set 34 and
contact element type 34 has been set up.  The pilot node 5642 is used
to apply the force which connects to other element 5629.  Internal MPC
will be built.
The used degrees of freedom set is  UX   UY   UZ   ROTX ROTY ROTZ
****************************************


*** NOTE ***                            CP =       1.484   TIME= 13:19:49
Force-distributed-surface identified by real constant set 36 and
contact element type 36 has been set up.  The pilot node 5644 is used
to apply the force which connects to other element 5633.  Internal MPC
will be built.
The used degrees of freedom set is  UX   UY   UZ   ROTX ROTY ROTZ
****************************************


*** NOTE ***                            CP =       1.484   TIME= 13:19:49
Force-distributed-surface identified by real constant set 38 and
contact element type 38 has been set up.  The pilot node 5646 is used
to apply the force which connects to other element 5637.  Internal MPC
will be built.
The used degrees of freedom set is  UX   UY   UZ   ROTX ROTY ROTZ
****************************************


*** NOTE ***                            CP =       1.484   TIME= 13:19:49
Force-distributed-surface identified by real constant set 40 and
contact element type 40 has been set up.  The pilot node 5648 is used
to apply the force which connects to other element 5641.  Internal MPC
will be built.
The used degrees of freedom set is  UX   UY   UZ   ROTX ROTY ROTZ
****************************************


*** NOTE ***                            CP =       1.484   TIME= 13:19:49
```

Force-distributed-surface identified by real constant set 42 and
contact element type 42 has been set up. The pilot node 5650 is used
to apply the force which connects to other element 5645. Internal MPC
will be built.
The used degrees of freedom set is UX   UY   UZ   ROTX ROTY ROTZ
****

*** NOTE ***   CP =   1.484   TIME= 13:19:49
Force-distributed-surface identified by real constant set 44 and
contact element type 44 has been set up. The pilot node 5652 is used
to apply the force which connects to other element 5649. Internal MPC
will be built.
The used degrees of freedom set is UX   UY   UZ   ROTX ROTY ROTZ
****

*** NOTE ***   CP =   1.484   TIME= 13:19:49
Force-distributed-surface identified by real constant set 46 and
contact element type 46 has been set up. The pilot node 5654 is used
to apply the force which connects to other element 5653. Internal MPC
will be built.
The used degrees of freedom set is UX   UY   UZ   ROTX ROTY ROTZ
****

*** NOTE ***   CP =   1.484   TIME= 13:19:49
Force-distributed-surface identified by real constant set 48 and
contact element type 48 has been set up. The pilot node 5656 is used
to apply the force which connects to other element 5657. Internal MPC
will be built.
The used degrees of freedom set is UX   UY   UZ   ROTX ROTY ROTZ
****

*** NOTE ***   CP =   1.484   TIME= 13:19:49
Force-distributed-surface identified by real constant set 50 and
contact element type 50 has been set up. The pilot node 5658 is used
to apply the force which connects to other element 5661. Internal MPC
will be built.
The used degrees of freedom set is UX   UY   UZ   ROTX ROTY ROTZ
****

*** NOTE ***   CP =   1.484   TIME= 13:19:49
Force-distributed-surface identified by real constant set 52 and
contact element type 52 has been set up. The pilot node 5660 is used
to apply the force which connects to other element 5665. Internal MPC

will be built.
The used degrees of freedom set is UX   UY   UZ   ROTX ROTY ROTZ
****

*** NOTE ***   CP =   1.484   TIME= 13:19:49
Force-distributed-surface identified by real constant set 54 and
contact element type 54 has been set up. The pilot node 5662 is used
to apply the force which connects to other element 5669. Internal MPC
will be built.
The used degrees of freedom set is UX   UY   UZ   ROTX ROTY ROTZ
****

*** NOTE ***   CP =   1.484   TIME= 13:19:49
Force-distributed-surface identified by real constant set 56 and
contact element type 56 has been set up. The pilot node 5664 is used
to apply the force which connects to other element 5673. Internal MPC
will be built.
The used degrees of freedom set is UX   UY   UZ   ROTX ROTY ROTZ
****

*** NOTE ***   CP =   1.484   TIME= 13:19:49
Force-distributed-surface identified by real constant set 58 and
contact element type 58 has been set up. The pilot node 5666 is used
to apply the force which connects to other element 5677. Internal MPC
will be built.
The used degrees of freedom set is UX   UY   UZ   ROTX ROTY ROTZ
****

*** NOTE ***   CP =   1.484   TIME= 13:19:49
Force-distributed-surface identified by real constant set 60 and
contact element type 60 has been set up. The pilot node 5668 is used
to apply the force which connects to other element 5681. Internal MPC
will be built.
The used degrees of freedom set is UX   UY   UZ   ROTX ROTY ROTZ
****

*** NOTE ***   CP =   1.484   TIME= 13:19:49
Force-distributed-surface identified by real constant set 62 and
contact element type 62 has been set up. The pilot node 5670 is used
to apply the force which connects to other element 5685. Internal MPC
will be built.
The used degrees of freedom set is UX   UY   UZ   ROTX ROTY ROTZ
****

```
*** NOTE ***                              CP =       1.484   TIME= 13:19:49
Force-distributed-surface identified by real constant set 64 and
contact element type 64 has been set up.  The pilot node 5672 is used
to apply the force which connects to other element 5689.  Internal MPC
will be built.
The used degrees of freedom set is  UX   UY   UZ   ROTX ROTY ROTZ
****************************************


*** NOTE ***                              CP =       1.484   TIME= 13:19:49
Force-distributed-surface identified by real constant set 66 and
contact element type 66 has been set up.  The pilot node 5674 is used
to apply the force which connects to other element 5693.  Internal MPC
will be built.
The used degrees of freedom set is  UX   UY   UZ   ROTX ROTY ROTZ
****************************************


*** NOTE ***                              CP =       1.484   TIME= 13:19:49
Force-distributed-surface identified by real constant set 68 and
contact element type 68 has been set up.  The pilot node 5676 is used
to apply the force which connects to other element 5697.  Internal MPC
will be built.
The used degrees of freedom set is  UX   UY   UZ   ROTX ROTY ROTZ
****************************************


*** NOTE ***                              CP =       1.484   TIME= 13:19:49
Force-distributed-surface identified by real constant set 70 and
contact element type 70 has been set up.  The pilot node 5678 is used
to apply the force which connects to other element 5701.  Internal MPC
will be built.
The used degrees of freedom set is  UX   UY   UZ   ROTX ROTY ROTZ
****************************************


*** NOTE ***                              CP =       1.484   TIME= 13:19:49
Force-distributed-surface identified by real constant set 72 and
contact element type 72 has been set up.  The pilot node 5680 is used
to apply the force which connects to other element 5705.  Internal MPC
will be built.
The used degrees of freedom set is  UX   UY   UZ   ROTX ROTY ROTZ
****************************************


*** NOTE ***                              CP =       1.484   TIME= 13:19:49
```

Force-distributed-surface identified by real constant set 74 and
contact element type 74 has been set up. The pilot node 5682 is used
to apply the force which connects to other element 5709. Internal MPC
will be built.
The used degrees of freedom set is UX   UY   UZ   ROTX ROTY ROTZ
****

*** NOTE ***   CP =   1.484   TIME= 13:19:49
Force-distributed-surface identified by real constant set 76 and
contact element type 76 has been set up. The pilot node 5684 is used
to apply the force which connects to other element 5713. Internal MPC
will be built.
The used degrees of freedom set is UX   UY   UZ   ROTX ROTY ROTZ
****

*** NOTE ***   CP =   1.484   TIME= 13:19:49
Force-distributed-surface identified by real constant set 78 and
contact element type 78 has been set up. The pilot node 5686 is used
to apply the force which connects to other element 5717. Internal MPC
will be built.
The used degrees of freedom set is UX   UY   UZ   ROTX ROTY ROTZ
****

*** NOTE ***   CP =   1.484   TIME= 13:19:49
Force-distributed-surface identified by real constant set 80 and
contact element type 80 has been set up. The pilot node 5688 is used
to apply the force which connects to other element 5721. Internal MPC
will be built.
The used degrees of freedom set is UX   UY   UZ   ROTX ROTY ROTZ
****

*** NOTE ***   CP =   1.484   TIME= 13:19:49
Force-distributed-surface identified by real constant set 82 and
contact element type 82 has been set up. The pilot node 5690 is used
to apply the force which connects to other element 5725. Internal MPC
will be built.
The used degrees of freedom set is UX   UY   UZ   ROTX ROTY ROTZ
****

*** NOTE ***   CP =   1.484   TIME= 13:19:49
Force-distributed-surface identified by real constant set 84 and
contact element type 84 has been set up. The pilot node 5692 is used
to apply the force which connects to other element 5729. Internal MPC

will be built.
The used degrees of freedom set is UX   UY   UZ   ROTX ROTY ROTZ
****

 *** NOTE ***   CP =   1.484   TIME= 13:19:49
 Force-distributed-surface identified by real constant set 86 and
 contact element type 86 has been set up. The pilot node 5694 is used
 to apply the force which connects to other element 5733. Internal MPC
 will be built.
 The used degrees of freedom set is UX   UY   UZ   ROTX ROTY ROTZ
 ****

 *** NOTE ***   CP =   1.484   TIME= 13:19:49
 Force-distributed-surface identified by real constant set 88 and
 contact element type 88 has been set up. The pilot node 5696 is used
 to apply the force which connects to other element 5737. Internal MPC
 will be built.
 The used degrees of freedom set is UX   UY   UZ   ROTX ROTY ROTZ
 ****

 *** NOTE ***   CP =   1.484   TIME= 13:19:49
 Force-distributed-surface identified by real constant set 90 and
 contact element type 90 has been set up. The pilot node 5698 is used
 to apply the force which connects to other element 5741. Internal MPC
 will be built.
 The used degrees of freedom set is UX   UY   UZ   ROTX ROTY ROTZ
 ****

 *** NOTE ***   CP =   1.484   TIME= 13:19:49
 Force-distributed-surface identified by real constant set 92 and
 contact element type 92 has been set up. The pilot node 5700 is used
 to apply the force which connects to other element 5745. Internal MPC
 will be built.
 The used degrees of freedom set is UX   UY   UZ   ROTX ROTY ROTZ
 ****

 *** NOTE ***   CP =   1.484   TIME= 13:19:49
 Force-distributed-surface identified by real constant set 94 and
 contact element type 94 has been set up. The pilot node 5702 is used
 to apply the force which connects to other element 5749. Internal MPC
 will be built.
 The used degrees of freedom set is UX   UY   UZ   ROTX ROTY ROTZ
 ****

```
*** NOTE ***                              CP =      1.484   TIME= 13:19:49
Force-distributed-surface identified by real constant set 96 and
contact element type 96 has been set up.  The pilot node 5704 is used
to apply the force which connects to other element 5753.  Internal MPC
will be built.
The used degrees of freedom set is  UX   UY   UZ   ROTX ROTY ROTZ
***************************************


*** NOTE ***                              CP =      1.484   TIME= 13:19:49
Force-distributed-surface identified by real constant set 98 and
contact element type 98 has been set up.  The pilot node 5706 is used
to apply the force which connects to other element 5757.  Internal MPC
will be built.
The used degrees of freedom set is  UX   UY   UZ   ROTX ROTY ROTZ
***************************************


*** NOTE ***                              CP =      1.484   TIME= 13:19:49
Force-distributed-surface identified by real constant set 100 and
contact element type 100 has been set up.  The pilot node 5708 is used
to apply the force which connects to other element 5761.  Internal MPC
will be built.
The used degrees of freedom set is  UX   UY   UZ   ROTX ROTY ROTZ
***************************************


*** NOTE ***                              CP =      1.484   TIME= 13:19:49
Force-distributed-surface identified by real constant set 102 and
contact element type 102 has been set up.  The pilot node 5710 is used
to apply the force which connects to other element 5765.  Internal MPC
will be built.
The used degrees of freedom set is  UX   UY   UZ   ROTX ROTY ROTZ
***************************************


*** NOTE ***                              CP =      1.484   TIME= 13:19:49
Force-distributed-surface identified by real constant set 104 and
contact element type 104 has been set up.  The pilot node 5712 is used
to apply the force which connects to other element 5769.  Internal MPC
will be built.
The used degrees of freedom set is  UX   UY   UZ   ROTX ROTY ROTZ
***************************************


*** NOTE ***                              CP =      1.484   TIME= 13:19:49
```

Force-distributed-surface identified by real constant set 106 and
contact element type 106 has been set up. The pilot node 5714 is used
to apply the force which connects to other element 5773. Internal MPC
will be built.
The used degrees of freedom set is UX   UY   UZ   ROTX ROTY ROTZ
****

*** NOTE ***   CP =   1.484   TIME= 13:19:49
Force-distributed-surface identified by real constant set 108 and
contact element type 108 has been set up. The pilot node 5716 is used
to apply the force which connects to other element 5777. Internal MPC
will be built.
The used degrees of freedom set is UX   UY   UZ   ROTX ROTY ROTZ
WARNING: Certain contact elements (for example 7194&5861) overlap
each other.
****

*** WARNING ***   CP =   1.484   TIME= 13:19:49
Overconstraint may occur for Lagrange multiplier or MPC based contact
algorithm.
The reasons for possible overconstraint are:
*Certain contact elements (for example 7194 & 5861) overlap with other.
****

MAXIMUM NUMBER OF EQUILIBRIUM ITERATIONS HAS BEEN MODIFIED
 TO BE, NEQIT = 26, BY SOLUTION CONTROL LOGIC.

*** NOTE ***   CP =   1.547   TIME= 13:19:49
Predictor is ON by default for structural elements with rotational
degrees of freedom. Use the PRED,OFF command to turn the predictor
OFF if it adversely affects the convergence.

The FEA model contains 0 external CE equations and 582 internal CE
equations.

```
         ***********  PRECISE MASS SUMMARY  ***********

    TOTAL RIGID BODY MASS MATRIX ABOUT ORIGIN
              Translational mass        |  Coupled translational/rotational mass
          2.6087       0.0000      0.0000   |    0.0000      0.35525E-03   -313.04
          0.0000       2.6087      0.0000   |  -0.35525E-03   0.0000      -0.29323E-04
          0.0000       0.0000      2.6087   |   313.04       0.29323E-04   0.0000
      ---------------------------------------- | ----------------------------------------
                                            |          Rotational mass (inertia)
                                            |    50254.      0.35130E-02   0.19866E-01
                                            |   0.35130E-02   232.75      -0.42636E-01
                                            |   0.19866E-01  -0.42636E-01   50151.


    TOTAL MASS =  2.6087
      The mass principal axes coincide with the global Cartesian axes


    CENTER OF MASS (X,Y,Z)=  -0.11241E-04    120.00        0.13618E-03


    TOTAL INERTIA ABOUT CENTER OF MASS
          12689.       -0.57822E-05   0.19866E-01
       -0.57822E-05     232.75       -0.61754E-05
        0.19866E-01   -0.61754E-05    12587.
      The inertia principal axes coincide with the global Cartesian axes



   *** MASS SUMMARY BY ELEMENT TYPE ***


   TYPE      MASS
     1    2.60867


  Range of element maximum matrix coefficients in global coordinates
  Maximum = 2396838.35 at element 4236.
  Minimum = 1.032861979E-02 at element 7206.


  *** WARNING ***                          CP =     23.156   TIME= 13:20:10
  Coefficient ratio exceeds 1.0e8 - Check results.

    *** ELEMENT MATRIX FORMULATION TIMES
   TYPE    NUMBER   ENAME     TOTAL CP  AVE CP


      1     5566  SHELL181    42.422   0.007622
      5       46  SURF156      0.000   0.000000
      6       46  CONTA175     0.000   0.000000
      7        1  TARGE170     0.000   0.000000
      8       10  CONTA174     0.000   0.000000
      9        1  TARGE170     0.000   0.000000
     10       22  CONTA174     0.000   0.000000
     11        1  TARGE170     0.000   0.000000
     12       22  CONTA174     0.000   0.000000
```

```
13        1    TARGE170    0.000    0.000000
14       22    CONTA174    0.000    0.000000
15        1    TARGE170    0.000    0.000000
16       22    CONTA174    0.000    0.000000
17        1    TARGE170    0.000    0.000000
18       21    CONTA174    0.000    0.000000
19        1    TARGE170    0.000    0.000000
20       22    CONTA174    0.000    0.000000
21        1    TARGE170    0.000    0.000000
22       22    CONTA174    0.000    0.000000
23        1    TARGE170    0.000    0.000000
24       23    CONTA174    0.000    0.000000
25        1    TARGE170    0.000    0.000000
26       23    CONTA174    0.000    0.000000
27        1    TARGE170    0.000    0.000000
28       24    CONTA174    0.000    0.000000
29        1    TARGE170    0.000    0.000000
30       23    CONTA174    0.000    0.000000
31        1    TARGE170    0.000    0.000000
32       23    CONTA174    0.000    0.000000
33        1    TARGE170    0.000    0.000000
34       22    CONTA174    0.000    0.000000
35        1    TARGE170    0.000    0.000000
36       22    CONTA174    0.000    0.000000
37        1    TARGE170    0.000    0.000000
38       21    CONTA174    0.000    0.000000
39        1    TARGE170    0.000    0.000000
40       22    CONTA174    0.000    0.000000
41        1    TARGE170    0.000    0.000000
42       22    CONTA174    0.000    0.000000
43        1    TARGE170    0.000    0.000000
44       22    CONTA174    0.000    0.000000
45        1    TARGE170    0.000    0.000000
46       22    CONTA174    0.000    0.000000
47        1    TARGE170    0.000    0.000000
48       20    CONTA174    0.000    0.000000
49        1    TARGE170    0.000    0.000000
50       41    CONTA174    0.031    0.000762
51        1    TARGE170    0.000    0.000000
52       41    CONTA174    0.000    0.000000
53        1    TARGE170    0.000    0.000000
54       44    CONTA174    0.031    0.000710
55        1    TARGE170    0.000    0.000000
56       43    CONTA174    0.000    0.000000
57        1    TARGE170    0.000    0.000000
58       42    CONTA174    0.000    0.000000
59        1    TARGE170    0.000    0.000000
60       43    CONTA174    0.000    0.000000
```

61	1	TARGE170	0.000	0.000000
62	44	CONTA174	0.000	0.000000
63	1	TARGE170	0.000	0.000000
64	41	CONTA174	0.000	0.000000
65	1	TARGE170	0.000	0.000000
66	41	CONTA174	0.000	0.000000
67	1	TARGE170	0.000	0.000000
68	10	CONTA174	0.000	0.000000
69	1	TARGE170	0.000	0.000000
70	22	CONTA174	0.000	0.000000
71	1	TARGE170	0.000	0.000000
72	22	CONTA174	0.000	0.000000
73	1	TARGE170	0.000	0.000000
74	22	CONTA174	0.000	0.000000
75	1	TARGE170	0.000	0.000000
76	22	CONTA174	0.000	0.000000
77	1	TARGE170	0.016	0.015625
78	22	CONTA174	0.000	0.000000
79	1	TARGE170	0.000	0.000000
80	21	CONTA174	0.000	0.000000
81	1	TARGE170	0.000	0.000000
82	22	CONTA174	0.000	0.000000
83	1	TARGE170	0.031	0.031250
84	23	CONTA174	0.000	0.000000
85	1	TARGE170	0.000	0.000000
86	23	CONTA174	0.000	0.000000
87	1	TARGE170	0.016	0.015625
88	24	CONTA174	0.000	0.000000
89	1	TARGE170	0.000	0.000000
90	23	CONTA174	0.000	0.000000
91	1	TARGE170	0.016	0.015625
92	23	CONTA174	0.000	0.000000
93	1	TARGE170	0.000	0.000000
94	22	CONTA174	0.000	0.000000
95	1	TARGE170	0.000	0.000000
96	21	CONTA174	0.000	0.000000
97	1	TARGE170	0.016	0.015625
98	22	CONTA174	0.000	0.000000
99	1	TARGE170	0.000	0.000000
100	22	CONTA174	0.000	0.000000
101	1	TARGE170	0.000	0.000000
102	22	CONTA174	0.000	0.000000
103	1	TARGE170	0.000	0.000000
104	22	CONTA174	0.000	0.000000
105	1	TARGE170	0.000	0.000000
106	22	CONTA174	0.000	0.000000
107	1	TARGE170	0.000	0.000000
108	10	CONTA174	0.000	0.000000

```
109        1  TARGE170   0.000   0.000000
110        1  COMBIN39   0.016   0.015625
111        1  COMBIN39   0.000   0.000000
112        1  COMBIN39   0.000   0.000000
113        1  COMBIN39   0.000   0.000000
114        1  COMBIN39   0.000   0.000000
115        1  COMBIN39   0.000   0.000000
116        1  COMBIN39   0.000   0.000000
117        1  COMBIN39   0.000   0.000000
118        1  COMBIN39   0.000   0.000000
119        1  COMBIN39   0.000   0.000000
120        1  COMBIN39   0.000   0.000000
121        1  COMBIN39   0.000   0.000000
122        1  COMBIN39   0.000   0.000000
123        1  COMBIN39   0.000   0.000000
124        1  COMBIN39   0.000   0.000000
125        1  COMBIN39   0.000   0.000000
126        1  COMBIN39   0.000   0.000000
127        1  COMBIN39   0.000   0.000000
128        1  COMBIN39   0.000   0.000000
129        1  COMBIN39   0.000   0.000000
130        1  COMBIN39   0.000   0.000000
131        1  COMBIN39   0.000   0.000000
132        1  COMBIN39   0.000   0.000000
133        1  COMBIN39   0.000   0.000000
134        1  COMBIN39   0.000   0.000000
135        1  COMBIN39   0.000   0.000000
136        1  COMBIN39   0.016   0.015625
137        1  COMBIN39   0.000   0.000000
138        1  COMBIN39   0.000   0.000000
139        1  COMBIN39   0.000   0.000000
140        1  COMBIN39   0.000   0.000000
141        1  COMBIN39   0.000   0.000000
142        1  COMBIN39   0.031   0.031250
143        1  COMBIN39   0.016   0.015625
144        1  COMBIN39   0.016   0.015625
145        1  COMBIN39   0.000   0.000000
146        1  COMBIN39   0.016   0.015625
147        1  COMBIN39   0.016   0.015625
148        1  COMBIN39   0.016   0.015625
149        1  COMBIN39   0.000   0.000000
150        1  COMBIN39   0.000   0.000000
151        1  COMBIN39   0.016   0.015625
152        1  COMBIN39   0.000   0.000000
153        1  COMBIN39   0.000   0.000000
154        1  COMBIN39   0.000   0.000000
155        1  COMBIN39   0.000   0.000000
156        1  COMBIN39   0.000   0.000000
```

```
    157          1  COMBIN39      0.000   0.000000
    158          1  COMBIN39      0.000   0.000000
    159          1  COMBIN39      0.000   0.000000
    160          1  COMBIN39      0.000   0.000000
    161          1  COMBIN39      0.000   0.000000
    162         24  COMBIN14      0.016   0.000651
Time at end of element matrix formulation CP = 23.15625.


ALL CURRENT ANSYS DATA WRITTEN TO FILE NAME= file.rdb
 FOR POSSIBLE RESUME FROM THIS POINT
    FORCE CONVERGENCE VALUE  = 0.1139E+08  CRITERION= 0.5811E+05
    MOMENT CONVERGENCE VALUE = 0.1469E+08  CRITERION= 0.7496E+05


SPARSE MATRIX DIRECT SOLVER.
 Number of equations =        33356,    Maximum wavefront =    360
 Memory allocated for solver =        131.022 MB
 Memory required for in-core =        113.439 MB
 Memory required for out-of-core =     23.922 MB



*** NOTE ***                         CP =      23.984   TIME= 13:20:12
The Sparse Matrix solver is currently running in the in-core memory
mode.  This memory mode uses the most amount of memory in order to
avoid using the hard drive as much as possible, which most often
results in the fastest solution time.  This mode is recommended if
enough physical memory is present to accommodate all of the solver
data.
curEqn= 33356  totEqn=  33356 Job CP sec=      24.641
     Factor Done= 100% Factor Wall sec=       0.198 rate=   13884.2 Mflops
Sparse solver maximum pivot= 970675347 at node 5614 ROTY.
Sparse solver minimum pivot= 4346.20939 at node 3052 UZ.
Sparse solver minimum pivot in absolute value= 4346.20939 at node 3052
UZ.
    DISP CONVERGENCE VALUE   =  4.000      CRITERION= 0.2041
   EQUIL ITER   1 COMPLETED.  NEW TRIANG MATRIX.  MAX DOF INC=   4.000
    DISP CONVERGENCE VALUE   =  4.000      CRITERION= 0.2082
    LINE SEARCH PARAMETER =   1.000     SCALED MAX DOF INC =   4.000
    FORCE CONVERGENCE VALUE  =  8264.      CRITERION=  83.68
    MOMENT CONVERGENCE VALUE =  46.08      CRITERION=  35.07
   EQUIL ITER   2 COMPLETED.  NEW TRIANG MATRIX.  MAX DOF INC=  -1.704
    DISP CONVERGENCE VALUE   =  1.704      CRITERION= 0.2125
    LINE SEARCH PARAMETER =   1.000     SCALED MAX DOF INC =  -1.704
    FORCE CONVERGENCE VALUE  =  3298.      CRITERION=  86.79
    MOMENT CONVERGENCE VALUE =  57.44      CRITERION=  36.38
   EQUIL ITER   3 COMPLETED.  NEW TRIANG MATRIX.  MAX DOF INC=  -34.61
    DISP CONVERGENCE VALUE   =  34.61      CRITERION=  2.000
    LINE SEARCH PARAMETER =   1.000     SCALED MAX DOF INC =  -34.61
    FORCE CONVERGENCE VALUE  =  1787.      CRITERION=  92.71
```

```
    MOMENT CONVERGENCE VALUE =  48.17     CRITERION=  38.86
  EQUIL ITER   4 COMPLETED.  NEW TRIANG MATRIX.  MAX DOF INC=  -98.88
   DISP CONVERGENCE VALUE   =  98.88      CRITERION=  7.510
   LINE SEARCH PARAMETER =   1.000     SCALED MAX DOF INC =  -98.88
   FORCE CONVERGENCE VALUE  = 0.3176E-03  CRITERION=  106.4     <<< CONVERGED
   MOMENT CONVERGENCE VALUE = 0.1801E-04  CRITERION=  44.62     <<< CONVERGED
  EQUIL ITER   5 COMPLETED.  NEW TRIANG MATRIX.  MAX DOF INC= -0.3430E-04
   DISP CONVERGENCE VALUE   = 0.3430E-04  CRITERION=  7.664     <<< CONVERGED
   LINE SEARCH PARAMETER =   1.000     SCALED MAX DOF INC = -0.3430E-04
   >>> SOLUTION CONVERGED AFTER EQUILIBRIUM ITERATION   5


   *** ELEMENT RESULT CALCULATION TIMES
 TYPE    NUMBER   ENAME     TOTAL CP  AVE CP

    1     5566  SHELL181    30.156   0.005418
    5       46  SURF156      0.000   0.000000
    6       46  CONTA175     0.000   0.000000
    8       10  CONTA174     0.000   0.000000
   10       22  CONTA174     0.000   0.000000
   12       22  CONTA174     0.000   0.000000
   14       22  CONTA174     0.000   0.000000
   16       22  CONTA174     0.000   0.000000
   18       21  CONTA174     0.000   0.000000
   20       22  CONTA174     0.000   0.000000
   22       22  CONTA174     0.000   0.000000
   24       23  CONTA174     0.000   0.000000
   26       23  CONTA174     0.000   0.000000
   28       24  CONTA174     0.000   0.000000
   30       23  CONTA174     0.000   0.000000
   32       23  CONTA174     0.000   0.000000
   34       22  CONTA174     0.000   0.000000
   36       22  CONTA174     0.000   0.000000
   38       21  CONTA174     0.000   0.000000
   40       22  CONTA174     0.000   0.000000
   42       22  CONTA174     0.000   0.000000
   44       22  CONTA174     0.000   0.000000
   46       22  CONTA174     0.000   0.000000
   48       20  CONTA174     0.000   0.000000
   50       41  CONTA174     0.000   0.000000
   52       41  CONTA174     0.000   0.000000
   54       44  CONTA174     0.000   0.000000
   56       43  CONTA174     0.000   0.000000
   58       42  CONTA174     0.000   0.000000
   60       43  CONTA174     0.000   0.000000
   62       44  CONTA174     0.000   0.000000
   64       41  CONTA174     0.000   0.000000
   66       41  CONTA174     0.000   0.000000
   68       10  CONTA174     0.000   0.000000
```

```
 70      22   CONTA174      0.000    0.000000
 72      22   CONTA174      0.000    0.000000
 74      22   CONTA174      0.000    0.000000
 76      22   CONTA174      0.000    0.000000
 78      22   CONTA174      0.000    0.000000
 80      21   CONTA174      0.000    0.000000
 82      22   CONTA174      0.000    0.000000
 84      23   CONTA174      0.000    0.000000
 86      23   CONTA174      0.000    0.000000
 88      24   CONTA174      0.000    0.000000
 90      23   CONTA174      0.000    0.000000
 92      23   CONTA174      0.000    0.000000
 94      22   CONTA174      0.000    0.000000
 96      21   CONTA174      0.000    0.000000
 98      22   CONTA174      0.000    0.000000
100      22   CONTA174      0.000    0.000000
102      22   CONTA174      0.000    0.000000
104      22   CONTA174      0.000    0.000000
106      22   CONTA174      0.000    0.000000
108      10   CONTA174      0.000    0.000000
110       1   COMBIN39      0.016    0.015625
111       1   COMBIN39      0.000    0.000000
112       1   COMBIN39      0.000    0.000000
113       1   COMBIN39      0.000    0.000000
114       1   COMBIN39      0.000    0.000000
115       1   COMBIN39      0.000    0.000000
116       1   COMBIN39      0.000    0.000000
117       1   COMBIN39      0.000    0.000000
118       1   COMBIN39      0.000    0.000000
119       1   COMBIN39      0.000    0.000000
120       1   COMBIN39      0.000    0.000000
121       1   COMBIN39      0.000    0.000000
122       1   COMBIN39      0.000    0.000000
123       1   COMBIN39      0.000    0.000000
124       1   COMBIN39      0.000    0.000000
125       1   COMBIN39      0.016    0.015625
126       1   COMBIN39      0.000    0.000000
127       1   COMBIN39      0.000    0.000000
128       1   COMBIN39      0.000    0.000000
129       1   COMBIN39      0.000    0.000000
130       1   COMBIN39      0.000    0.000000
131       1   COMBIN39      0.000    0.000000
132       1   COMBIN39      0.000    0.000000
133       1   COMBIN39      0.000    0.000000
134       1   COMBIN39      0.000    0.000000
135       1   COMBIN39      0.000    0.000000
136       1   COMBIN39      0.000    0.000000
137       1   COMBIN39      0.000    0.000000
```

```
138      1   COMBIN39    0.000    0.000000
139      1   COMBIN39    0.000    0.000000
140      1   COMBIN39    0.000    0.000000
141      1   COMBIN39    0.000    0.000000
142      1   COMBIN39    0.000    0.000000
143      1   COMBIN39    0.000    0.000000
144      1   COMBIN39    0.000    0.000000
145      1   COMBIN39    0.000    0.000000
146      1   COMBIN39    0.000    0.000000
147      1   COMBIN39    0.000    0.000000
148      1   COMBIN39    0.000    0.000000
149      1   COMBIN39    0.000    0.000000
150      1   COMBIN39    0.000    0.000000
151      1   COMBIN39    0.000    0.000000
152      1   COMBIN39    0.000    0.000000
153      1   COMBIN39    0.000    0.000000
154      1   COMBIN39    0.000    0.000000
155      1   COMBIN39    0.000    0.000000
156      1   COMBIN39    0.000    0.000000
157      1   COMBIN39    0.000    0.000000
158      1   COMBIN39    0.000    0.000000
159      1   COMBIN39    0.000    0.000000
160      1   COMBIN39    0.000    0.000000
161      1   COMBIN39    0.000    0.000000
162     24   COMBIN14    0.000    0.000000


 *** NODAL LOAD CALCULATION TIMES
 TYPE    NUMBER   ENAME     TOTAL CP  AVE CP


    1    5566   SHELL181    0.234    0.000042
    5      46   SURF156     0.000    0.000000
    6      46   CONTA175    0.000    0.000000
    8      10   CONTA174    0.000    0.000000
   10      22   CONTA174    0.000    0.000000
   12      22   CONTA174    0.000    0.000000
   14      22   CONTA174    0.000    0.000000
   16      22   CONTA174    0.000    0.000000
   18      21   CONTA174    0.000    0.000000
   20      22   CONTA174    0.000    0.000000
   22      22   CONTA174    0.000    0.000000
   24      23   CONTA174    0.000    0.000000
   26      23   CONTA174    0.000    0.000000
   28      24   CONTA174    0.000    0.000000
   30      23   CONTA174    0.000    0.000000
   32      23   CONTA174    0.000    0.000000
   34      22   CONTA174    0.000    0.000000
   36      22   CONTA174    0.000    0.000000
   38      21   CONTA174    0.000    0.000000
```

```
 40        22   CONTA174     0.000    0.000000
 42        22   CONTA174     0.000    0.000000
 44        22   CONTA174     0.000    0.000000
 46        22   CONTA174     0.000    0.000000
 48        20   CONTA174     0.000    0.000000
 50        41   CONTA174     0.000    0.000000
 52        41   CONTA174     0.000    0.000000
 54        44   CONTA174     0.000    0.000000
 56        43   CONTA174     0.000    0.000000
 58        42   CONTA174     0.000    0.000000
 60        43   CONTA174     0.000    0.000000
 62        44   CONTA174     0.000    0.000000
 64        41   CONTA174     0.000    0.000000
 66        41   CONTA174     0.000    0.000000
 68        10   CONTA174     0.000    0.000000
 70        22   CONTA174     0.000    0.000000
 72        22   CONTA174     0.000    0.000000
 74        22   CONTA174     0.000    0.000000
 76        22   CONTA174     0.000    0.000000
 78        22   CONTA174     0.000    0.000000
 80        21   CONTA174     0.000    0.000000
 82        22   CONTA174     0.000    0.000000
 84        23   CONTA174     0.000    0.000000
 86        23   CONTA174     0.000    0.000000
 88        24   CONTA174     0.000    0.000000
 90        23   CONTA174     0.000    0.000000
 92        23   CONTA174     0.000    0.000000
 94        22   CONTA174     0.000    0.000000
 96        21   CONTA174     0.000    0.000000
 98        22   CONTA174     0.000    0.000000
100        22   CONTA174     0.000    0.000000
102        22   CONTA174     0.000    0.000000
104        22   CONTA174     0.000    0.000000
106        22   CONTA174     0.000    0.000000
108        10   CONTA174     0.000    0.000000
110         1   COMBIN39     0.000    0.000000
111         1   COMBIN39     0.000    0.000000
112         1   COMBIN39     0.000    0.000000
113         1   COMBIN39     0.000    0.000000
114         1   COMBIN39     0.000    0.000000
115         1   COMBIN39     0.000    0.000000
116         1   COMBIN39     0.000    0.000000
117         1   COMBIN39     0.000    0.000000
118         1   COMBIN39     0.000    0.000000
119         1   COMBIN39     0.000    0.000000
120         1   COMBIN39     0.000    0.000000
121         1   COMBIN39     0.000    0.000000
122         1   COMBIN39     0.000    0.000000
```

231

```
123      1  COMBIN39    0.000   0.000000
124      1  COMBIN39    0.000   0.000000
125      1  COMBIN39    0.000   0.000000
126      1  COMBIN39    0.000   0.000000
127      1  COMBIN39    0.000   0.000000
128      1  COMBIN39    0.000   0.000000
129      1  COMBIN39    0.000   0.000000
130      1  COMBIN39    0.000   0.000000
131      1  COMBIN39    0.000   0.000000
132      1  COMBIN39    0.000   0.000000
133      1  COMBIN39    0.000   0.000000
134      1  COMBIN39    0.000   0.000000
135      1  COMBIN39    0.000   0.000000
136      1  COMBIN39    0.000   0.000000
137      1  COMBIN39    0.000   0.000000
138      1  COMBIN39    0.000   0.000000
139      1  COMBIN39    0.000   0.000000
140      1  COMBIN39    0.000   0.000000
141      1  COMBIN39    0.000   0.000000
142      1  COMBIN39    0.000   0.000000
143      1  COMBIN39    0.000   0.000000
144      1  COMBIN39    0.000   0.000000
145      1  COMBIN39    0.000   0.000000
146      1  COMBIN39    0.000   0.000000
147      1  COMBIN39    0.000   0.000000
148      1  COMBIN39    0.000   0.000000
149      1  COMBIN39    0.000   0.000000
150      1  COMBIN39    0.000   0.000000
151      1  COMBIN39    0.000   0.000000
152      1  COMBIN39    0.000   0.000000
153      1  COMBIN39    0.000   0.000000
154      1  COMBIN39    0.000   0.000000
155      1  COMBIN39    0.000   0.000000
156      1  COMBIN39    0.000   0.000000
157      1  COMBIN39    0.000   0.000000
158      1  COMBIN39    0.000   0.000000
159      1  COMBIN39    0.000   0.000000
160      1  COMBIN39    0.000   0.000000
161      1  COMBIN39    0.000   0.000000
162     24  COMBIN14    0.016   0.000651
*** LOAD STEP    1   SUBSTEP    1  COMPLETED.    CUM ITER =       5
*** TIME =   1.00000        TIME INC =   1.00000


*** ANSYS BINARY FILE STATISTICS
 BUFFER SIZE USED= 16384
       0.875 MB WRITTEN ON ELEMENT MATRIX FILE: file.emat
     285.250 MB WRITTEN ON ELEMENT SAVED DATA FILE: file.esav
```

```
        17.188 MB WRITTEN ON ASSEMBLED MATRIX FILE: file.full
        39.562 MB WRITTEN ON RESULTS FILE: file.rst
 *************** Write FE CONNECTORS *********


 WRITE OUT CONSTRAINT EQUATIONS TO FILE=
file.ce




 *****************************************************
 *************** FINISHED SOLVE FOR LS 1 *************


 PARAMETER _DS_PROGRESS  DELETED.


 *GET  _WALLASOL  FROM  ACTI  ITEM=TIME WALL  VALUE=  13.3822222


 PRINTOUT RESUMED BY /GOP


 FINISH SOLUTION PROCESSING


 ***** ROUTINE COMPLETED *****  CP =        186.125




 *** ANSYS - ENGINEERING ANALYSIS SYSTEM  RELEASE Release 16.2     16.2      ***
 ANSYS Academic Research
 00427805  VERSION=WINDOWS x64   13:22:56  FEB 20, 2016 CP=     186.125


 FRP305 - Varying Orientation Angle and Vertical Load in Soft Clay - Constant 4




          ***** ANSYS RESULTS INTERPRETATION (POST1) *****


 *** NOTE ***                           CP =      186.125   TIME= 13:22:56
 Reading results into the database (SET command) will update the current
 displacement and force boundary conditions in the database with the
 values from the results file for that load set.  Note that any
 subsequent solutions will use these values unless action is taken to
 either SAVE the current values or not overwrite them (/EXIT,NOSAVE).


 Set Encoding of XML File to:ISO-8859-1


 Set Output of XML File to:
     PARM,       ,     ,     ,     ,     ,     ,     ,     ,     ,     ,     ,
            ,     ,     ,     ,     ,     ,     ,
```

DATABASE WRITTEN ON
FILE   parm.xml

EXIT THE ANSYS POST1 DATABASE PROCESSOR

 ***** ROUTINE COMPLETED ***** CP =   186.125

 PRINTOUT RESUMED BY /GOP

 *GET _WALLDONE FROM ACTI ITEM=TIME WALL VALUE= 13.3822222

 PARAMETER _PREPTIME =   0.000000000

 PARAMETER _SOLVTIME =   187.0000000

 PARAMETER _POSTTIME =   0.000000000

 PARAMETER _TOTALTIM =   187.0000000

 EXIT ANSYS WITHOUT SAVING DATABASE

 NUMBER OF WARNING MESSAGES ENCOUNTERED=   4
 NUMBER OF ERROR   MESSAGES ENCOUNTERED=   0

 *** WARNING ***   CP =   186.141   TIME= 13:22:59
 During this session the elapsed time exceeds the CPU time by 104%.
 Often this indicates either a lack of physical memory (RAM) required
 to efficiently handle this simulation or it indicates a particularly
 slow hard drive configuration. This simulation can be expected to run
 faster on identical hardware if additional RAM or a faster hard drive
 configuration is made available. For more details, please see the
 ANSYS Performance Guide which is part of the ANSYS Help system.

 +--------------------- A N S Y S   S T A T I S T I C S ----------------------+

 Release: Release 16.2   Build: 16.2   Update: UP20150629   Platform: WINDOWS
 x64
 Date Run: 02/20/2016   Time: 13:22
 Windows Process ID: 10296

 Processor Model: Intel(R) Core(TM) i7-4700MQ CPU @ 2.40GHz

```
Compiler: Intel(R) FORTRAN Compiler Version 14.0.0  (Build: 20140422)
          Intel(R) C/C++ Compiler Version 14.0.0  (Build: 20140422)
          Intel(R) Math Kernel Library Version 11.1.3 Product Build 20140917


Total number of cores available        :    8
Number of physical cores available     :    4
Number of processes requested          :    1
Number of threads per process requested :   2
Total number of cores requested        :    2 (Shared Memory
Parallel)


GPU Acceleration: Not Requested


Job Name: file
Working Directory: E:\FRP\_ProjectScratch\ScrEB4D


Total CPU time for main thread                   :       93.9 seconds
Total CPU time summed for all threads            :      186.1 seconds


Elapsed time spent pre-processing model (/PREP7)  :        0.1 seconds
Elapsed time spent solution - preprocessing       :        0.1 seconds
Elapsed time spent computing solution             :      186.3 seconds
Elapsed time spent solution - postprocessing      :        0.0 seconds
Elapsed time spent post-processing model (/POST1) :        0.0 seconds


Equation solver computational rate                :     9855.6 Mflops
Equation solver effective I/O rate                :     7047.5 MB/sec


Maximum total memory used                         :      211.0 MB
Maximum total memory allocated                    :     2112.0 MB
Maximum total memory available                    :       16 GB


+------------------ E N D   A N S Y S   S T A T I S T I C S ------------------+


 *----------------------------------------------------------------------------*
 |                                                                            |
 |                          ANSYS RUN COMPLETED                               |
 |                                                                            |
 |----------------------------------------------------------------------------|
 |                                                                            |
 | Ansys Release 16.2        Build 16.2        UP20150629     WINDOWS x64 |
 |                                                                            |
 |----------------------------------------------------------------------------|
 |                                                                            |
 | Database Requested(-db)  1024 MB     Scratch Memory Requested    1024 MB |
 | Maximum Database Used        8 MB     Maximum Scratch Memory Used    203 MB |
```

```
|                                                                       |
|-----------------------------------------------------------------------|
|                                                                       |
|       CP Time      (sec) =         186.141       Time  =  13:22:59     |
|       Elapsed Time (sec) =         192.000       Date  =  02/20/2016   |
|                                                                       |
*-----------------------------------------------------------------------*
```

14.2. *Project Schematic view*

Summary

Project:	FRP305 - Varying Orientation Angle and Vertical Load in Soft Clay - Constant 4 in displacement , material and 24x12 in pile dimension
Date:	3/16/2016
Time:	9:16:08 PM
Product Version:	Release 16.2
Last Saved Version:	Release 16.2

Project Schematic View
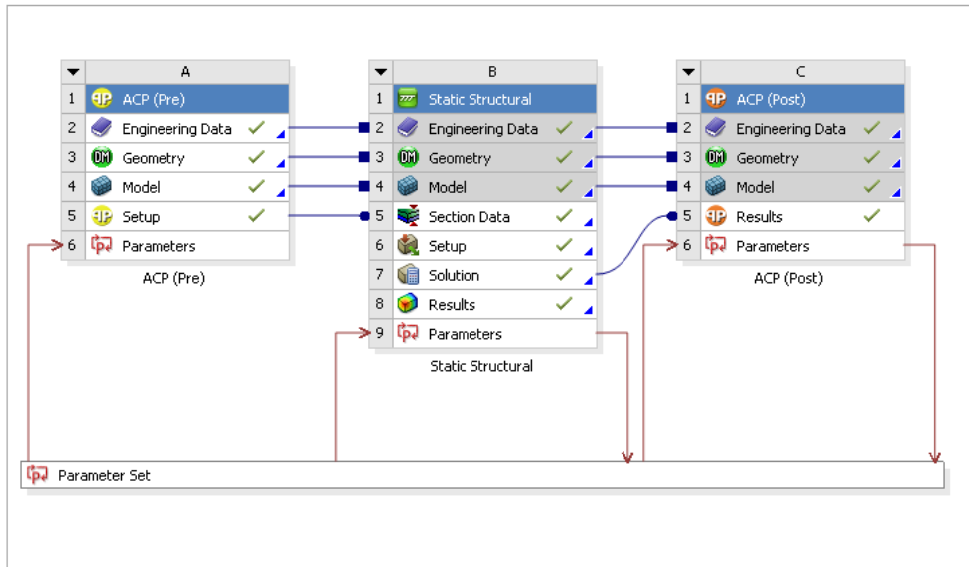
Figure 123 – Project schematic view

14.3. *Outline of All Parameters*

Table 32 – Outline of all Parameters

ID	Parameter Name	Value	Unit
⊞⊟Input Parameters			
⊞⊟ ACP (Pre)			
P1	ZXPlane.H1	12	in
P2	ZXPlane.V2	6	in
P3	ModelingPly.1.ply_angle	0	
P4	ModelingPly.2.ply_angle	0	
P5	ModelingPly.3.ply_angle	0	
P6	ModelingPly.4.ply_angle	0	
P7	ModelingPly.5.ply_angle	0	
P8	ModelingPly.6.ply_angle	0	
P9	ModelingPly.7.ply_angle	0	
P10	ModelingPly.8.ply_angle	0	
P11	ModelingPly.9.ply_angle	0	
P12	ModelingPly.10.ply_angle	0	
⊞⊟ Static Structural			
P17	Displacement X Component	4	in
P18	Force Y Component	-50000	lbf
⊞⊟Output Parameters			
⊞⊟ Static Structural			
P13	Maximum Principal Stress Maximum	1544.7	psi
P15	Maximum Shear Stress Maximum	1595.2	psi
⊞⊟ ACP (Post)			
P16	Parameter.1	0.3186	

238

14.4. *Report Preview*

Project

First Saved	Wednesday, December 02, 2015
Last Saved	Saturday, February 20, 2016
Product Version	16.2 Release
Save Project Before Solution	No
Save Project After Solution	No
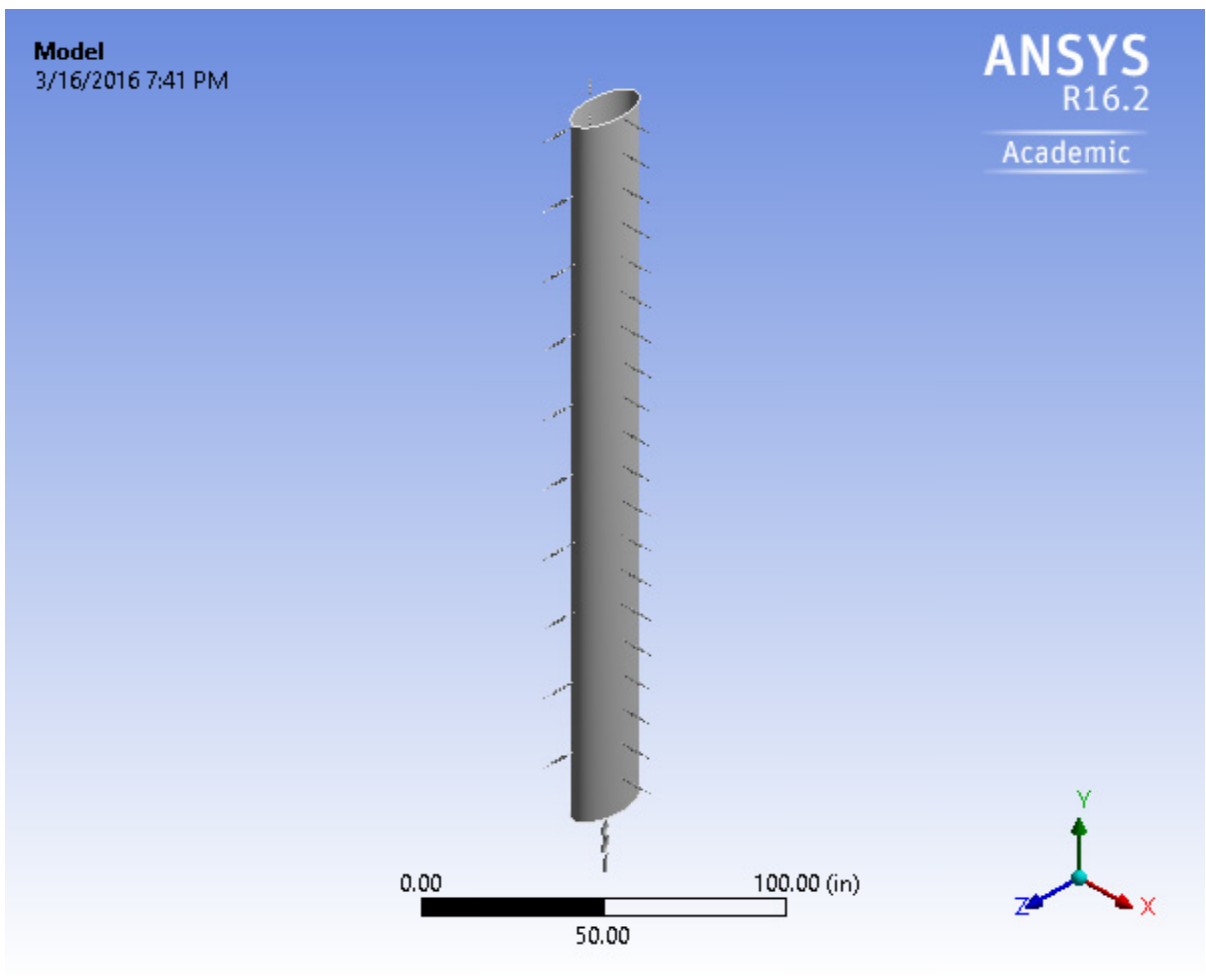
Figure 124 – Project Model

Contents

Units

Table 33 - Units

Unit System	U.S. Customary (in, lbm, lbf, s, V, A) Degrees rad/s Fahrenheit
Angle	Degrees
Rotational Velocity	rad/s
Temperature	Fahrenheit

Model (A4, B4, C4)

Geometry

Table 34 - Model (A4, B4, C4) > Geometry

Object Name	*Geometry*
State	Fully Defined
Definition	
Source	E:\FRP\1 - FE Models\FRP305 - Varying Orientation Angle and Vertical Load in Soft Clay - Constant 4 in displacement , material and 24x12 in pile dimension_files\dp4\ACP-Pre\DM\ACP-Pre.agdb
Type	DesignModeler
Length Unit	Meters
Element Control	Program Controlled
Display Style	Body Color
Bounding Box	
Length X	12. in
Length Y	240. in
Length Z	24. in
Properties	
Volume	1396.6 in³
Mass	100.91 lbm
Surface Area(approx.)	13966 in²
Scale Factor Value	1.
Statistics	
Bodies	1
Active Bodies	1
Nodes	5612
Elements	5566
Mesh Metric	None
Basic Geometry Options	
Parameters	Yes
Parameter Key	DS
Attributes	No
Named Selections	No
Material Properties	No
Advanced Geometry Options	
Use Associativity	Yes
Coordinate Systems	No
Reader Mode Saves Updated File	No
Use Instances	Yes
Smart CAD Update	No
Compare Parts On Update	No
Attach File Via Temp File	Yes
Temporary Directory	C:\Users\Yahya\AppData\Roaming\Ansys\v162
Analysis Type	3-D
Decompose Disjoint Geometry	Yes
Enclosure and Symmetry Processing	Yes

Table 35 - Model (A4, B4, C4) > Geometry > Parts

Object Name	*Surface Body*
State	Meshed
Graphics Properties	
Visible	Yes
Transparency	1
Definition	
Suppressed	No
Stiffness Behavior	Flexible
Coordinate System	Default Coordinate System
Reference Temperature	By Environment
Thickness	0.1 in
Thickness Mode	Manual
Offset Type	Middle
Material	
Assignment	Epoxy E-Glass UD
Nonlinear Effects	Yes
Thermal Strain Effects	Yes
Bounding Box	
Length X	12. in
Length Y	240. in
Length Z	24. in
Properties	
Volume	1396.6 in³
Mass	100.91 lbm
Centroid X	3.3327e-005 in
Centroid Y	120. in
Centroid Z	1.7908e-005 in
Moment of Inertia Ip1	4.8938e+005 lbm·in²
Moment of Inertia Ip2	8148.9 lbm·in²
Moment of Inertia Ip3	4.8538e+005 lbm·in²
Surface Area(approx.)	13966 in²
Statistics	
Nodes	5612
Elements	5566
Mesh Metric	None

Coordinate Systems

Table 36 - Model (A4, B4, C4) > Coordinate Systems > Coordinate System

Object Name	*Global Coordinate System*
State	Fully Defined
Definition	
Type	Cartesian
Coordinate System ID	0.
Origin	
Origin X	0. in
Origin Y	0. in
Origin Z	0. in
Directional Vectors	
X Axis Data	[1. 0. 0.]
Y Axis Data	[0. 1. 0.]
Z Axis Data	[0. 0. 1.]

Connections

Table 37 - Model (A4, B4, C4) > Connections

Object Name	*Connections*
State	Fully Defined
Auto Detection	
Generate Automatic Connection On Refresh	Yes
Transparency	
Enabled	Yes

Table 38 - Model (A4, B4, C4) > Connections > Springs

Object Name	Longitudinal - Ground To Surface Body 1	Longitudinal - Ground To Surface Body 2	Longitudinal - Ground To Surface Body 3	Longitudinal - Ground To Surface Body 4	Longitudinal - Ground To Surface Body 5	Longitudinal - Ground To Surface Body 6	Longitudinal - Ground To Surface Body 7	Longitudinal - Ground To Surface Body 8	Longitudinal - Ground To Surface Body 9	Longitudinal - Ground To Surface Body 10	Longitudinal - Ground To Surface Body 11
State	Fully Defined										
Graphics Properties											
Visible	Yes										
Definition											
Type	Longitudinal										
Spring Behavior	Both										
Longitudinal Stiffness	Tabular Data										
Longitudinal Damping	0. lbf·s/in										
Preload	None										
Suppressed	No										
Spring Length	24. in	12. in									
Scope											
Scope	Body-Ground										
Reference											
Coordinate System	Global Coordinate System										
Reference X Coordinate	0. in	18. in									
Reference Z Coordinate	0. in										
Reference Location	Defined										
Mobile											
Scoping Method	Geometry Selection										
Applied By	Remote Attachment										
Scope	1 Edge	1 Face									
Body	Surface Body										
Coordinate System	Global Coordinate System										
Mobile X Coordinate	0. in	6. in									
Mobile Z Coordinate	0. in										
Mobile Location	Defined										
Behavior	Rigid	Deformable									
Pinball Region	All	5. in									

246

Figure 125 - Model (A4, B4, C4) > Connections > Longitudinal - Ground To Surface Body

Table 39 - Model (A4, B4, C4) > Connections > Longitudinal - Ground To Surface Body

Displacement [in]	Force [lbf]
0.	0.
0.25	11846
0.5	12419
0.75	12622
1.	12727
1.25	12790
1.5	12833
1.75	12863
2.	12886
2.25	12904
2.5	12919
2.75	12931
3.	12940
3.25	12949
3.5	12956
3.75	12962
4.	12968

Figure 126 - Model (A4, B4, C4) > Connections > Longitudinal - Ground To Surface Body

Table 40 - Model (A4, B4, C4) > Connections > Longitudinal - Ground To Surface Body

Displacement [in]	Force [lbf]
0.	0.
0.25	292.82
0.5	395.17
0.75	447.28
1.	478.85
1.25	500.03
1.5	515.22
1.75	526.65
2.	535.56
2.25	542.7
2.5	548.55
2.75	553.43
3.	557.57
3.25	561.12
3.5	564.19
3.75	566.89
4.	569.27

Figure 127 - Model (A4, B4, C4) > Connections > Longitudinal - Ground To Surface Body 3

Table 41 - Model (A4, B4, C4) > Connections > Longitudinal - Ground To Surface Body 3

Displacement [in]	Force [lbf]
0.	0.
0.25	292.82
0.5	395.17
0.75	447.28
1.	478.85
1.25	500.03
1.5	515.22
1.75	526.65
2.	535.56
2.25	542.7
2.5	548.55
2.75	553.43
3.	557.57
3.25	561.12
3.5	564.19
3.75	566.89
4.	569.27

249

Figure 128 - Model (A4, B4, C4) > Connections > Longitudinal - Ground To Surface Body 4

Table 42 - Model (A4, B4, C4) > Connections > Longitudinal - Ground To Surface Body 4

Displacement [in]	Force [lbf]
0.	0.
0.25	292.82
0.5	395.17
0.75	447.28
1.	478.85
1.25	500.03
1.5	515.22
1.75	526.65
2.	535.56
2.25	542.7
2.5	548.55
2.75	553.43
3.	557.57
3.25	561.12
3.5	564.19
3.75	566.89
4.	569.27

250

Figure 129 - Model (A4, B4, C4) > Connections > Longitudinal - Ground To Surface Body 5

Table 43 - Model (A4, B4, C4) > Connections > Longitudinal - Ground To Surface Body 5

Displacement [in]	Force [lbf]
0.	0.
0.25	292.82
0.5	395.17
0.75	447.28
1.	478.85
1.25	500.03
1.5	515.22
1.75	526.65
2.	535.56
2.25	542.7
2.5	548.55
2.75	553.43
3.	557.57
3.25	561.12
3.5	564.19
3.75	566.89
4.	569.27

Figure 130 - Model (A4, B4, C4) > Connections > Longitudinal - Ground To Surface Body 6

Table 44 - Model (A4, B4, C4) > Connections > Longitudinal - Ground To Surface Body 6

Displacement [in]	Force [lbf]
0.	0.
0.25	292.82
0.5	395.17
0.75	447.28
1.	478.85
1.25	500.03
1.5	515.22
1.75	526.65
2.	535.56
2.25	542.7
2.5	548.55
2.75	553.43
3.	557.57
3.25	561.12
3.5	564.19
3.75	566.89
4.	569.27

Figure 131 - Model (A4, B4, C4) > Connections > Longitudinal - Ground To Surface Body 7

Table 45 - Model (A4, B4, C4) > Connections > Longitudinal - Ground To Surface Body 7

Displacement [in]	Force [lbf]
0.	0.
0.25	292.82
0.5	395.17
0.75	447.28
1.	478.85
1.25	500.03
1.5	515.22
1.75	526.65
2.	535.56
2.25	542.7
2.5	548.55
2.75	553.43
3.	557.57
3.25	561.12
3.5	564.19
3.75	566.89
4.	569.27

253

Figure 132 - Model (A4, B4, C4) > Connections > Longitudinal - Ground To Surface Body 8

Table 46 - Model (A4, B4, C4) > Connections > Longitudinal - Ground To Surface Body 8

Displacement [in]	Force [lbf]
0.	0.
0.25	292.82
0.5	395.17
0.75	447.28
1.	478.85
1.25	500.03
1.5	515.22
1.75	526.65
2.	535.56
2.25	542.7
2.5	548.55
2.75	553.43
3.	557.57
3.25	561.12
3.5	564.19
3.75	566.89
4.	569.27

Figure 133 - Model (A4, B4, C4) > Connections > Longitudinal - Ground To Surface Body 9

Table 47 - Model (A4, B4, C4) > Connections > Longitudinal - Ground To Surface Body 9

Displacement [in]	Force [lbf]
0.	0.
0.25	292.82
0.5	395.17
0.75	447.28
1.	478.85
1.25	500.03
1.5	515.22
1.75	526.65
2.	535.56
2.25	542.7
2.5	548.55
2.75	553.43
3.	557.57
3.25	561.12
3.5	564.19
3.75	566.89
4.	569.27

255

Figure 134 - Model (A4, B4, C4) > Connections > Longitudinal - Ground To Surface Body 10

Table 48 - Model (A4, B4, C4) > Connections > Longitudinal - Ground To Surface Body 10

Displacement [in]	Force [lbf]
0.	0.
0.25	292.82
0.5	395.17
0.75	447.28
1.	478.85
1.25	500.03
1.5	515.22
1.75	526.65
2.	535.56
2.25	542.7
2.5	548.55
2.75	553.43
3.	557.57
3.25	561.12
3.5	564.19
3.75	566.89
4.	569.27

Figure 135 - Model (A4, B4, C4) > Connections > Longitudinal - Ground To Surface Body 11

Table 49 - Model (A4, B4, C4) > Connections > Longitudinal - Ground To Surface Body 11

Displacement [in]	Force [lbf]
0.	0.
0.25	292.82
0.5	395.17
0.75	447.28
1.	478.85
1.25	500.03
1.5	515.22
1.75	526.65
2.	535.56
2.25	542.7
2.5	548.55
2.75	553.43
3.	557.57
3.25	561.12
3.5	564.19
3.75	566.89
4.	569.27

Table 50 - Model (A4, B4, C4) > Connections > Springs

	Longitudinal - Ground To Surface Body 12	Longitudinal - Ground To Surface Body 13	Longitudinal - Ground To Surface Body 14	Longitudinal - Ground To Surface Body 15	Longitudinal - Ground To Surface Body 16	Longitudinal - Ground To Surface Body 17	Longitudinal - Ground To Surface Body 18	Longitudinal - Ground To Surface Body 19	Longitudinal - Ground To Surface Body 20	Longitudinal - Ground To Surface Body 21	Longitudinal - Ground To Surface Body 22
State	Fully Defined										
Graphics Properties											
Visible	Yes										
Definition											
Type	Longitudinal										
Spring Behavior	Both										
Longitudinal Stiffness	Tabular Data										
Longitudinal Damping	0. lbf·s/in										
Preload	None										
Suppressed	No										
Spring Length	12. in										
Scope											
Scope	Body-Ground										
Reference											
Coordinate System	Global Coordinate System										
Reference X Coordinate	18. in										0. in
Reference Y Coordinate	120. in	108. in	96. in	84. in	72. in	60. in	48. in	36. in	24. in	12. in	240. in
Reference Z Coordinate	0. in										24. in
Reference Location	Defined										
Mobile											
Scoping Method	Geometry Selection										
Applied By	Remote Attachment										
Scope	1 Face										
Body	Surface Body										
Coordinate System	Global Coordinate System										
Mobile X Coordinate	6. in										0. in
Mobile Y Coordinate	120. in	108. in	96. in	84. in	72. in	60. in	48. in	36. in	24. in	12. in	240. in
Mobile Z Coordinate	0. in										12. in
Mobile Location	Defined										
Behavior	Deformable										
Pinball Region	5. in										

Figure 136 - Model (A4, B4, C4) > Connections > Longitudinal - Ground To Surface Body 12

Table 51 - Model (A4, B4, C4) > Connections > Longitudinal - Ground To Surface Body 12

Displacement [in]	Force [lbf]
0.	0.
0.25	292.82
0.5	395.17
0.75	447.28
1.	478.85
1.25	500.03
1.5	515.22
1.75	526.65
2.	535.56
2.25	542.7
2.5	548.55
2.75	553.43
3.	557.57
3.25	561.12
3.5	564.19
3.75	566.89
4.	569.27

259

Figure 137 - Model (A4, B4, C4) > Connections > Longitudinal - Ground To Surface Body 13

Table 52 - Model (A4, B4, C4) > Connections > Longitudinal - Ground To Surface Body 13

Displacement [in]	Force [lbf]
0.	0.
0.25	292.82
0.5	395.17
0.75	447.28
1.	478.85
1.25	500.03
1.5	515.22
1.75	526.65
2.	535.56
2.25	542.7
2.5	548.55
2.75	553.43
3.	557.57
3.25	561.12
3.5	564.19
3.75	566.89
4.	569.27

Figure 138 - Model (A4, B4, C4) > Connections > Longitudinal - Ground To Surface Body 14

Table 53 - Model (A4, B4, C4) > Connections > Longitudinal - Ground To Surface Body 14

Displacement [in]	Force [lbf]
0.	0.
0.25	292.82
0.5	395.17
0.75	447.28
1.	478.85
1.25	500.03
1.5	515.22
1.75	526.65
2.	535.56
2.25	542.7
2.5	548.55
2.75	553.43
3.	557.57
3.25	561.12
3.5	564.19
3.75	566.89
4.	569.27

Figure 139 - Model (A4, B4, C4) > Connections > Longitudinal - Ground To Surface Body 15

Table 54 - Model (A4, B4, C4) > Connections > Longitudinal - Ground To Surface Body 15

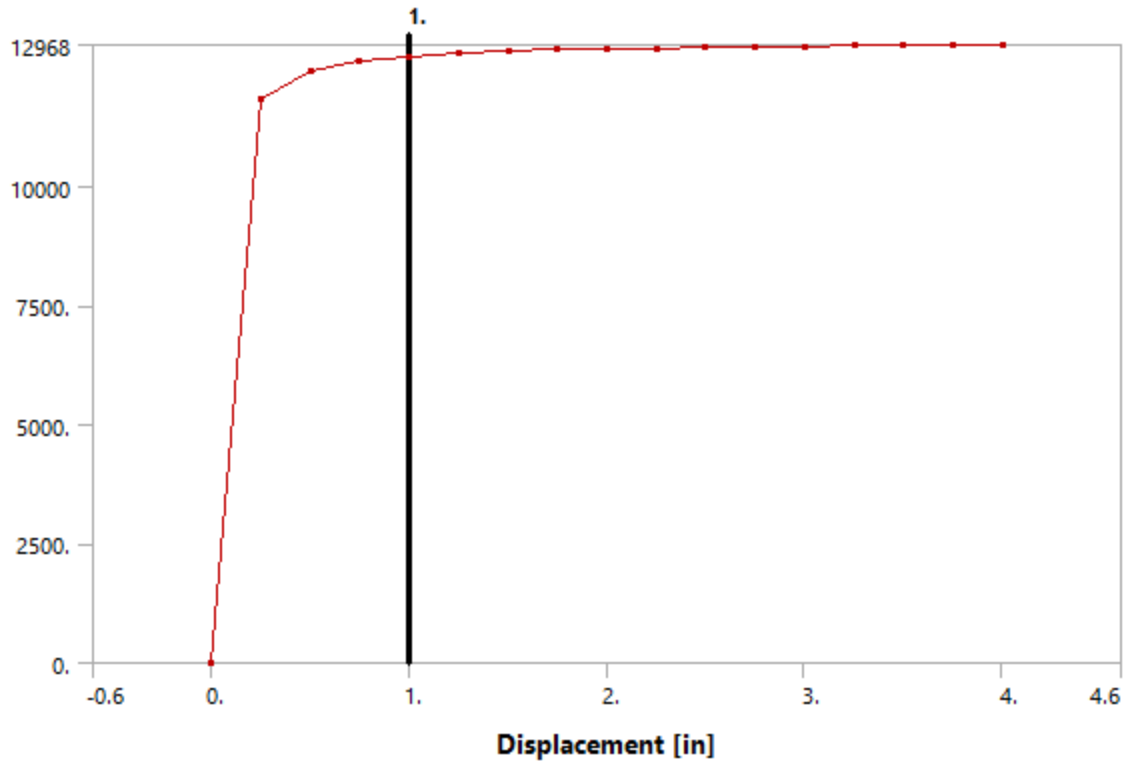| Displacement [in]	Force [lbf]
0.	0.
0.25	292.82
0.5	395.17
0.75	447.28
1.	478.85
1.25	500.03
1.5	515.22
1.75	526.65
2.	535.56
2.25	542.7
2.5	548.55
2.75	553.43
3.	557.57
3.25	561.12
3.5	564.19
3.75	566.89
4.	569.27

Figure 140 - Model (A4, B4, C4) > Connections > Longitudinal - Ground To Surface Body 16

Table 55 - Model (A4, B4, C4) > Connections > Longitudinal - Ground To Surface Body 16

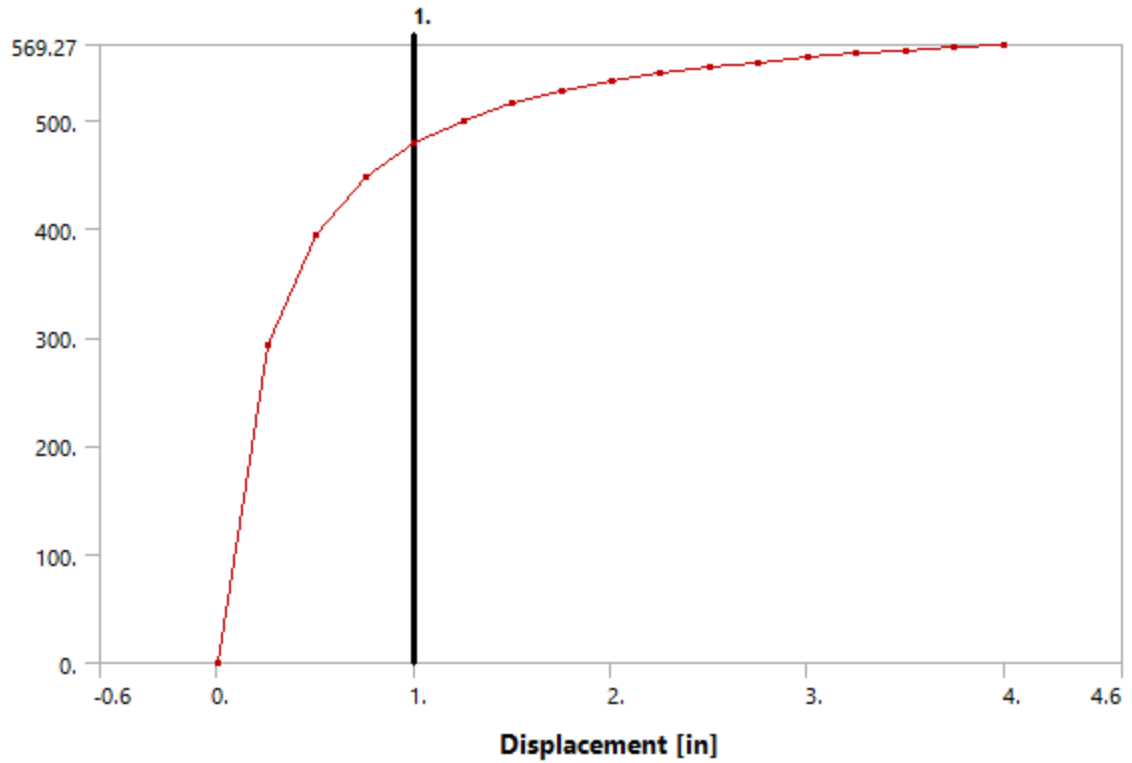| Displacement [in]	Force [lbf]
0.	0.
0.25	292.82
0.5	395.17
0.75	447.28
1.	478.85
1.25	500.03
1.5	515.22
1.75	526.65
2.	535.56
2.25	542.7
2.5	548.55
2.75	553.43
3.	557.57
3.25	561.12
3.5	564.19
3.75	566.89
4.	569.27

Figure 141 - Model (A4, B4, C4) > Connections > Longitudinal - Ground To Surface Body 17

Table 56 - Model (A4, B4, C4) > Connections > Longitudinal - Ground To Surface Body 17

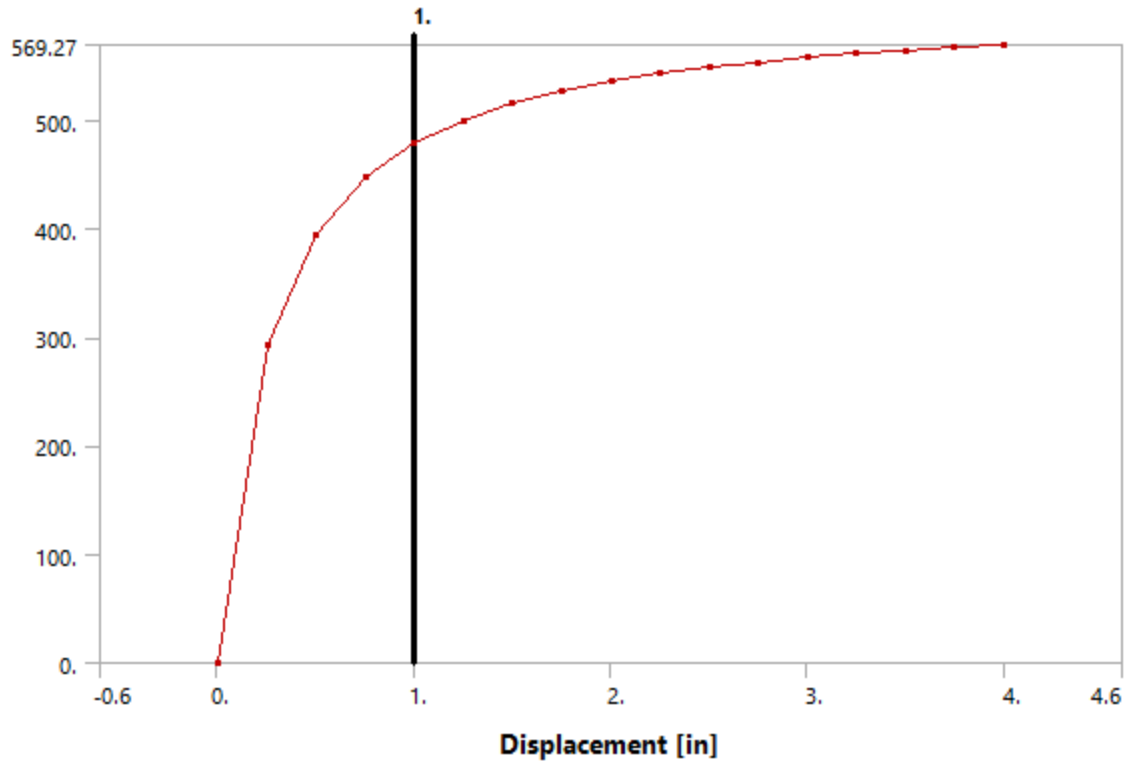| Displacement [in]	Force [lbf]
0.	0.
0.25	292.82
0.5	395.17
0.75	447.28
1.	478.85
1.25	500.03
1.5	515.22
1.75	526.65
2.	535.56
2.25	542.7
2.5	548.55
2.75	553.43
3.	557.57
3.25	561.12
3.5	564.19
3.75	566.89
4.	569.27

Figure 142 - Model (A4, B4, C4) > Connections > Longitudinal - Ground To Surface Body 18

Table 57 - Model (A4, B4, C4) > Connections > Longitudinal - Ground To Surface Body 18

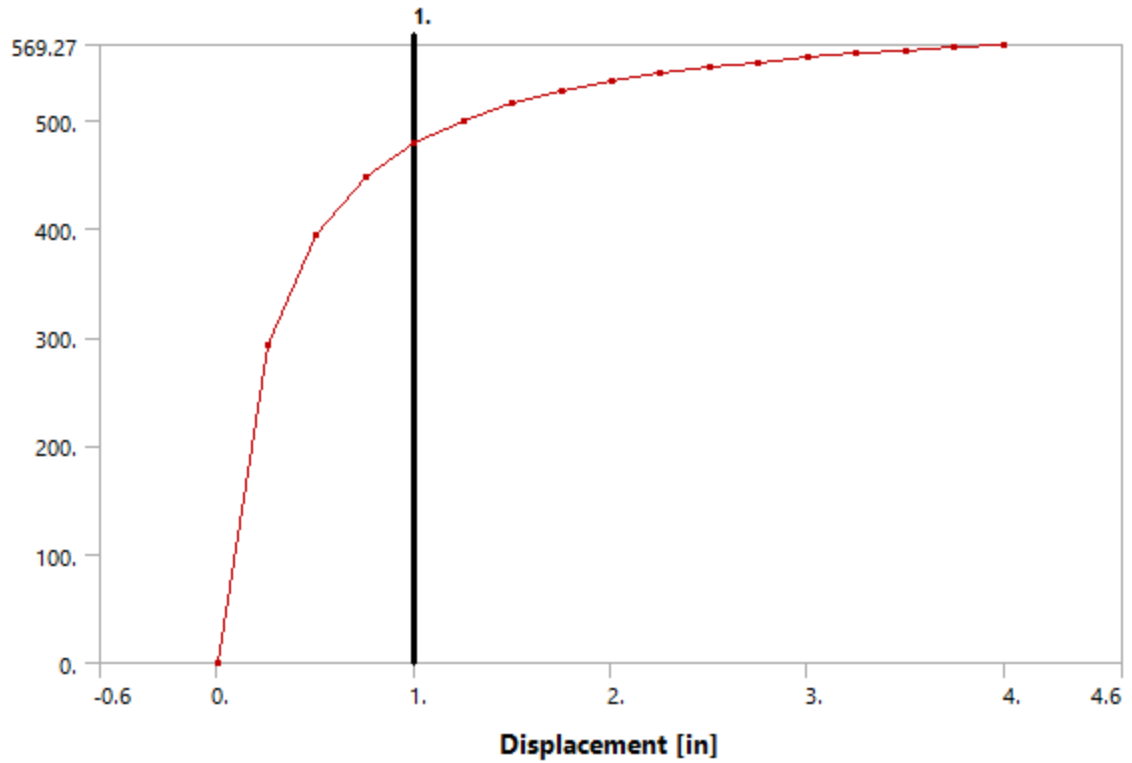| Displacement [in]	Force [lbf]
0.	0.
0.25	292.82
0.5	395.17
0.75	447.28
1.	478.85
1.25	500.03
1.5	515.22
1.75	526.65
2.	535.56
2.25	542.7
2.5	548.55
2.75	553.43
3.	557.57
3.25	561.12
3.5	564.19
3.75	566.89
4.	569.27

Figure 143 - Model (A4, B4, C4) > Connections > Longitudinal - Ground To Surface Body 19

Table 58 - Model (A4, B4, C4) > Connections > Longitudinal - Ground To Surface Body 19

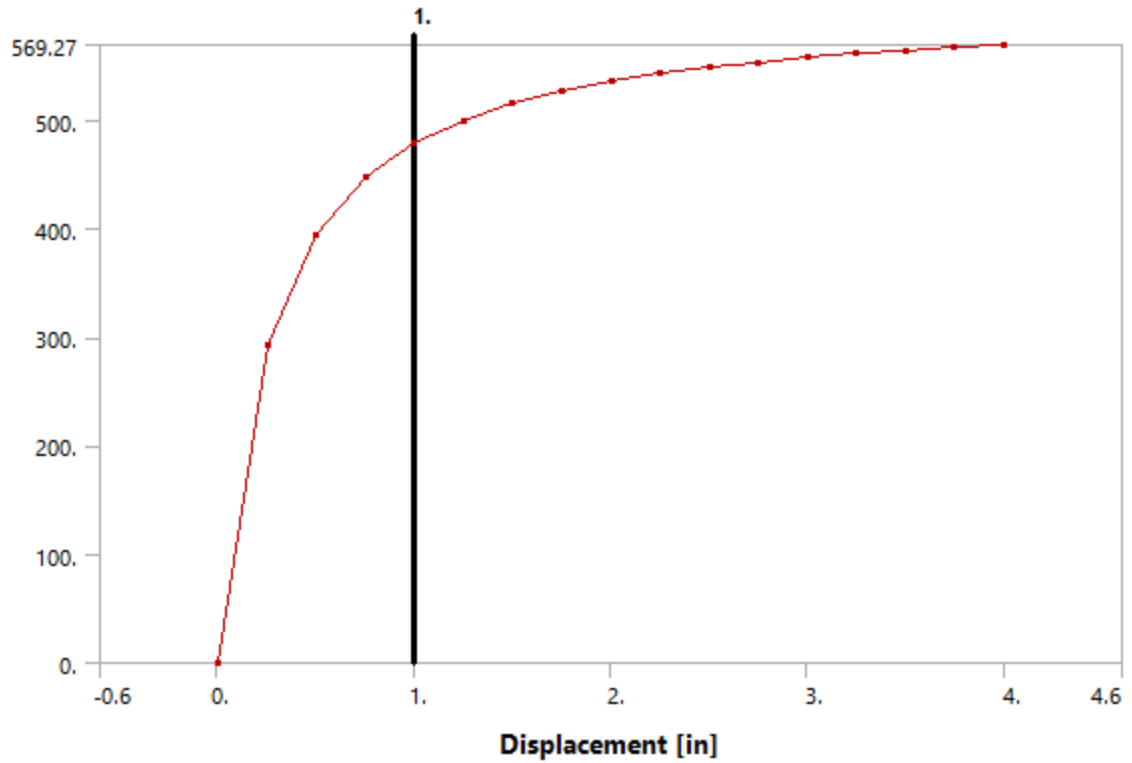| Displacement [in]	Force [lbf]
0.	0.
0.25	292.82
0.5	395.17
0.75	447.28
1.	478.85
1.25	500.03
1.5	515.22
1.75	526.65
2.	535.56
2.25	542.7
2.5	548.55
2.75	553.43
3.	557.57
3.25	561.12
3.5	564.19
3.75	566.89
4.	569.27

Figure 144 - Model (A4, B4, C4) > Connections > Longitudinal - Ground To Surface Body 20

Table 59 - Model (A4, B4, C4) > Connections > Longitudinal - Ground To Surface Body 20

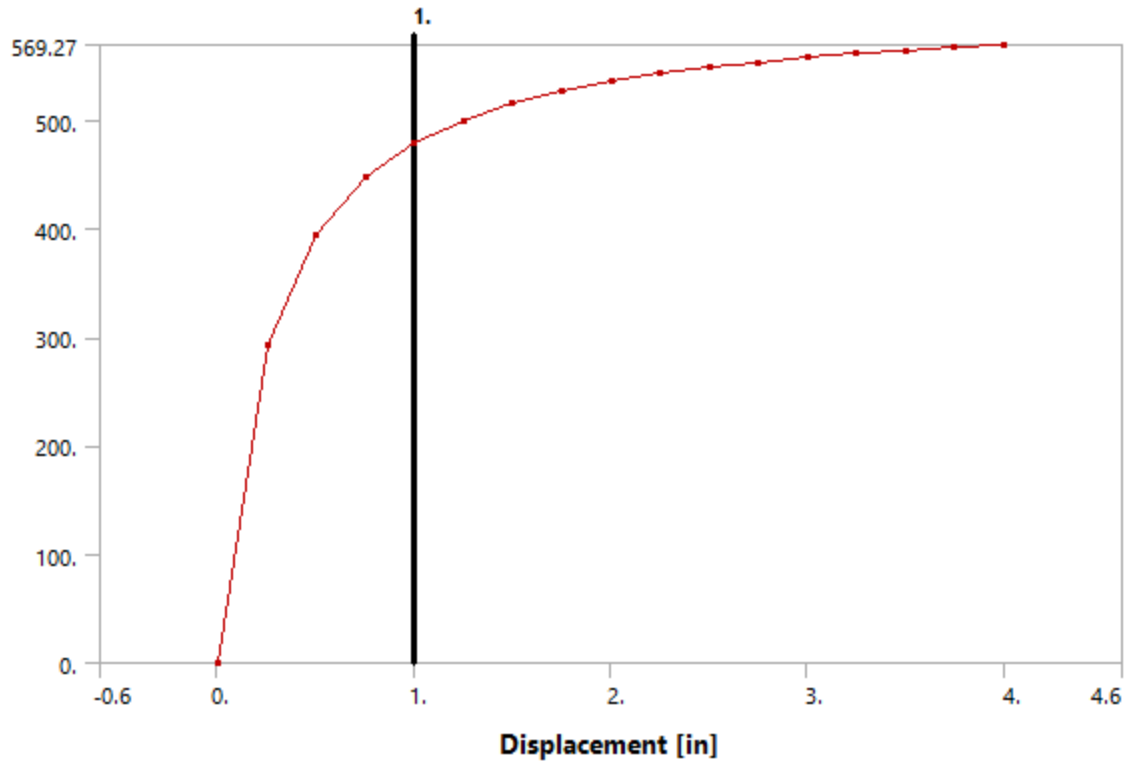| Displacement [in]	Force [lbf]
0.	0.
0.25	292.82
0.5	395.17
0.75	447.28
1.	478.85
1.25	500.03
1.5	515.22
1.75	526.65
2.	535.56
2.25	542.7
2.5	548.55
2.75	553.43
3.	557.57
3.25	561.12
3.5	564.19
3.75	566.89
4.	569.27

Figure 145 - Model (A4, B4, C4) > Connections > Longitudinal - Ground To Surface Body 21

Table 60 - Model (A4, B4, C4) > Connections > Longitudinal - Ground To Surface Body 21

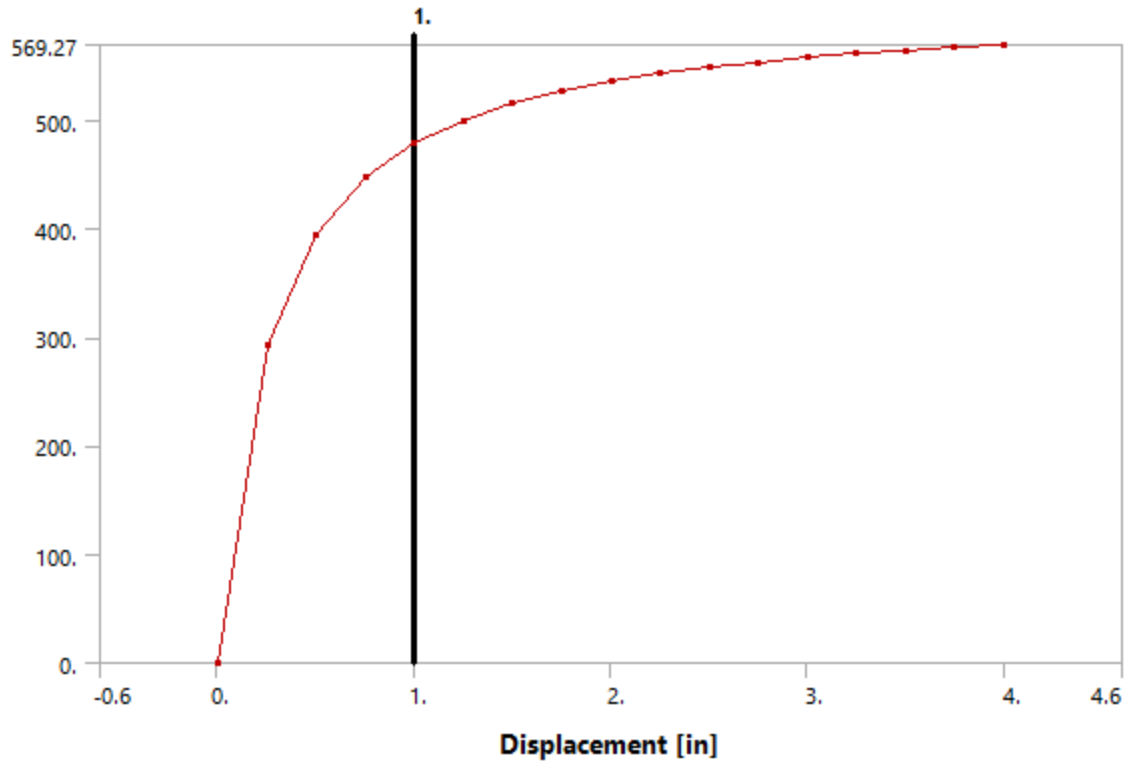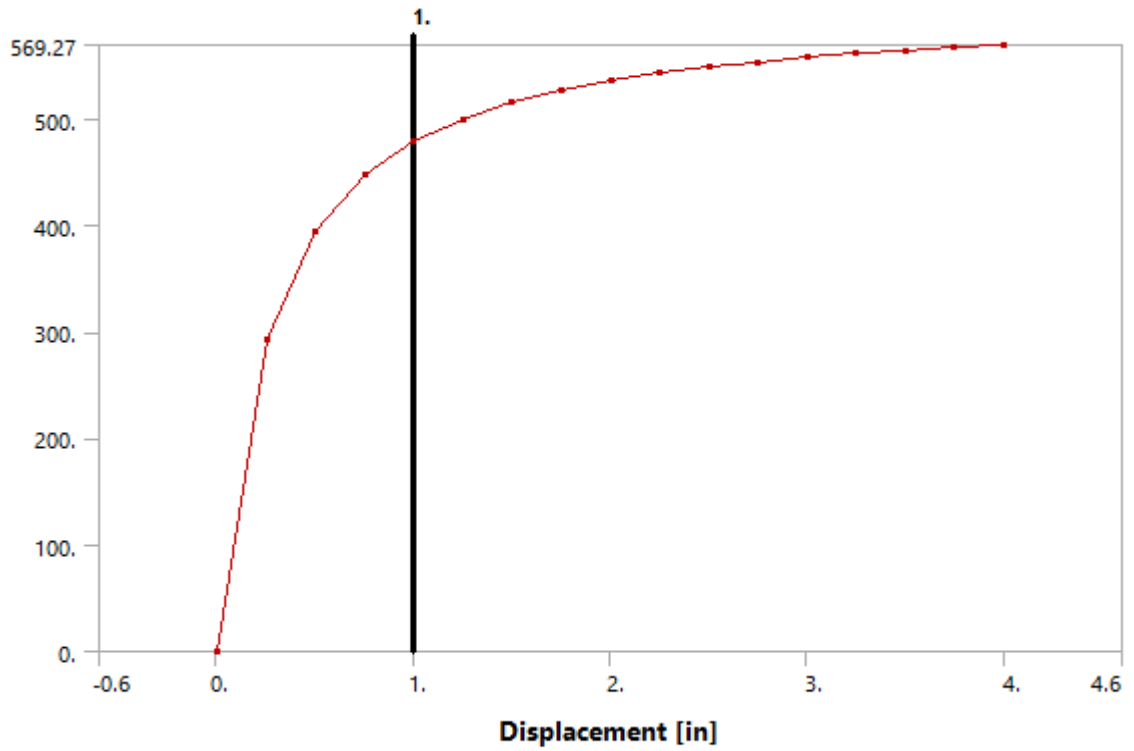| Displacement [in]	Force [lbf]
0.	0.
0.25	292.82
0.5	395.17
0.75	447.28
1.	478.85
1.25	500.03
1.5	515.22
1.75	526.65
2.	535.56
2.25	542.7
2.5	548.55
2.75	553.43
3.	557.57
3.25	561.12
3.5	564.19
3.75	566.89
4.	569.27

268

Figure 146 - Model (A4, B4, C4) > Connections > Longitudinal - Ground To Surface Body 22

Table 61 - Model (A4, B4, C4) > Connections > Longitudinal - Ground To Surface Body 22

Displacement [in]	Force [lbf]
0.	0.
0.25	292.82
0.5	395.17
0.75	447.28
1.	478.85
1.25	500.03
1.5	515.22
1.75	526.65
2.	535.56
2.25	542.7
2.5	548.55
2.75	553.43
3.	557.57
3.25	561.12
3.5	564.19
3.75	566.89
4.	569.27

Table 62 - Model (A4, B4, C4) > Connections > Springs

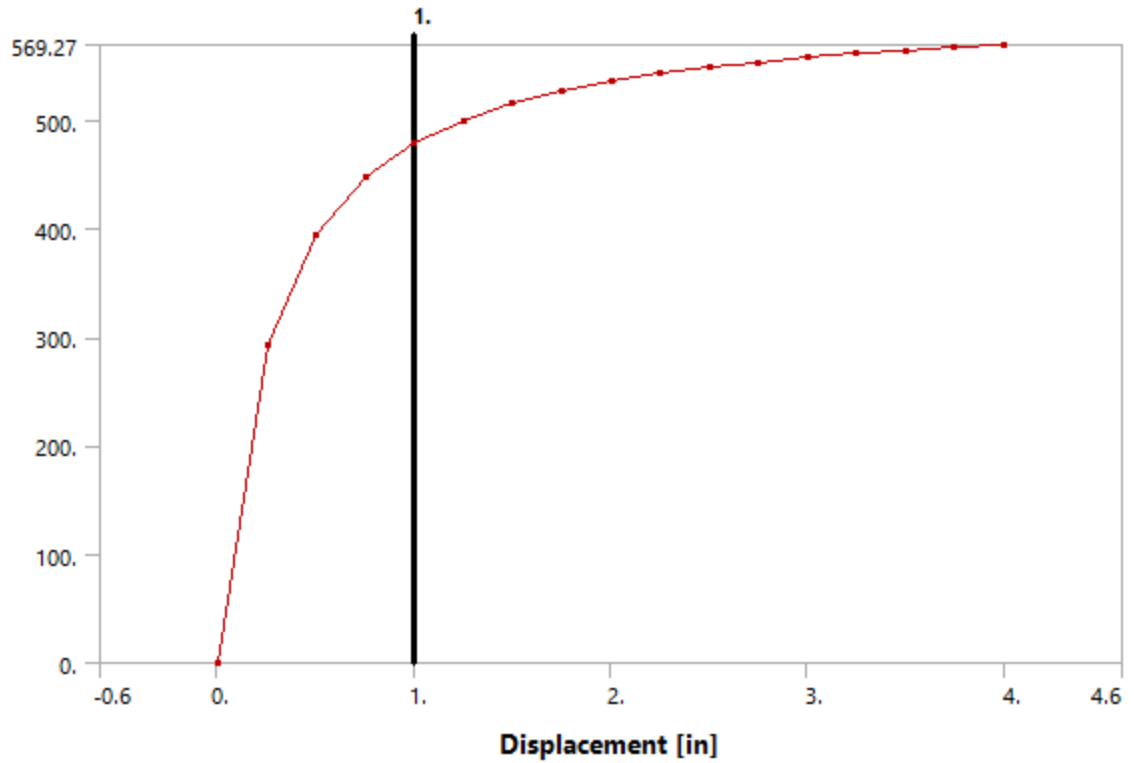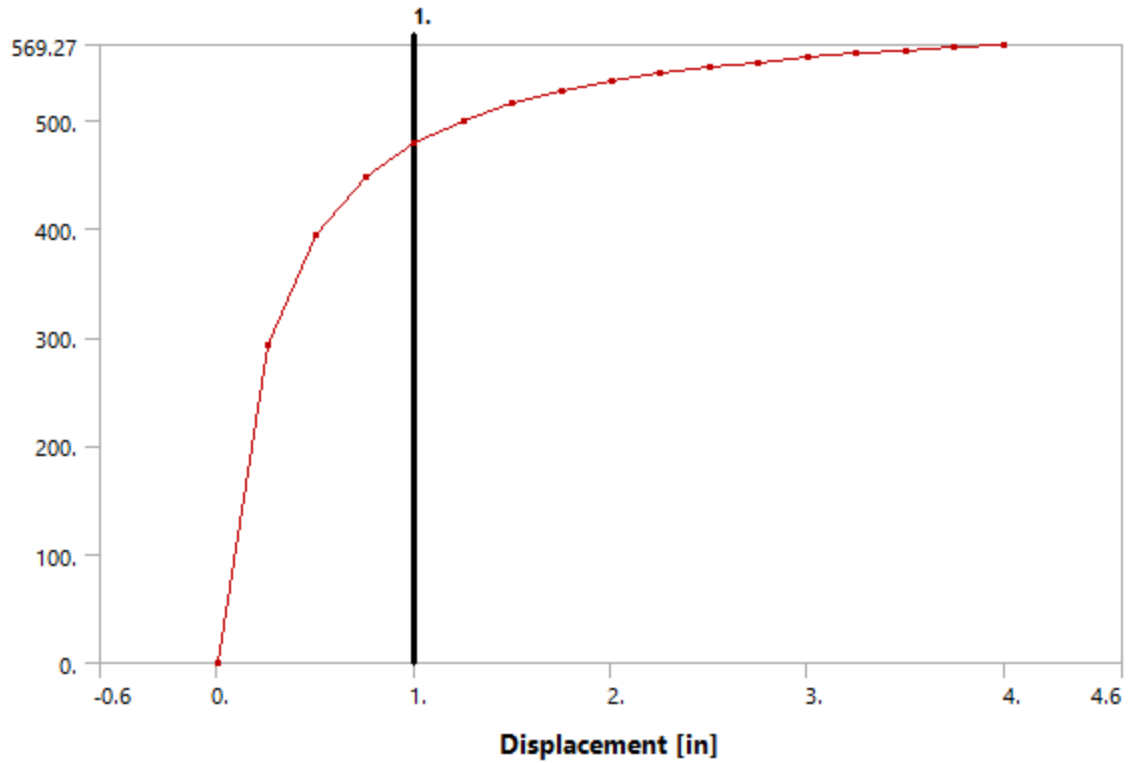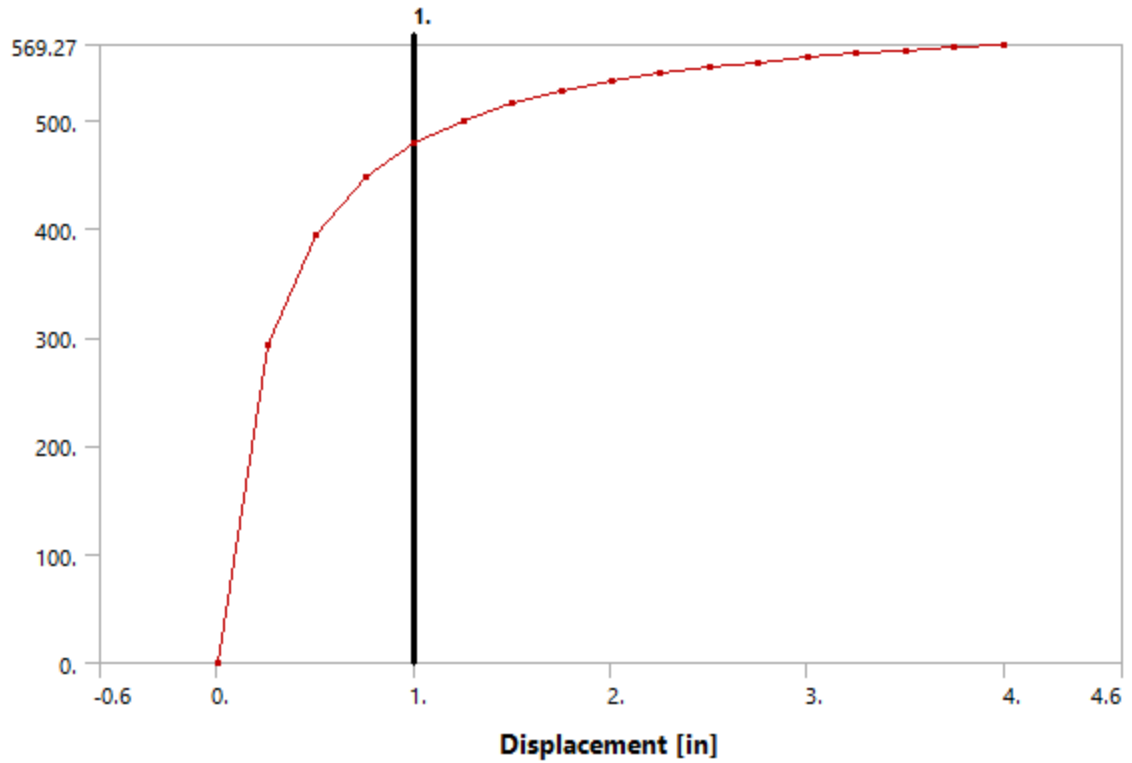| Object Name	Longitudinal - Ground To Surface Body 23	Longitudinal - Ground To Surface Body 24	Longitudinal - Ground To Surface Body 25	Longitudinal - Ground To Surface Body 26	Longitudinal - Ground To Surface Body 27	Longitudinal - Ground To Surface Body 28	Longitudinal - Ground To Surface Body 29	Longitudinal - Ground To Surface Body 30	Longitudinal - Ground To Surface Body 31	Longitudinal - Ground To Surface Body 32	Longitudinal - Ground To Surface Body 33
State	Fully Defined										
Graphics Properties											
Visible	Yes										
Definition											
Type	Longitudinal										
Spring Behavior	Both										
Longitudinal Stiffness	Tabular Data										
Longitudinal Damping	0. lbf·s/in										
Preload	None										
Suppressed	No										
Spring Length	12. in									9. in	
Scope											
Scope	Body-Ground										
Reference											
Coordinate System	Global Coordinate System										
Reference X Coordinate	0. in									-6. in	
Reference Y Coordinate	216. in	192. in	168. in	144. in	120. in	96. in	72. in	48. in	24. in	249. in	237. in
Reference Z Coordinate	24. in									0. in	
Reference Location	Defined										
Mobile											
Scoping Method	Geometry Selection										
Applied By	Remote Attachment										
Scope	1 Face										
Body	Surface Body										
Coordinate System	Global Coordinate System										
Mobile X Coordinate	0. in									-6. in	
Mobile Y Coordinate	216. in	192. in	168. in	144. in	120. in	96. in	72. in	48. in	24. in	240. in	228. in
Mobile Z Coordinate	12. in									0. in	
Mobile Location	Defined										
Behavior	Deformable										
Pinball Region	5. in										

Figure 147 - Model (A4, B4, C4) > Connections > Longitudinal - Ground To Surface Body 23

Table 63 - Model (A4, B4, C4) > Connections > Longitudinal - Ground To Surface Body 23

Displacement [in]	Force [lbf]
0.	0.
0.25	292.82
0.5	395.17
0.75	447.28
1.	478.85
1.25	500.03
1.5	515.22
1.75	526.65
2.	535.56
2.25	542.7
2.5	548.55
2.75	553.43
3.	557.57
3.25	561.12
3.5	564.19
3.75	566.89
4.	569.27

Figure 148 - Model (A4, B4, C4) > Connections > Longitudinal - Ground To Surface Body 24

Table 64 - Model (A4, B4, C4) > Connections > Longitudinal - Ground To Surface Body 24

Displacement [in]	Force [lbf]
0.	0.
0.25	292.82
0.5	395.17
0.75	447.28
1.	478.85
1.25	500.03
1.5	515.22
1.75	526.65
2.	535.56
2.25	542.7
2.5	548.55
2.75	553.43
3.	557.57
3.25	561.12
3.5	564.19
3.75	566.89
4.	569.27

Figure 149 - Model (A4, B4, C4) > Connections > Longitudinal - Ground To Surface Body 25

Table 65 - Model (A4, B4, C4) > Connections > Longitudinal - Ground To Surface Body 25

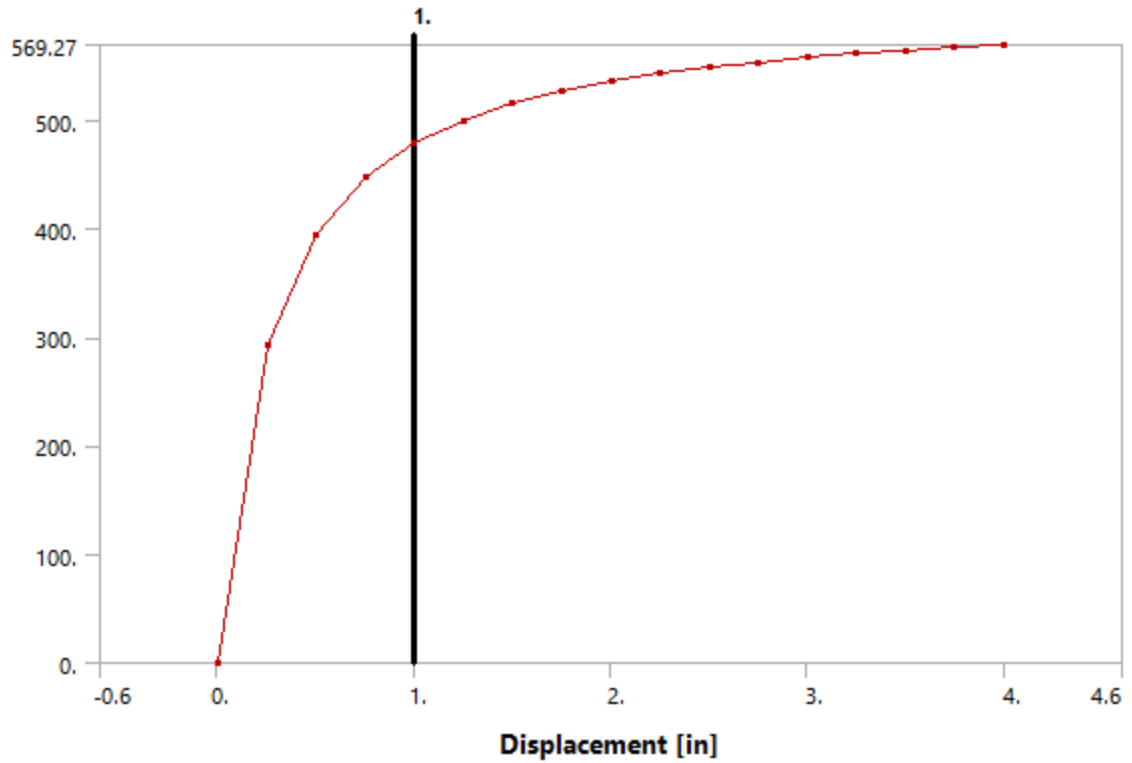| Displacement [in]	Force [lbf]
0.	0.
0.25	292.82
0.5	395.17
0.75	447.28
1.	478.85
1.25	500.03
1.5	515.22
1.75	526.65
2.	535.56
2.25	542.7
2.5	548.55
2.75	553.43
3.	557.57
3.25	561.12
3.5	564.19
3.75	566.89
4.	569.27

273

Figure 150 - Model (A4, B4, C4) > Connections > Longitudinal - Ground To Surface Body 26

Table 66 - Model (A4, B4, C4) > Connections > Longitudinal - Ground To Surface Body 26

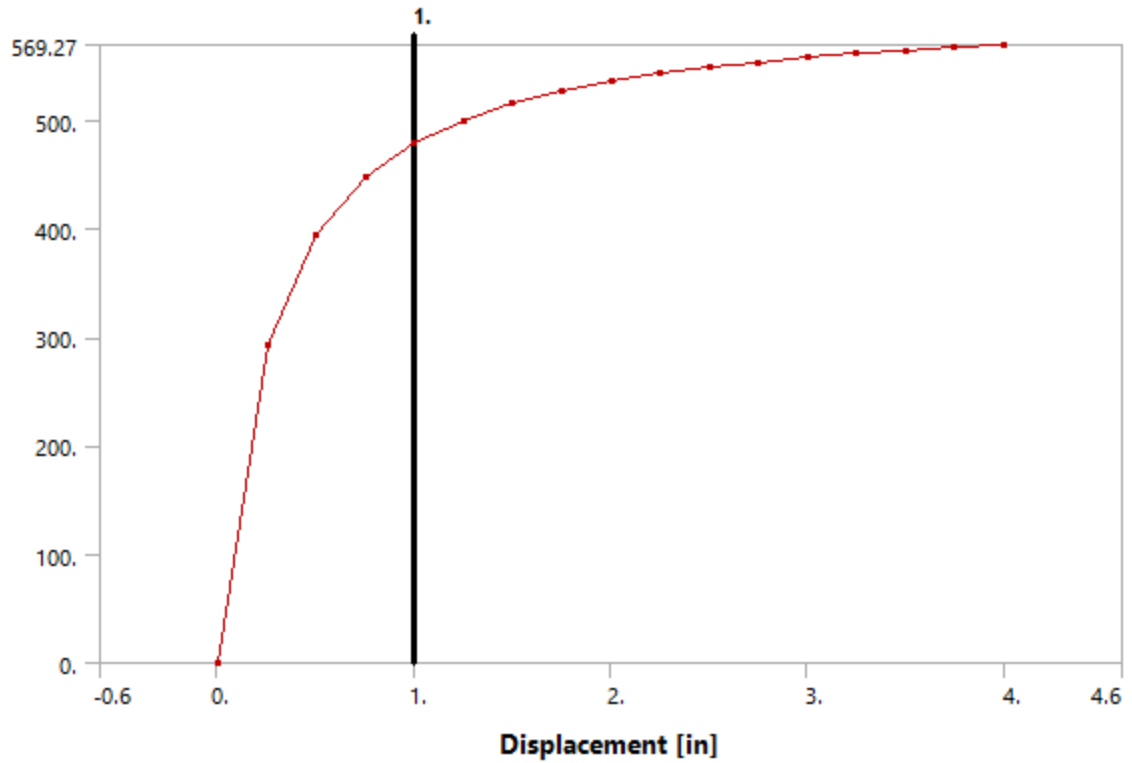| Displacement [in]	Force [lbf]
0.	0.
0.25	292.82
0.5	395.17
0.75	447.28
1.	478.85
1.25	500.03
1.5	515.22
1.75	526.65
2.	535.56
2.25	542.7
2.5	548.55
2.75	553.43
3.	557.57
3.25	561.12
3.5	564.19
3.75	566.89
4.	569.27

Figure 151 - Model (A4, B4, C4) > Connections > Longitudinal - Ground To Surface Body 27

Table 67 - Model (A4, B4, C4) > Connections > Longitudinal - Ground To Surface Body 27

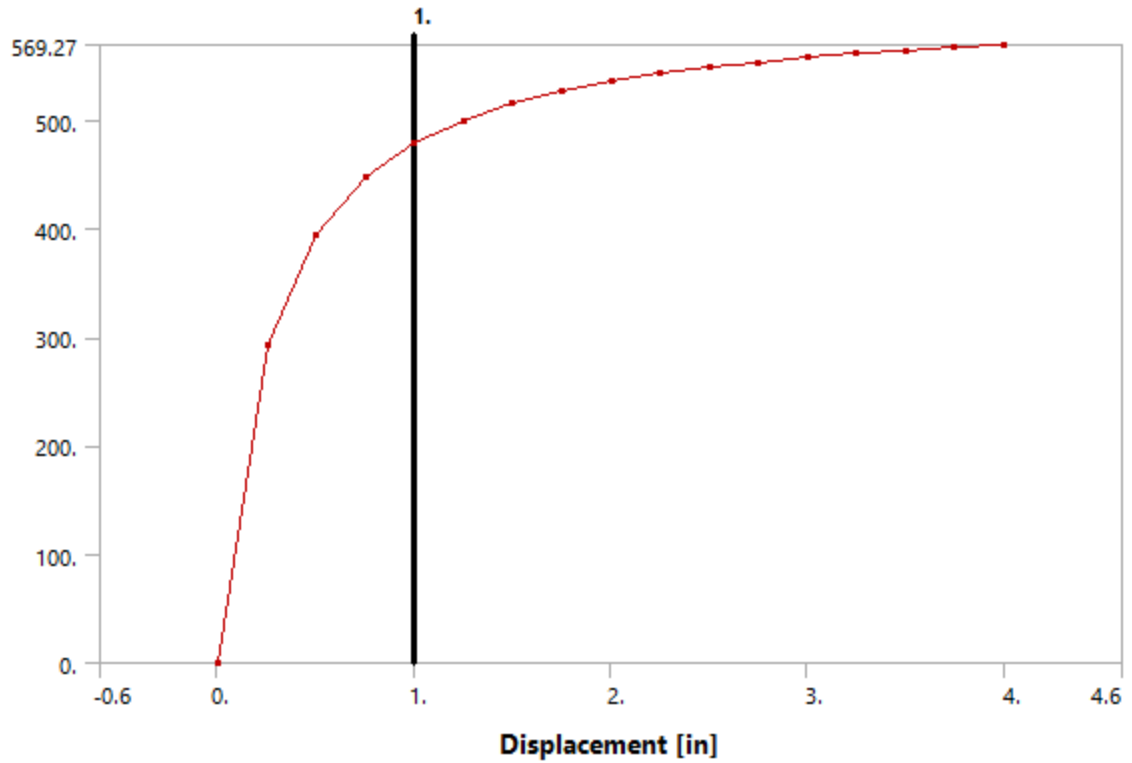| Displacement [in]	Force [lbf]
0.	0.
0.25	292.82
0.5	395.17
0.75	447.28
1.	478.85
1.25	500.03
1.5	515.22
1.75	526.65
2.	535.56
2.25	542.7
2.5	548.55
2.75	553.43
3.	557.57
3.25	561.12
3.5	564.19
3.75	566.89
4.	569.27

Figure 152 - Model (A4, B4, C4) > Connections > Longitudinal - Ground To Surface Body 28

Table 68 - Model (A4, B4, C4) > Connections > Longitudinal - Ground To Surface Body 28

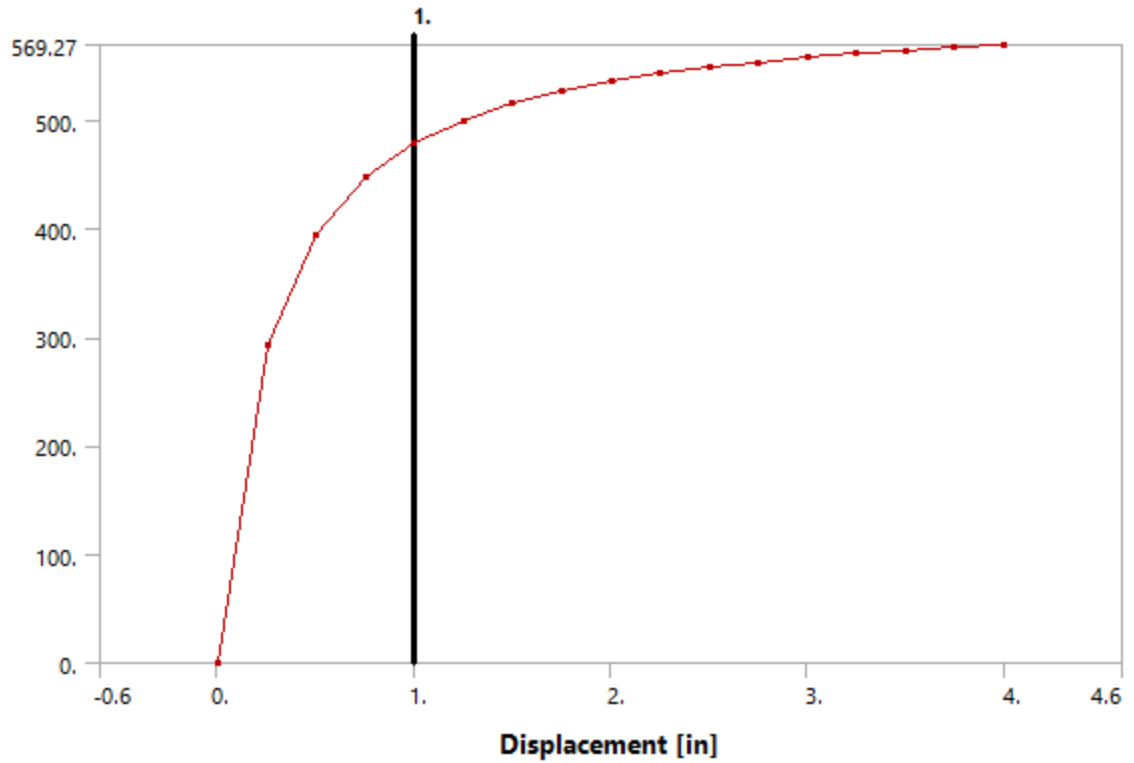| Displacement [in]	Force [lbf]
0.	0.
0.25	292.82
0.5	395.17
0.75	447.28
1.	478.85
1.25	500.03
1.5	515.22
1.75	526.65
2.	535.56
2.25	542.7
2.5	548.55
2.75	553.43
3.	557.57
3.25	561.12
3.5	564.19
3.75	566.89
4.	569.27

Figure 153 - Model (A4, B4, C4) > Connections > Longitudinal - Ground To Surface Body 29

Table 69 - Model (A4, B4, C4) > Connections > Longitudinal - Ground To Surface Body 29

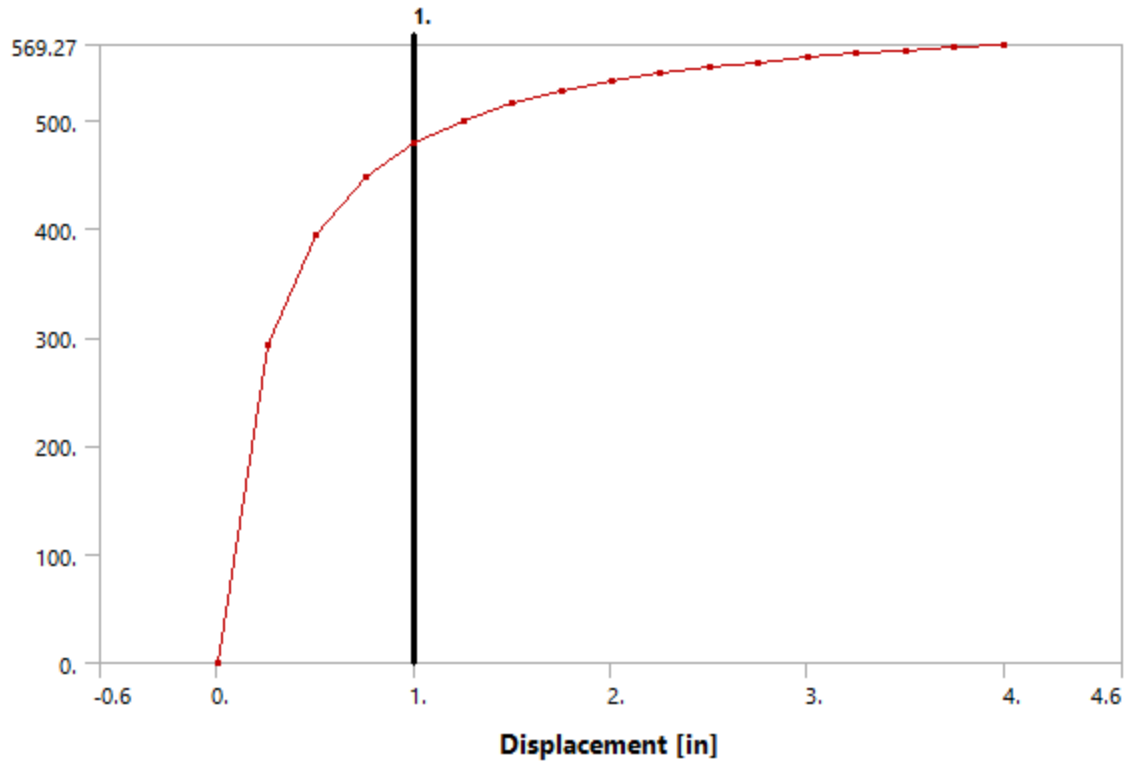| Displacement [in]	Force [lbf]
0.	0.
0.25	292.82
0.5	395.17
0.75	447.28
1.	478.85
1.25	500.03
1.5	515.22
1.75	526.65
2.	535.56
2.25	542.7
2.5	548.55
2.75	553.43
3.	557.57
3.25	561.12
3.5	564.19
3.75	566.89
4.	569.27

Figure 154 - Model (A4, B4, C4) > Connections > Longitudinal - Ground To Surface Body 30

Table 70 - Model (A4, B4, C4) > Connections > Longitudinal - Ground To Surface Body 30

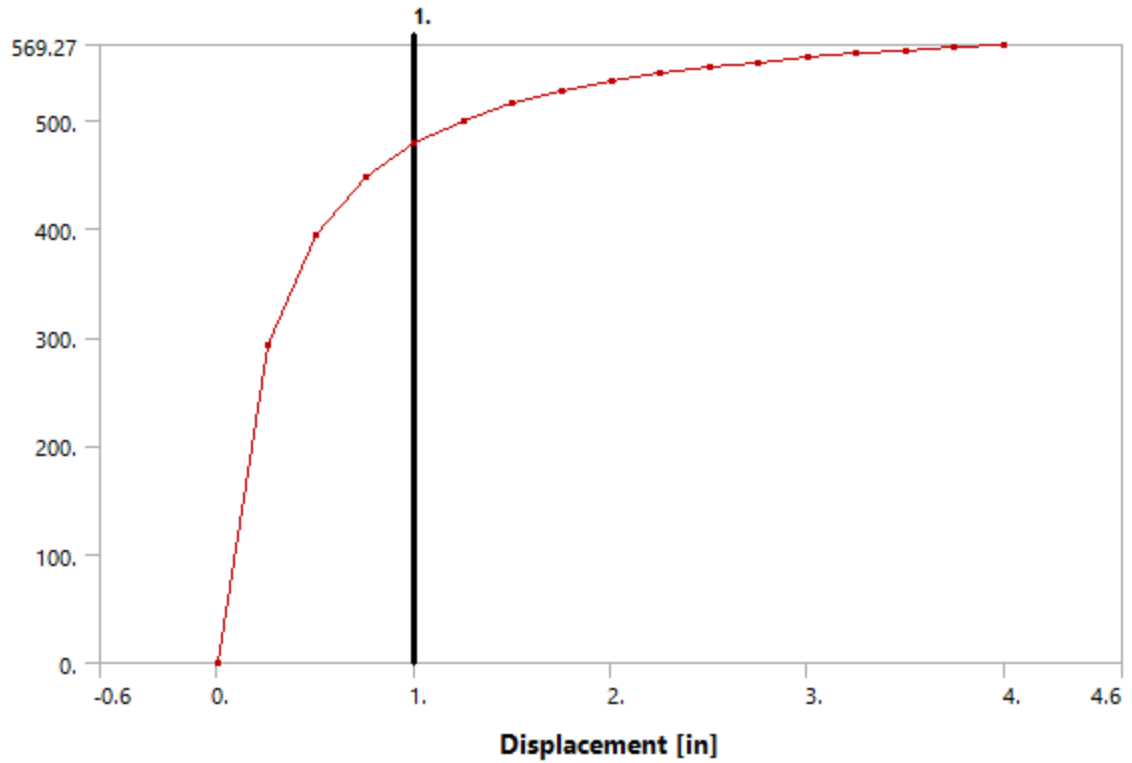| Displacement [in]	Force [lbf]
0.	0.
0.25	292.82
0.5	395.17
0.75	447.28
1.	478.85
1.25	500.03
1.5	515.22
1.75	526.65
2.	535.56
2.25	542.7
2.5	548.55
2.75	553.43
3.	557.57
3.25	561.12
3.5	564.19
3.75	566.89
4.	569.27

Figure 155 - Model (A4, B4, C4) > Connections > Longitudinal - Ground To Surface Body 31

Table 71 - Model (A4, B4, C4) > Connections > Longitudinal - Ground To Surface Body 31

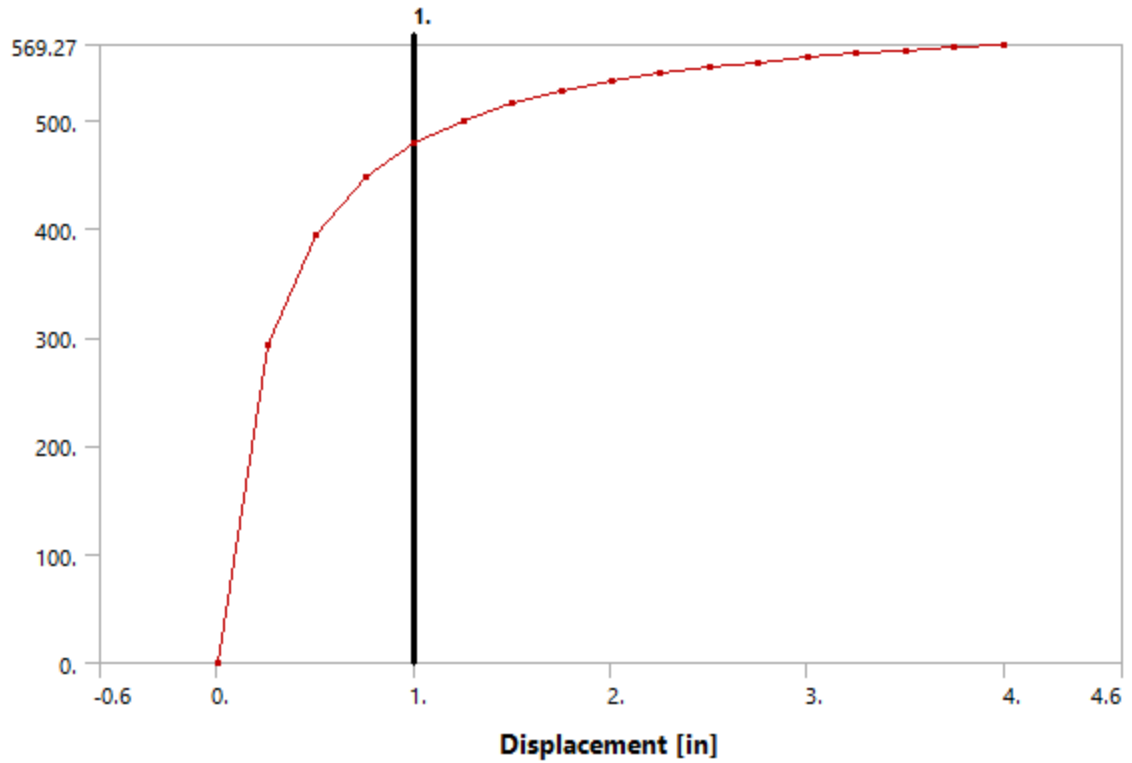| Displacement [in]	Force [lbf]
0.	0.
0.25	292.82
0.5	395.17
0.75	447.28
1.	478.85
1.25	500.03
1.5	515.22
1.75	526.65
2.	535.56
2.25	542.7
2.5	548.55
2.75	553.43
3.	557.57
3.25	561.12
3.5	564.19
3.75	566.89
4.	569.27

Figure 156 - Model (A4, B4, C4) > Connections > Longitudinal - Ground To Surface Body 32

Table 72 - Model (A4, B4, C4) > Connections > Longitudinal - Ground To Surface Body 32

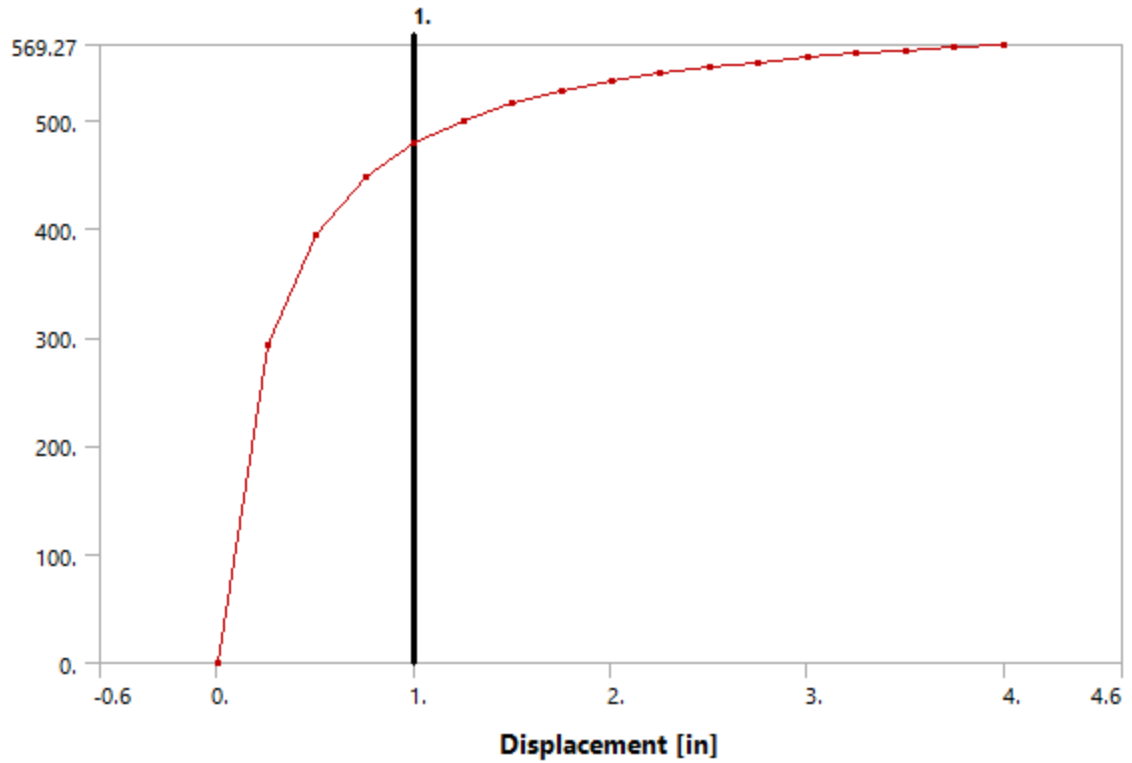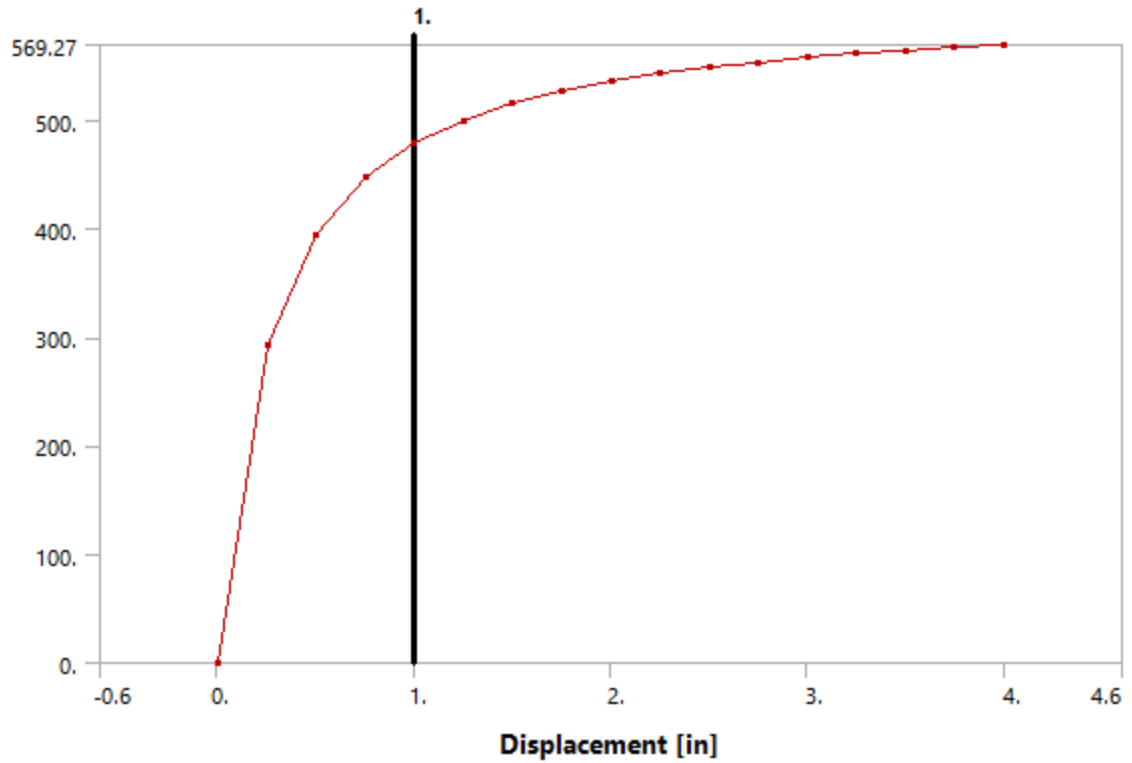| Displacement [in]	Force [lbf]
0.	0.
0.25	1217.6
0.5	1275.9
0.75	1296.6
1.	1307.2
1.25	1313.6
1.5	1317.9
1.75	1321.
2.	1323.4
2.25	1325.2
2.5	1326.7
2.75	1327.9
3.	1328.9
3.25	1329.7
3.5	1330.5
3.75	1331.1
4.	1331.6

280

Figure 157 - Model (A4, B4, C4) > Connections > Longitudinal - Ground To Surface Body 33

Table 73 - Model (A4, B4, C4) > Connections > Longitudinal - Ground To Surface Body 33

Displacement [in]	Force [lbf]
0.	0.
0.25	1217.6
0.5	1275.9
0.75	1296.6
1.	1307.2
1.25	1313.6
1.5	1317.9
1.75	1321.
2.	1323.4
2.25	1325.2
2.5	1326.7
2.75	1327.9
3.	1328.9
3.25	1329.7
3.5	1330.5
3.75	1331.1
4.	1331.6

Table 74 - Model (A4, B4, C4) > Connections > Springs

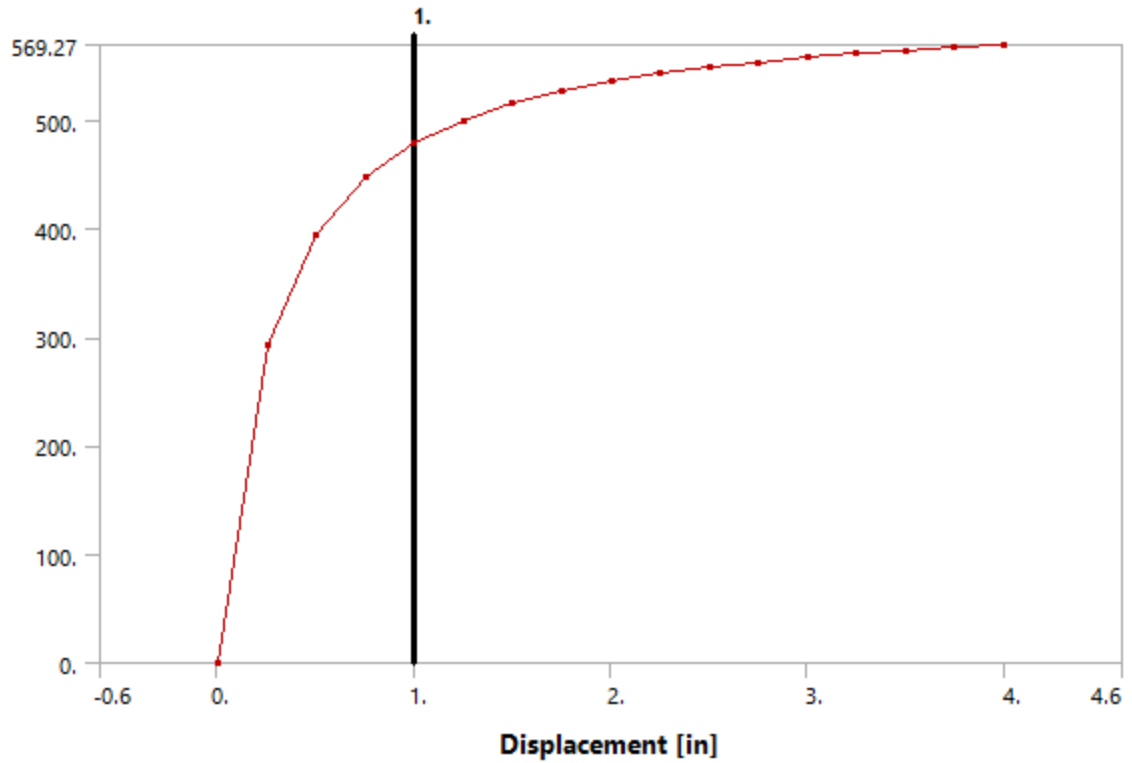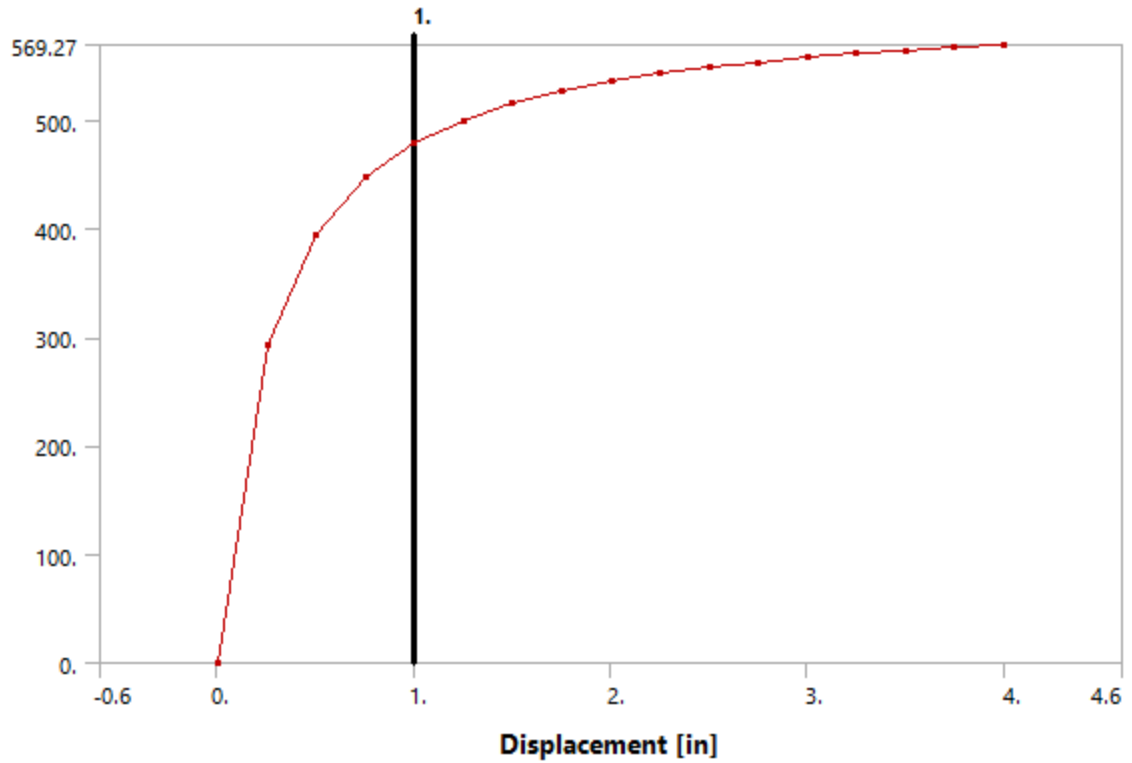| Object Name	Longitudinal - Ground To Surface Body 34	Longitudinal - Ground To Surface Body 35	Longitudinal - Ground To Surface Body 36	Longitudinal - Ground To Surface Body 37	Longitudinal - Ground To Surface Body 38	Longitudinal - Ground To Surface Body 39	Longitudinal - Ground To Surface Body 40	Longitudinal - Ground To Surface Body 41	Longitudinal - Ground To Surface Body 42	Longitudinal - Ground To Surface Body 43	Longitudinal - Ground To Surface Body 44
State	Fully Defined										
Graphics Properties											
Visible	Yes										
Definition											
Type	Longitudinal										
Spring Behavior	Both										
Longitudinal Stiffness	Tabular Data										
Longitudinal Damping	0. lbf·s/in										
Preload	None										
Suppressed	No										
Spring Length	9. in										
Scope											
Scope	Body-Ground										
Reference											
Coordinate System	Global Coordinate System										
Reference X Coordinate	-6. in										
Reference Y Coordinate	225. in	213. in	201. in	189. in	177. in	165. in	153. in	141. in	129. in	117. in	105. in
Reference Z Coordinate	0. in										
Reference Location	Defined										
Mobile											
Scoping Method	Geometry Selection										
Applied By	Remote Attachment										
Scope	1 Face										
Body	Surface Body										
Coordinate System	Global Coordinate System										
Mobile X Coordinate	-6. in										
Mobile Y Coordinate	216. in	204. in	192. in	180. in	168. in	156. in	144. in	132. in	120. in	108. in	96. in
Mobile Z Coordinate	0. in										
Mobile Location	Defined										
Behavior	Deformable										
Pinball Region	5. in										

Figure 158 - Model (A4, B4, C4) > Connections > Longitudinal - Ground To Surface Body 34

Table 75 – Model (A4, B4, C4) > Connections > Longitudinal - Ground To Surface Body 34

Displacement [in]	Force [lbf]
0.	0.
0.25	1217.6
0.5	1275.9
0.75	1296.6
1.	1307.2
1.25	1313.6
1.5	1317.9
1.75	1321.
2.	1323.4
2.25	1325.2
2.5	1326.7
2.75	1327.9
3.	1328.9
3.25	1329.7
3.5	1330.5
3.75	1331.1
4.	1331.6

283

Figure 159 - Model (A4, B4, C4) > Connections > Longitudinal - Ground To Surface Body 35

Table 76 - Model (A4, B4, C4) > Connections > Longitudinal - Ground To Surface Body 35

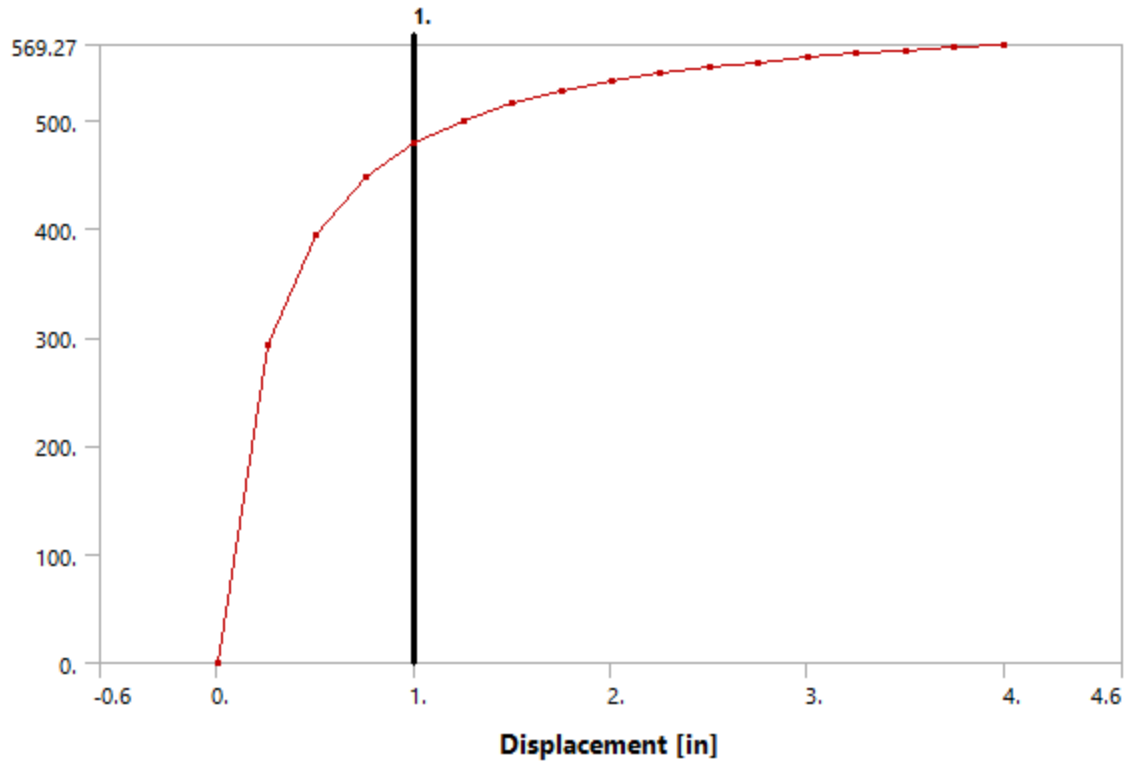| Displacement [in]	Force [lbf]
0.	0.
0.25	1217.6
0.5	1275.9
0.75	1296.6
1.	1307.2
1.25	1313.6
1.5	1317.9
1.75	1321.
2.	1323.4
2.25	1325.2
2.5	1326.7
2.75	1327.9
3.	1328.9
3.25	1329.7
3.5	1330.5
3.75	1331.1
4.	1331.6

Figure 160 - Model (A4, B4, C4) > Connections > Longitudinal - Ground To Surface Body 36

Table 77 - Model (A4, B4, C4) > Connections > Longitudinal - Ground To Surface Body 36

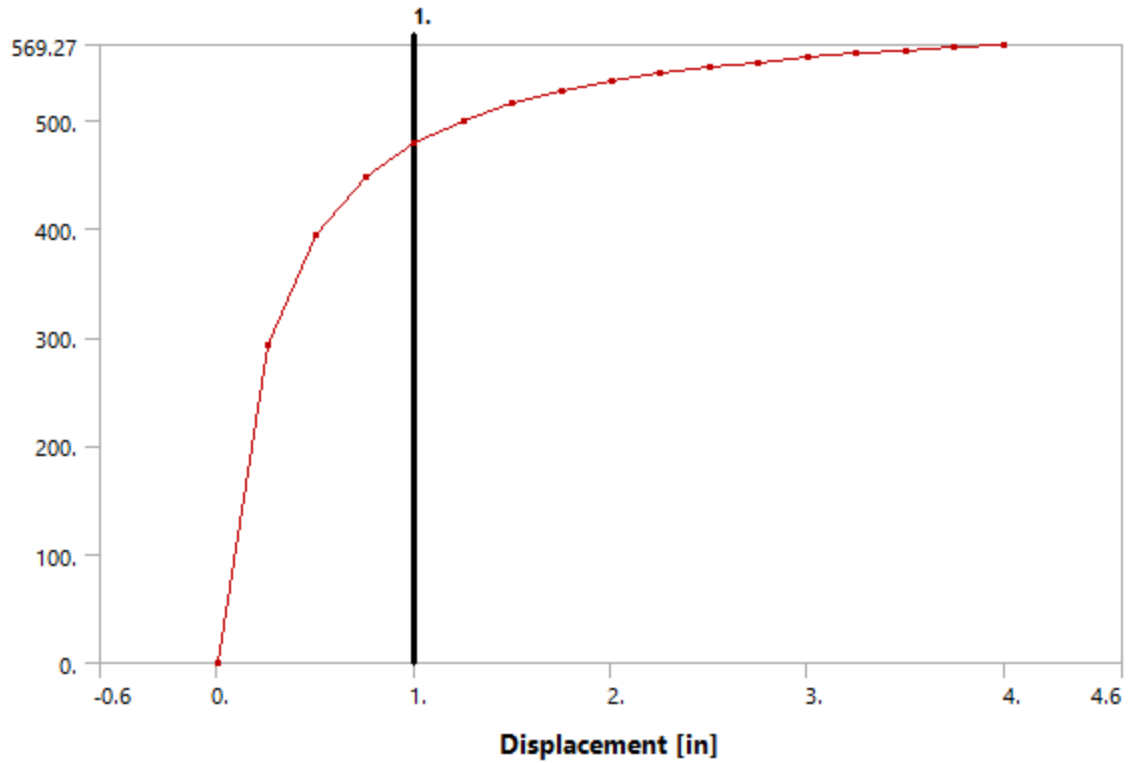| Displacement [in]	Force [lbf]
0.	0.
0.25	1217.6
0.5	1275.9
0.75	1296.6
1.	1307.2
1.25	1313.6
1.5	1317.9
1.75	1321.
2.	1323.4
2.25	1325.2
2.5	1326.7
2.75	1327.9
3.	1328.9
3.25	1329.7
3.5	1330.5
3.75	1331.1
4.	1331.6

Figure 161 - Model (A4, B4, C4) > Connections > Longitudinal - Ground To Surface Body 37

Table 78 - Model (A4, B4, C4) > Connections > Longitudinal - Ground To Surface Body 37

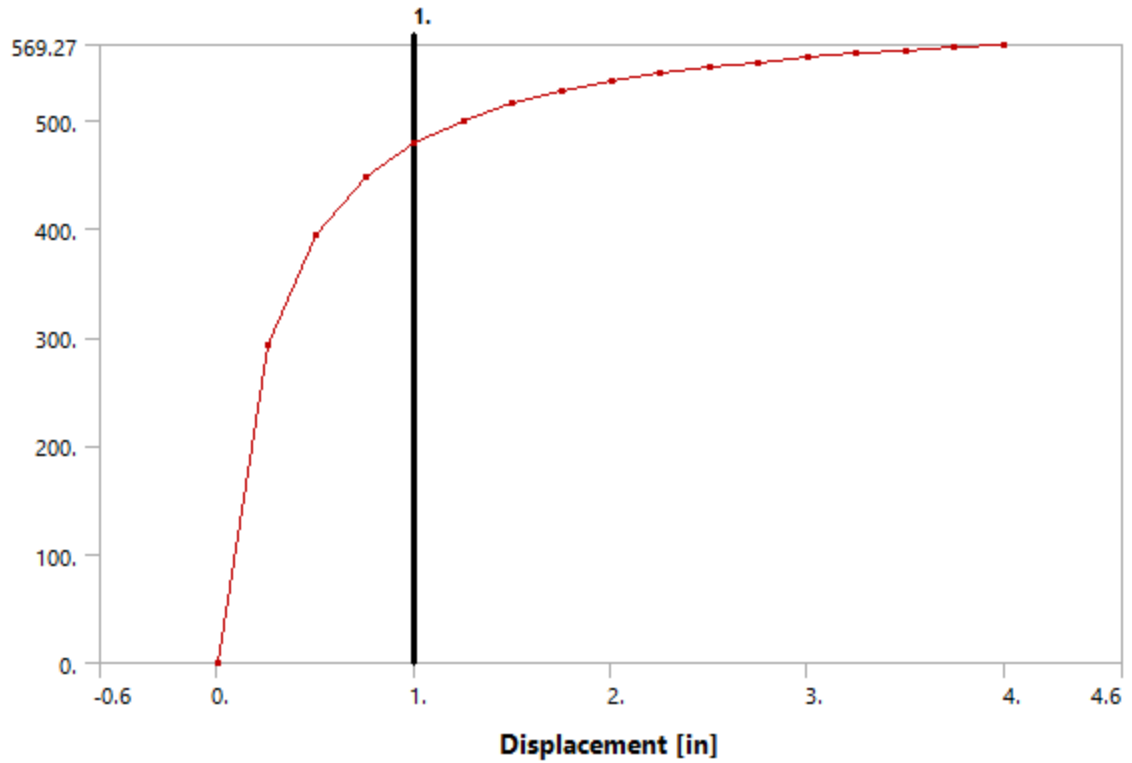| Displacement [in]	Force [lbf]
0.	0.
0.25	1217.6
0.5	1275.9
0.75	1296.6
1.	1307.2
1.25	1313.6
1.5	1317.9
1.75	1321.
2.	1323.4
2.25	1325.2
2.5	1326.7
2.75	1327.9
3.	1328.9
3.25	1329.7
3.5	1330.5
3.75	1331.1
4.	1331.6

Figure 162 - Model (A4, B4, C4) > Connections > Longitudinal - Ground To Surface Body 38

Table 79 - Model (A4, B4, C4) > Connections > Longitudinal - Ground To Surface Body 38

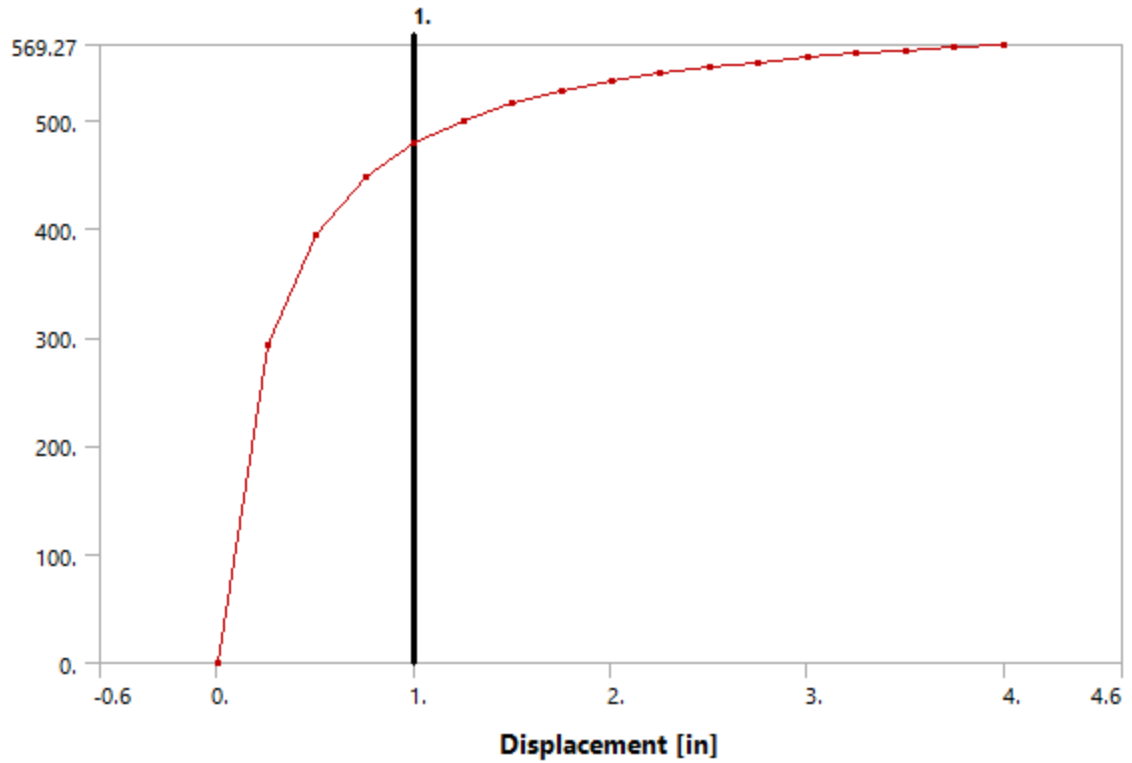| Displacement [in]	Force [lbf]
0.	0.
0.25	1217.6
0.5	1275.9
0.75	1296.6
1.	1307.2
1.25	1313.6
1.5	1317.9
1.75	1321.
2.	1323.4
2.25	1325.2
2.5	1326.7
2.75	1327.9
3.	1328.9
3.25	1329.7
3.5	1330.5
3.75	1331.1
4.	1331.6

Figure 163 - Model (A4, B4, C4) > Connections > Longitudinal - Ground To Surface Body 39

Table 80 - Model (A4, B4, C4) > Connections > Longitudinal - Ground To Surface Body 39

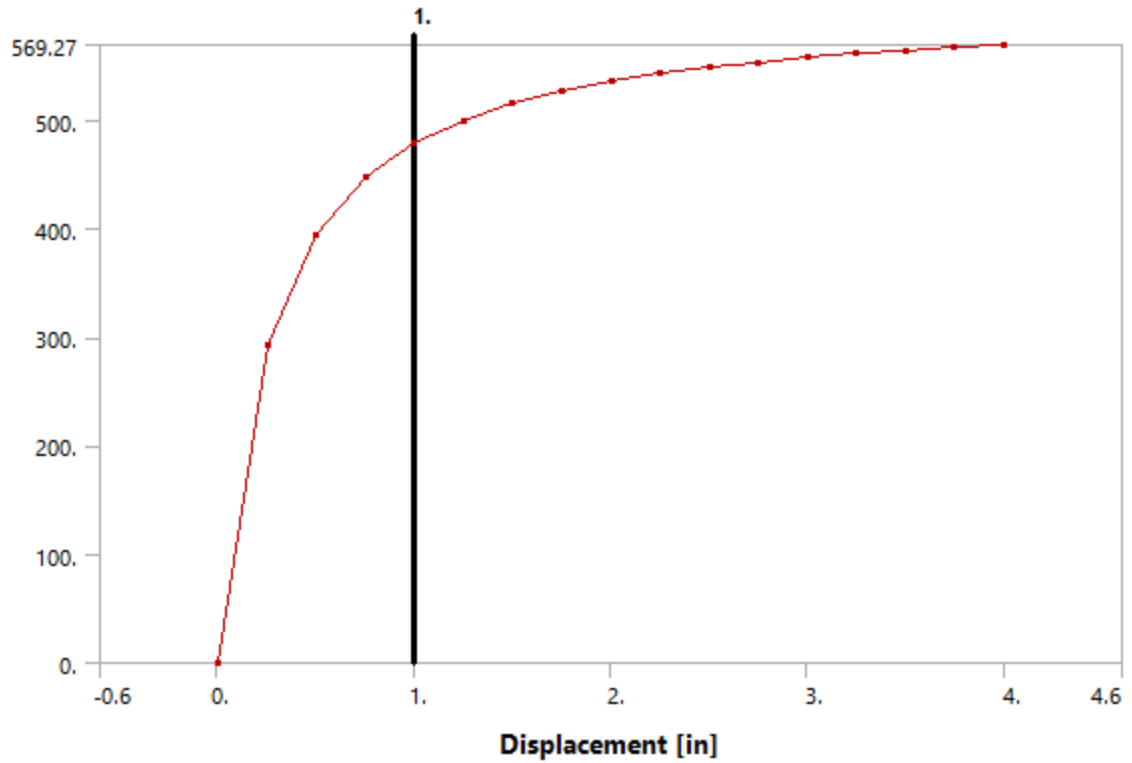| Displacement [in]	Force [lbf]
0.	0.
0.25	1217.6
0.5	1275.9
0.75	1296.6
1.	1307.2
1.25	1313.6
1.5	1317.9
1.75	1321.
2.	1323.4
2.25	1325.2
2.5	1326.7
2.75	1327.9
3.	1328.9
3.25	1329.7
3.5	1330.5
3.75	1331.1
4.	1331.6

288

Figure 164 - Model (A4, B4, C4) > Connections > Longitudinal - Ground To Surface Body 40

Table 81 - Model (A4, B4, C4) > Connections > Longitudinal - Ground To Surface Body 40

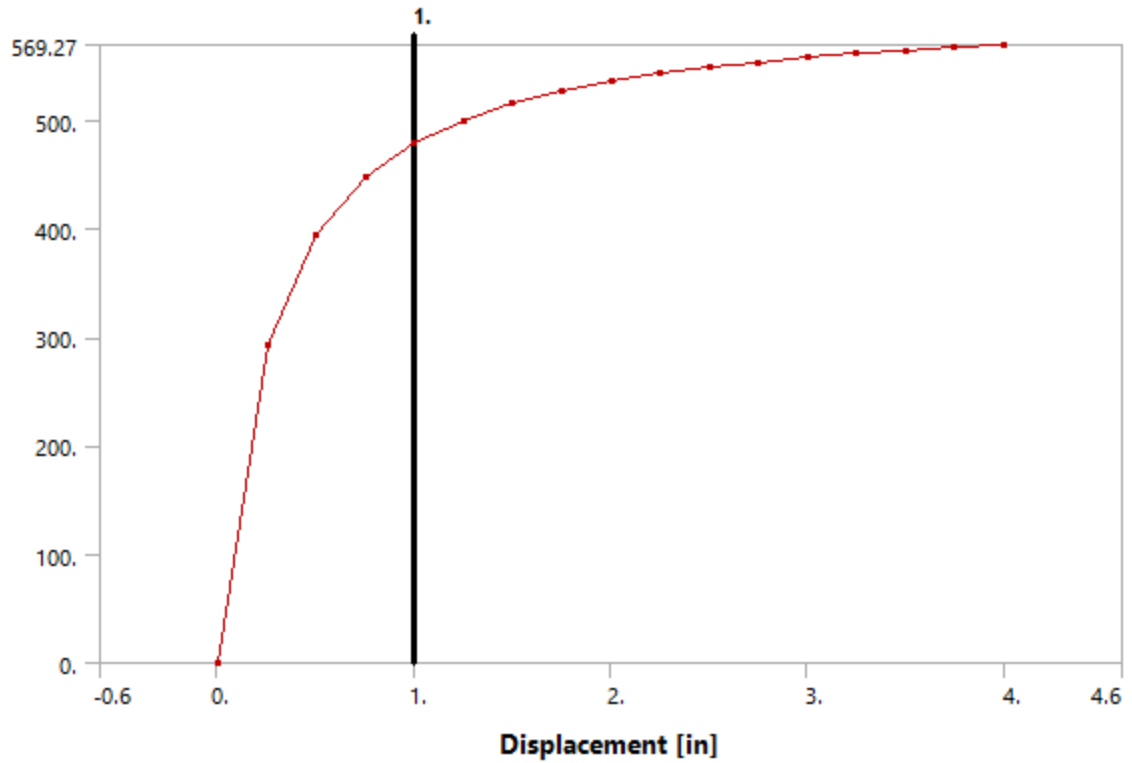| Displacement [in]	Force [lbf]
0.	0.
0.25	1217.6
0.5	1275.9
0.75	1296.6
1.	1307.2
1.25	1313.6
1.5	1317.9
1.75	1321.
2.	1323.4
2.25	1325.2
2.5	1326.7
2.75	1327.9
3.	1328.9
3.25	1329.7
3.5	1330.5
3.75	1331.1
4.	1331.6
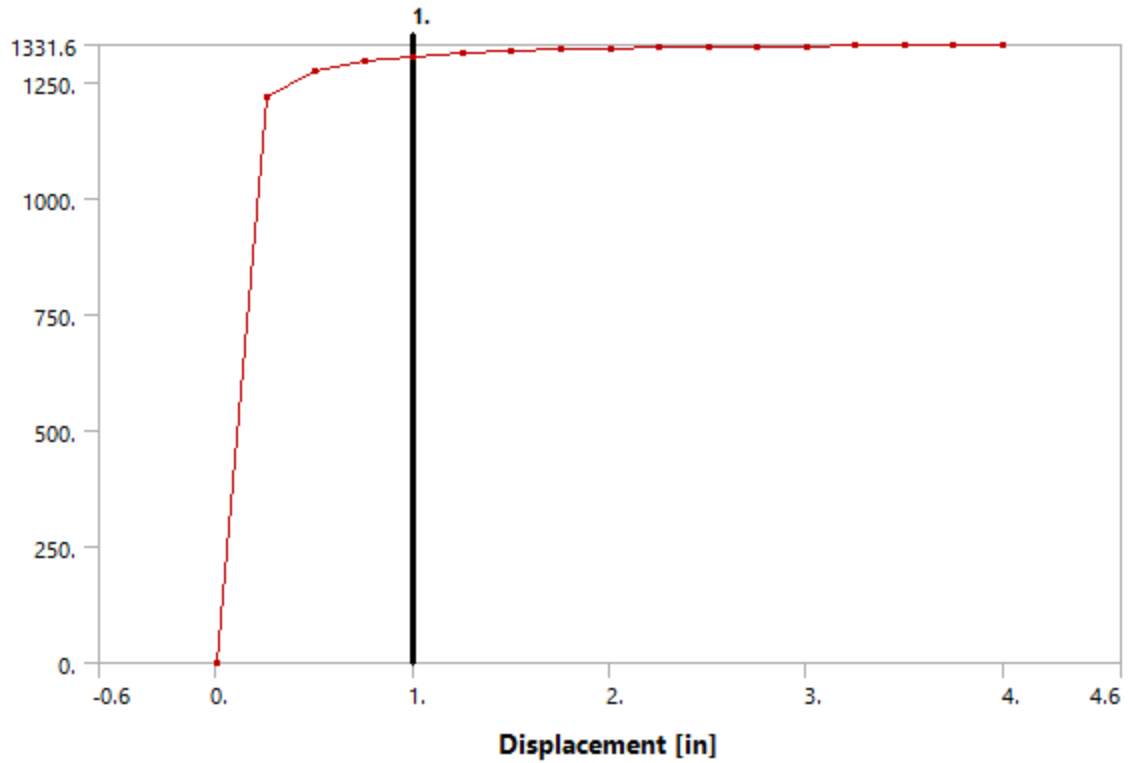
Figure 165 - Model (A4, B4, C4) > Connections > Longitudinal - Ground To Surface Body 41

Table 82 - Model (A4, B4, C4) > Connections > Longitudinal - Ground To Surface Body 41

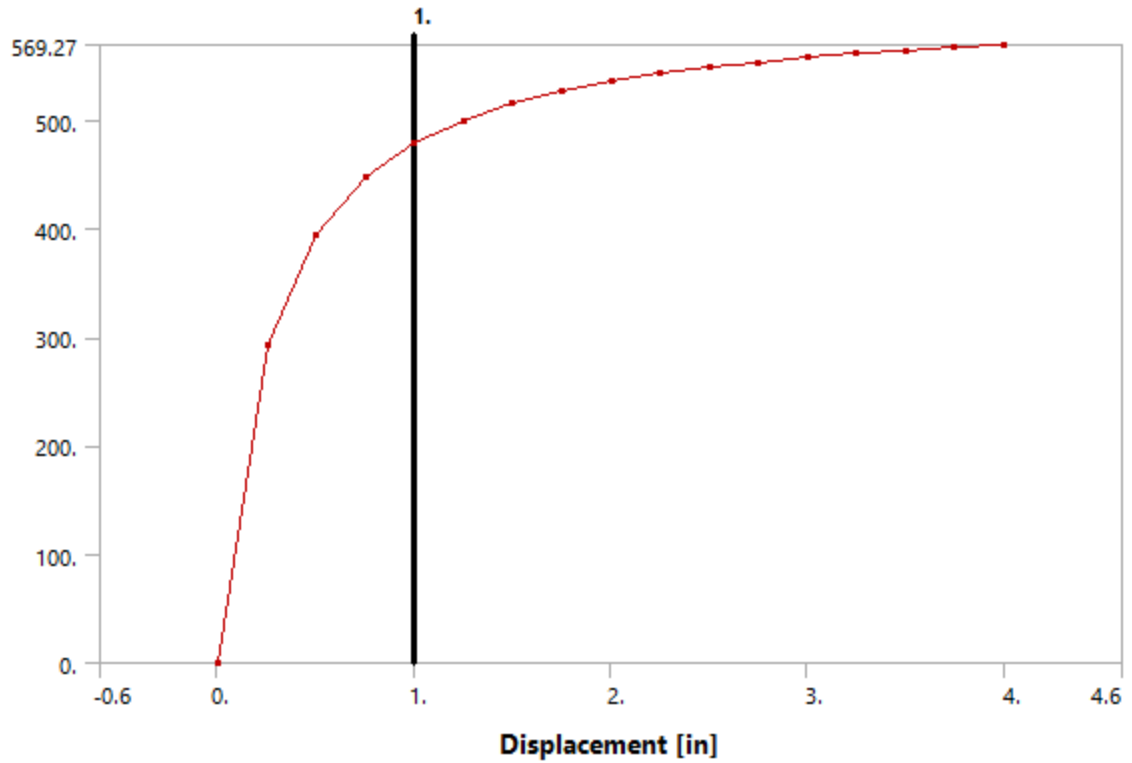| Displacement [in]	Force [lbf]
0.	0.
0.25	1217.6
0.5	1275.9
0.75	1296.6
1.	1307.2
1.25	1313.6
1.5	1317.9
1.75	1321.
2.	1323.4
2.25	1325.2
2.5	1326.7
2.75	1327.9
3.	1328.9
3.25	1329.7
3.5	1330.5
3.75	1331.1
4.	1331.6

Figure 166 - Model (A4, B4, C4) > Connections > Longitudinal - Ground To Surface Body 42

Table 83 - Model (A4, B4, C4) > Connections > Longitudinal - Ground To Surface Body 42

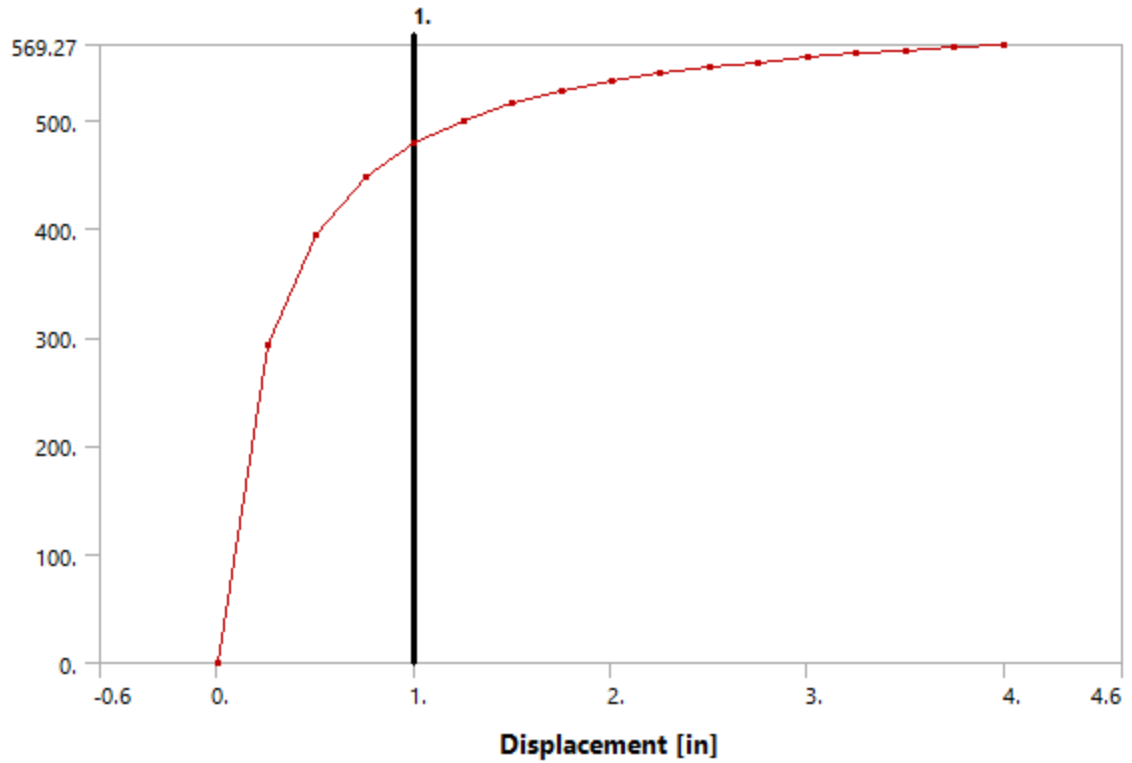| Displacement [in]	Force [lbf]
0.	0.
0.25	1217.6
0.5	1275.9
0.75	1296.6
1.	1307.2
1.25	1313.6
1.5	1317.9
1.75	1321.
2.	1323.4
2.25	1325.2
2.5	1326.7
2.75	1327.9
3.	1328.9
3.25	1329.7
3.5	1330.5
3.75	1331.1
4.	1331.6

Figure 167 - Model (A4, B4, C4) > Connections > Longitudinal - Ground To Surface Body 43

Table 84 - Model (A4, B4, C4) > Connections > Longitudinal - Ground To Surface Body 43

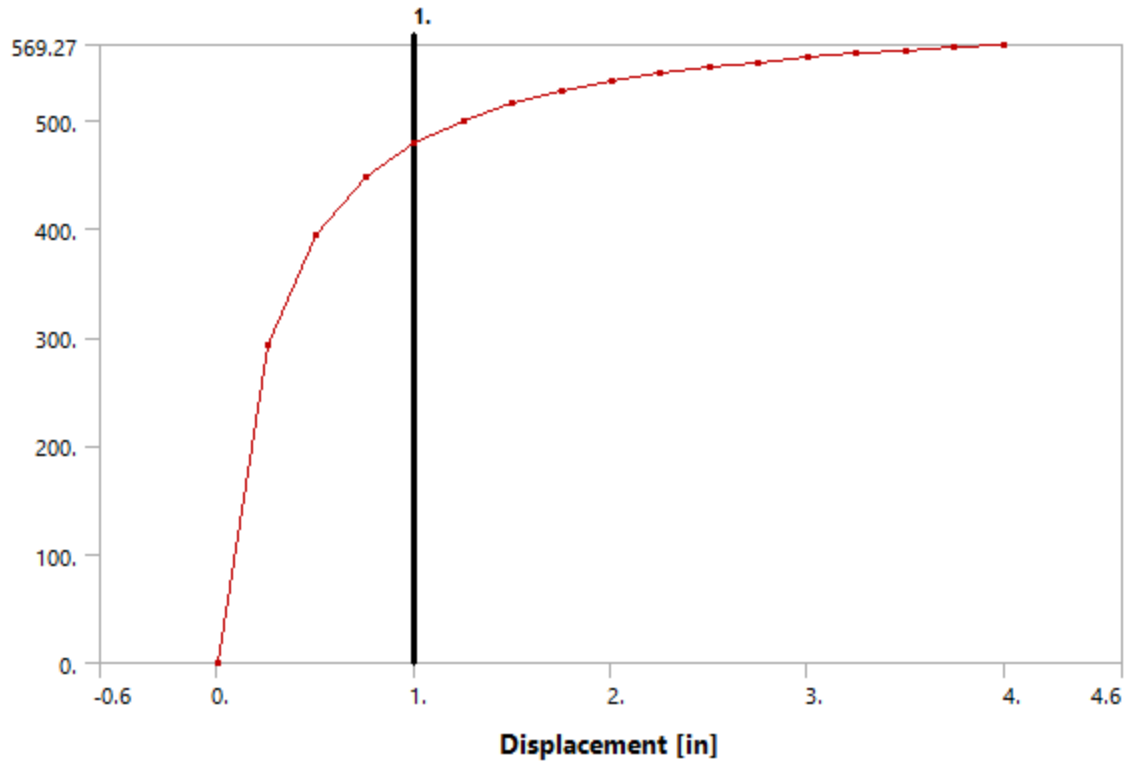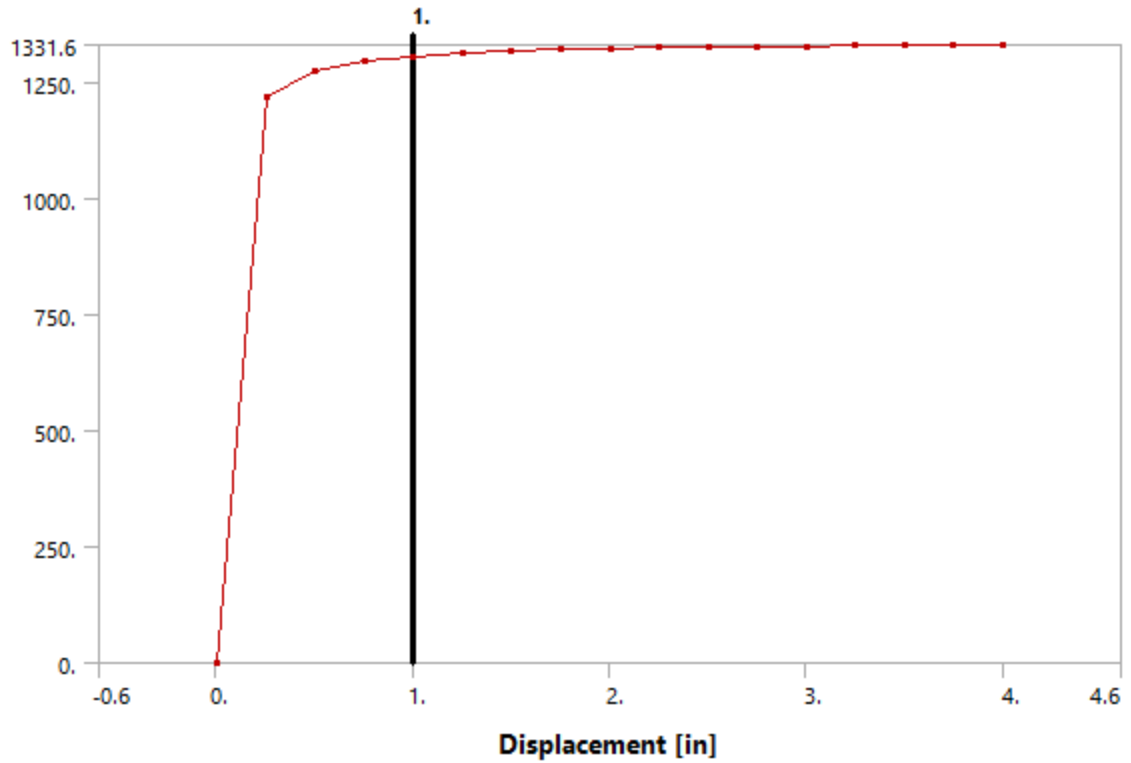| Displacement [in]	Force [lbf]
0.	0.
0.25	1217.6
0.5	1275.9
0.75	1296.6
1.	1307.2
1.25	1313.6
1.5	1317.9
1.75	1321.
2.	1323.4
2.25	1325.2
2.5	1326.7
2.75	1327.9
3.	1328.9
3.25	1329.7
3.5	1330.5
3.75	1331.1
4.	1331.6

Figure 168 - Model (A4, B4, C4) > Connections > Longitudinal - Ground To Surface Body 44

Table 85 - Model (A4, B4, C4) > Connections > Longitudinal - Ground To Surface Body 44

Displacement [in]	Force [lbf]
0.	0.
0.25	1217.6
0.5	1275.9
0.75	1296.6
1.	1307.2
1.25	1313.6
1.5	1317.9
1.75	1321.
2.	1323.4
2.25	1325.2
2.5	1326.7
2.75	1327.9
3.	1328.9
3.25	1329.7
3.5	1330.5
3.75	1331.1
4.	1331.6

Table 86 - Model (A4, B4, C4) > Connections > Springs

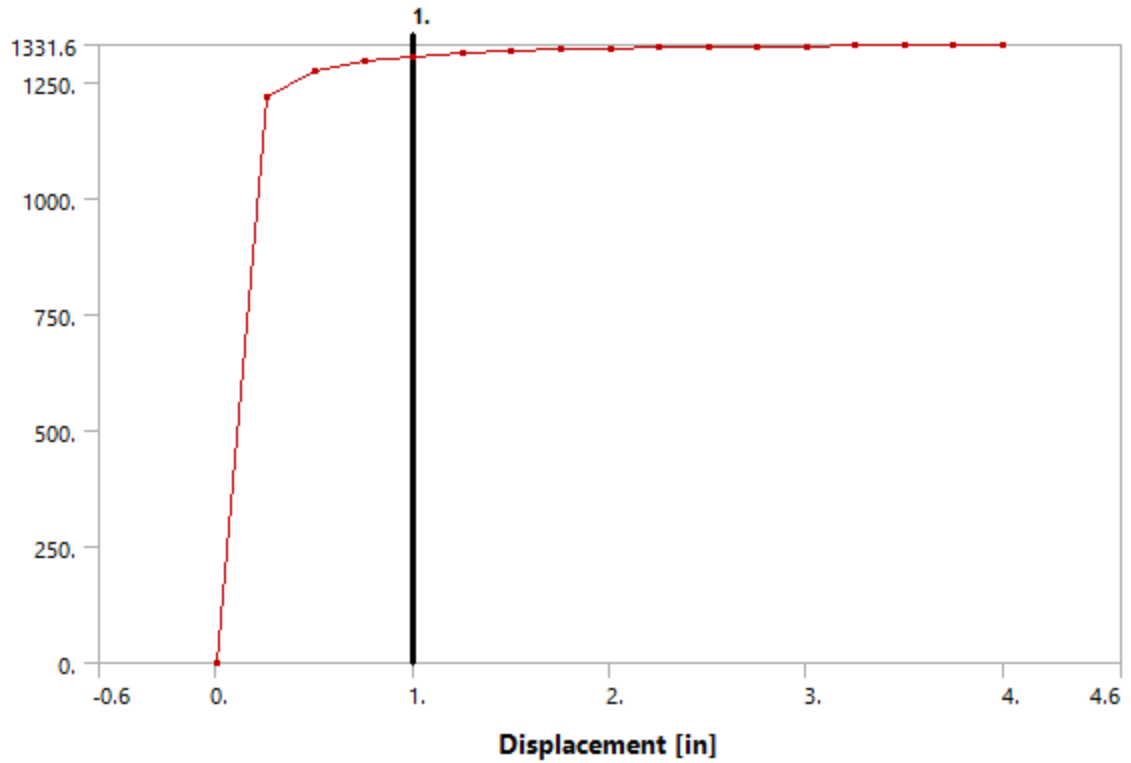| Object Name	Longitudinal - Ground To Surface Body 45	Longitudinal - Ground To Surface Body 46	Longitudinal - Ground To Surface Body 47	Longitudinal - Ground To Surface Body 48	Longitudinal - Ground To Surface Body 49	Longitudinal - Ground To Surface Body 50	Longitudinal - Ground To Surface Body 51	Longitudinal - Ground To Surface Body 52
State	Fully Defined							
Graphics Properties								
Visible	Yes							
Definition								
Type	Longitudinal							
Spring Behavior	Both							
Longitudinal Stiffness	Tabular Data							
Longitudinal Damping	0. lbf·s/in							
Preload	None							
Suppressed	No							
Spring Length	9. in							
Scope								
Scope	Body-Ground							
Reference								
Coordinate System	Global Coordinate System							
Reference X Coordinate	-6. in							
Reference Y Coordinate	93. in	81. in	69. in	57. in	45. in	33. in	21. in	9. in
Reference Z Coordinate	0. in							
Reference Location	Defined							
Mobile								
Scoping Method	Geometry Selection							
Applied By	Remote Attachment							
Scope	1 Face							
Body	Surface Body							
Coordinate System	Global Coordinate System							
Mobile X Coordinate	-6. in							
Mobile Y Coordinate	84. in	72. in	60. in	48. in	36. in	24. in	12. in	0. in
Mobile Z Coordinate	0. in							
Mobile Location	Defined							
Behavior	Deformable							
Pinball Region	5. in							

294

Figure 169 - Model (A4, B4, C4) > Connections > Longitudinal - Ground To Surface Body 45

Table 87 - Model (A4, B4, C4) > Connections > Longitudinal - Ground To Surface Body 45

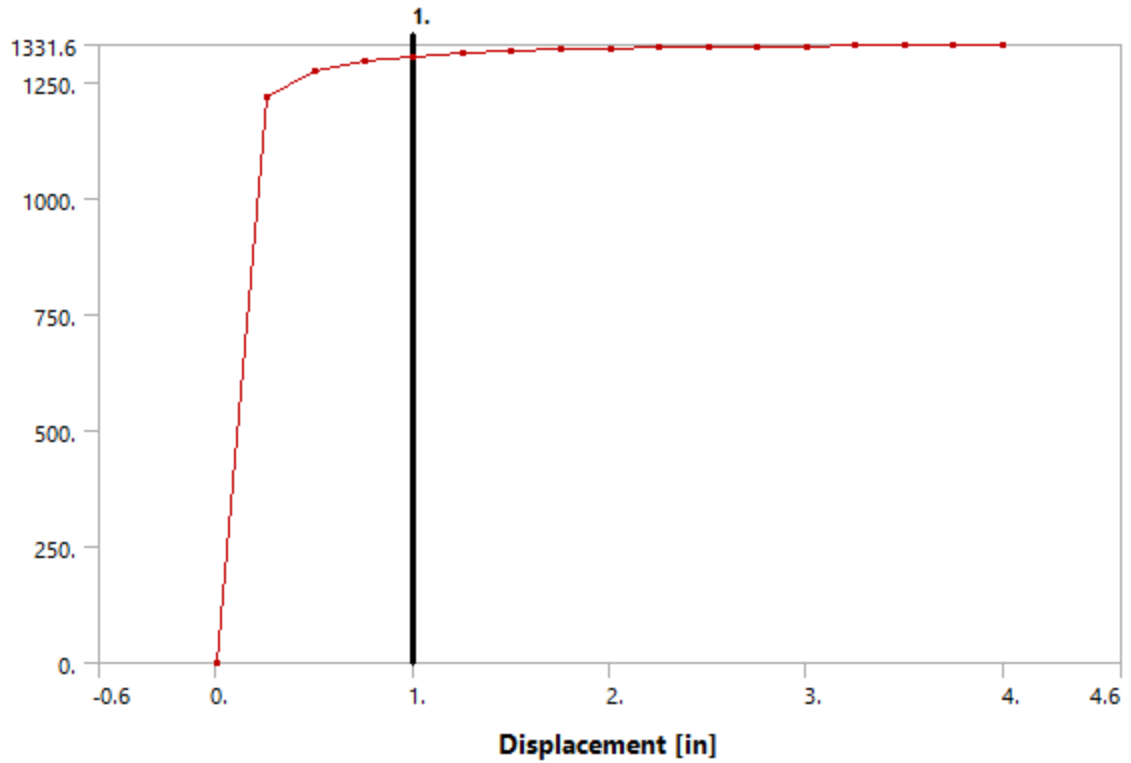| Displacement [in]	Force [lbf]
0.	0.
0.25	1217.6
0.5	1275.9
0.75	1296.6
1.	1307.2
1.25	1313.6
1.5	1317.9
1.75	1321.
2.	1323.4
2.25	1325.2
2.5	1326.7
2.75	1327.9
3.	1328.9
3.25	1329.7
3.5	1330.5
3.75	1331.1
4.	1331.6

295
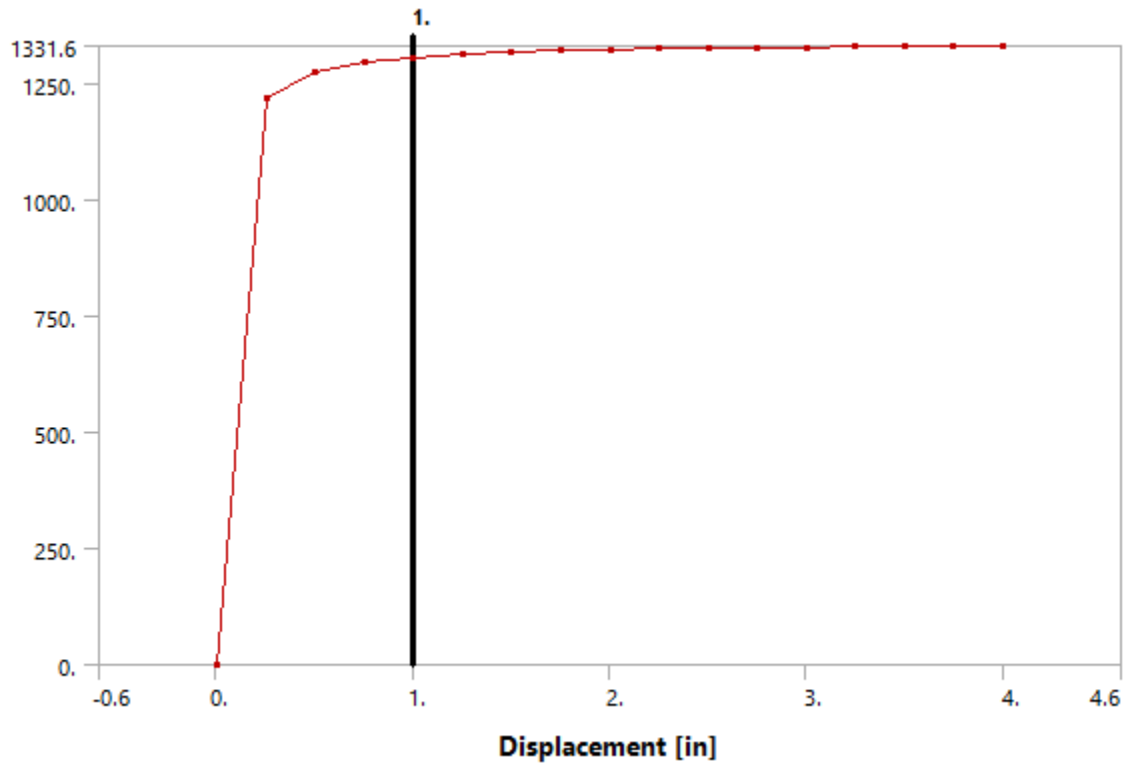
Figure 170 - Model (A4, B4, C4) > Connections > Longitudinal - Ground To Surface Body 46

Table 88 - Model (A4, B4, C4) > Connections > Longitudinal - Ground To Surface Body 46

Displacement [in]	Force [lbf]
0.	0.
0.25	1217.6
0.5	1275.9
0.75	1296.6
1.	1307.2
1.25	1313.6
1.5	1317.9
1.75	1321.
2.	1323.4
2.25	1325.2
2.5	1326.7
2.75	1327.9
3.	1328.9
3.25	1329.7
3.5	1330.5
3.75	1331.1
4.	1331.6
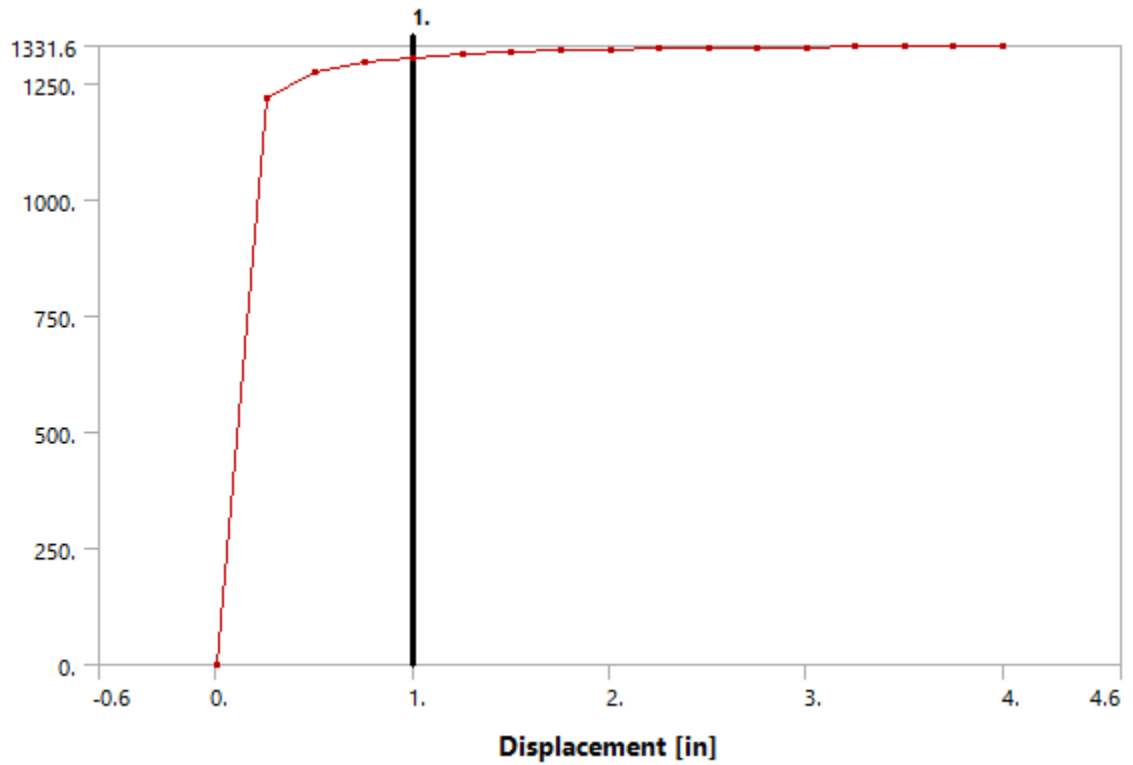
Figure 171 - Model (A4, B4, C4) > Connections > Longitudinal - Ground To Surface Body 47

Table 89 - Model (A4, B4, C4) > Connections > Longitudinal - Ground To Surface Body 47

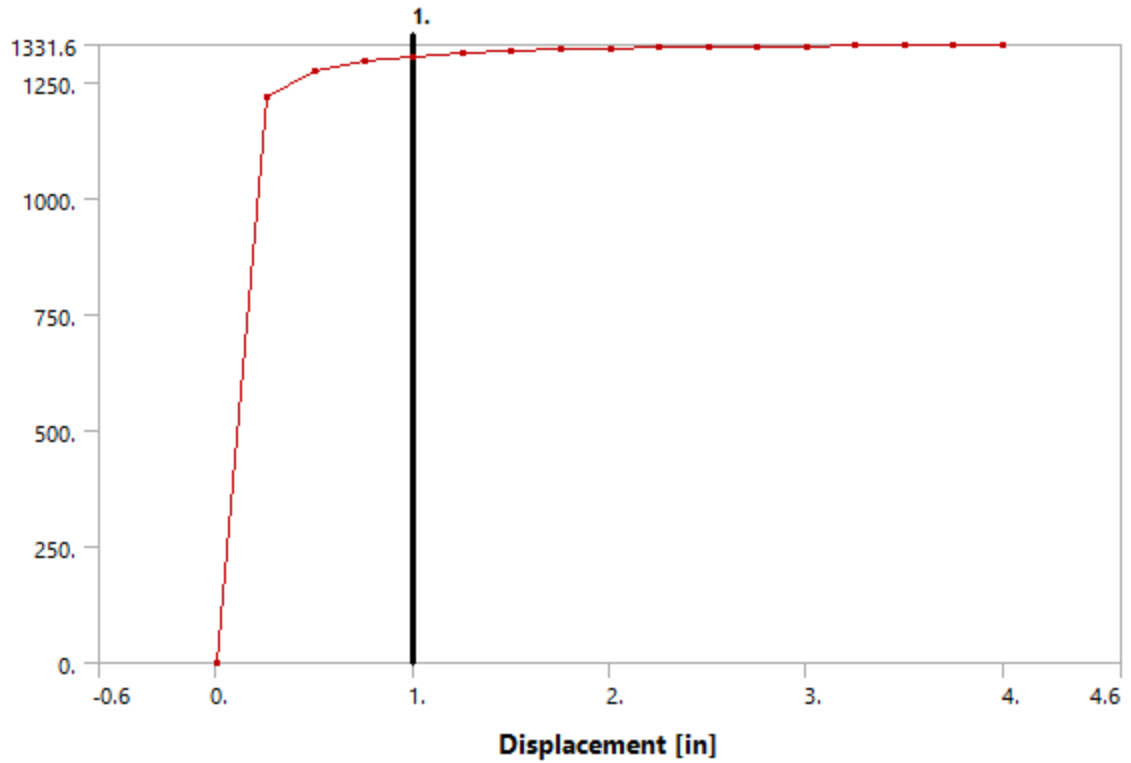| Displacement [in]	Force [lbf]
0.	0.
0.25	1217.6
0.5	1275.9
0.75	1296.6
1.	1307.2
1.25	1313.6
1.5	1317.9
1.75	1321.
2.	1323.4
2.25	1325.2
2.5	1326.7
2.75	1327.9
3.	1328.9
3.25	1329.7
3.5	1330.5
3.75	1331.1
4.	1331.6

297
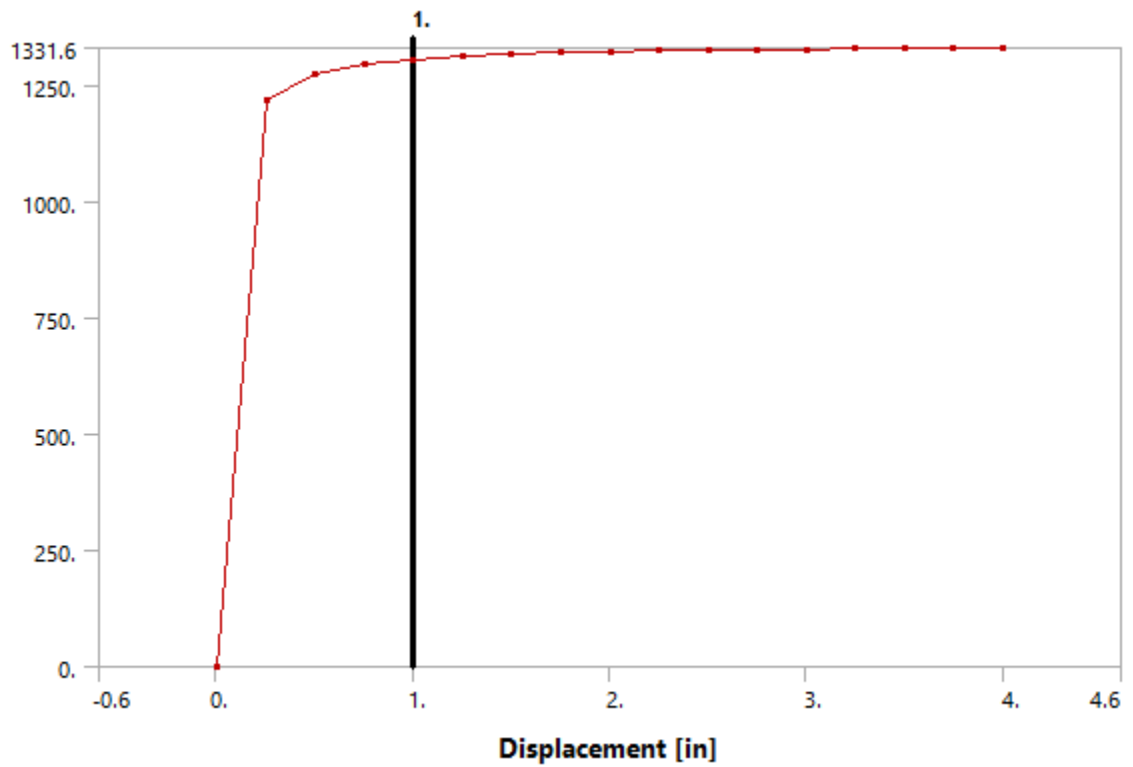
Figure 172 - Model (A4, B4, C4) > Connections > Longitudinal - Ground To Surface Body 48

Table 90 - Model (A4, B4, C4) > Connections > Longitudinal - Ground To Surface Body 48

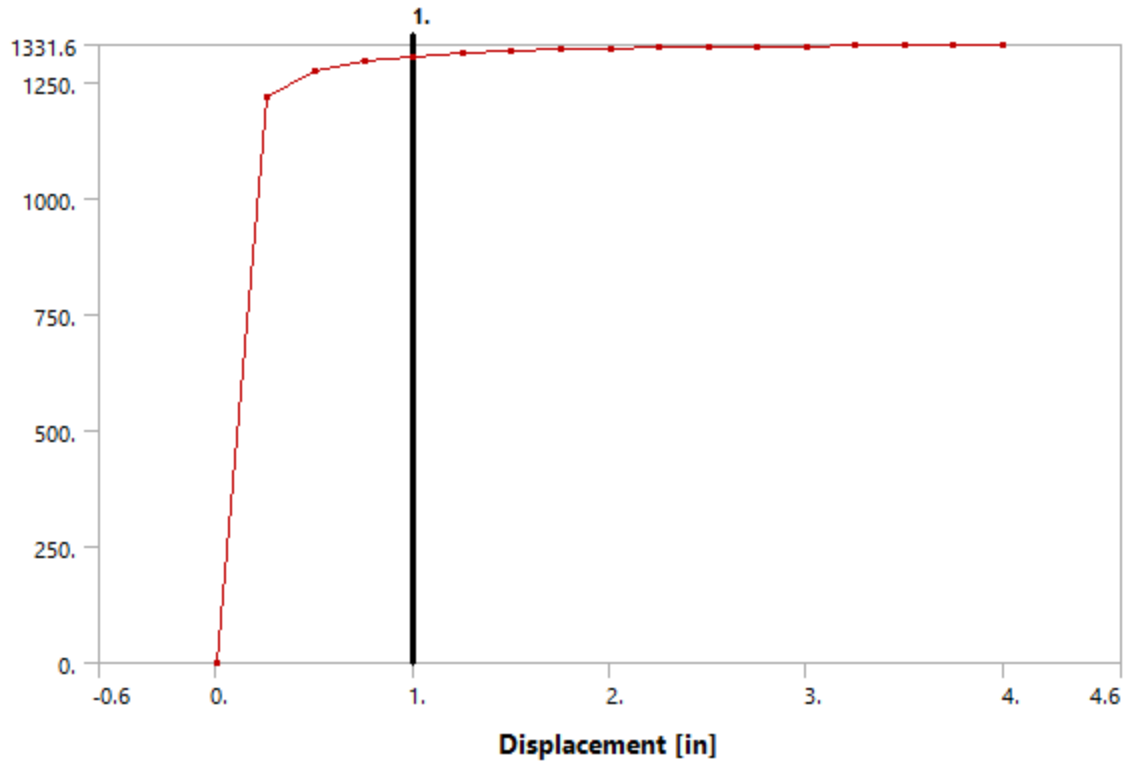| Displacement [in]	Force [lbf]
0.	0.
0.25	1217.6
0.5	1275.9
0.75	1296.6
1.	1307.2
1.25	1313.6
1.5	1317.9
1.75	1321.
2.	1323.4
2.25	1325.2
2.5	1326.7
2.75	1327.9
3.	1328.9
3.25	1329.7
3.5	1330.5
3.75	1331.1
4.	1331.6

298
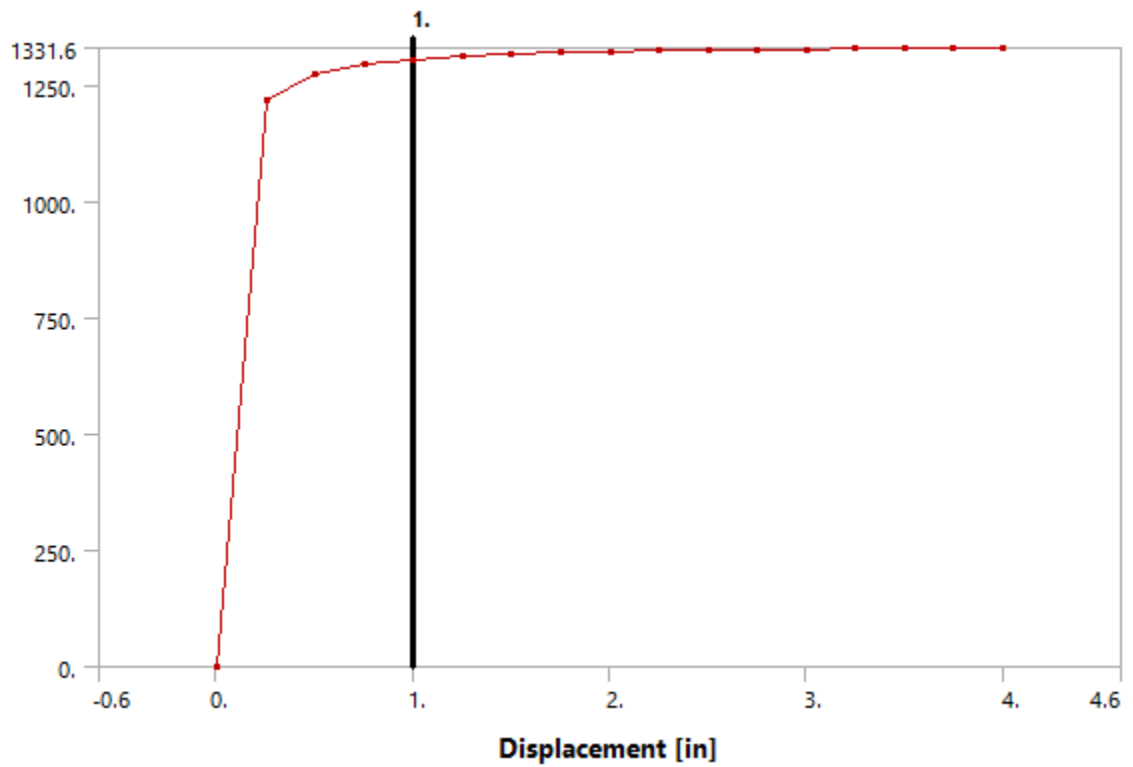
Figure 173 - Model (A4, B4, C4) > Connections > Longitudinal - Ground To Surface Body 49

Table 91 - Model (A4, B4, C4) > Connections > Longitudinal - Ground To Surface Body 49

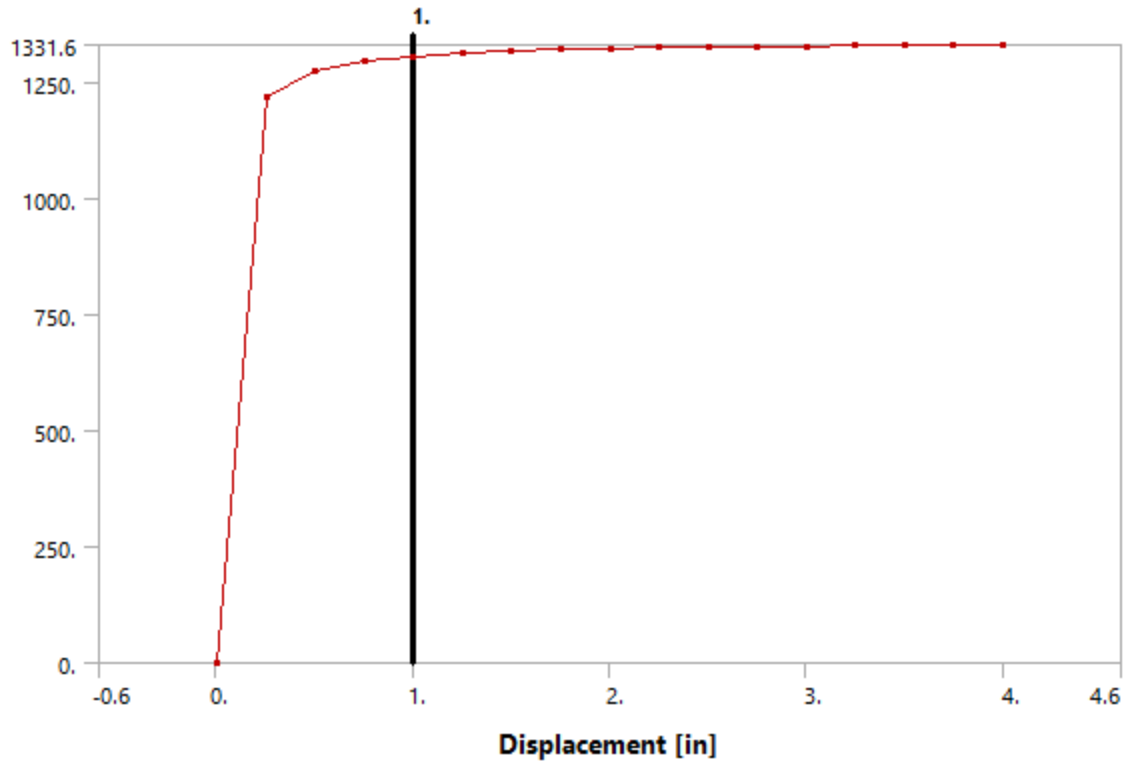| Displacement [in]	Force [lbf]
0.	0.
0.25	1217.6
0.5	1275.9
0.75	1296.6
1.	1307.2
1.25	1313.6
1.5	1317.9
1.75	1321.
2.	1323.4
2.25	1325.2
2.5	1326.7
2.75	1327.9
3.	1328.9
3.25	1329.7
3.5	1330.5
3.75	1331.1
4.	1331.6

299
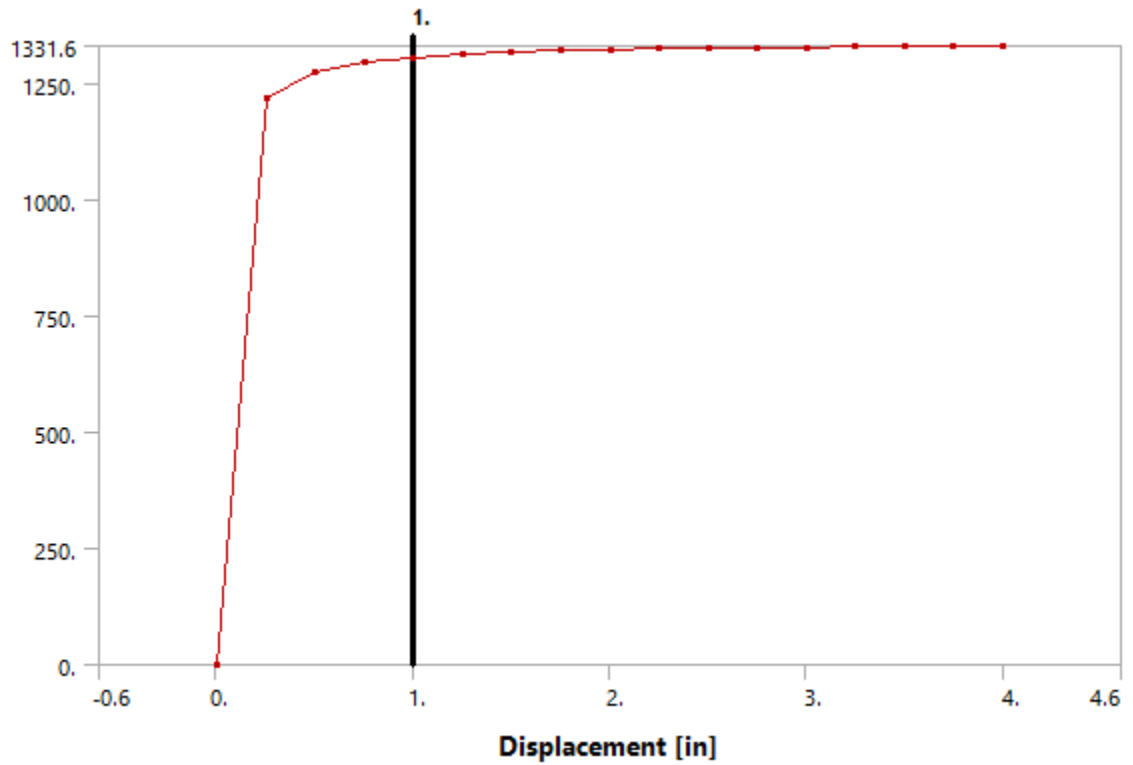
Figure 174 - Model (A4, B4, C4) > Connections > Longitudinal - Ground To Surface Body 50

Table 92 - Model (A4, B4, C4) > Connections > Longitudinal - Ground To Surface Body 50

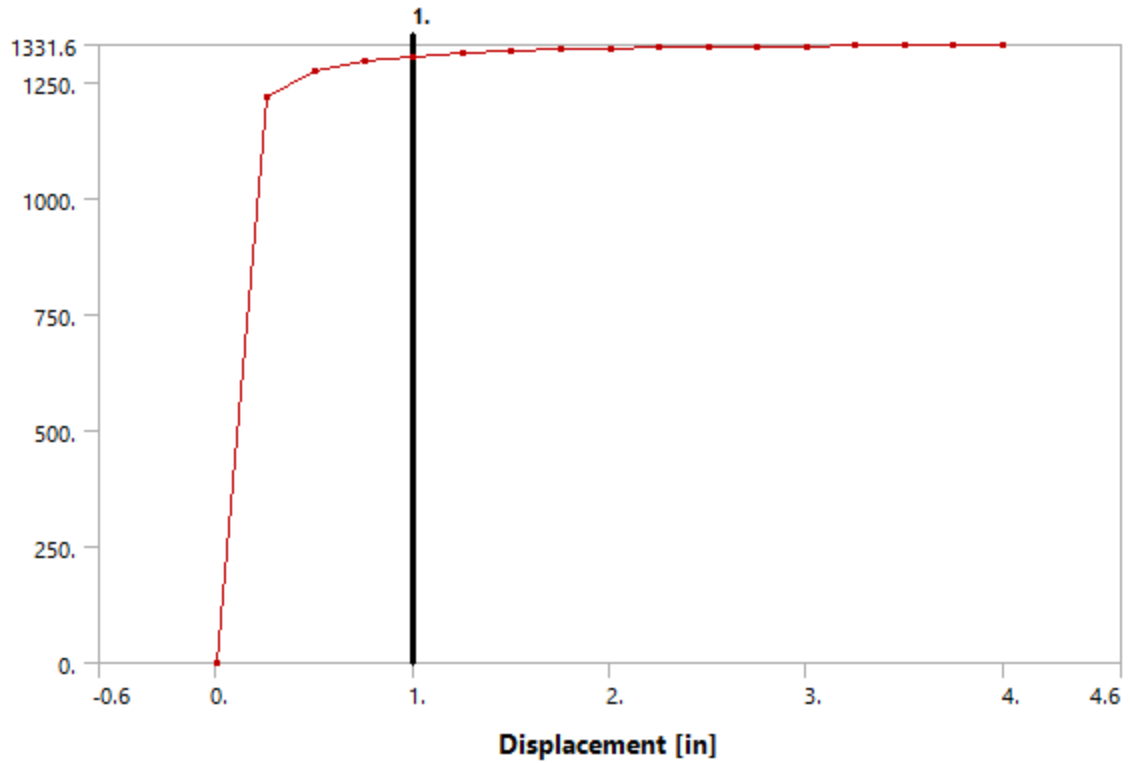| Displacement [in]	Force [lbf]
0.	0.
0.25	1217.6
0.5	1275.9
0.75	1296.6
1.	1307.2
1.25	1313.6
1.5	1317.9
1.75	1321.
2.	1323.4
2.25	1325.2
2.5	1326.7
2.75	1327.9
3.	1328.9
3.25	1329.7
3.5	1330.5
3.75	1331.1
4.	1331.6
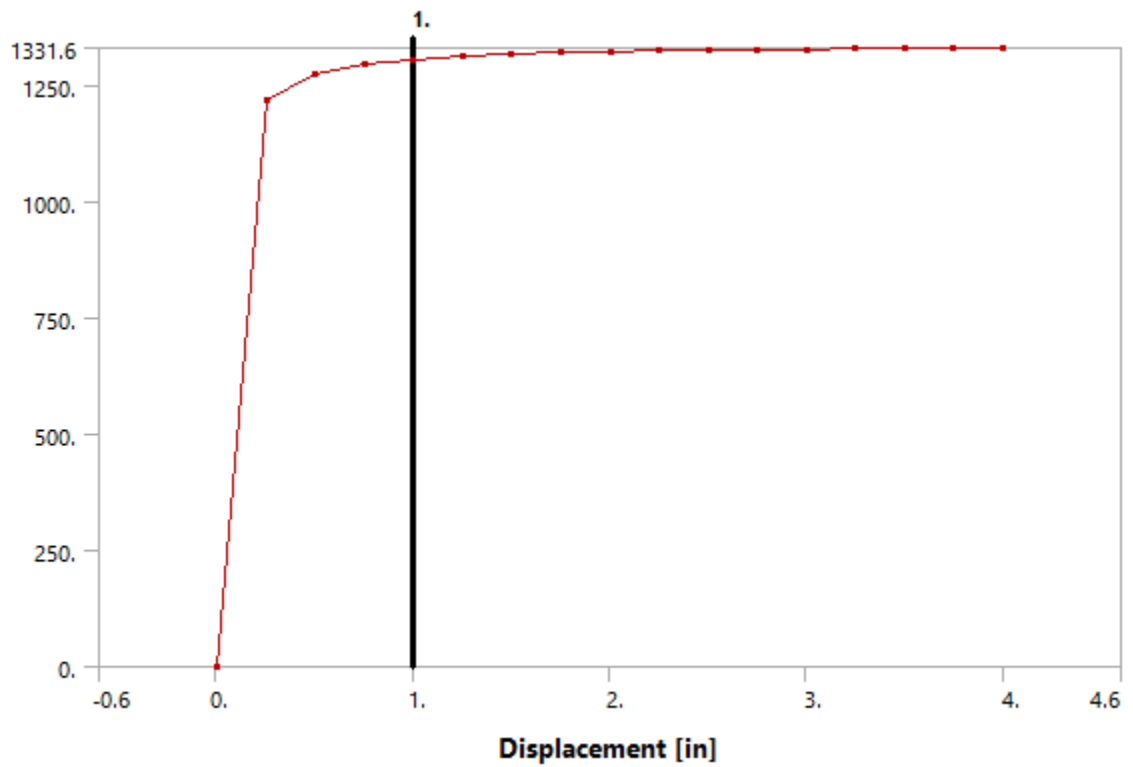
Figure 175 - Model (A4, B4, C4) > Connections > Longitudinal - Ground To Surface Body 51

Table 93 - Model (A4, B4, C4) > Connections > Longitudinal - Ground To Surface Body 51

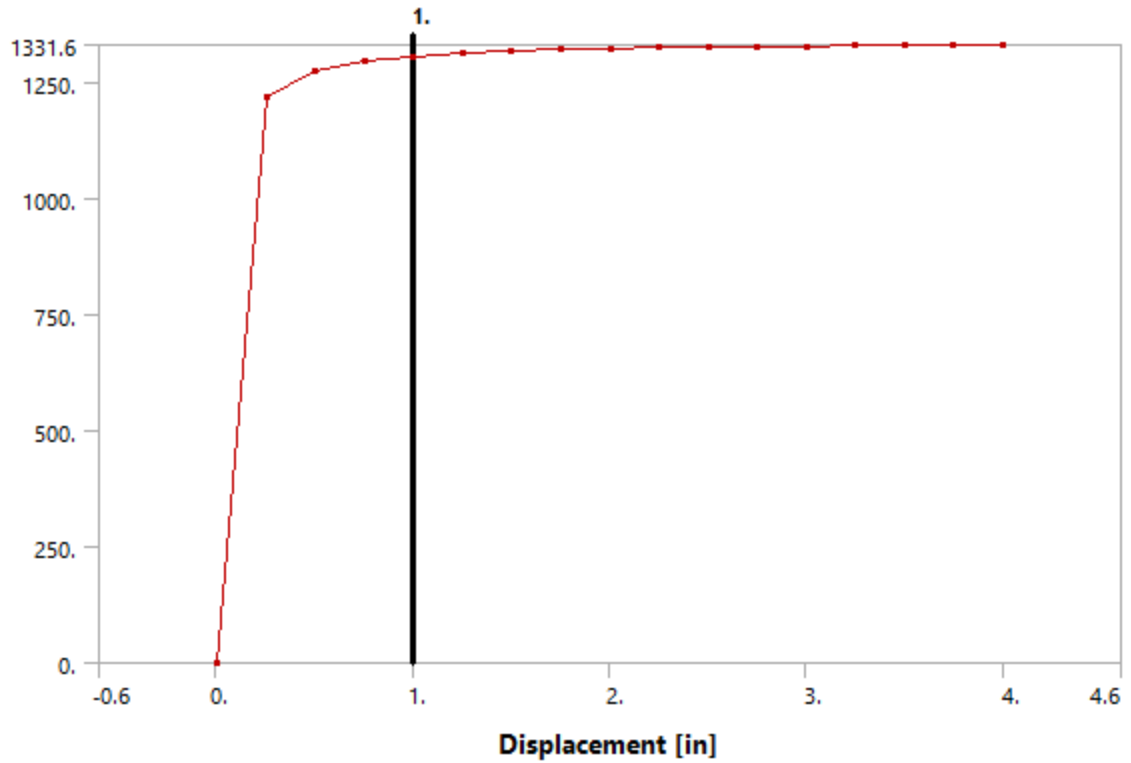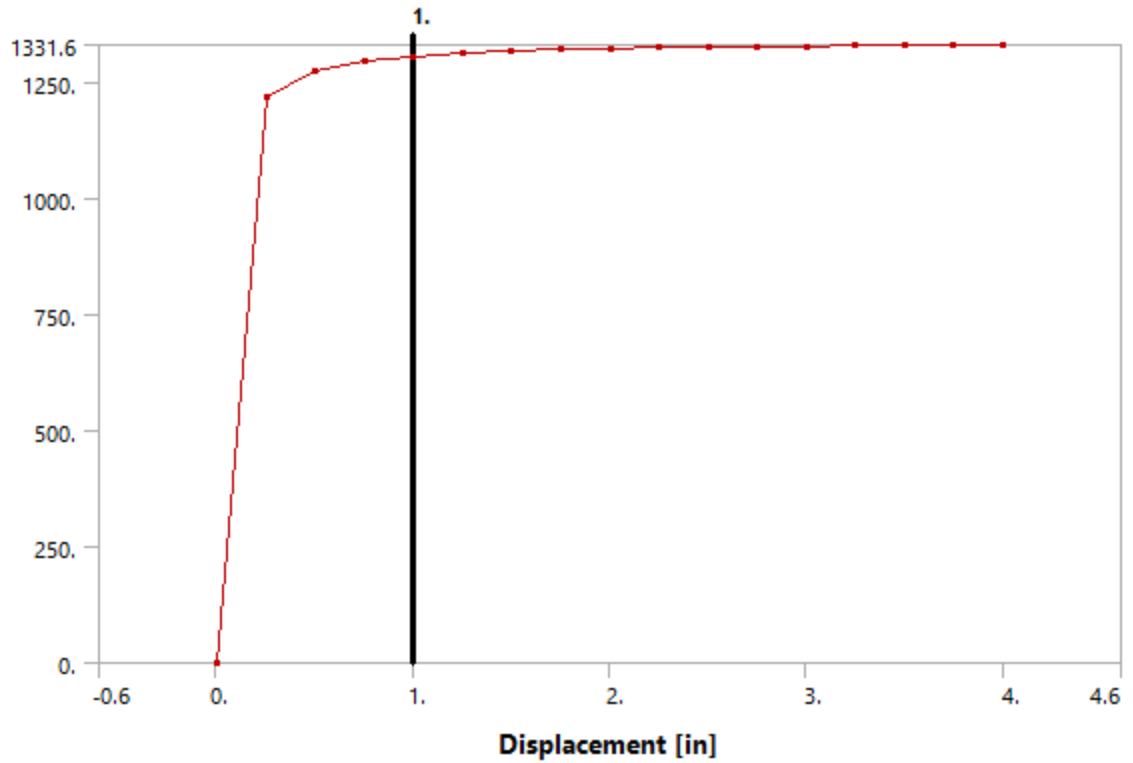| Displacement [in]	Force [lbf]
0.	0.
0.25	1217.6
0.5	1275.9
0.75	1296.6
1.	1307.2
1.25	1313.6
1.5	1317.9
1.75	1321.
2.	1323.4
2.25	1325.2
2.5	1326.7
2.75	1327.9
3.	1328.9
3.25	1329.7
3.5	1330.5
3.75	1331.1
4.	1331.6

301
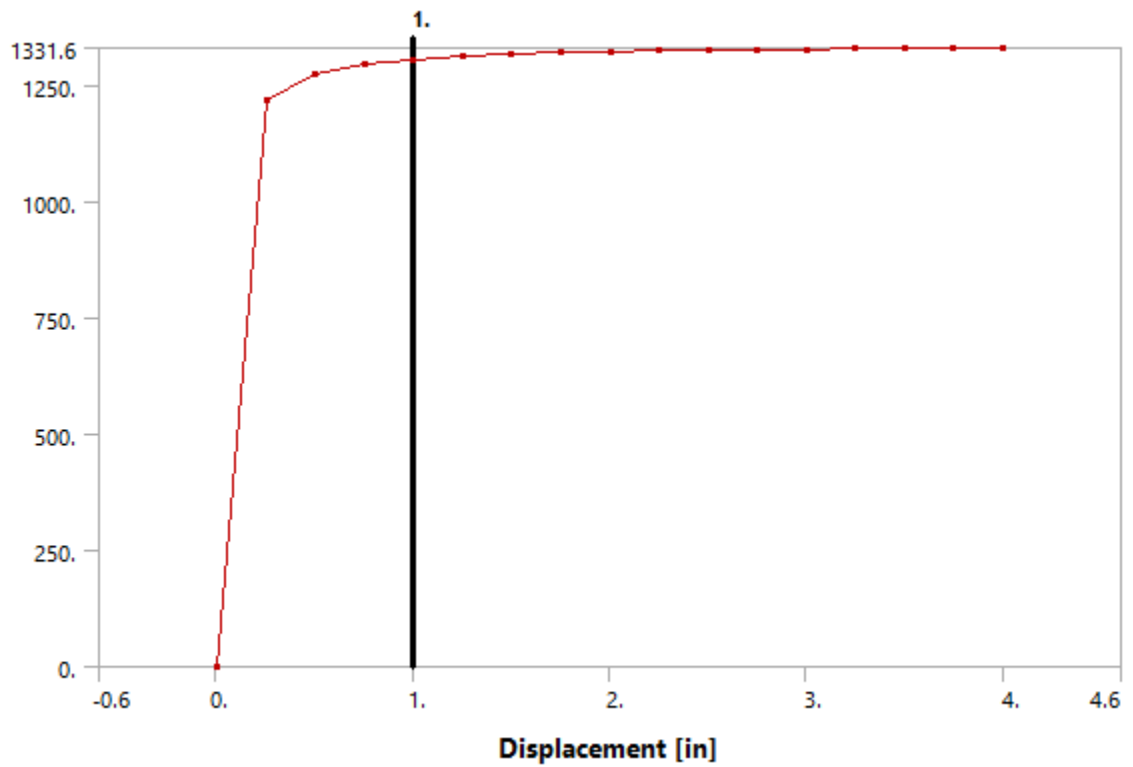
Figure 176 - Model (A4, B4, C4) > Connections > Longitudinal - Ground To Surface Body 52

Table 94 - Model (A4, B4, C4) > Connections > Longitudinal - Ground To Surface Body 52

Displacement [in]	Force [lbf]
0.	0.
0.25	1217.6
0.5	1275.9
0.75	1296.6
1.	1307.2
1.25	1313.6
1.5	1317.9
1.75	1321.
2.	1323.4
2.25	1325.2
2.5	1326.7
2.75	1327.9
3.	1328.9
3.25	1329.7
3.5	1330.5
3.75	1331.1
4.	1331.6

Mesh

Table 95 - Model (A4, B4, C4) > Mesh

Object Name	*Mesh*
State	Solved
Display	
Display Style	Body Color
Defaults	
Physics Preference	Mechanical
Relevance	0
Sizing	
Use Advanced Size Function	On: Curvature
Relevance Center	Coarse
Initial Size Seed	Active Assembly
Smoothing	Medium
Span Angle Center	Coarse
Curvature Normal Angle	5.0 °
Min Size	1.0 in
Max Face Size	2.0 in
Growth Rate	Default
Minimum Edge Length	58.1310 in
Inflation	
Use Automatic Inflation	None
Inflation Option	Smooth Transition
Transition Ratio	0.272
Maximum Layers	2
Growth Rate	1.2
Inflation Algorithm	Pre
View Advanced Options	No
Patch Conforming Options	
Triangle Surface Mesher	Program Controlled
Patch Independent Options	
Topology Checking	No
Advanced	
Number of CPUs for Parallel Part Meshing	Program Controlled
Shape Checking	Standard Mechanical
Element Midside Nodes	Program Controlled
Straight Sided Elements	No
Number of Retries	Default (4)
Extra Retries For Assembly	Yes
Rigid Body Behavior	Dimensionally Reduced
Mesh Morphing	Disabled

Table 96 – Meshing Data

Defeaturing	
Use Sheet Thickness for Pinch	No
Pinch Tolerance	Default (0.90 in)
Generate Pinch on Refresh	No
Sheet Loop Removal	No
Automatic Mesh Based Defeaturing	On
Defeaturing Tolerance	Default (0.750 in)
Statistics	
Nodes	5612
Elements	5566
Mesh Metric	None

Table 97 - Model (A4, B4, C4) > Mesh > Mesh Controls

Object Name	*MultiZone Quad/Tri Method*
State	Fully Defined
Scope	
Scoping Method	Geometry Selection
Geometry	1 Body
Definition	
Suppressed	No
Method	MultiZone Quad/Tri
Surface Mesh Method	Program Controlled
Element Midside Nodes	Use Global Setting
Free Face Mesh Type	All Quad
Advanced	
Preserve Boundaries	Protected
Mesh Based Defeaturing	On
Defeaturing Tolerance	Default(0.75 in)
Sheet Loop Removal	No
Minimum Edge Length	58.131 in
Write ICEM CFD Files	No

Table 98 - Model (A4, B4, C4) > Imported Plies

Object Name	*Imported Plies*
State	Solved
Definition	
Type	Imported Plies
Suppressed	No
Material	
Nonlinear Effects	Yes
Thermal Strain Effects	Yes
Graphics Properties	
Layer To Display	All Layers

ModelingGroup.1

ModelingPly.1

P1__ModelingPly.1

Table 99 - Model (A4, B4, C4) > Imported Plies > ModelingGroup.1 > ModelingPly.1 >

P1__ModelingPly.1 > P1L1__ModelingPly.1

Object Name	*P1L1__ModelingPly.1*
State	No State
Definition	
Name in Source	P1L1__ModelingPly.1
ID in Source	P1L1__ModelingPly.1
Material	Epoxy E-Glass UD
Thickness	0.1 in
Angle	0. °
Number of Elements	5566.

ModelingPly.2

P1__ModelingPly.2

Table 100 - Model (A4, B4, C4) > Imported Plies > ModelingGroup.1 > ModelingPly.2 >

P1__ModelingPly.2 > P1L1__ModelingPly.2

Object Name	*P1L1__ModelingPly.2*
State	No State
Definition	
Name in Source	P1L1__ModelingPly.2
ID in Source	P1L1__ModelingPly.2
Material	Epoxy E-Glass UD
Thickness	0.1 in
Angle	0. °
Number of Elements	5566.

ModelingPly.3

P1__ModelingPly.3

Table 101 - Model (A4, B4, C4) > Imported Plies > ModelingGroup.1 > ModelingPly.3 >

P1__ModelingPly.3 > P1L1__ModelingPly.3

Object Name	*P1L1__ModelingPly.3*
State	No State
Definition	
Name in Source	P1L1__ModelingPly.3
ID in Source	P1L1__ModelingPly.3
Material	Epoxy E-Glass UD
Thickness	0.1 in
Angle	0. °
Number of Elements	5566.

ModelingPly.4

P1__ModelingPly.4

Table 102 - Model (A4, B4, C4) > Imported Plies > ModelingGroup.1 > ModelingPly.4 >

P1__ModelingPly.4 > P1L1__ModelingPly.4

Object Name	*P1L1__ModelingPly.4*
State	No State
Definition	
Name in Source	P1L1__ModelingPly.4
ID in Source	P1L1__ModelingPly.4
Material	Epoxy E-Glass UD
Thickness	0.1 in
Angle	0. °
Number of Elements	5566.

ModelingPly.5

P1__ModelingPly.5

Table 103 - Model (A4, B4, C4) > Imported Plies > ModelingGroup.1 > ModelingPly.5 >

P1__ModelingPly.5 > P1L1__ModelingPly.5

Object Name	*P1L1__ModelingPly.5*
State	No State
Definition	
Name in Source	P1L1__ModelingPly.5
ID in Source	P1L1__ModelingPly.5
Material	Epoxy E-Glass UD
Thickness	0.1 in
Angle	0. °
Number of Elements	5566.

ModelingPly.6

P1__ModelingPly.6

Table 104 - Model (A4, B4, C4) > Imported Plies > ModelingGroup.1 > ModelingPly.6 >

P1__ModelingPly.6 > P1L1__ModelingPly.6

Object Name	*P1L1__ModelingPly.6*
State	No State
Definition	
Name in Source	P1L1__ModelingPly.6
ID in Source	P1L1__ModelingPly.6
Material	Epoxy E-Glass UD
Thickness	0.1 in
Angle	0. °
Number of Elements	5566.

ModelingPly.7

P1__ModelingPly.7

Table 105 - Model (A4, B4, C4) > Imported Plies > ModelingGroup.1 > ModelingPly.7 >

P1__ModelingPly.7 > P1L1__ModelingPly.7

Object Name	*P1L1__ModelingPly.7*
State	No State
Definition	
Name in Source	P1L1__ModelingPly.7
ID in Source	P1L1__ModelingPly.7
Material	Epoxy E-Glass UD
Thickness	0.1 in
Angle	0. °
Number of Elements	5566.

ModelingPly.8

P1__ModelingPly.8

Table 106 - Model (A4, B4, C4) > Imported Plies > ModelingGroup.1 > ModelingPly.8 >

P1__ModelingPly.8 > P1L1__ModelingPly.8

Object Name	*P1L1__ModelingPly.8*
State	No State
Definition	
Name in Source	P1L1__ModelingPly.8
ID in Source	P1L1__ModelingPly.8
Material	Epoxy E-Glass UD
Thickness	0.1 in
Angle	0. °
Number of Elements	5566.

ModelingPly.9

P1__ModelingPly.9

Table 107 - Model (A4, B4, C4) > Imported Plies > ModelingGroup.1 > ModelingPly.9 >

P1__ModelingPly.9 > P1L1__ModelingPly.9

Object Name	*P1L1__ModelingPly.9*
State	No State
Definition	
Name in Source	P1L1__ModelingPly.9
ID in Source	P1L1__ModelingPly.9
Material	Epoxy E-Glass UD
Thickness	0.1 in
Angle	0. °
Number of Elements	5566.

ModelingPly.10

P1__ModelingPly.10

Table 108 - Model (A4, B4, C4) > Imported Plies > ModelingGroup.1 > ModelingPly.10 >

P1__ModelingPly.10 > P1L1__ModelingPly.10

Object Name	*P1L1__ModelingPly.10*
State	No State
Definition	
Name in Source	P1L1__ModelingPly.10
ID in Source	P1L1__ModelingPly.10
Material	Epoxy E-Glass UD
Thickness	0.1 in
Angle	0. °
Number of Elements	5566.

Static Structural (B6)

Table 109 - Model (A4, B4, C4) > Analysis

Object Name	*Static Structural (B6)*
State	Solved
Definition	
Physics Type	Structural
Analysis Type	Static Structural
Solver Target	Mechanical APDL
Options	
Environment Temperature	71.6 °F
Generate Input Only	No

Table 110 - Model (A4, B4, C4) > Static Structural (B6) > Analysis Settings

Object Name	Analysis Settings
State	Fully Defined
Step Controls	
Number Of Steps	1.
Current Step Number	1.
Step End Time	1. s
Auto Time Stepping	Program Controlled
Solver Controls	
Solver Type	Program Controlled
Weak Springs	Program Controlled
Solver Pivot Checking	Program Controlled
Large Deflection	Off
Inertia Relief	Off
Restart Controls	
Generate Restart Points	Program Controlled
Retain Files After Full Solve	No
Nonlinear Controls	
Newton-Raphson Option	Program Controlled
Force Convergence	Program Controlled
Moment Convergence	Program Controlled
Displacement Convergence	Program Controlled
Rotation Convergence	Program Controlled
Line Search	Program Controlled
Stabilization	Off
Output Controls	
Stress	Yes
Strain	Yes
Nodal Forces	No
Contact Miscellaneous	No
General Miscellaneous	No
Store Results At	All Time Points
Analysis Data Management	
Solver Files Directory	E:\FRP\1 - FE Models\FRP305
Future Analysis	None
Scratch Solver Files Directory	
Save MAPDL db	No
Delete Unneeded Files	Yes
Nonlinear Solution	Yes
Solver Units	Active System
Solver Unit System	Bin

Table 111 - Model (A4, B4, C4) > Static Structural (B6) > Loads

Object Name	*Displacement*	*Force*
State	Fully Defined	
Scope		
Scoping Method	Geometry Selection	
Geometry	1 Edge	
Definition		
Type	Displacement	Force
Define By	Components	
Coordinate System	Global Coordinate System	
X Component	4. in (ramped)	0. lbf (ramped)
Y Component	Free	-50000 lbf (ramped)
Z Component	Free	0. lbf (ramped)
Suppressed	No	
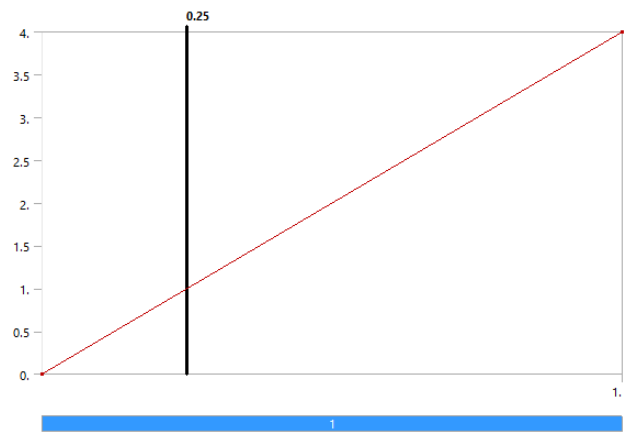
Figure 177 - Model (A4, B4, C4) > Static Structural (B6) > Displacement
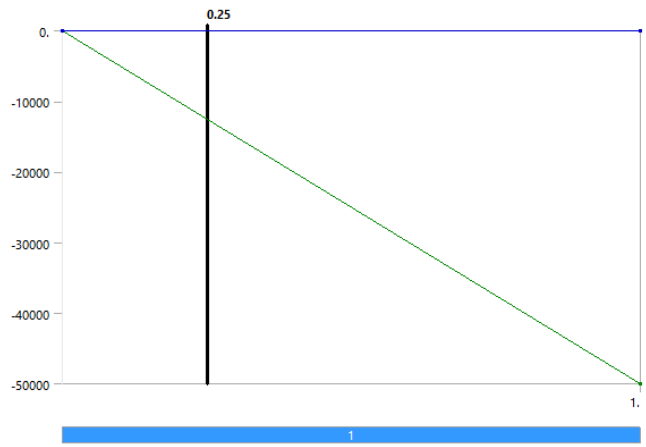
Figure 178 - Model (A4, B4, C4) > Static Structural (B6) > Force

Solution (B7)

Table 112 - Model (A4, B4, C4) > Static Structural (B6) > Solution

Object Name	*Solution (B7)*
State	Solved
Adaptive Mesh Refinement	
Max Refinement Loops	1.
Refinement Depth	2.
Information	
Status	Done
Post Processing	
Calculate Beam Section Results	No

Table 113 - Model (A4, B4, C4) > Static Structural (B6) > Solution (B7) > Solution Information

Object Name	*Solution Information*
State	Solved
Solution Information	
Solution Output	Solver Output
Newton-Raphson Residuals	0
Update Interval	2.5 s
Display Points	All
FE Connection Visibility	
Activate Visibility	Yes
Display	All FE Connectors
Draw Connections Attached To	All Nodes
Line Color	Connection Type
Visible on Results	No
Line Thickness	Single
Display Type	Lines

Table 114 - Model (A4, B4, C4) > Static Structural (B6) > Solution (B7) > Results

	Maximum Principal Stress	Maximum Shear Stress	Directional Deformation
Object Name	*Maximum Principal Stress*	*Maximum Shear Stress*	*Directional Deformation*
State	Solved		
Scope			
Scoping Method	Geometry Selection		
Geometry	All Bodies		
Sub Scope By	Layer		
Layer	Entire Section		
Position	Top/Bottom		
Definition			
Type	Maximum Principal Stress	Maximum Shear Stress	Directional Deformation
By	Time		
Display Time	Last		
Calculate Time History	Yes		
Identifier			
Suppressed	No		
Orientation			X Axis
Coordinate System			Global Coordinate System
Integration Point Results			
Display Option	Averaged		
Average Across Bodies	No		
Results			
Minimum	-13.23 psi	13.439 psi	-2.3313 in
Maximum	1544.7 psi	1595.2 psi	4. in
Information			
Time	1. s		
Load Step	1		
Substep	1		
Iteration Number	5		
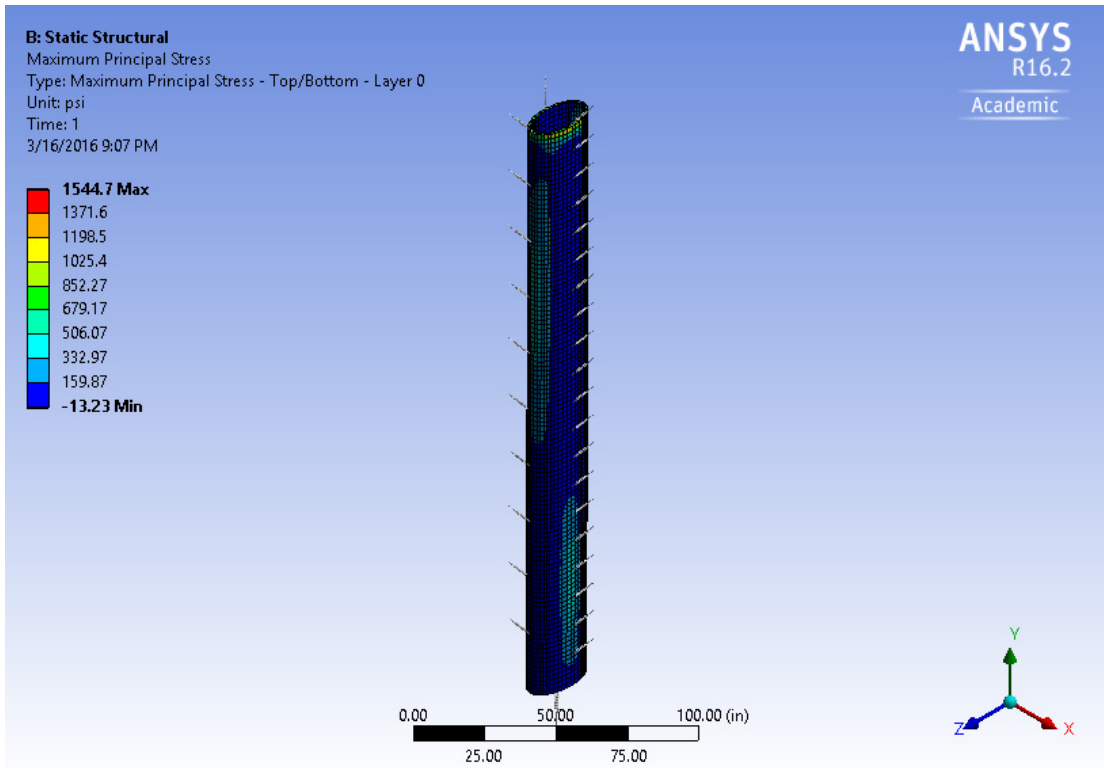
Figure 179 - Model (A4, B4, C4) > Static Structural (B6) > Solution (B7) > Maximum Principal Stress

Table 115 - Model (A4, B4, C4) > Static Structural (B6) > Solution (B7) > Maximum Principal Stress

Time [s]	Minimum [psi]	Maximum [psi]
1.	-13.23	1544.7
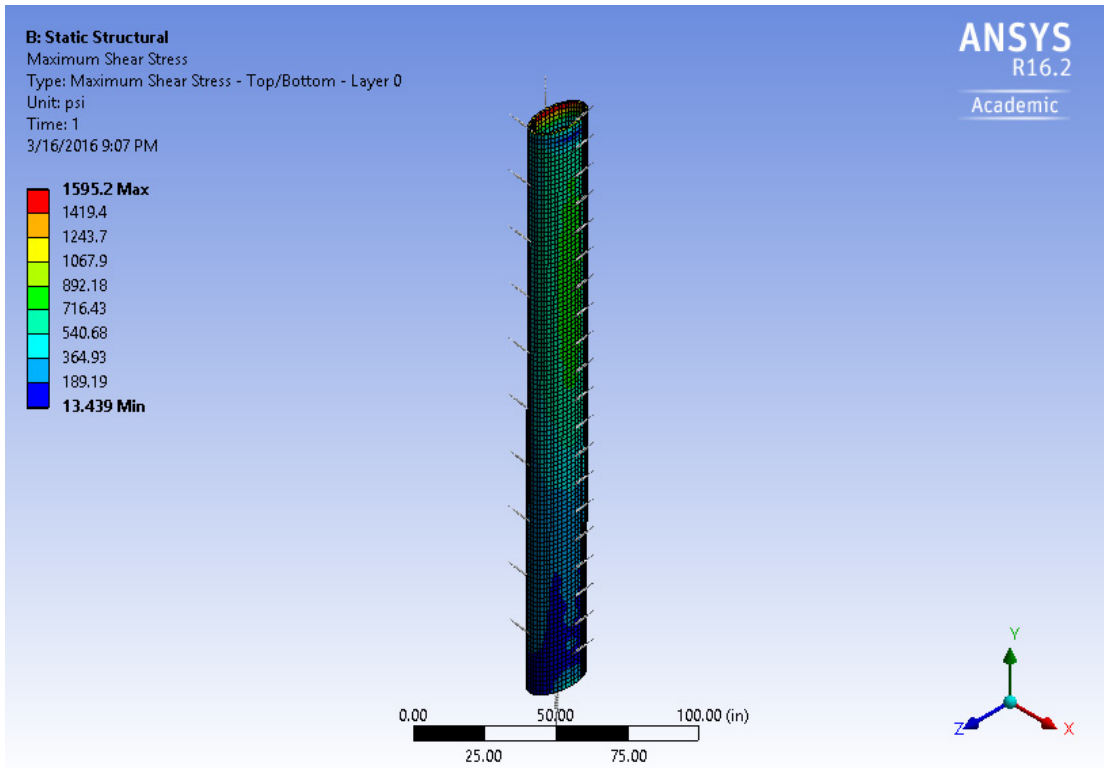
Figure 180 - Model (A4, B4, C4) > Static Structural (B6) > Solution (B7) > Maximum Shear Stress

Table 116 - Model (A4, B4, C4) > Static Structural (B6) > Solution (B7) > Maximum Shear Stress

Time [s]	Minimum [psi]	Maximum [psi]
1.	13.439	1595.2

315
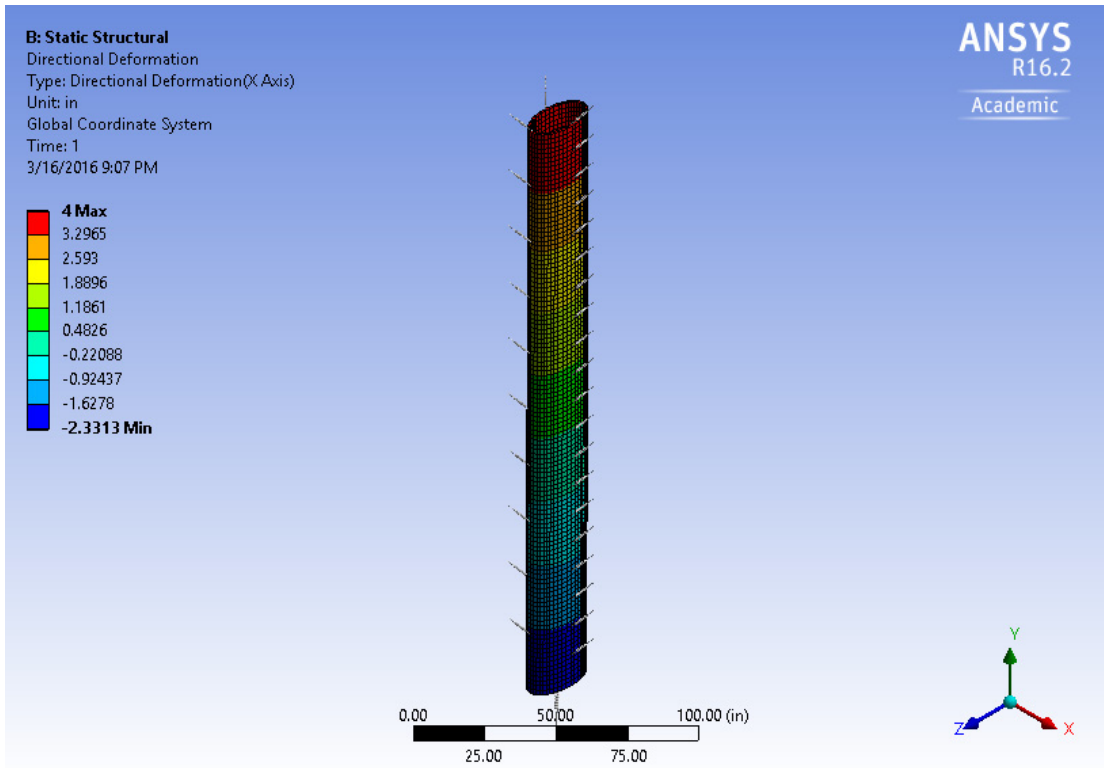
Figure 181 - Model (A4, B4, C4) > Static Structural (B6) > Solution (B7) > Directional Deformation

Table 117 - Model (A4, B4, C4) > Static Structural (B6) > Solution (B7) > Directional Deformation

Time [s]	Minimum [in]	Maximum [in]
1.	-2.3313	4.

316

Material Data

Epoxy E-Glass UD

Table 118 - Epoxy E-Glass UD > Constants

Density	7.2255e-002 lbm in^-3

Table 119 - Epoxy E-Glass UD > Orthotropic Elasticity

Temperature F	Young's Modulus X direction psi	Young's Modulus Y direction psi	Young's Modulus Z direction psi	Poisson's Ratio XY	Poisson's Ratio YZ	Poisson's Ratio XZ	Shear Modulus XY psi	Shear Modulus YZ psi	Shear Modulus XZ psi
	6.5267e+006	1.4504e+006	1.4504e+006	0.3	0.4	0.3	7.2519e+005	5.5784e+005	7.2519e+005

Table 120 - Epoxy E-Glass UD > Orthotropic Strain Limits

Temperature F	Tensile X direction	Tensile Y direction	Tensile Z direction	Compressive X direction	Compressive Y direction	Compressive Z direction	Shear XY	Shear YZ	Shear XZ
	2.44e-002	3.5e-003	3.5e-003	-1.5e-002	-1.2e-002	-1.2e-002	1.6e-002	1.2e-002	1.6e-002

Table 121 - Epoxy E-Glass UD > Orthotropic Stress Limits

Temperature F	Tensile X direction psi	Tensile Y direction psi	Tensile Z direction psi	Compressive X direction psi	Compressive Y direction psi	Compressive Z direction psi	Shear XY psi	Shear YZ psi	Shear XZ psi
	1.5954e+005	5076.3	5076.3	-97900	-17405	-17405	11603	6694	11603

Table 122 - Epoxy E-Glass UD > Puck Constants

Temperature F	Compressive Inclination XZ	Compressive Inclination YZ	Tensile Inclination XZ	Tensile Inclination YZ
	0.25	0.2	0.3	0.2

Table 123 - Epoxy E-Glass UD > Additional Puck Constants

Interface Weakening Factor	Degradation Parameter s	Degradation Parameter M
0.8	0.5	0.5

Table 124 - Epoxy E-Glass UD > Tsai-Wu Constants

Temperature F	Coupling Coefficient XY	Coupling Coefficient YZ	Coupling Coefficient XZ
	-1	-1	-1

14.5. *Exported Data*

Name	P1	P2	P3	P4	P5	P6	P7	P8	P9	P10	P11	P12	P17	P18	P13	P15	P16
#																	
# 02/23/2016 09:38:58																	
# The parameters defined in the project are:																	
# P1 - Z	P2 -	P3 -	P4 -	P5 -	P6 -	P7 -	P8 -	P9 -	P10	P11	P12	P17	P18 -	P13 - Ma	P15 - Maxi	P16 - Parameter.1	
#																	
# The following header line defines the name of the columns by reference to the parameters.																	
Name	P1	P2	P3	P4	P5	P6	P7	P8	P9	P10	P11	P12	P17	P18	P13	P15	P16
DP 0	12	6	0	0	0	0	0	0	0	0	0	0	4	-10000	675.3786	692.5828	0.153646
DP 1	12	6	0	0	0	0	0	0	0	0	0	0	4	-20000	709.6636	849.3414	0.190338
DP 2	12	6	0	0	0	0	0	0	0	0	0	0	4	-30000	985.6399	1017.157	0.23509
DP 3	12	6	0	0	0	0	0	0	0	0	0	0	4	-40000	1262.273	1287.418	0.27657
DP 4	12	6	0	0	0	0	0	0	0	0	0	0	4	-50000	1544.671	1595.166	0.318598
DP 5	12	6	0	0	0	0	0	0	0	0	0	0	4	-60000	1827.106	1902.98	0.369125
DP 6	12	6	0	0	0	0	0	0	0	0	0	0	4	-70000	2109.306	2210.7	0.422244
DP 7	12	6	0	0	0	0	0	0	0	0	0	0	4	-80000	2391.237	2518.311	0.47639
DP 8	12	6	0	0	0	0	0	0	0	0	0	0	4	-90000	2672.898	2825.809	0.530417
DP 9	12	6	0	0	0	0	0	0	0	0	0	0	4	-100000	2954.329	3133.214	0.587486
DP 10	12	6	10	-10	10	-10	10	-10	10	-10	10	-10	4	-10000	695.2113	896.3109	0.167289
DP 11	12	6	10	-10	10	-10	10	-10	10	-10	10	-10	4	-20000	718.1101	1062.485	0.212795
DP 12	12	6	10	-10	10	-10	10	-10	10	-10	10	-10	4	-30000	990.3566	1230.647	0.25204
DP 13	12	6	10	-10	10	-10	10	-10	10	-10	10	-10	4	-40000	1274.363	1433.67	0.291004
DP 14	12	6	10	-10	10	-10	10	-10	10	-10	10	-10	4	-50000	1563.752	1678.345	0.332616
DP 15	12	6	10	-10	10	-10	10	-10	10	-10	10	-10	4	-60000	1853.822	1974.002	0.37529
DP 16	12	6	10	-10	10	-10	10	-10	10	-10	10	-10	4	-70000	2145.075	2291.806	0.429352
DP 17	12	6	10	-10	10	-10	10	-10	10	-10	10	-10	4	-80000	2436.122	2609.447	0.483326
DP 18	12	6	10	-10	10	-10	10	-10	10	-10	10	-10	4	-90000	2728.448	2926.918	0.537216
DP 19	12	6	10	-10	10	-10	10	-10	10	-10	10	-10	4	-100000	3022.699	3244.245	0.59268
DP 20	12	6	20	-20	20	-20	20	-20	20	-20	20	-20	4	-10000	891.4478	1076.993	0.175075
DP 21	12	6	20	-20	20	-20	20	-20	20	-20	20	-20	4	-20000	904.5936	1256.022	0.220328
DP 22	12	6	20	-20	20	-20	20	-20	20	-20	20	-20	4	-30000	1042.994	1417.313	0.260709
DP 23	12	6	20	-20	20	-20	20	-20	20	-20	20	-20	4	-40000	1307.39	1632.891	0.301958
DP 24	12	6	20	-20	20	-20	20	-20	20	-20	20	-20	4	-50000	1620.842	1887.512	0.346578
DP 25	12	6	20	-20	20	-20	20	-20	20	-20	20	-20	4	-60000	1934.742	2144.411	0.391274
DP 26	12	6	20	-20	20	-20	20	-20	20	-20	20	-20	4	-70000	2248.674	2441.498	0.443432
DP 27	12	6	20	-20	20	-20	20	-20	20	-20	20	-20	4	-80000	2562.671	2778.078	0.499774
DP 28	12	6	20	-20	20	-20	20	-20	20	-20	20	-20	4	-90000	2880.11	3114.453	0.556051
DP 29	12	6	20	-20	20	-20	20	-20	20	-20	20	-20	4	-100000	3197.475	3450.652	0.612274
DP 30	12	6	30	-30	30	-30	30	-30	30	-30	30	-30	4	-10000	1054.122	1185.499	0.171084
DP 31	12	6	30	-30	30	-30	30	-30	30	-30	30	-30	4	-20000	1008.024	1353.325	0.2187
DP 32	12	6	30	-30	30	-30	30	-30	30	-30	30	-30	4	-30000	1110.438	1574.944	0.266223
DP 33	12	6	30	-30	30	-30	30	-30	30	-30	30	-30	4	-40000	1359.539	1812.044	0.313405
DP 34	12	6	30	-30	30	-30	30	-30	30	-30	30	-30	4	-50000	1691.477	2070.443	0.363818
DP 35	12	6	30	-30	30	-30	30	-30	30	-30	30	-30	4	-60000	2024.239	2330.607	0.41434
DP 36	12	6	30	-30	30	-30	30	-30	30	-30	30	-30	4	-70000	2361.139	2647.991	0.467133
DP 37	12	6	30	-30	30	-30	30	-30	30	-30	30	-30	4	-80000	2699.166	3010.253	0.527322
DP 38	12	6	30	-30	30	-30	30	-30	30	-30	30	-30	4	-90000	3037.252	3373.624	0.587444
DP 39	12	6	30	-30	30	-30	30	-30	30	-30	30	-30	4	-100000	3375.368	3736.812	0.647536
DP 40	12	6	40	-40	40	-40	40	-40	40	-40	40	-40	4	-10000	1218.908	1224.22	0.161584
DP 41	12	6	40	-40	40	-40	40	-40	40	-40	40	-40	4	-20000	1100.363	1464.628	0.218547
DP 42	12	6	40	-40	40	-40	40	-40	40	-40	40	-40	4	-30000	1138.582	1702.019	0.274066
DP 43	12	6	40	-40	40	-40	40	-40	40	-40	40	-40	4	-40000	1375.039	1937.532	0.331007
DP 44	12	6	40	-40	40	-40	40	-40	40	-40	40	-40	4	-50000	1719.869	2197.376	0.390386
DP 45	12	6	40	-40	40	-40	40	-40	40	-40	40	-40	4	-60000	2066.234	2489.845	0.449565
DP 46	12	6	40	-40	40	-40	40	-40	40	-40	40	-40	4	-70000	2413.387	2880.118	0.514413

318

DP 47	12	6	40	-40	40	-40	40	-40	40	-40	40	-40	4	-80000	2761.006	3271.173	0.582101
DP 48	12	6	40	-40	40	-40	40	-40	40	-40	40	-40	4	-90000	3123.129	3662.002	0.650194
DP 49	12	6	40	-40	40	-40	40	-40	40	-40	40	-40	4	-100000	3488.363	4052.631	0.718584
DP 50	12	6	50	-50	50	-50	50	-50	50	-50	50	-50	4	-10000	1332.383	1266.806	0.159632
DP 51	12	6	50	-50	50	-50	50	-50	50	-50	50	-50	4	-20000	1003.554	1496.805	0.224124
DP 52	12	6	50	-50	50	-50	50	-50	50	-50	50	-50	4	-30000	1041.56	1718.318	0.293192
DP 53	12	6	50	-50	50	-50	50	-50	50	-50	50	-50	4	-40000	1374.439	1938.566	0.367468
DP 54	12	6	50	-50	50	-50	50	-50	50	-50	50	-50	4	-50000	1711.051	2247.543	0.450592
DP 55	12	6	50	-50	50	-50	50	-50	50	-50	50	-50	4	-60000	2064.977	2655.505	0.533724
DP 56	12	6	50	-50	50	-50	50	-50	50	-50	50	-50	4	-70000	2420.132	3065.565	0.616809
DP 57	12	6	50	-50	50	-50	50	-50	50	-50	50	-50	4	-80000	2775.562	3475.31	0.699824
DP 58	12	6	50	-50	50	-50	50	-50	50	-50	50	-50	4	-90000	3131.174	3884.816	0.782788
DP 59	12	6	50	-50	50	-50	50	-50	50	-50	50	-50	4	-100000	3486.909	4294.09	0.865704
DP 60	12	6	60	-60	60	-60	60	-60	60	-60	60	-60	4	-10000	1375.386	1213.727	0.169273
DP 61	12	6	60	-60	60	-60	60	-60	60	-60	60	-60	4	-20000	1180.394	1411.263	0.240992
DP 62	12	6	60	-60	60	-60	60	-60	60	-60	60	-60	4	-30000	1242.292	1592.51	0.334292
DP 63	12	6	60	-60	60	-60	60	-60	60	-60	60	-60	4	-40000	1499.58	1881.444	0.4308
DP 64	12	6	60	-60	60	-60	60	-60	60	-60	60	-60	4	-50000	1858.251	2283.648	0.528866
DP 65	12	6	60	-60	60	-60	60	-60	60	-60	60	-60	4	-60000	2221.041	2689.375	0.626856
DP 66	12	6	60	-60	60	-60	60	-60	60	-60	60	-60	4	-70000	2583.904	3096.4	0.724747
DP 67	12	6	60	-60	60	-60	60	-60	60	-60	60	-60	4	-80000	2946.672	3503.005	0.822519
DP 68	12	6	60	-60	60	-60	60	-60	60	-60	60	-60	4	-90000	3309.402	3909.395	0.920218
DP 69	12	6	60	-60	60	-60	60	-60	60	-60	60	-60	4	-100000	3672.059	4315.506	1.017844
DP 70	12	6	70	-70	70	-70	70	-70	70	-70	70	-70	4	-10000	1368.986	1095.497	0.16568
DP 71	12	6	70	-70	70	-70	70	-70	70	-70	70	-70	4	-20000	1313.006	1238.354	0.268868
DP 72	12	6	70	-70	70	-70	70	-70	70	-70	70	-70	4	-30000	1517.175	1426.076	0.369426
DP 73	12	6	70	-70	70	-70	70	-70	70	-70	70	-73	4	-40000	1733.287	1779.304	0.47342
DP 74	12	6	70	-70	70	-70	70	-70	70	-70	70	-70	4	-50000	1977.629	2147.368	0.579269
DP 75	12	6	70	-70	70	-70	70	-70	70	-70	70	-70	4	-60000	2226.103	2517.986	0.684975
DP 76	12	6	70	-70	70	-70	70	-70	70	-70	70	-70	4	-70000	2476.345	2891.165	0.790515
DP 77	12	6	70	-70	70	-70	70	-70	70	-70	70	-70	4	-80000	2802.427	3263.976	0.895886
DP 78	12	6	70	-70	70	-70	70	-70	70	-70	70	-70	4	-90000	3134.651	3636.614	1.001151
DP 79	12	6	70	-70	70	-70	70	-70	70	-70	70	-70	4	-100000	3472.259	4008.971	1.10631
DP 80	12	6	80	-80	80	-80	80	-80	80	-80	80	-80	4	-10000	1221.944	918.6146	0.178134
DP 81	12	6	80	-80	80	-80	80	-80	80	-80	80	-80	4	-20000	1240.034	1018.343	0.281019
DP 82	12	6	80	-80	80	-80	80	-80	80	-80	80	-80	4	-30000	1538.817	1264.475	0.379158
DP 83	12	6	80	-80	80	-80	80	-80	80	-80	80	-80	4	-40000	1850.344	1563.259	0.481044
DP 84	12	6	80	-80	80	-80	80	-80	80	-80	80	-80	4	-50000	2184.19	1876.707	0.586059
DP 85	12	6	80	-80	80	-80	80	-80	80	-80	80	-80	4	-60000	2521.867	2191.439	0.690884
DP 86	12	6	80	-80	80	-80	80	-80	80	-80	80	-80	4	-70000	2861.236	2506.56	0.795494
DP 87	12	6	80	-80	80	-80	80	-80	80	-80	80	-80	4	-80000	3201.281	2824.541	0.899895
DP 88	12	6	80	-80	80	-80	80	-80	80	-80	80	-80	4	-90000	3541.963	3143.042	1.004167
DP 89	12	6	80	-80	80	-80	80	-80	80	-80	80	-80	4	-100000	3882.837	3461.382	1.108304
DP 90	12	6	90	-90	90	-90	90	-90	90	-90	90	-90	4	-10000	847.6283	717.8108	0.181785
DP 91	12	6	90	-90	90	-90	90	-90	90	-90	90	-90	4	-20000	880.9169	874.4762	0.282454
DP 92	12	6	90	-90	90	-90	90	-90	90	-90	90	-90	4	-30000	1230.726	1082.321	0.376281
DP 93	12	6	90	-90	90	-90	90	-90	90	-90	90	-90	4	-40000	1605.315	1372.318	0.46951
DP 94	12	6	90	-90	90	-90	90	-90	90	-90	90	-90	4	-50000	1994.967	1697.28	0.568019
DP 95	12	6	90	-90	90	-90	90	-90	90	-90	90	-90	4	-60000	2389.785	2027.409	0.667649
DP 96	12	6	90	-90	90	-90	90	-90	90	-90	90	-90	4	-70000	2787.547	2360.481	0.767204
DP 97	12	6	90	-90	90	-90	90	-90	90	-90	90	-90	4	-80000	3187.17	2695.417	0.866531
DP 98	12	6	90	-90	90	-90	90	-90	90	-90	90	-90	4	-90000	3588.091	3031.649	0.965715
DP 99	12	6	90	-90	90	-90	90	-90	90	-90	90	-90	4	-100000	3989.929	3368.8	1.064951

15.   References

Abrate, Serge. "Criteria for Yielding or Failure of Cellular Materials." *Journal of Sandwitch Structures and Materials, Vol. 10*, January 2008: 5-47.

Aero Consultants AG. *Aero Consultants AG.* 2015. http://www.aero-consultants.ch/en/Airtech-Hilfsmaterialien/Vacuum-Bagging-and-Composite-Tooling.htm.

Alok, Bhowmick. "Design and construction of integral bridges - An innovative concept." *The Indian concrete journal*, 2003: 1203-1209.

Amde, A. M., Aggour, M.S. and Chini, S.A. *Structural and Soil Provisions for Approaches to Bridges.* Phase I, Maryland Department of Transportation, July 1987, 96 pages.

Amde, A. M., Aggour, M.S. *Structural and Soil Provisions For Approaches to Bridges.* AW089-321-046, FHWA/MD-90/01, June 1990, 16 pages.

Amde, A. M., Aggour, M.S., Moumena, L. and Chini, S.A. *Structural and Soil Provisions for Approaches to Bridges.* AW 089-321-046, FHWA/MD-89/12, December 1989, 350 pages.

Amde, A. M., and Greimann, L. F. "Design Model for Piles in Jointless bridges." *Journal of Structural Engineering, ASCE, Vol. 114, No. 6*, June 1988: 1354-1371.

Amde, A. M., and Greimann, L. F. "General Design Details for Integral Abutment Bridges." *Journal of Civil Engineering Practice, BSCE/ASCE,ISSN: 0886-9685, Vol. 3, No. 2*, Fall 1988: 7-20.

Amde, A. M., and Klinger, J. E. *Integral Abutment Bridges Design and Construction.* College Park: Department of Civil Engineering, University of Maryland, Final Report, January 1987.

Amde, A. M., and L., and Johnson, B. Greimann. "Performance of Bridge Abutments." *The Journal of theInternational Association for Bridge and Structural Engineering, IABSE PERIODICA 1*, 1983: 17-34.

Amde, A. M., Chini, S. A., and Mafi, M. "Model Study of H-piles Subjected to Combined Loading." *Geotechnical and Geological Engineering*, August 1997: 343-355.

Amde, A. M., Chini, S.A. and Mafi, M. "Experimental Study of Piles in Integral Abutment Bridges." *International Journal of Geotechnical and Geological Engineering Vol. 15*, 1997: 343-355.

Amde, A. M., Chini, S.A. and Moumena, L. "Finite Element Representation of Approach Slabs." *Proceedings of the Fifth International Conference on Computing in Civil and Building Engineering.* Anaheim, California, June 7-9, 1993. 184-188.

Amde, A. M., Greimann, L. F., and Yang, P. S. "Nonlinear Analysis of Integral Abutment Bridges." *Journal of Structural Engineering, ASCE, Vol. 112,*, October 1986: 2263-2280.

Amde, A. M., Greimann, L. F., and Yang, P. S. *Nonlinear Pile Behavior in Integral Abutment Bridges.* Ames, Iowa: Final Report, Iowa DOT Project HR-227, ISU-ERIAmes, 1982.

Amde, A. M., Greimann, L. F., and Yang, P. S. *Skewed Bridges with Integral Abutment.* Washington DC: Bridges and Culverts, Transportation Research Record 903, Transportation Research Board, National Academy of Sciences, 1983, 64-72.

Amde, A. M., Greimann, L. F., Yang, P. S., and Edmunds, S. K. *Design of Piles for Integral Abutment Bridges.* Iowa Department of Transportation, Project H-252, ISU-ERI-Ames 84286, 277 pages, August 1984.

Amde, A. M., Greimann, L.F., and Yang, P.S. "End Bearing Piles in Jointless Bridges." *Journal of Structural Engineering, ASCE, Vol. 114, No. 8*, August 1988: 1870-1884.

Amde, A. M., Greimann, L.F., and Yang, P.S. "Non-linear Pile Behavior in Integral Abutment Bridges HR-227, ISU-ERI-Ames 82123." February 1982, 201 pages.

Amde, A. M., Klinger, J. E. and Mullangi R. "Bridge Decks Joint Rehabilitation or Retrofitting." *Department of Civil Engineering, University of Maryland*, 1988.

Amde, A. M., Klinger, J. E., and White, E. J. "Performance of Jointless Bridges." *Journal of the Performance of Constructed Facilities, ASCE, Vol. 2, No. 2,* , May 1988: 111-125.

Amde, A. M., Klinger, J. E., Mafi, M., Albrecht, P., White, J., and Buresly, N. *Performance and Design of Jointless Bridges.* U.S. Department of Transportation, Federal Highway Administration, 282 pages, June 1987.

Amde, A. M., Klinger, J. *The State-of-the-Art in Integral Abutment Bridge Design and Construction.* AW087-313-046, FHWA/MD-87/07, January 1987, 70 pages.

Amde, A. M., Klinger, J.E. ,and Mullangi R. *Bridge Deck Joint Rehabilitation or Retrofitting.* AW089-327-046, FHWA/MD-89/12, December 1988, 284 pages.

Amde, A. M., Lowwell Greinman. "General design details for integral abutment bridges." *Civil Engineering Practice, Journal of the Boston Society of Civil Engineers Section/ASCE, Vol. 3, No. 2, Fall, ISSN: 0886-9685*, 1988: 7-20.

Amde, A. M., Lowwell Greinman, Pe-Shen Yang. "End-Bearing Piles in Jointless Bridges." *ASCE - Journal of Structural Engineering Vol. 114, No. 8*, August 1989: 1870-1884.

Amde, A. M., Yang, P. S., and Greimann, L. F. *Nonlinear Finite Element Study of Piles in Integral Abutment Bridges.* Ames, Iowa: Iowa DOT, September 1982 , Final report.

Andrea Frangi, Peter Collin, Roman Geier. "Bridges with Integral Abutments: Introduction." *Structural Engineering International*, 2011: 144-150.

Andrew Lawver, Catherine French, and Carol K. Shield. "Field Performance of Integral Abutment Bridge." *Transportation research record*, 2000.

ANSYS Inc. "ANSYS16.2 Help." Canonsburg, , PA 15317, Feb 2016.

Arockiasamy, M. P.E., M. ASCE, and Sivakumar, M. "Time-dependent behavior of continuous composite integral abutment bridges." *Practice Periodical on Structural Design and Construction*, 2005: 161-170.

Arockiasamy, M. P.E., Narongrit Butrieng, and Sivakumar. "State-of-the-Art of
Integral Abutment Bridges: Design and Practice." *Journal of Bridge
Engineering*, 2004: 497-506.

Arsoy, Sami. "Proposed mathematical model for daily and seasonal thermal bridge
displacements." *Transportation Research Record*, 2008.

Barbero, Ever J. *Introduction to Composite Materials Design.* Boca Raton FL 33487:
CRC Press, 2011.

Bhowmick, Alok. "Design and detailing of integral bridges: Suggested guidelines."
The Indian Concrete Journal, 2005: 43-50.

Bloodworth, Alan G., Ming Xu, James R. Banks, and and Chris R. I. Clayton.
"Predicting the Earth Pressure on Integral Bridge Abutments." *Journal of
Bridge Engineering © ASCE*, 2012: 371-381.

Breña, Sergio F., Christine H. Bonczar, Scott A. Civjan, Jason T. DeJong, and and
Daniel S. Crovo. "Evaluation of Seasonal and Yearly Behavior of an Integral
Abutment Bridge." *Journal of Bridge Engineering*, 2007: 296-305.

Burdette, E.G., S.c. Howard, and J.H. and Goodpasture, D.W. Deatherage. "The use
of prestressed concrete piles to support integral abutments." *Structural
concrete*, 2007: 119-124.

By Lowell F. Greimann M. ASCE, Pe-Shen Yang, and Amde A. M., M. ASCE.
"Nonlinear Analysis of Integral Abutment Bridges." *Journal of Structural
Engineering*, 1986: 2263-2280.

Cabrera, S. *Shear strength and seismic performance of concrete filled tubes.* Orlando:
MS thesis, Univ. of Central Florida, Orlando, 1996.

Camanho, Pedro Ponces. "Failure Criteria for Fibre-Reinforced Polymer Composites." *Demegi*, 2002: 1-13.

Chaozhuan, LUO, PENG Dawen, and LIN Zhiping. "Multimodal Response Spectrum Method Analysis of Integral Abutment Curved Box Bridge." 2010.

Charles W. W. Ng, Member, ASCE, Sarah M. Springman/ and Alison R. M. Norrish. "Centrifuge modeling of spread-base integral bridge abutments." *Journal of Geotechnical and Geoenviromental Engineering*, 1998: 376-388.

Chini, S.A., Amde, A. M. and Aggour, S.M. "Drainage and Backfill Provisions for Approaches to Bridges." *Journal of the Transportation Research Record, No. 1425*, October 1993: 45-53.

Christensen, R.M. "Mechanics of Composite Materials." *National SAMPE Symposium and Exhibition.* Reno, NV, USA: SAMPE, Covina, Calif, USA, 1984. 994-1006.

"Circumference of Ellipse." *Wikipedia.* 3 9, 2016. https://en.wikipedia.org/wiki/Ellipse#Circumference.

Clayton, C.R.I. "A laboratory study of the development of earth pressure behind integral bridge." *Geotechnique*, 2006: 261-571.

Composite Material Handbook (DOD). "Polymer Matrix Composites Material Usage, Design and Analysis." In *Composite MaterialsHandbook Volume 3*. 2013.

Connal, John. "Integral Abutment Bridges – Australian and US Practice." 2004.

Creative Pultrusion. *Fiberglass Pultrusion Process.* 1 5, 2016. http://www.creativepultrusions.com/index.cfm/products-solutions/fiberglass-pultrusion-process/ (accessed 1 5, 2016).

Cuihong Ding, Guocai Wang. "Numerical Simulation Analysis on Effect of Pile Cap to Lateral Capacity of Single Pile." 2010.

Davol, A., R. Burgueño, and F. Seible. "Flexural behavior of circular concrete filled FRP shells." *J. Struct. Eng.*, 2001: 810–817.

Dicleli, Murat. "Integral Abutment-Backfill Behavior on Sand Soil—Pushover Analysis Approach." *Journal of Bridge Engineering*, 2005: 354-364.

Dicleli, Murat. "Rational design approach for prestressed-concrete-girder integral bridges." *Engineering Structures*, 2000: 230-245.

Dicleli, Murat. "Simplified model for computer-aided analysis of integral bridges." *Journal of Bridge Engineering*, 2000: 240-248.

Direct Industry. *Filament winding machine / computer-controlled.* May 5, 2015. http://www.directindustry.com/prod/magnum-venus-products/product-39130-427499.html.

Dupont. *Kevlar Brand.* May 1, 2015. http://www.dupont.com/products-and-services/fabrics-fibers-nonwovens/fibers/brands/kevlar.html.

Earl E. Ingram, Edwin G. Burdette. "Behavior of steel H-piles supporting integral abutments." *Proceedings of the 2004 Structures Congress - Building on the Past: Securing the Future*, 2004: 219-225.

Edwin G. Burdette, Samuel C. Howard. "Behavior of prestressed concrete piles supporting integral abutments." *ASCE*, 2004.

Emre Kalayci, Scott A. Civjan , Sergio F. Breña. "Parametric study on the thermal response of curved integral abutment bridges." *Engineering Structures*, 2012: 129-138.

England, George. "Design of soil loading for integral bridges." *The Indian concrete journal*, 2005: 53-59.

Erhan, M. Dicleli & S. "Distribution of live load effects in integral bridge abutments and piles." *Bridge Maintenance, Safety, Management and Life-Cycle Optimization*, 2010: 616.

Eric Steinberg, P.E., Shad M. Sargand, and and Christopher Bettinger. "Forces in Wingwalls of Skewed Semi-Integral Bridges." *Journal of Bridge Engineering © ASCE*, Nov/Dec 2004: 563-571.

Ernesto Guades, Thiru Aravinthan , Mainul Islam, Allan Manalo. "A review on the driving performance of FRP composite piles." *Composite Structures*, 2012: 1932 - 1941.

Fam, Amir, and Sami Rizkalla. "Behavior of axially loaded concrete-filled circular fiber-reinforced polymer tubes." *ACI Structural Journal*, 2001: 280-289.

Fan, L., W. Zhou, and Y. Xue. "Preliminary study of seismic performance of FRP tube confined concrete short columns." *1st Chinese National Conf. of Application Technology of FRP Materials in Civil Engineering.* Beijing: National Diagnosis and Rehabilitation of Industrial Building Research Center, 2000. 113–117.

Fennema, Jolene L., P.E. Jeffrey A. Laman, and P.E. and Daniel G. Linzell. "Predicted and measured response of an integral abutment bridge." *Journal of Bridge Engineering © ASCE*, 2005: 666-677.

Forouzani, Afshin, and Ismail Mohamed Taib. "Modern integral bridge designs for
east coast expressway." *Proceedings of the 4th International Conference on
Current and Future Trends*, 2006: 175-186.

Fu, Chung C., Hamed Alayed, Amde M. Amde, and Jeff Robert. "Field Performance
of the Fiber-Reinforced Polymer Deck of a Truss Bridge." *Journal of
Performance of Constructed Facilities*, 2007: v21 n1 (200702): 53-60.

Gaetano Russo, Prof. Ing., Univ. of Udine, Ing., Jesolo, Univ. of Udine, Venezia
Otello Bergamo, and Ing., Caorle, Venezia Luigi Damiani. "Retrofitting a
Short Span Bridge with a Semi-Integral Abutment Bridge: The Treviso
Bridge." *Structural Engineering International*, 2/2009: 137-141.

Gangarao, Hemanth K. Thippeswamy and Hota V. S. "Analysis of In-Service
Jointless Bridges." *Transportation Research Record*, 1995: 162-170.

Gol'denblat, I. I., and V. A. Kopnov. "General theory of criteria of strength for
isotropic and anisotropic materials." *Strength of Materials v3 n2 (197102)*,
1971: 184-188.

Grainman, L.F., Amde, A.M. , Yang, P.S. "Skewed Bridges with Integral
Abutments." *National Research Council*, 1983.

Greimann, A.M., Amde, A. M. and Yang, P.S. "Finite Element Model for Soil-Pile
Interaction in Integral Abutment Bridges." *International Journal of
Computers and Geotechnics, Elsevier Applied Science Publishers Ltd.,
England, Vol. 4*, 1987: 127-149.

Greimann, L., Edwards, S. and Amde, A. M. "Simplified Model for Piles in Integral

Abutment Bridges." *Canadian Society for Civil Engineering Annual*

Conference. Saskatoon, Saskatchewan, May 27-June 1 , 1985.

Greimann, L.F., Yang, P.S. and Amde, A. M. "Non-linear Analysis of Integral

Abutment Bridges." *Journal of Structural Engineering, ASCE, Vol. 112, No.*

10, Paper No. 20969, October 1986: 2263-2280.

Greimann, Yang, Edmunds, Amde. *Design of piles for integral abutment bridges.*

Iowa Department of Transportation, 1984.

Greinmann, Robert E. Abendroth and Lowell F. "Rational design approach for

integral abutment bridge piles." *Transportation research record*, 1989: 12-23.

Grien, M. J., and K. and Tavakolian, M. R. Truong. "Study of Mechanically

Stabilized Earth Structure Supporting Integral Bridge Abutment." *Earth*

Retention Conference, 2010: 772-779.

Hashin, Z. "Analysis of Properties of Fiber Composites with Anisotropic

Constituents." *Journal of Applied Mechanics, Transactions ASME*, 1979: 543-

550.

Hashin, Z. and Rosen, B.W. "The Elastic Moduli of Fiber-Reinforced Materials." *J.*

Appl. Mech. Vol 31, 1964: 223.

Hashin, Zvi. "Theory of Fiber Reinforced Materials." *NASA Contractor Reports*,

1974.

Houston Walker, P.E. *Eliminating Bridge Joints – A Preservation Strategy.* April 5,

2016. http://www.concretebridgeviews.com/i70/Article1.php.

Huang, Jimin, and Catherine French Carol Shield. "Behavior of an Integral Abutment
Bridge in Minnesota, US." *Structural Engineering International*, 2011: 320-
331.

Huang, Jimin, Carol Shield, and Catherine French. "Behavior of an Integral Abutment
Bridge in Minnesota, US." *Structural Engineering International*, 2011: 320-
331.

Ireman T., Thesken J.C., Greenhalgh E., Sharp R., Gädke M., Maison S., Ousset Y.,
Roudolff. "Damage Propagation in Composite Structural Element-Coupon
Experiment and Analyses." *Composite Structures*, 1996: 209-220.

Iskander, Magued G. "Sustainable Piling Made of Recycled Polymers: State of the
Art Review." *Journal of ASTM International* 9, no. 2 (2012): 523-544.

Iskander, Magued G., and Moataz Hassan. "State of Practice Review in FRP
Composite Piling." *Journal of Composites for Constructions*, 1998: 116-120.

Jamaloddin Noorzaei, Aeid. A. Abdulrazeg, Mohamed Saleh Jaafar, Omid
Kohnehpooshi. "Non-linear analysis of an integral bridge." *Journal of Civil
Engineering and Management*, 2010: 387-394.

Jason T. DeJong, M. ASCE, Dan S.Howei, S.M. ASCE. "Influence of daily and
annual thermal variations on integral abutment bridge performance."
Geotechnical special publication, 2004: 496-505.

Javier Rodriguez, Principia, Principia Francisco Martinez, and Principia Joaquin
Marti. "Integral Bridge for High-Speed Railway." *Structural Engineering
International*, March 29, 2011: 297-303.

Jimin Huang, M.ASCE, M.ASCE Carol K. Shield, and M.ASCE and Catherine E. W. French. "Parametric Study of Concrete Integral Abutment Bridges." *Journal of Bridge Engineering* , 2009: 511-526.

Jin-Hee Ahn, Ji-Hyun Yoon, Jong-Hak Kim, Sang-Hyo Kim. "Evaluation on the behavior of abutment–pile connection in integral abutment bridge." *Journal of Constructional Steel Research*, 2011: 1134-1148.

John S. Horvath, Ph.D., P.E. "Integral-Abutment Bridges: Problems and Innovative Solutions Using EPS Geofoam and Other Geosynthetics." *Manhattan College School of Engineering Civil Engineering Department*, 2000.

Jonathan Kunin, Associate Member, ASCE, and Sreenivas Alampalli. "Integral Abutment Bridges: Current Practice in United States and Canada." *Journal of Performance of Constructed Facilities*, 2000: 104-111.

Jorsenson, James. "Behavior of Abutment Piles in an Integral Abutment in Response to Bridge Movements." 1983: 72-79.

Juan C. Carvajal, Carlos E. Ventura, and Sharlie Huffman. "Ambient Vibration Testing of Multi-Span Bridges with Integral Deck-Abutment." *Society for Experimental Mechanics Inc.*, 2009.

Kalaycı, Emre, and Sergio F. Breña, Chad A. Allen Scott A. Civjan. "Load Testing and Modeling of Two Integral Abutment Bridges in Vermont, US." *Structural Engineering International*, 2011: 181-188.

Kenneth F. Dunker, P.E., M.ASCE, and P.E., S.E. and Dajin Liu. "Foundations for Integral Abutments." *Practice Periodical on Structural Design and Construction © ASCE*, 2007: 22-30.

Khodair, Y. A. "Lateral earth pressure behind an integral abutment." *Structure and Infrastructure Engineering*, 2006: 123-136.

Komornik, Ilan Juran and Uri. "Behavior of Fiber-Reinforced Polumer Composite Piles under Vertical Loads." *U.S. Department of Transportation*, Aug. 2006.

Lehane, B. M. "Lateral soil stiffness adjacent to deep integral bridge abutments." *Geotechnique*, 2011: 593-603.

Lehane, B.M. , Keogh, D.L. , O'Brien, E.J. "Simplified elastic model for restraining effects of backfill soil on integral bridges." *Computers and Structures*, 1999: 303-313.

Linzell, D., D. Hall, and and D. White. "Historical Perspective on Horizontally Curved I Girder Bridge Design in the United States." *Journal of Bridge Engineering © ASCE*, 2004: 218-229.

Lissenden, Dr. Clifford J. *The Department of Engineering Science and Mechanics.* 2015. http://www.esm.psu.edu/labs/axialtorsion/activities/ (accessed April 5, 2015).

Marx, Steffen, and Günter Seidl. "Integral Railway B ridges in Germany." *Structural Engineering International*, 2011: 332-340.

Michael Paul, Jeffrey A. Laman, and Daniel G. Linzell. "Thermally induced superstructure stresses in prestressed girder integral abutment bridges." *Journal of the Transportation Research Board*, 2005: 287-297.

Michael R. Simac, P.E., M ASCE and David J. Elton, P.E. M. ASCE. "Geosynthetic Reinforced Soil Walls as Integral Bridge Abutment Walls." *2010 Earth Retention Conference.* n.d. 604-611.

Mirmiran, Amir, and Mohsen Shahawy. "A new concrete-filled hollow FRP composite column." *Composites Part B: Engineering*, 1996: 263–268.

Mirmiran, Amir, and Mohsen Shahawy. "Novel FRP-concrete composite construction for the infrastructure." *Structures Congress - Proceedings*, 1995: 1663- 1666.

Mistry, Vasant C. "Integral Abutment and Jointless Bridges." *Federal Highway Administration*, 2000.

Moumena, L. and Amde, A. M. "Plasticity Analysis of Abutment Lateral Effect on Bridge Approaches." *Proceedings of the 13th Canadian Congress of Applied Mechanics.* Winnipeg, Manitoba, Canada, June 2-6 , 1991.

Moumena, L., Amde, A. M. and Aggour, S.M. "Analysis of `Approaches to Bridges." *Proceedings of the Second NSF Sponsored Workshop on Bridge Engineering Research in Progress, University of Nevada.* Reno, 29-30 October 1990.

Munoz, H., F. Tatsuoka, D. Hirakawa, H. Nishikiori, R. Soma, and M. and Watanabe K. Tateyama. "Dynamic stability of geosynthetic-reinforced soil integral bridge." *Geosynthetics International*, 2012: 11-38.

Murat Dicleli, P. Eng, Suhail M. Albhaisi. "Maximum length of integral bridges supported on steel H-piles driven in sand." *Engineering Structures*, 2003: 1491-1504.

Murat Dicleli, P.E., M.ASCE, and Suhail M. Albhaisi. "Estimation of Length Limits for Integral Bridges Built on Clay." *Journal of Bridge Engineering © ASCE*, 2004: 572-581.

NS Department of Transportation and Infrastructure Renewal. *Highway 125, Cape Breton County, NS.* 2010-2013. http://harboursideengineering.ca/Highway125 (accessed May 2, 2015).

Nuplex. *Filament winding.* May 1, 2015. http://www.nuplex.com/composites/processes/filament-winding (accessed May 5, 2015).

Pando, Miguel A., Carl D. Ealy, George M. Filz, J.J. Lesko, and E.J. and Hoppe. *A Laboratory and Field Study of Composite Piles for Bridge Substructures.* Charlottesville: Virginia Transportation Research Council, 2006.

"Pearson Pilings." *Pearson Pilings.* Feb 19, 2016. http://www.pearsonpilings.com/commercial_advantages.html.

Perie, D., and B.R. & Esmaeily, A. Shah. "Three-dimensional non-linear finite element modeling of integral abutment bridges." 2007: 679-684.

Phillip S. K. Ooi, P.E., M.ASCE, Xiaobin Lin, and P.E., F.ASCE and Harold S. Hamada. "Field Behavior of an Integral Abutment Bridge Supported on Drilled Shafts." *Journal of Bridge Engineering © ASCE*, 2010: 4-18.

Phillip S. K. Ooi, P.E., M.ASCE, Xiaobin Lin, and P.E., F.ASCE and Harold S. Hamada. "Numerical Study of an Integral Abutment Bridge Supported on Drilled Shafts." *Journal of Bridge Engineering © ASCE*, 2010.

Pugasap, K. Ph.D., P.E, W. Kim, and J. A. , Ph.D., P.E and Laman. "Long-Term Response Prediction of Integral Abutment Bridges." *Journal of Bridge Engineering © ASCE*, 2009: 129-139.

Qiuhong Zhao, Reza Vasheghani-Farahani and Edwin G. Burdette. "Seismic Analysis of Integral Abutment Bridges Including Soil-Structure Interaction." *Structures Congress 2011 © ASCE*, 2011: 289-303.

Rakesh K. Goel, Member, ASCE. "Earthquake Charasteristics of Bridges with Integral Abutments." *Journal of Bridge Engineering* , Nov. 1997: 1435-1443.

Robert E. Abendroth, Lowell F. Greimann. "Abutment pile design for jointless bridges." *Joumal of Structural Engineering*, 1989: 2914-2930.

Robert E. Abendroth, Lowell F. Greimann, and Michael D. LaViolette. "An Integral Abutment Bridge with Precast Concrete Piles." *Iowa Highway Research Board*, 2007: 1-60.

Sami Arsoy, Richard M. Barker, Ph.D. "The behavior of integral abutment bridges." *Virginia Transportation Research Council*, 1999.

Scott A. Civjan, Ph.D., P.E., Christine Bonczar, Sergio F. Breña, Jason DeJong, and and Daniel Crovo. "Integral Abutment Bridge Behavior: Parametric Analysis of a Massachusetts Bridge." *Journal of Bridge Engineering* , 2007: 64-71.

Seible, F., R. Burgueno, M.G. Abdallah, and R. Nuismer. "Development of advanced composite carbon shell systems for concrete columns in seismic zones." *11th World Conf. on Earthquake Engineering.* Oxford, UK: Pergamon–Elsevier Science, 1996. Paper No. 1375.

Semih Erhan, Murat Dicleli. "Live load distribution equations for integral bridge substructures." *Engineering Structures*, 2009: 1250-1264.

Sendeckyj, G.P. "Elastic Behavior of Composites." *Composite Materials*, 1974: 45-83.

Shoukry, Samir N., Gergis W. William, and Mourad Y. Riad. "Response of an

integral abutment bridge to lemperature variations." *Proceedings of the 2008

Structures Congress - Structures Congress 2008: Crossing the Borders.* 2008.

Shoukry, Samir N., Gergis W. William, and Mourad Y. Riad. "Structural Behaviour

of an Integral Abutment Bridge under Environmental Conditions." *Structures*,

2006.

Siddique, Abu B., Leon D. Wegner, and Bruce F. Sparling. "Application of vibration-

based damage detection to an integral abutment bridge." *Department of Civil

and Geological Engineering, University of Saskatchewan, Saskatoon, SK*,

2005: 225-235.

Singh, Satinder. "Integral abutments for bridges in seismic regions: Californian

practice." *The Indian concrete journal*, 2005: 17-21.

Sreenivas Alampalli, Arthur Yannotti. "In-service performance of integral bridges

and jointless decks." *Transportation research records*, 1998: 1-7.

Sri Sritharan, M.ASCE, Justin Vander Werff, M.ASCE , Wagdy G. Wassef, M.ASCE

Robert E. Abendroth, and F.ASCE and Lowell F. Greimann. "Seismic

Behavior of a Concrete/Steel Integral Bridge Pier System." *Journal of

Structural Engineering © ASCE*, July 2005: 1083-1094.

Stergios A. Mitoulis, M.Sc., Ph.D. and Ioanni s A. Tegos. "Two New Earthquake

Resistant Integral Abutments for Medium to Long Span Bridges." *Structural

Engineering International*, 2011: 157-161.

Strongwell. *Design Manual Documents.* 1 11, 2013.

http://www.strongwell.com/DesignManual/.

Susan Faraji, John M. Ting, Members, ASCE, Daniel S. Crovo, and Helmut Ernst. "Nonlinear Analysis of Integral Bridges." *Journal of Geotechnical and Geoenvironmental Engineering*, 2001: 454-461.

Synthane Taylor. *The Strength and Diversity of Pultruded Products.* May 5, 2015. http://www.synthanetaylor.com/blog/bid/252917/The-Strength-and-Diversity-of-Pultruded-Products.

Tabsh, Sehab Mourad and Sami W. "Pile Forces in Integral Abutment Bridges Subjected to Truck Loads." *Transportation Research Record*, 1998: 77-83.

Tabsh, Shehab Mourad and Sami W. "Deck Slab Stresses in Integral Abutment Bridges." *Journal of Bridge Engineering* , 1999: 125-130.

Tang, Benjamin. "Fiber Reinforced Polymer Composites Applications in USA." *First Korea/U.S.A. Road Workshop Proceedings.* DOT - Federal Highway Administration, 1997.

Tap Plastics. *Carbon Fiber.* May 5, 2015. http://www.tapplastics.com/product/fiberglass/carbon_specialty_fabrics/standard_carbon_twill/98.

Tatsuoka F., Hirakawa D., Nojiri M., Aizawa H., Nishikiori H., Soma R., Tateyama M. "A new type of integral bridge comprising geosynthetic-reinforced soil walls." *Geosynthetics international*, 2009: 301-326.

Tegou, Sevasti, and Ioannis Tegos. "A Proposal for a New Type of Integ ral Abutment with Seismi c Energy Dissipation Capabilities." *Structural Engineering International*, 4/2011: 471-480.

Thanoon, W. A., A. A. Abdulrazeg, J. Noorzaei, and M. S. Jaafar. "Soil Structure
    Interaction for Integral Abutment Bridge Using Spring Analogy Approach."
    IOP Science, 2011: 1-17.

Tobia Zordan, Bruno Briseghella , Cheng Lan. "Parametric and pushover analyses on
    integral abutment bridge." *Engineering Structures 33*, 2011: 502-515.

Tsai, S. W. and Wu, E. M. "A general theory of strength for anisotropic materials."
    Journal of Composite Materials. vol. 5, 1971: 58-80.

Tze-Wei Choo, Daniel G. Linzell,∗, Je Il Lee, James A. Swanson. "Response of a
    continuous, skewed, steel bridge during deck placement." *Journal of
    Constructional Steel Research*, 2004: 567-586.

Ultramet. *Fiber Interface Coatings.* 2015.
    http://www.ultramet.com/fiber_interface_scanning.html (accessed April 5,
    2015).

"University of Cambridge." *Failure of laminates and the Tsai–Hill criterion.* 3 7,
    2016.
    http://www.doitpoms.ac.uk/tlplib/fibre_composites/laminate_failure.php.

Wacker. *Hand Lay-up.* May 10, 2015.
    http://www.wacker.com/cms/en/industries/pl_composites/pl_comp_appl/handl
    ayup.jsp?country=US&language=en (accessed May 10, 2015).

Wang, Tianli. "The review about a new type of bridge structure - Semi-integral
    abutment jointless bridge." *Advanced materials research*, 2012: 72-75.

Warren, K.A., W. Schlatter, M. Adams, T. Stabile, and D. LeGrand. "Preliminary Results for a GRS Integrated Bridge System Supporting a Large Single Span Bridge." *2010 Earth Retention Conference.* ASCE 2010, 2010. 612-619.

Wasserman, Edward. "Integral abutment practices in the United States." *The Indian concrete journal*, 2005: 11-16.

White, II, H., H. Pétursson, and P. Collin. "Integral Abutment Bridges: The European Way." *Practice Periodical on Structural Design and Construction © ASCE*, Aug 2010: 201-208.

William G. Davids, P.E., M.ASCE, and P.E., M.ASCE Thomas Sandford. "Field-Measured Response of an Integral Abutment Bridge with Short Steel H-Piles." *Journal of Bridge Engineering © ASCE*, 2010: 32-43.

WooSeok Kim, Jeffrey A. Laman. "Integral abutment bridge response under thermal loading." *Engineering Structures 32*, 2010: 1495–1508.

WooSeok Kim, Jeffrey A. Laman. "Numerical analysis method for long-term behavior of integral abutment bridges." *Engineering Structures 32*, 2010: 2247-2257.

WooSeok Kim, Ph.D. and Jeffrey A. Laman, Ph.D., PE, M.ASCE. "Seven-Year Field Monitoring of Four Integral Abutment Bridges." *Journal of Performance of Constructed Facilities © ASCE*, Jan /Feb 2012: 54-64.

Xiong, Sophia Hassiotis and Kai. "Field Measurements of Passive Pressures Behind an Integral Abutment Bridge." *Seventh International Symposium on Field Measurements in Geomechanics*, 2007.

Xu, Ming, Alan G. Bloodworth, and and Chris R. I. Clayton. "Behavior of a Stiff
Clay behind Embedded Integral Abutments." *Journal of Geotechnical and
Geoenvironmental Engineering © ASCE*, June 2007: 721-730.

Yang, P.S., Amde, A. M., and Greimann, L.F. "Effects of Predrilling and Layered
Soils on Piles." *Journal of Geotechnical Engineering, ASCE, Vol. 111, No. 1*,
January 1985: 18-31.

Yang, P.S., Amde, A. M., and Greimann, L.F. "Non-linear Finite Element Study of
Piles in Integral Abutment Bridges, ERI 1501, ISU-ERI-Ames-83068."
September 1982: 153 pages.

Yasser A. Khodair, Sophia Hassiotis. "Analysis of soil–pile interaction in integral
abutment." *Computers and Geotechnics*, 2005: 201-209.

Yu, Tianlai. "Effect of bridge-soil interaction on behavior of integral bridge." *Applied
mechanics and materials*, 2012: 123-127.

Yuan, H., Y. Xue, X. Li, and M. Zhang. "Study on a novel hybrid GFRP/CFRP
composite beam." *2nd Conference of Application Technology of FRP
Materials in Civil Engineering.* Beijing: Tsinghua University Publication,
2002. 296–305.

Zordan, Tobia, Bruno Briseghella, and Cheng Lan. "Analytical Formulation for Limit
Length of Integral Abutment Bridges." *Structural Engineering International*,
May 2011: 304-310.

Zweben, C. *Introduction to Mechanical Behavior and Properties of Composites
Materials (Vol. 1).* 1989.